ATMOSPHERIC AND EXTRATERRESTRIAL EFFECTS ON RADIO WAVE PROPAGATION

TIS R60EMH36

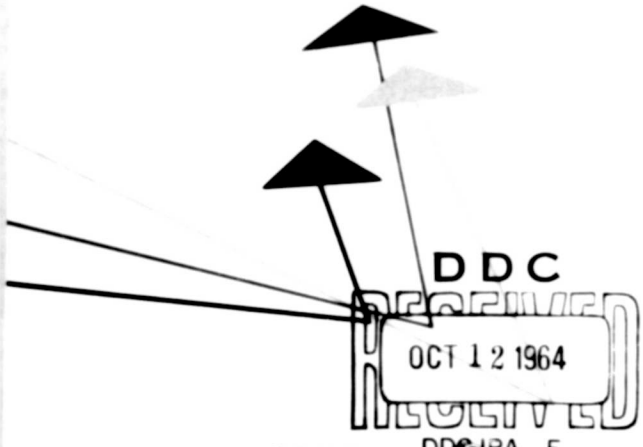

GENERAL ELECTRIC

MISSILE DETECTION SYSTEMS SECTION

CLEARINGHOUSE FOR FEDERAL SCIENTIFIC AND TECHNICAL INFORMATION CFSTI
DOCUMENT MANAGEMENT BRANCH 410.11

LIMITATIONS IN REPRODUCTION QUALITY

ACCESSION # AD 606137

☒ 1. WE REGRET THAT LEGIBILITY OF THIS DOCUMENT IS IN PART UNSATISFACTORY. REPRODUCTION HAS BEEN MADE FROM BEST AVAILABLE COPY.

☐ 2. A PORTION OF THE ORIGINAL DOCUMENT CONTAINS FINE DETAIL WHICH MAY MAKE READING OF PHOTOCOPY DIFFICULT.

☐ 3. THE ORIGINAL DOCUMENT CONTAINS COLOR, BUT DISTRIBUTION COPIES ARE AVAILABLE IN BLACK-AND-WHITE REPRODUCTION ONLY.

☐ 4. THE INITIAL DISTRIBUTION COPIES CONTAIN COLOR WHICH WILL BE SHOWN IN BLACK-AND-WHITE WHEN IT IS NECESSARY TO REPRINT.

☐ 5. LIMITED SUPPLY ON HAND: WHEN EXHAUSTED, DOCUMENT WILL BE AVAILABLE IN MICROFICHE ONLY.

☐ 6. LIMITED SUPPLY ON HAND: WHEN EXHAUSTED DOCUMENT WILL NOT BE AVAILABLE.

☐ 7. DOCUMENT IS AVAILABLE IN MICROFICHE ONLY.

☐ 8. DOCUMENT AVAILABLE ON LOAN FROM CFSTI (TT DOCUMENTS ONLY).

☐ 9.

PROCESSOR:

TSL-107-10 64

GENERAL ELECTRIC

ELECTRONICS DIVISION

RTD-1048-21 REV (1-58)

TECHNICAL INFORMATION SERIES

Title Page

AUTHOR	SUBJECT CATEGORY	NO. R60EMH36
G. H. Millman	Radar Propagation	DATE June 1960*

TITLE Atmosphere and Extraterrestrial Effects on Radio Wave Propagation

ABSTRACT

This report consists of material presented by the author as a Visiting Lecturer at the 1960 Special Summer Session, The Moore School of Electrical Engineering, University of Pennsylvania. These notes are lectures five and six of the "Modern Radar Techniques" course conducted during the period June 20 - July 1, 1960 and are for the most part revised material originally contained in the General Electric Company Technical Information Series, Report No. R56EMH31.

G.E. CLASS	REPRODUCIBLE COPY FILED AT	NO. PAGES
1	Technical Publications CSP 9-12, Syracuse, New York	174
GOV. CLASS Unclassified		

CONCLUSIONS

*Revised December 1960

By cutting out this rectangle and folding on the center line, the above information can be fitted into a standard card file.

For list of contents—drawings, photos, etc. and for distribution see next page (RTD 1011-21 or revision).

FOR GENERAL TIS INSTRUCTIONS SEE EDI 1.3

GE ACCOUNTING REFERENCE HMED 310

COLLABORATORS

COUNTERSIGNED DEPT HMED LOCATION CSP 9-46

61-07-6387

TABLE OF CONTENTS

TABLE OF CONTENTS (Cont.)

TABLE OF CONTENTS (Cont.)

LIST OF ILLUSTRATIONS

LIST OF ILLUSTRATIONS (Cont.)

LIST OF ILLUSTRATIONS (Cont.)

LIST OF ILLUSTRATIONS (Cont.)

LIST OF TABLES

5.1 - INTRODUCTION

An important consideration which must be taken into account in the formulation and design of any radar system is the degradation in the signal-target information introduced by the atmosphere. From a study of the propagational anomalies, it becomes somewhat apparent that the future development of radar equipments possessing highly accurate measurement capabilities may be ultimately limited by the characteristics of the propagating medium. In general, the regions of the atmosphere which affect the propagation of electromagnetic waves are the troposphere and the ionosphere.

Signal deterioration results from the fact that there exists in the atmosphere spatial inhomogeneities which are continuously varying as a function of time. The spatial variations, in essence, produce statistical-bias errors while the time-varying component results in the fluctuating or root-mean-square inaccuracies.

The propagational effects which are prevalent when radio waves traverse the atmosphere manifest themselves as refractive bending, time delays, Doppler errors, rotation of the plane of polarization (Faraday effect) and attenuation. In addition, the presence of celestial radio noise sources such as the sun and radio stars are capable of reducing the overall system sensitivity. Moreover, auroral and meteoric ionization at ionospheric heights, and the moon also introduce interference and clutter problems.

In the ensuing discussion, these phenomena are described and assessed with application to frequencies in the VHF and UHF range. The calculations which are presented are based on a normal static, undisturbed atmosphere. Atmospheric anomalies brought about by man-made artificial devices are not considered.

5 2 - ATMOSPHERIC MODELS

A. INTRODUCTION

A study of the effects of the atmosphere on radio wave propagation necessitates a knowledge of the height-variation of the dielectric constant, or refractive index, in the tropospheric and ionospheric regions. Since the magnitude of the dielectric constant is a function of such parameters as the geographic location on the earth, weather, time of day and season of the year, it becomes an overwhelming task to completely analyze atmospheric propagational effects under all parametric conditions. To simplify the analytical problem, atmospheric models which are representative of average conditions, are employed.

B. THE TROPOSPHERE

In the troposphere, the index of refraction which is a function of meteorological variables such as water vapor, air temperature and air pressure, can be represented by

$$(n - 1) \times 10^6 = \frac{a}{T}\left(p + \frac{be}{T}\right) \qquad (5.2\text{-}1)$$

where n is the refractive index; T, the air temperature in degrees Kelvin; p, the total pressure in millibars; and e, the partial pressure of water vapor in millibars. The first term, ap/T, applies both to optical and radio frequencies while the second term, abe/T^2, is the explicit water vapor relationship required only at radio frequencies.

According to Kerr (1), the constants, a and b, are approximately equal to 79° K/mb and 4800° K respectively Campen and Cole (2) quote 74 4° K/mb and 4973° K as the values of a and b Through consideration of various propagation experiments, Smith and Weintraub (3) arrive at the values of 77 6° K/mb and 4810°K

The above expression for the refractivity of air, is independent of frequency in the 100 mc/sec - 10,000 mc/sec range According to Smith and Weintraub (3), this expression is considered to be valid to 0 5% in $(n-1) \times 10^6$ units for frequencies up to 30,000 mc/sec and normally encountered ranges of temperature, pressure and humidity

The analytical expressions of refractive index for a standard atmosphere utilized in this study were derived by Campen and Cole (2).

In the Standard Atmosphere which represents average conditions in the temperate zone, the temperature is given by

$$T = 288 - 6\ 5Z \qquad (5.2\text{-}2)$$

where Z is the altitude in kilometers This equation is based on a surface temperature of 15°C and a lapse rate of 6 5°C/km up to an altitude of 11 km The lapse rate is defined as the decrease in temperature per unit increase in altitude.

The pressure in a Standard Atmosphere which is based on a sea level pressure of 1013 millibars decreasing with height up to 11 km, is given by

$$p = 1013\left[1 - 0.02257Z\right]^{5.2561} \qquad (5.2\text{-}3)$$

Campen and Cole, assuming the ratio of water vapor at altitudes below 10 km to the water vapor pressure at the earth's surface may be approximated by

$$\frac{e}{e_o} = (1 - 0.064Z)^6 \qquad (5.2\text{-}4)$$

arrive at the following polynomial expression for the refractive index of a completely wet (one hundred percent relative humidity at all levels) Standard Atmosphere.

$$N_w = 338 - 50.9Z + 4.39Z^2 - 0.245Z^3 + 0.0071Z^4 - 0.00006Z^5 \qquad (5.2\text{-}5)$$

where

$$N_w = (n_w - 1) \times 10^6 \qquad (5.2\text{-}6)$$

For a completely dry (zero percent relative humidity at all levels) Standard Atmosphere, the refractive index becomes

$$N_d = 262 - 25.1Z + 0.92Z^2 - 0.016Z^3 + 0.0001Z^4 \qquad (5.2\text{-}7)$$

Equations (5.2-5) and (5.2-7) are valid for $0 \leq Z \leq 10$ km. Above 10 km altitude, the refractive index is assumed to decay exponentially as

$$N_{w,d} = N_{ow,d}\, e^{-\frac{h}{25}} \qquad (5.2\text{-}8)$$

where h is the altitude in thousands of feet and N_{ow} and N_{od} are the values of N_w and N_d, respectively, at the earth's surface. It is evident from the definitions of N_w and N_d that N_{ow} and N_{od} are 338 and 262 units, respectively. The values of N_w and N_d at 100,000 ft., which is assumed to be the upper extent of the troposphere, are 6.2 and 4.8 units, respectively.

The index of refraction as a function of altitude for Standard Atmospheres having zero and one hundred percent relative humidity is plotted in Figure 5.2-1. A smoothing curve was applied to the zero percent curve to avoid discontinuities in the region connecting the index of refraction given by Equations (5.2-7) and (5.2-8).

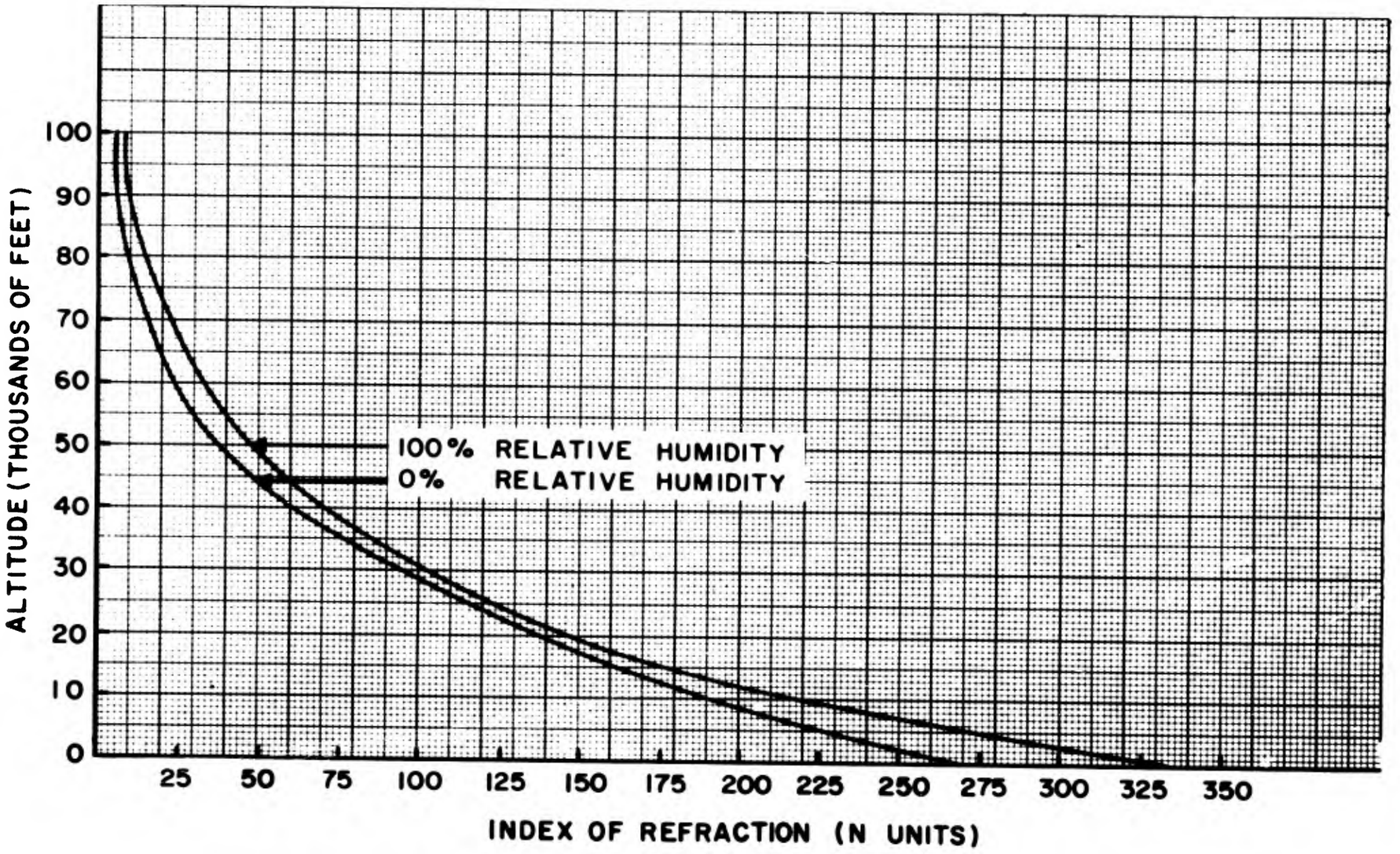

Figure 5.2-1. Index of Refraction in the Troposphere for a Standard Atmosphere

C. THE IONOSPHERE

According to the theory of Eccles and Larmor (4), the refractive index of a medium containing free electrons is given by

$$n = \left[1 - \frac{4\pi N_e e^2}{m\omega^2}\right]^{\frac{1}{2}} \qquad (5\ 2\text{-}9)$$

where N_e is the electron density in electrons/cm^3; e, the electron charge (4.8×10^{-10} esu); m, electron mass (9.1×10^{-28}gm), and ω the angular frequency of the incident wave in radians/sec. This relationship is valid when the earth's magnetic field and the collisions of electrons with ions and neutral particles are neglected.

The distribution of electron density with height under equilibrium conditions, as formulated by Chapman (4), is;

$$N_e = N_m e^{\frac{1}{2}\left[1 - Z - \sec\chi\ e^{-Z}\right]} \qquad (5\ 2\text{-}10)$$

where N_m is the electron density at the level of maximum ionization; Z, the normalized height; and χ, the solar zenith angle.

The normalized height is given by

$$Z = \frac{h - h_m}{H} \qquad (5.2\text{-}11)$$

where h_m is the height of maximum ionization density. The scale height, H, which is the height of the homogeneous atmosphere at a given temperature, is defined by

$$H = \frac{kT}{mg} \qquad (5.2\text{-}12)$$

where k is Boltzmann's constant (1.38×10^{-16} erg/degree Kelvin); T, the temperature in degrees Kelvin; m, the mean molecular mass of air (4.8×10^{-23} gm); and g, the gravitational constant (32.16 ft/sec^2)

The approximate average values of H for different ionospheric regions, as calculated by Mitra (4), are presented in Table 5.2-1 These calulations were based on the hypothesis that the ionospheric regions are all the Chapman type which is the simplest type of ionized layer that can be predicted theoretically. The Chapman layer is formed under highly idealized conditions, namely, the atmosphere is isothermal, the ionizing radiation from the sun is monochromatic and the recombination coefficient, or ion decay, is constant with height.

TABLE 5.2-1

IONOSPHERIC SCALE HEIGHTS

ALTITUDE (km)	SCALE HEIGHT - H (km)
70	6
100	10
200	35 (Winter Noon)
200	50 (Summer Noon)
250	50 (Winter Noon)
300	70 (Summer Noon)

The distribution of electron densities under consideration in this analysis are assumed to follow the Chapman theory. The assumed magnitudes and levels of maximum ionization and scale heights given in Tables 5.2-2 and 5.2-3 are for both the daytime and nighttime ionospheric models.

TABLE 5.2-2

DAYTIME PARAMETERS OF ELECTRON DENSITY

LAYER	H - (km)	h_m - (km)	N_m - (Electrons/cm^3)
E	10	100	1.5×10^5
F_1	40	200	3.0×10^5
F_2	50	300	12.5×10^5

TABLE 5.2-3

NIGHTTIME PARAMETERS OF ELECTRON DENSITY

LAYER	H - (km)	h_m - (km)	N_m - (Electrons/cm^3)
E	10	120	0.8×10^4
F	45	250	4.0×10^5

The ionospheric electron density models are illustrated in Figure 5.2-2. An arbitrary "fill-in" region having a minimum electron density at 128 km and 213 km for the daytime model and at 137 km for the nighttime model was constructed to join the layers smoothly.

In the upper atmosphere, electron collisions occur due to the presence of neutral particles and heavy ions. The ultimate effect of collisions is to cause absorption of energy from the electromagnetic waves traversing the ionized medium. If it is assumed that the atmosphere is chemically homogeneous and isothermal, the angular collisional frequency of the electrons, ν, with the particles should obey the exponential law

$$\nu = \nu_G \, e^{-\frac{h}{H}} \tag{5.2-13}$$

where ν_G is the collision frequency at the surface of the earth in radians per second and H is the scale height in the region. This expression can also be written in the form

$$\nu = \nu' \, e^{-\frac{h' - h}{H}} \tag{5.2-14}$$

where ν' is now the collision frequency at the altitude, h'.

The parameters which describe the electron collision frequency model shown in Figure 5.2-3, are presented in Table 5.2-4.

TABLE 5.2-4

COLLISION FREQUENCY PARAMETERS

LAYER	H - (km)	h' - (km)	ν' - (Radians/sec)
E	10	100	3×10^5
F	45	134	10^4

To extend the curve into the F region, the E region logarithmic curve was plotted to 134 km. The resultant collision frequency of 10^4 radians/sec at 134 km was then used for ν' in Equation (5.2-14) with the scale height abruptly changing to 45 km. To avoid discontinuities at 134 km, a smoothing curve was employed.

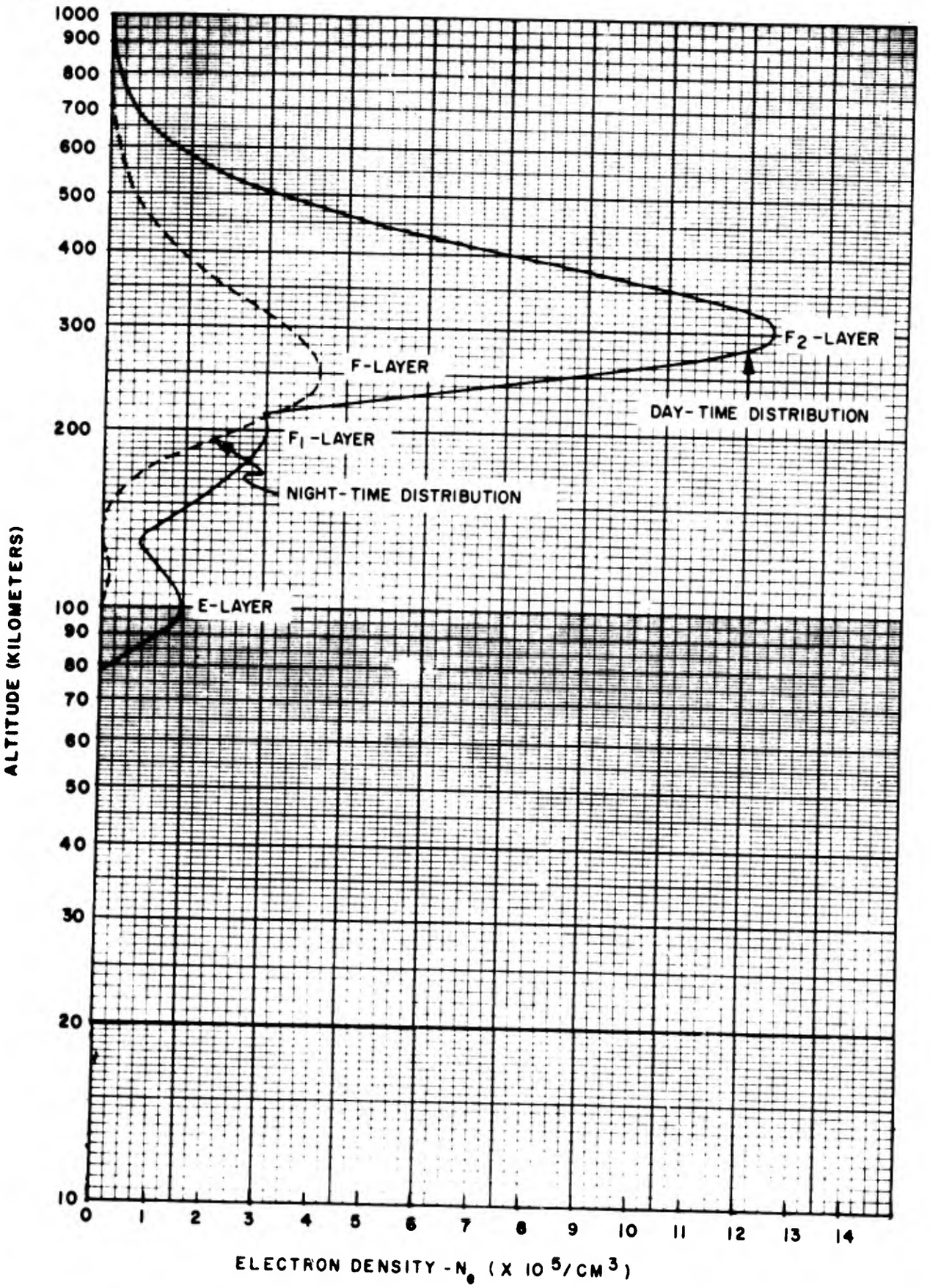

Figure 5.2-2. Chapman Distribution of Ionospheric Density

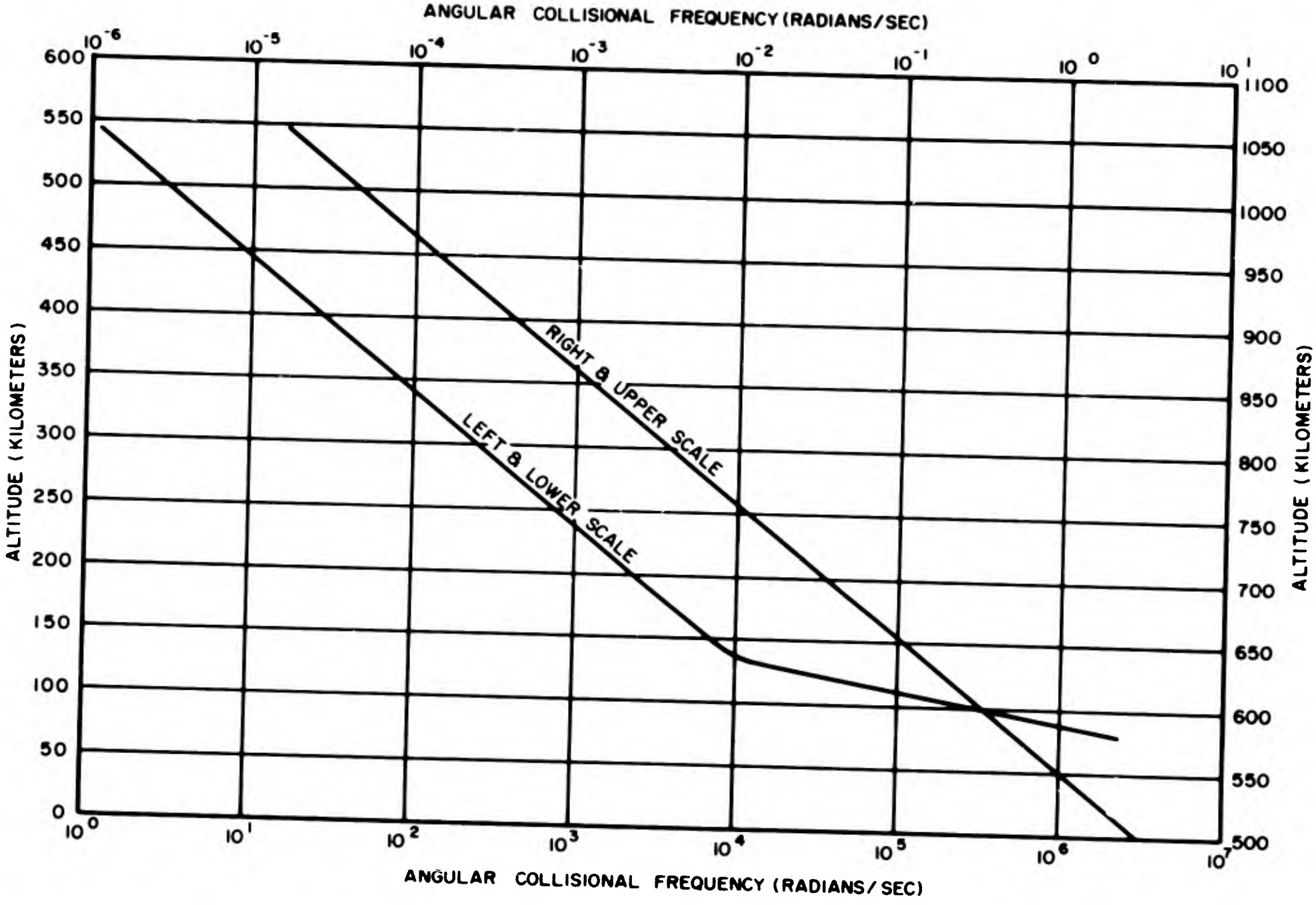

Figure 5.2-3. Collision Frequency Model for the Atmosphere

D. IONOSPHERIC TERMINOLOGY

1. IONOSPHERIC LAYERS

The ionization in the upper atmosphere is not uniform but appears to be concentrated into layers, each at a different altitude (4).

The D-layer, located at an altitude of approximately 70 kilometers, has been theoretically postulated to account for large variations in absorption of radio waves between summer and winter and between daytime and evening.

The E-layer maximum ionization density is at a height of 100-120 kilometers. The ionization density which is a maximum during the daytime is controlled by the solar zenith angle and solar activity. At night the ionization greatly decreases.

The F-layer height is approximately between 200-300 kilometers. During a summer daytime, this layer sometimes separates into two parts, the F_1 -layer and F_2 -layer. This division is not very distinct and, in fact, is often observed as an inflection in the F-layer electron density distribution. The F_1 -layer is believed to be formed by solar radiation; its ionization density follows the regular solar zenith variation similar to the E-layer. The F_2 -layer, on the other hand, although also formed by solar radiation, does not correlate its maximum ionization density with solar movement.

2. IONOSPHERIC ABNORMALITY

The abnormal or sporadic E-layer which is imbedded in the normal E-layer at approximately 100 km, reflects radio waves at frequencies higher than the normal E-layer and sometimes at frequencies higher than the normal F-layer. Because of this, it must necessarily contain highly dense concentrations of ionization. In the equatorial region, sporadic-E ionization exists throughout the daylight hours and is weak. In the temperate zone, sporadic-E occurs most frequently in the early morning and evening. It is most often present in the summer time in both the equatorial and temperate zone. It does not appear to be dependent on the solar cycle. Near the auroral zone, sporadic-E appears with great frequency at night. Meteor ionization, thunderstorm effect and bombardment by solar corpuscles near the auroral zone, have all been suggested to account for the origin of sporadic-E. Sporadic-E clouds are sometimes of the order of 100-200 kilometers in diameter and appear to have an effective thickness of one kilometer. They have been known to move with an apparent velocity of 60-100 meters/sec and have a lifetime of 2-3 hours. Because of the high ionization density in the clouds, high frequency waves passing through this region will suffer greater phase retardations, time delays and direction deviations than normally expected.

3. IONOSPHERIC DISTURBANCES

A sudden ionospheric disturbance, or S.I.D., is caused by intense ultraviolet radiation penetrating into the atmosphere and increasing the ionization in the lower ionospheric regions. This phenomenon, which occurs almost simultaneously with observed solar flares during the daylight hours, results in increased absorption for frequencies of short and medium wavelengths. For frequencies below 500 Kc/sec, the increase in ionization causes an increase in signal strength.

Ionospheric and magnetic storms are atmospheric disturbances accompanying one another and believed to be produced by the corpuscular matter which are ejected from the sun during a sloar flare and then surround the entire earth in a cloud of ionization. It takes about 48 hours for the corpuscles to reach the earth. The disturbances usually last two or three days. Auroral activity is an indication of the magnetic disturbance. A sudden decrease in the ionization density and increase in the virtual height of the F_2 -layer are an indication of the ionospheric storm in the high latitude. In the middle latitudes, the ionization density usually increases. The frequency and severity of these disturbances are greatest in the northern latitudes The normal ionospheric structure will be distorted by the appearance of spread echoes and ionization clouds. High frequency signals undergo an increase in fading rate while low frequency radio waves which are normally reflected from the lower E-layer are not affected. An increase in absorption often results in a complete polar "black-out."

4. IONOSPHERE STRUCTURE IN NORTHERN LATITUDES

The structure of the ionosphere near the auroral zone is different from that of other regions of the earth. This is attributed to the fact that the sun is not present during the winter months and that the ionization in the polar regions is influenced to a great extent by the presence of charged solar corpuscles ejected by the sun. A normal ionosphere in the northern latitude is considered an abnormal one in the middle latitudes. During the summer months the diurnal variation of the ionospheric layers are quite normal. At the winter solstice, the ionization density is a minimum.

E. REFERENCES

1. Kerr, D. E.; "Propagation of Short Radio Waves", Radiation Laboratory Series, Vol. 13, McGraw-Hill Book Co., 1951.

2. Campen, C. F. and Cole, A. E., "Tropospheric Variations of Refractive Index at Microwave Frequencies," Air Force Surveys in Geophysics, No. 79, Geophysical Reasearch Directorate, Oct. 1955.

3. Smith, E K , Jr and Weintraub, S.; "The Constants in the Equation for Atmospheric Refractive Index at Radio Frequencies", Central Radio Propagation Laboratory, N.B.S. Report No. 1938, Sept. 1952

4. Mitra, S.K., "The Upper Atmosphere", The Asiatic Society of Calcutta, 1952.

5.3 - MATHEMATICAL TECHNIQUES FOR REFRACTION AND TIME DELAY COMPUTATION

A. INTRODUCTION

When electromagnetic waves are propagated through a medium whose dielectric constant or index of refraction is a varying function of the path, the waves undergo a change in direction, or refractive bending, and a retardation in the velocity of propagation. Since the earth's atmosphere is such a medium, errors are evidently introduced in the radar angular and range measurements of target position.

In this section, two methods are discussed, i.e., the integral and the stratified layer method, which can be used to calculate the angular deviation and range inaccuracy introduced when electromagnetic waves traverse a medium other than free space. The latter method, although only approximate in nature, is capable of rendering theoretical estimates of propagational errors to a rather high degree of accuracy.

B. INTEGRAL METHOD

1. REFRACTION ERROR

The relationship expressing the angular bending of a ray of light can be determined from geometric optics by the application of Fermat's principle of least time which states that the path chosen by a ray joining two points is that which can be traveled over in the least possible time.

The velocity of propagation of a monochromatic ray, V, is related to the refractive index of the medium, n, by V = (c/n) where c is the free space velocity of light. The time, t, required for the ray to travel between the points s_1 and s_2 is, therefore, given by

$$t = \frac{1}{c} \int_{s_1}^{s_2} n\,ds \tag{5.3-1}$$

In applying Fermat's principle, it is necessary to minimize the integral such that

$$\delta I = \delta \int n\,ds = 0 \tag{5.3-2}$$

As shown in Figure 5.3-1, the incremental distance, ds, can be expressed in terms of polar coordinates, in the case of a spherical earth, by the function

$$ds^2 = dr^2 + r^2\,d\theta^2 \tag{5.3-3}$$

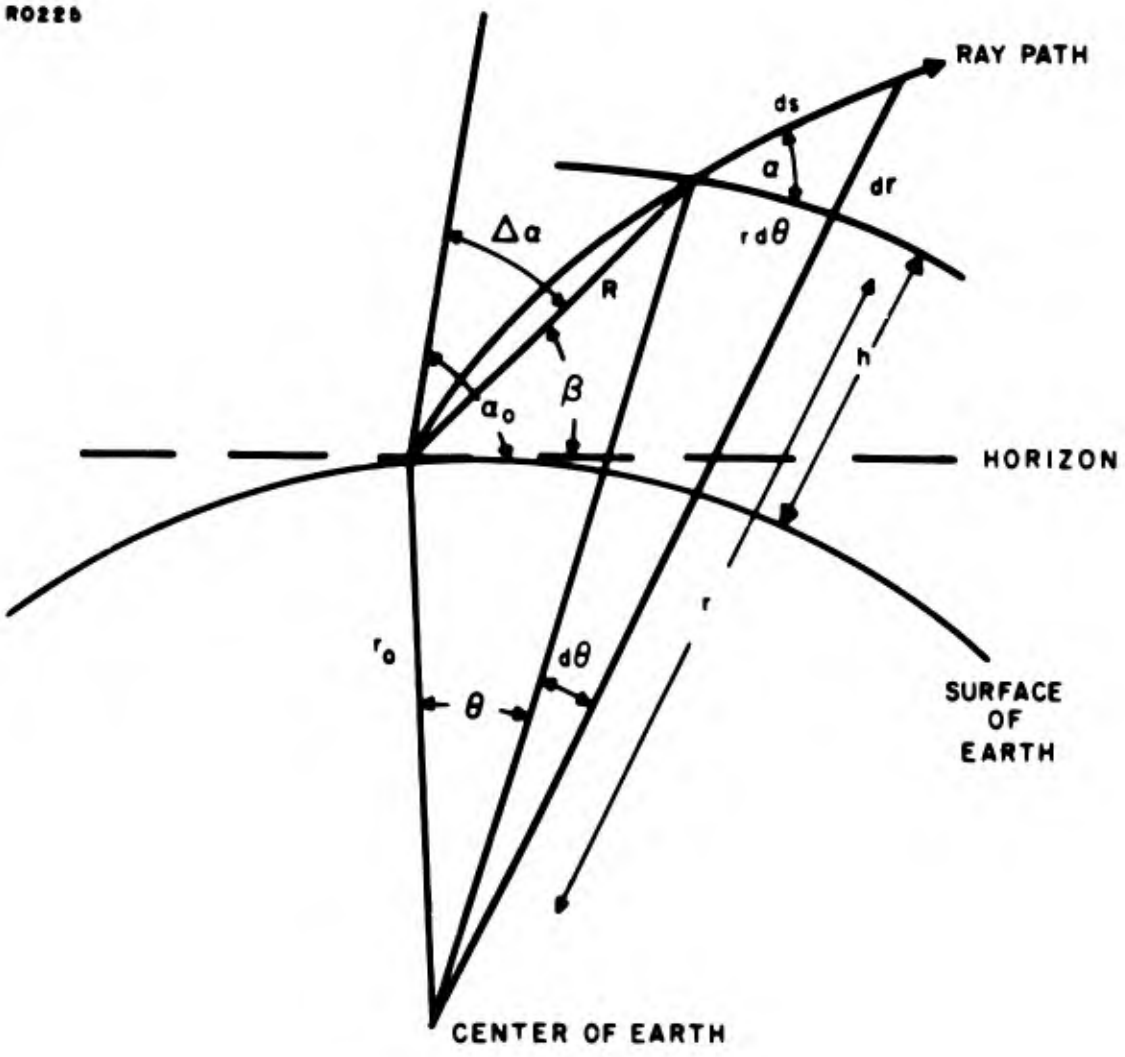

Figure 5.3-1. Ray Path Geometry

Assuming that the refractive index is only a function of height or the radial distance, r, and employing r as an independent variable, it follows that Equation (5.3-2) can be written as

$$\delta \int_{r_1}^{r_2} f(r, \dot{\Theta})\, d\, r = 0 \tag{5.3-4}$$

where

$$f(r, \dot{\Theta}) = n \left[1 + r^2 (\dot{\Theta})^2 \right]^{\frac{1}{2}} \tag{5.3-5}$$

and where $\dot{\Theta} = (d\Theta/dr)$

For Equation (5.3-4) to hold, the necessary condition that must be satisfied is that

$$\frac{d}{dr} \left(\frac{\partial f}{\partial \dot{\Theta}} \right) - \left(\frac{\partial f}{\partial \Theta} \right) = 0 \tag{5.3-6}$$

Since $f(r, \dot{\Theta})$ is not a function of Θ, this expression reduces to

$$\frac{d}{dr} \left[\frac{n r^2 \dot{\Theta}}{\left[1 + r^2 (\dot{\Theta})^2 \right]^{\frac{1}{2}}} \right] = 0 \tag{5.3-7}$$

The integration of this equation results in

$$\frac{n r^2 \dot{\Theta}}{\left[1 + r^2 (\dot{\Theta})^2 \right]^{\frac{1}{2}}} = K \tag{5.3-8}$$

where K is a constant. From Figure 5.3-1, it is seen that

$$\cos \alpha = \frac{r \dot{\Theta}}{\left[1 + r^2 (\dot{\Theta})^2 \right]^{\frac{1}{2}}} \tag{5.3-9}$$

It follows, therefore, that

$$nr \cos \alpha = K \tag{5.3-10}$$

For the condition that $\alpha = \alpha_o$, $r = r_o$ and $n = n_o$ then

$$K = n_o r_o \cos \alpha_o \tag{5.3-11}$$

where α_o is the apparent elevation angle of the ray at the earth's surface; r_o, the radius of the earth; n_o, the index of refraction at the earth's surface. Equation (5.3-10) which is a form of Snell's law for spherically symmetrical surfaces is also known as "Bouger's Rule."

Rewriting Equation (5.3-8) in terms of $(d\Theta/dr)$ and then integrating once again, there results

$$\Theta\Big]_{\Theta_o}^{\Theta} = \int_{r_o}^{r} \frac{dr}{r\left[\left(\frac{nr}{n_o r_o \cos \alpha_o}\right)^2 - 1\right]^{\frac{1}{2}}} \qquad (5.3\text{-}12)$$

According to Figure 5.3-1, the refraction angle error, $\Delta\alpha$, can be evaluated from the relationship

$$\Delta\alpha = \alpha_o - \beta \qquad (5.3\text{-}13)$$

where β is the true elevation angle. From the law of sines, it is seen that

$$\beta = \cos^{-1}\left[\frac{r_o + h}{R} \sin\Theta\right] \qquad (5.3\text{-}14)$$

where

$$R = \left[r_o^2 + (r_o + h)^2 - 2r_o (r_o + h) \cos\Theta\right]^{\frac{1}{2}} \qquad (5.3\text{-}15)$$

2. TIME DELAY CORRECTION

a. The Troposphere

With regard to atmospheric time delay or range error, for a non-dispersive medium, such as the troposphere, the apparent radar range, R_a, according to Equation (5.3-1), is simply given by

$$R_a = \int_{s_1}^{s_2} n\,ds \qquad (5.3\text{-}16)$$

According to Figure 5.3-1, the element of path length, ds, can be expressed in terms of the element of height or radial distance, dr, by

$$ds = \frac{dr}{\sin\alpha} \qquad (5\ 3\text{-}17)$$

From Equations (5.3-10) and (5.3-11), it is seen that

$$\sin\alpha = \left[1 - \left(\frac{n_o r_o \cos\alpha_o}{nr}\right)^2\right]^{\frac{1}{2}} \qquad (5.3\text{-}18)$$

Substituting Equation (5.3-17) and (5.3-18) in Equation (5.3-16), it follows that

$$R_a = \frac{1}{n_o r_o \cos \alpha_o} \int_{r_o}^{r} \frac{n^2 r dr}{\left[\left(\frac{nr}{n_o r_o \cos \alpha_o}\right)^2 - 1\right]^{\frac{1}{2}}} \tag{5.3-19}$$

It is noted the integrand of this expression resembles that for the central angle, Θ, given by Equation (5.3-12).

The range error, ΔR, is the difference between the apparent radar range and the true range, R, defined by Equation (5.3-15). In other words,

$$\Delta R = R_a - R \tag{5.3-20}$$

b. The Ionosphere

The group velocity of a wave packet must be used when problems of pulsed electromagnetic waves are concerned. In the troposphere, the group and phase velocity are synonymous since, in the frequency range of interest, the index of refraction is independent of frequency. For the ionosphere, however, the refractive index of the medium is a function of the transmitted frequency. As discussed in Section 6.1, in the simple case when the earth's magnetic field and electron collisions are neglected, the group velocity, V_g, is related to the phase velocity, V_p, by

$$V_p V_g = c^2 \tag{5.3-21}$$

Since by definition, the phase velocity is $V_p = (c/n)$, it follows that in the ionosphere, the time of travel for a ray to traverse a distance from point s_1 to s_2, is

$$t = \frac{1}{c} \int_{s_1}^{s_2} \frac{ds}{n} \tag{5.3-22}$$

In other words, the apparent radar range becomes

$$R_a = \int_{s_1}^{s_2} \frac{ds}{n} \tag{5.3-23}$$

From Equations (5.3-17) and (5.3-18), it is seen that this expression reduces to

$$R_a = \frac{1}{n_o r_o \cos \alpha_o} \int_{r_o}^{r} \frac{rdr}{\left[\left(\frac{nr}{n_o r_o \cos \alpha_o}\right)^2 - 1\right]^{\frac{1}{2}}} \tag{5.3-24}$$

The range error is similarly defined by Equation (5.3-20).

C. STRATIFIED LAYER METHOD

1. REFRACTION ERROR

The basic assumption which the proposed mathematical approach embodies is that the atmosphere is considered to be stratified into m spherical layers of thickness, h_m and constant refractive index, n_m. This type of stratification is illustrated in Figure 5.3-2, where α_o is the apparent elevation angle, and α_{om} is the true elevation angle.

From the law of sines, the angle of incidence, i_o, is found to be

$$\frac{\sin i_o}{r_0} = \frac{\sin (\frac{\pi}{2} + \alpha_o)}{r_1} \tag{5.3-25}$$

where r_o is the radius of the earth and $r_1 = r_o + h_o$.

The angle that the ray makes with the horizon in layer -1, α_1, is readily obtainable from Snell's law for a spherically symmetrical surface which for this example states that

$$n_o r_o \cos \alpha_o = n_1 r_1 \cos \alpha_1 \tag{5.3-26}$$

From Equations (5.3-25) and (5.3-26), it is seen that the general expressions for α_m and i_m are given by

$$\alpha_m = \cos^{-1} \left[\frac{n_{m-1} r_{m-1}}{n_m r_m} \cos \alpha_{m-1} \right] \tag{5.3-27}$$

and

$$i_m = \sin^{-1} \left[\frac{r_m}{r_{m+1}} \cos \alpha_m \right] \tag{5.3-28}$$

where the radial distance, r_{m+1}, is merely the summation of the various layers expressed by

$$r_{m+1} = r_o + \sum_{j=0}^{m} h_j \tag{5.3-29}$$

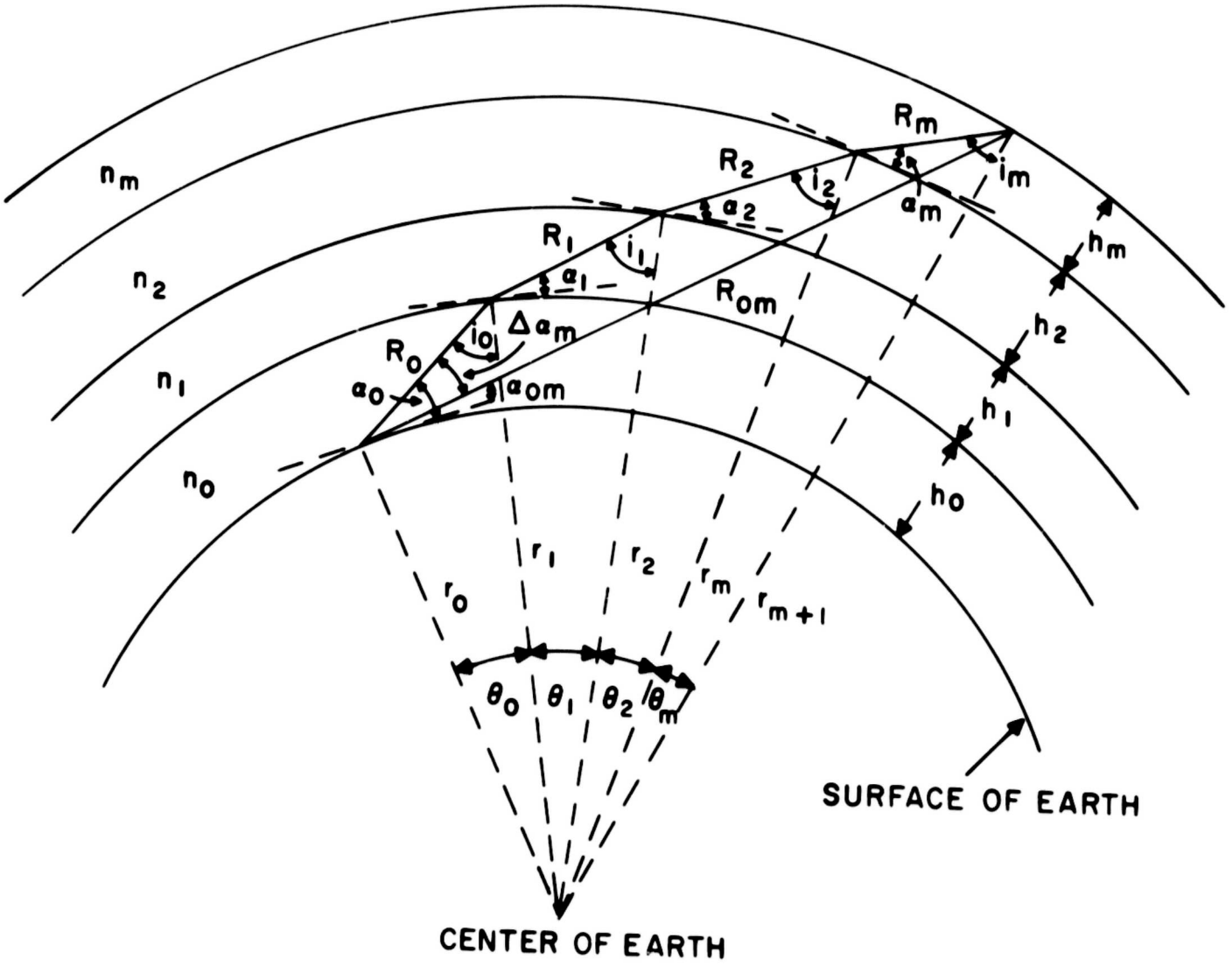

Figure 5.3-2. Atmospheric Layer Stratification

Applying the law of sines again for the direct path, it follows that

$$\alpha_{om} = \cos^{-1}\left\{\frac{r_{m+1}}{R_{om}} \sin\left[\sum_{j=0}^{m} \theta_j\right]\right\} \qquad (5.3\text{-}30)$$

where

$$R_{om}^2 = r_o^2 + r_{m+1}^2 - 2r_o\, r_{m+1} \cos\left[\sum_{j=0}^{m} \theta_j\right] \qquad (5.3\text{-}31)$$

and

$$\theta_j = \frac{\pi}{2} - \alpha_j - i_j \qquad (5.3\text{-}32)$$

The refraction angle error, $\Delta\alpha_m$, which is the difference between the apparent elevation angle and the true elevation angle can then be determined from

$$\Delta\alpha_m = \alpha_o - \alpha_{om} \qquad (5.3\text{-}33)$$

It should be noted that, in terms of the above nomenclature, for m = 0

$$R_{oo} = R_o, \qquad \Delta\alpha_m = 0$$

and for $\alpha_o = 90^o$.

$$R_{om} = \sum_{j=0}^{m} h_j$$

2. TIME DELAY CORRECTION

a. The Troposphere

Referring to Figure 5.3-2, it is seen that the time of travel along the ray path, R_o, is $t_o = (R_o/V_{po})$ where V_{po} is the phase velocity in the first layer defined by $V_{po} = (c/n_o)$. It follows, therefore, that the total time of travel of the refracted beam in the stratified layers becomes

$$t_t = \frac{1}{c} \sum_{j=0}^{m} n_j R_j \qquad (5.3\text{-}34)$$

Since the free space travel time of the unrefracted ray is $t_{om} = (R_{om}/c)$, the range error, ΔR, which results from the velocity of propagation being less than the free space velocity and from an increase in path length brought about by the refractive bending of the ray, reduces to

$$\Delta R = \sum_{j=0}^{m} n_j R_j - R_{om} \qquad (5.3\text{-}35)$$

where the distance, R_j, is given by

$$R_j^2 = r_j^2 + r_{j+1}^2 - 2r_j\, r_{j+1} \cos \Theta_j \qquad (5.3\text{-}36)$$

and where R_{om}, r_j and Θ_j are the parameters defined in the previous section.

b. The Ionosphere

As mentioned previously, for the ionosphere, which is a dispersive medium, i..e., the index of refraction is a function of frequency, the group velocity must be employed when estimating the range errors of pulsed radar measurements.

Since the group velocity, V_g, is given by $V_g = nc$, the total time of travel in the deviating medium is

$$t_t = \frac{1}{c} \sum_{j=0}^{m} \frac{R_j}{n_j} \qquad (5.3\text{-}37)$$

It follows that the expression for the range error becomes

$$\Delta R = \sum_{j=0}^{m} \frac{R_j}{n_j} - R_{om} \qquad (5.3\text{-}38)$$

3. EFFECT OF LAYER THICKNESS ON COMPUTATION ACCURACY

The effect of altering the number of layers or, in other words, the depth of each height element on the $\Delta\alpha_m$ and ΔR calculations are depicted in Figures 5.3-3 and 5.3-4, respectively. The atmospheric model employed in this example is a relatively simple analytical function proposed by Fannin (1)

$$N = 542.90 + 4.8544h - 100.859\ \sqrt{h + 3.9187} \qquad (5.3\text{-}39)$$

for $0 \leq h \leq 103.87$ where h is in thousands of feet and N is the refractivity given by

$$N = (n-1) \times 10^6 \qquad (5.3\text{-}40)$$

It is seen that, when the number of stratified layers is increased, the magnitude of the refraction error increases while the range error decreases. At an altitude of 100,000 feet, the difference between the $\Delta\alpha_m$'s and the ΔR's computed for the 1000 and 25 layer atmospheric model are approximately 0.24 milliradian and 100 feet, respectively. A comparison of the 1000 layer and 200 layer results indicate a difference of only 0.03 milliradian and one foot.

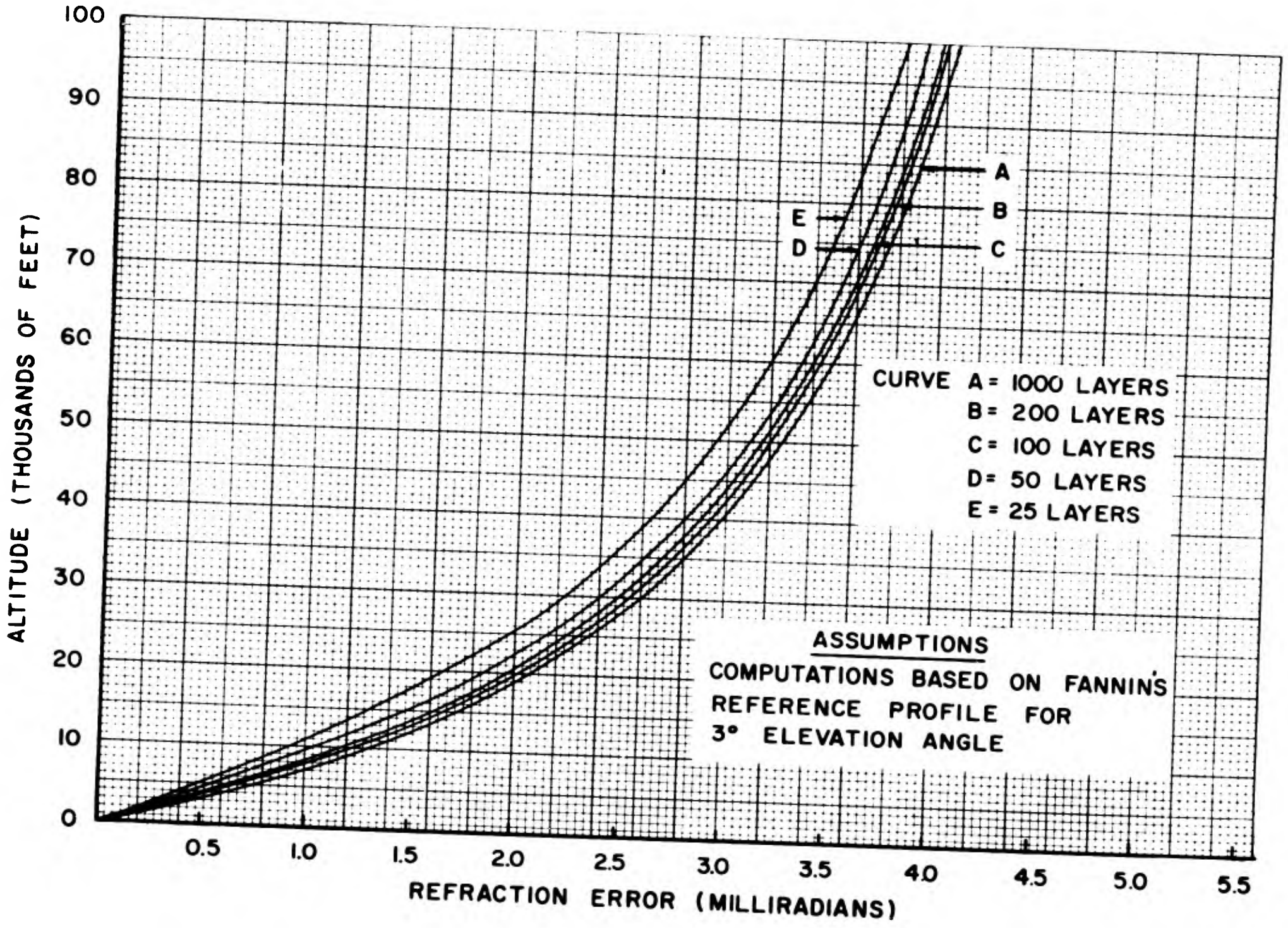

Figure 5.3-3. Effect of Layer Stratification on Refraction Errors

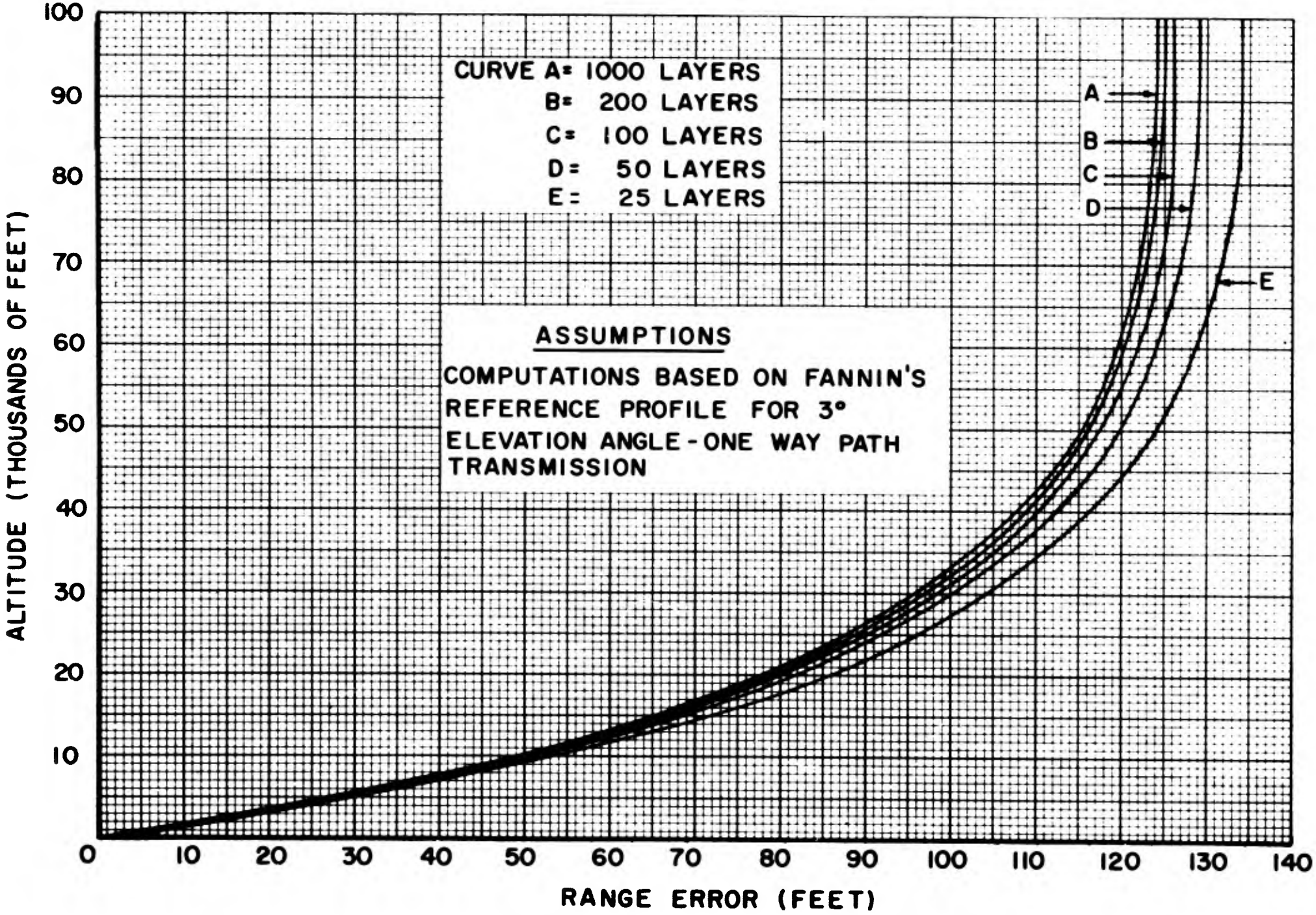

Figure 5.3-4. Effect of Layer Stratification on Range Errors

D. COMPARISON OF STRATIFIED LAYER METHOD WITH FANNIN'S METHOD

In order to ascertain the accuracy of stratified layers of constant refractive indices as a first approximation in the solution of atmospheric refraction and time delay, this method is compared with the theoretical technique proposed by Fannin (1).

Fannin has derived a mathematical expression for the elevation angle error, $\Delta\alpha$, in terms of a definite integral

$$\Delta\alpha = \frac{\cot \alpha_o}{Z} \int_0^z (n_o - n)\, dZ \qquad (5.3\text{-}41)$$

where $Z = y/y_1$ and

$$y = 1 - \text{Sin}\ \alpha_o \left[\left(\frac{r}{r_o}\right)^2 - \text{Cos}^2 \alpha_o \right]^{-1/2} \qquad (5\ 3\text{-}42)$$

and where α_o is the apparent elevation angle; and n_o, the refractive index at the earth's surface. The term, y_1, denotes the value of y at $h=h_1$. Equation (5.3-41) is valid for $\alpha_o \geq 3^o$ and for slant ranges less than 100 nautical miles.

The range error is given by

$$\Delta R = \int_o^h \frac{(n-1)}{\text{Sin}\ \alpha}\, d\,h \qquad (5.3\text{-}43)$$

where

$$\text{Sin}\ \alpha = \left[1 - \left(\frac{n_o r_o}{n\, r}\right)^2 \text{Cos}^2 \alpha_o \right]^{1/2} \qquad (5.3\text{-}44)$$

and $r = r_o + h$

The elevation angular errors and range errors computed by Fannin for the atmospheric model defined by Equation (5 3-39) are plotted in Figures 5.3-5 and 5.3-6, together with the calculations derived on the basis of an assumed 200-layer stratified atmosphere. It is clearly evident that the results of both methods are in excellent agreement for elevation angles at 5^o and above. It appears, however, that for low elevation angles, the Fannin refraction computations are somewhat less than the stratified results. According to Figure 5.3-5, at an altitude of 50,000 feet and a 3^o elevation angle, the percentage difference in the numerical answers of refraction error calculated by the two different analytical approaches is approximately eight per cent

E. REFERENCES

1. B. M. Fannin, "Radar Elevation Angle and Range Errors in Representative Air Masses," Report No. 7-01, Electrical Engineering Research Laboratory, University of Texas, June, 1954.

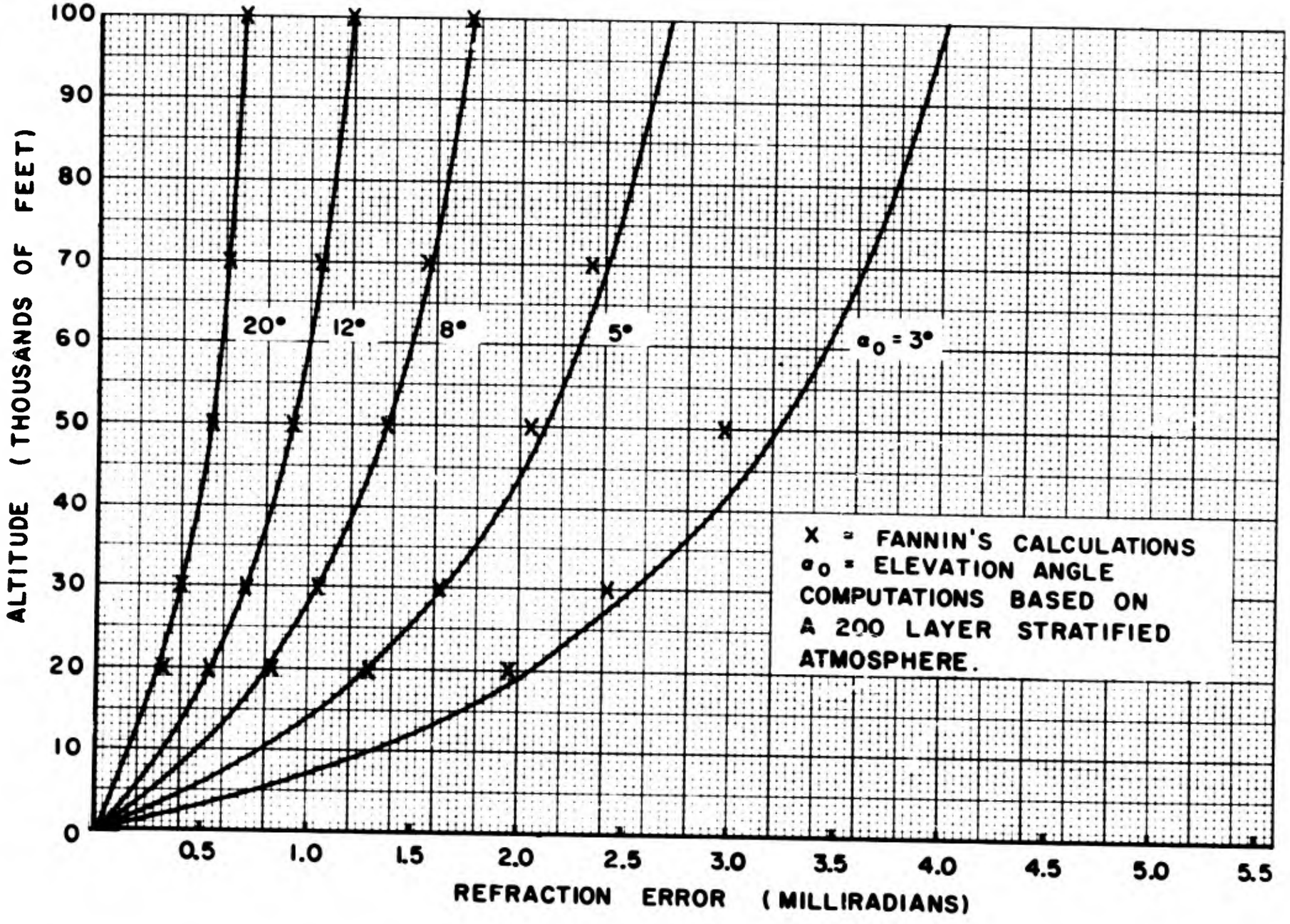

Figure 5.3-5. Refraction Errors for Fannin's Reference Profile

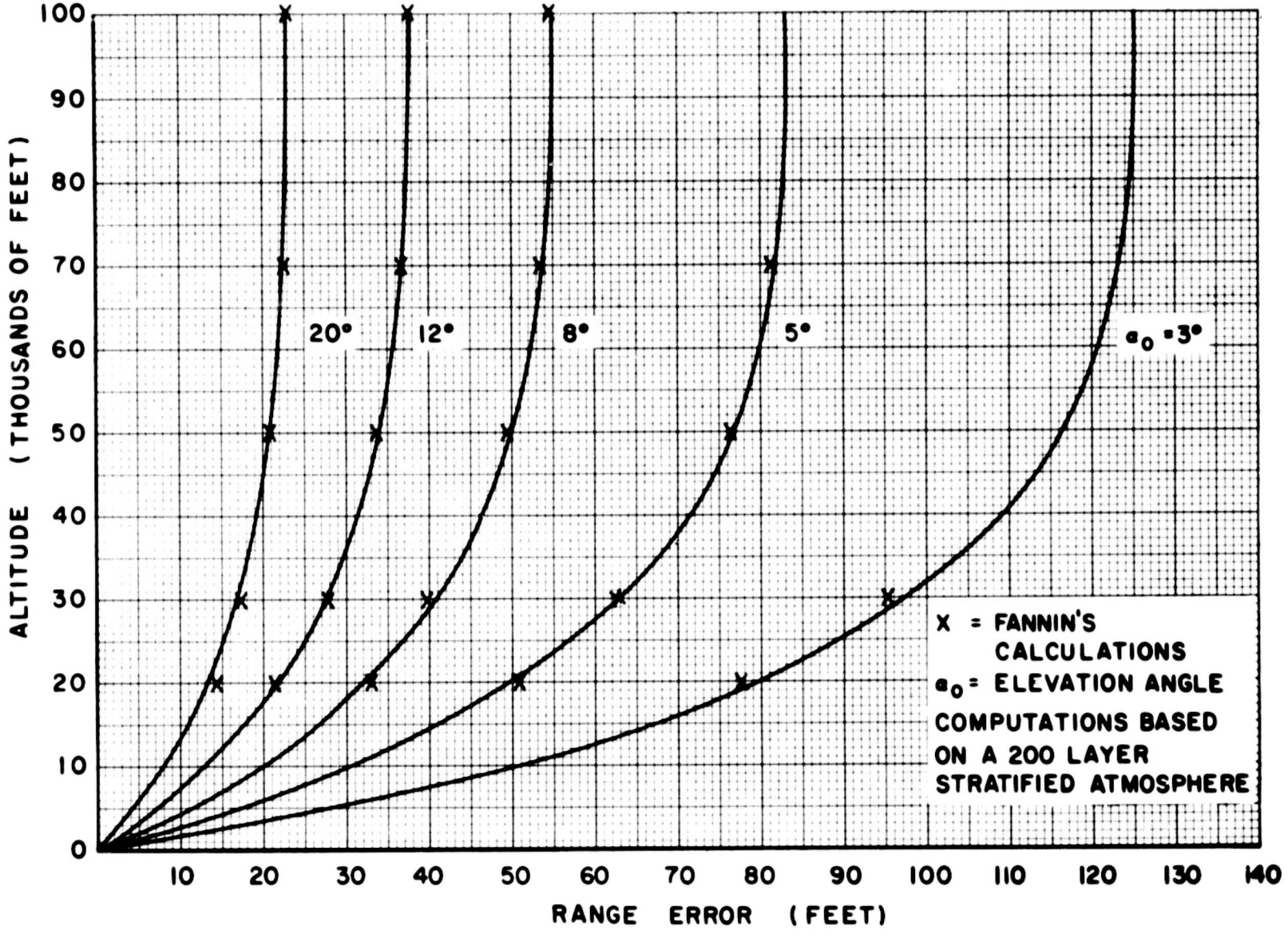

Figure 5.3-6. Range Errors for Fannin's Reference Profile, One-Way Transmission Path

5 4 - ATMOSPHERIC REFRACTION EFFECTS

A. INTRODUCTION

Because of the non-isotropic characteristics of the troposphere and the ionosphere, radio waves on their passage through the atmosphere experience an angular deviation.

Calculations of the predictable-bias errors based on assumed static atmospheric models are presented together with the unpredictable angular errors. The latter are basically due to the non-stationary inhomogeneities which are present along the path traversed by the waves.

In calculating the average or bias refractive errors, the stratified layer method, discussed in Section 5.3, has been employed. In the derivation of this method, it is assumed that the atmosphere is stratified into spherical layers of constant refractive index. The results obtained by this assumption are quite valid when the incremental layer heights are kept small.

It should be mentioned that the solutions of the mathematical equations of the stratified layer method were obtained by means of an IBM 704 computer employing a double precision computational technique. This was necessary to insure a reasonable degree of accuracy in evaluating the refraction angle error.

A typical ray path trajectory of radio waves traversing the atmosphere, in the vertical plane, is shown in Figure 5.4-1. It is assumed that (1) the troposphere extends to approximately 100,000 feet, with refractive index decreasing uniformly with height; (2) the ionosphere lies between 85 - 1000 kilometers with a minimum refractive index at the level of maximum electron density, (3) free space prevails between the tropospheric and ionospheric regions. The elevation-angle error due to refraction is the angle between the apparent path direction and the direct line-of-sight path.

B. AVERAGE REFRACTIVE ERRORS

1. TROPOSPHERIC REFRACTION

The standard atmospheric models used in this analysis are those formulated by Campen and Cole (1) (see Section 5.2).

The computations of the refraction errors presented in Figures 5.4-2 and 5.4-3 are based on a 190 layer stratification. Constant layer thicknesses of 100 feet are taken from the ground level to an altitude of 10,000 feet. Between the 10,000 and 100,000 foot level, 1000 foot increments are employed. The region above 100,000 feet is assumed to consist of unity refraction index

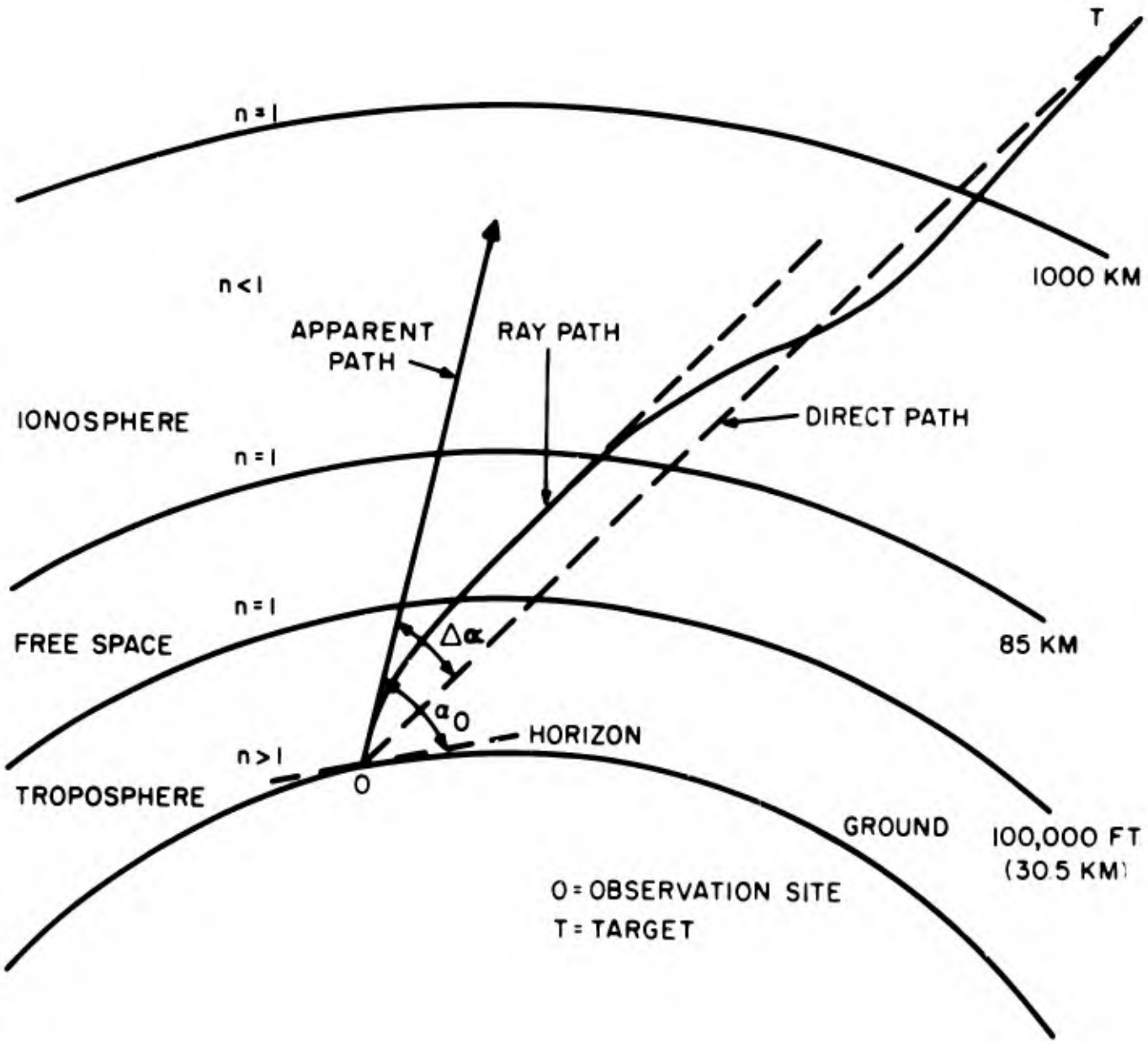

Figure 5.4-1. Typical Ray Path Trajectory

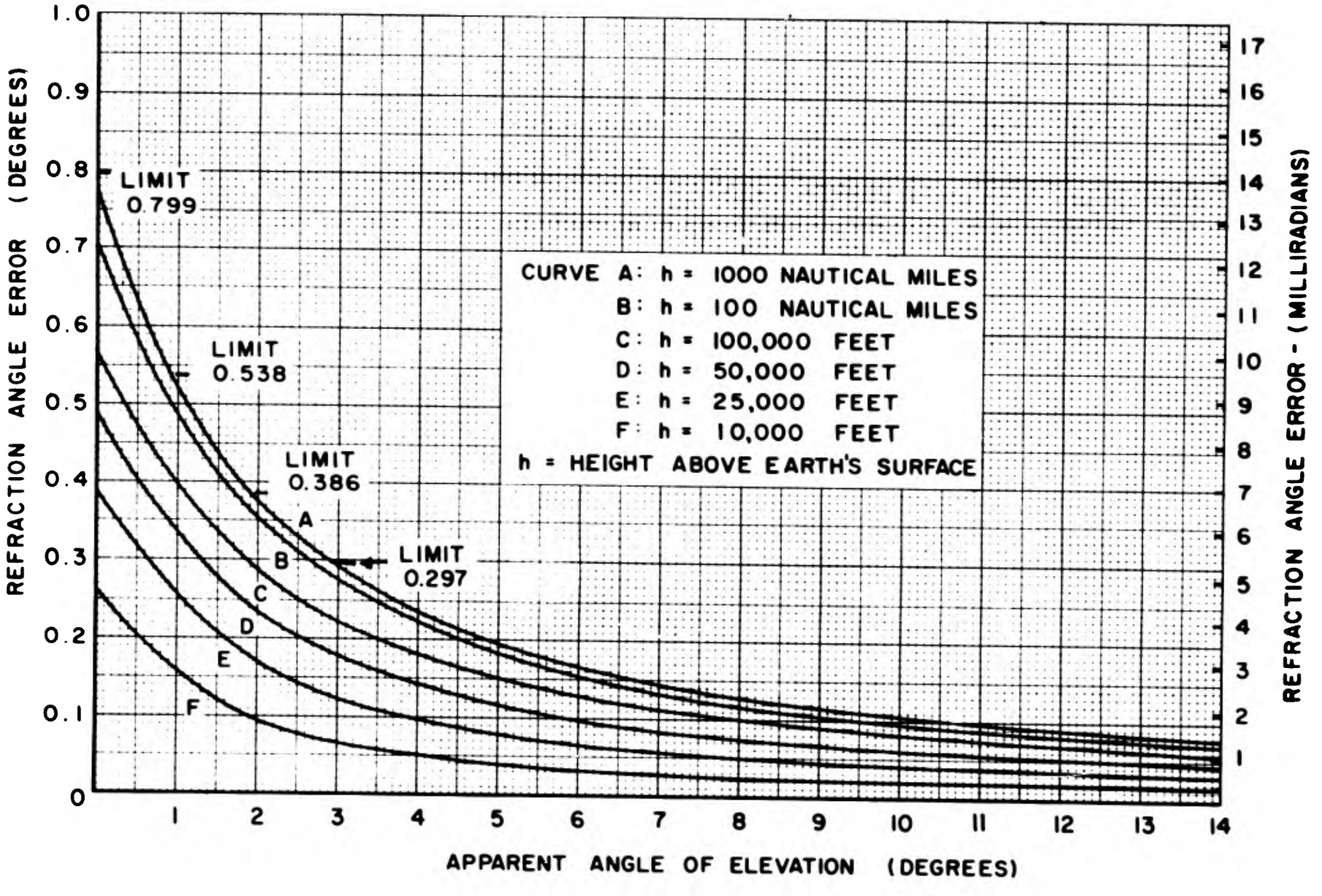

Figure 5.4-2. Atmospheric Refraction Errors for a Standard Atmosphere with 100 Per Cent Relative Humidity

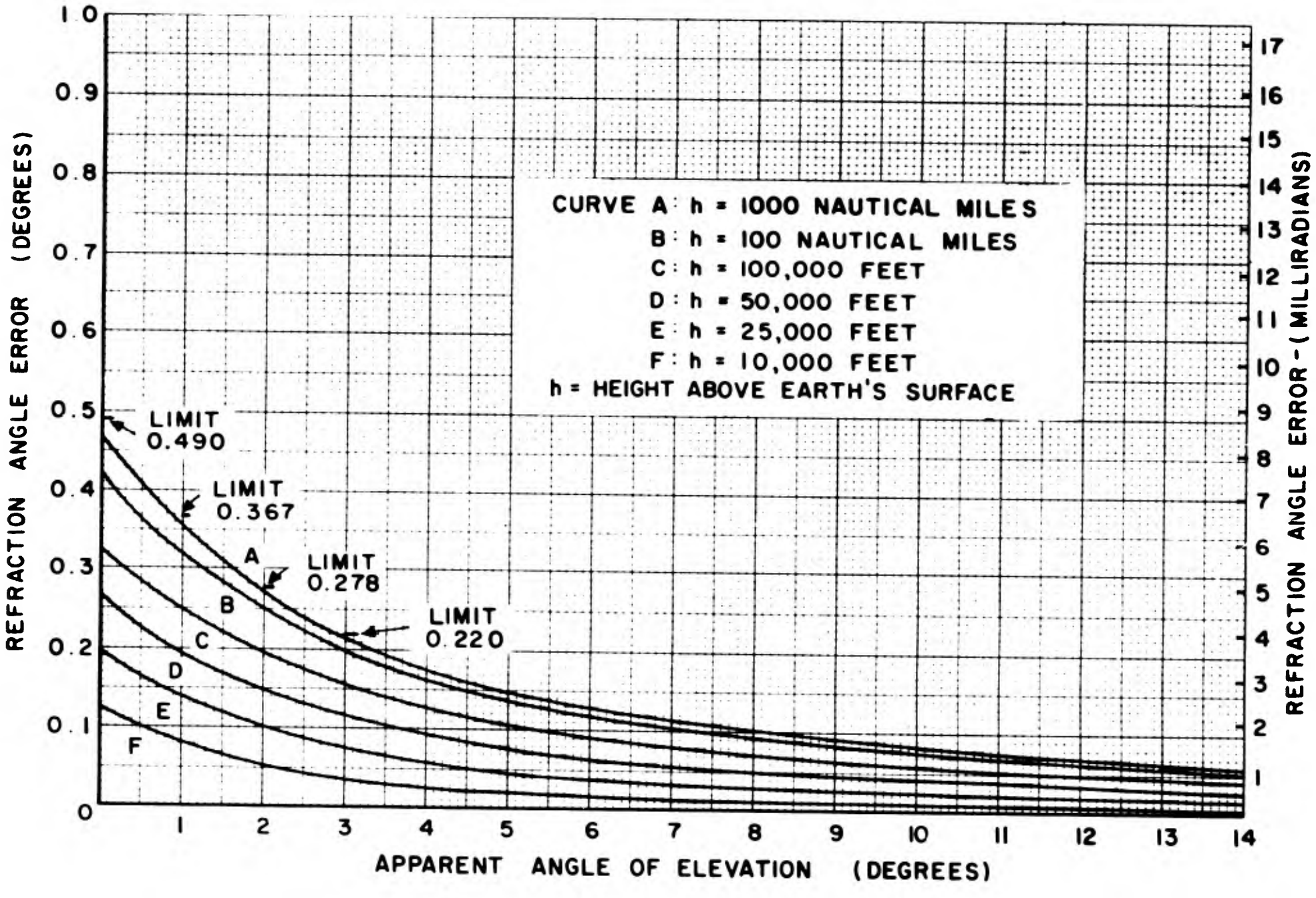

Figure 5.4-3. Atmospheric Refraction Errors for a Standard Atmosphere with Zero Per Cent Relative Humidity

It is seen that maximum refraction occurs along the horizon and at heights beyond the deviating medium. It should also be noted that the refraction error resulting from the wet atmospheric model is about 2.1 times greater than the dry model when examined at 10,000 foot altitude and zero degree elevation angle. At 50,000 feet, it is approximately 1.8 times greater. When propagation at 5^{o} and heights of 10,000 and 50,000 feet are considered, this factor reduces to 1.9 and 1.5, respectively.

The limits of refraction error illustrated in Figure 5.4-4 are derived on the basis of distances on the order of the sun-earth separation. The maximum error possible is about 0.8 degree for the atmosphere containing 100 per cent relative humidity and 0.49 degree for zero per cent relative humidity.

The percentages of total refraction as a function of altitude are plotted in Figures 5.4-5 and 5.4-6. For propagation at five degree elevation angle in the completely wet atmosphere, approximately 20 per cent of its total refraction error is reached at an altitude of 1.5 nautical miles, 40 per cent at the four nautical mile level and 64 per cent at ten nautical miles. With regard to the dry atmosphere, approximately 13 per cent of the total bending is accomplished at 1.5 nautical mile altitude, 31 per cent at four nautical miles and 58 per cent at ten nautical miles. It is of interest to note that for both atmospheric models, and five degree elevation angle, 98 per cent of the total bending has taken place at an altitude of 1000 nautical miles.

With regard to azimuthal refraction, this effect arises whenever there are horizontal gradients of refractive index. Meteorological observations do show, however, that such horizontal variations are small compared to the vertical variation of the indices of refraction. Measurements of azimuthal refraction indicates an average value of 0.1 milliradian on cloudy days and 0.03 milliradian on clear days (1).

It should be mentioned that, in addition to the normal refraction effects, at times, depending upon meteorological conditions in the tropospheric region, radio waves transmitted at very low elevation angles may experience a duct mode of propagation. That is, the waves are guided somewhat along the earth's surface to great distances. The ducting phenomenon occurs when there is a minimum change of approximately 48 N-units per thousand feet altitude. (See Section 5.2 for a discussion on the refractivity, N.)

2. IONOSPHERIC REFRACTION

The electron density profiles, described in Section 5.2, were employed in the analysis of ionospheric refraction effects. For the daytime model, the ionosphere was stratified into 350 layers varying in thickness of 2 km between the 80-575 km heights, and 5 km between the 575-1000 km region. Beyond the 1000 km height, miscellaneous intervals were taken. In the case of the nighttime model only 340 layers were employed with the bottom of the ionization region commencing at a height of 100 km.

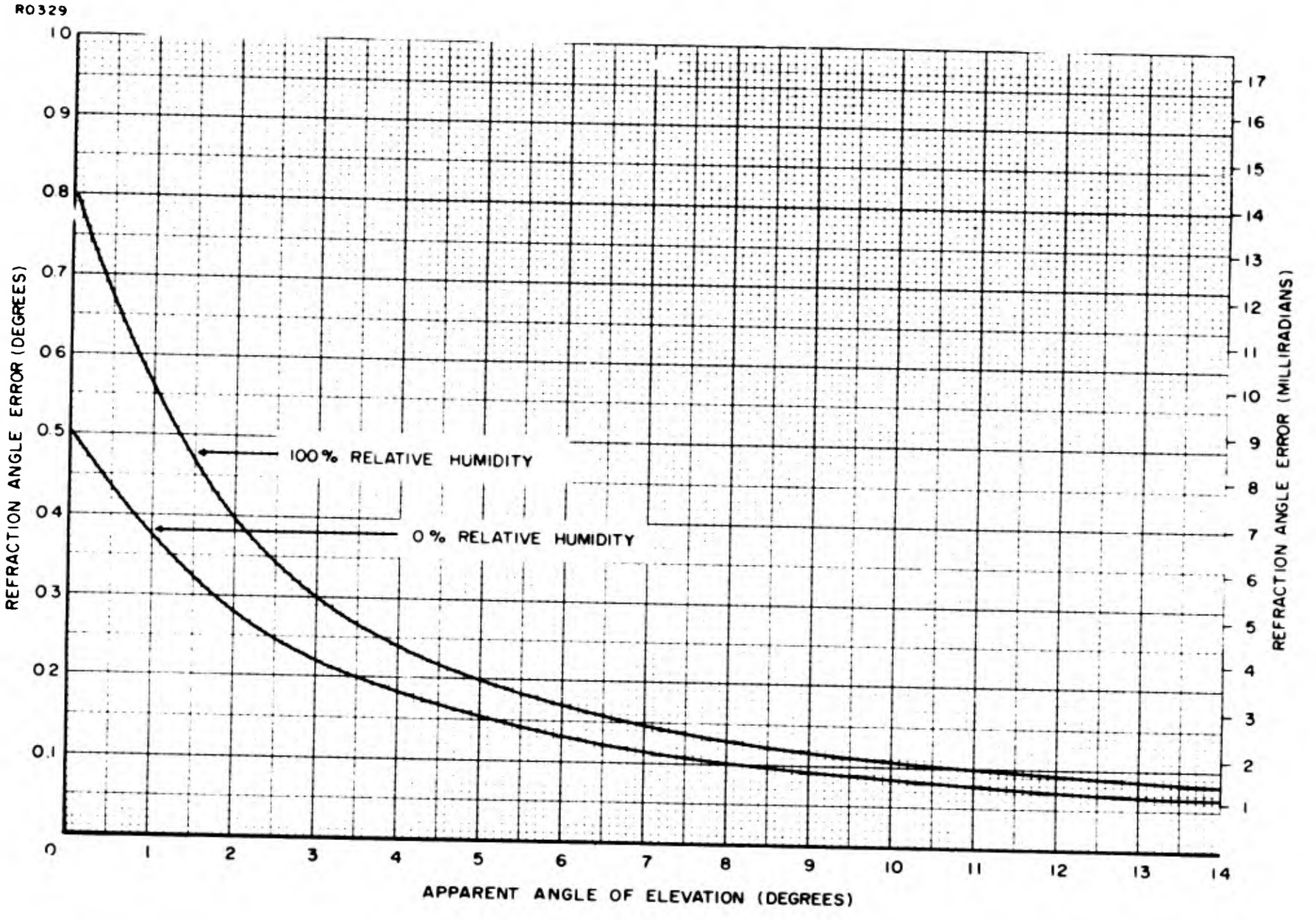

Figure 5.4-4. Limits of Atmospheric Refraction Errors for a Standard Atmosphere

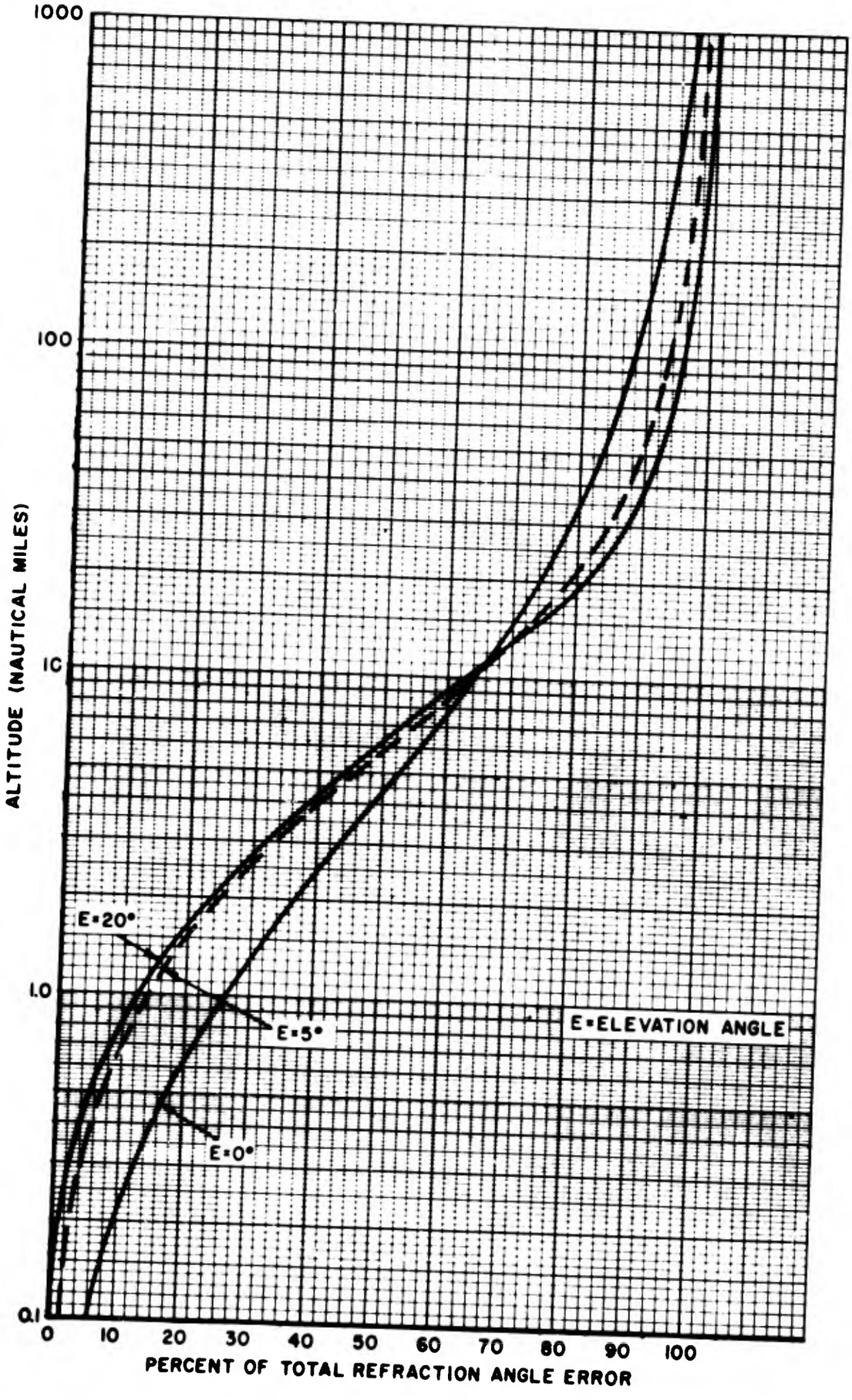

Figure 5.4-5. Percentage of Total Refraction for a Standard Atmosphere with 100 Per Cent Relative Humidity

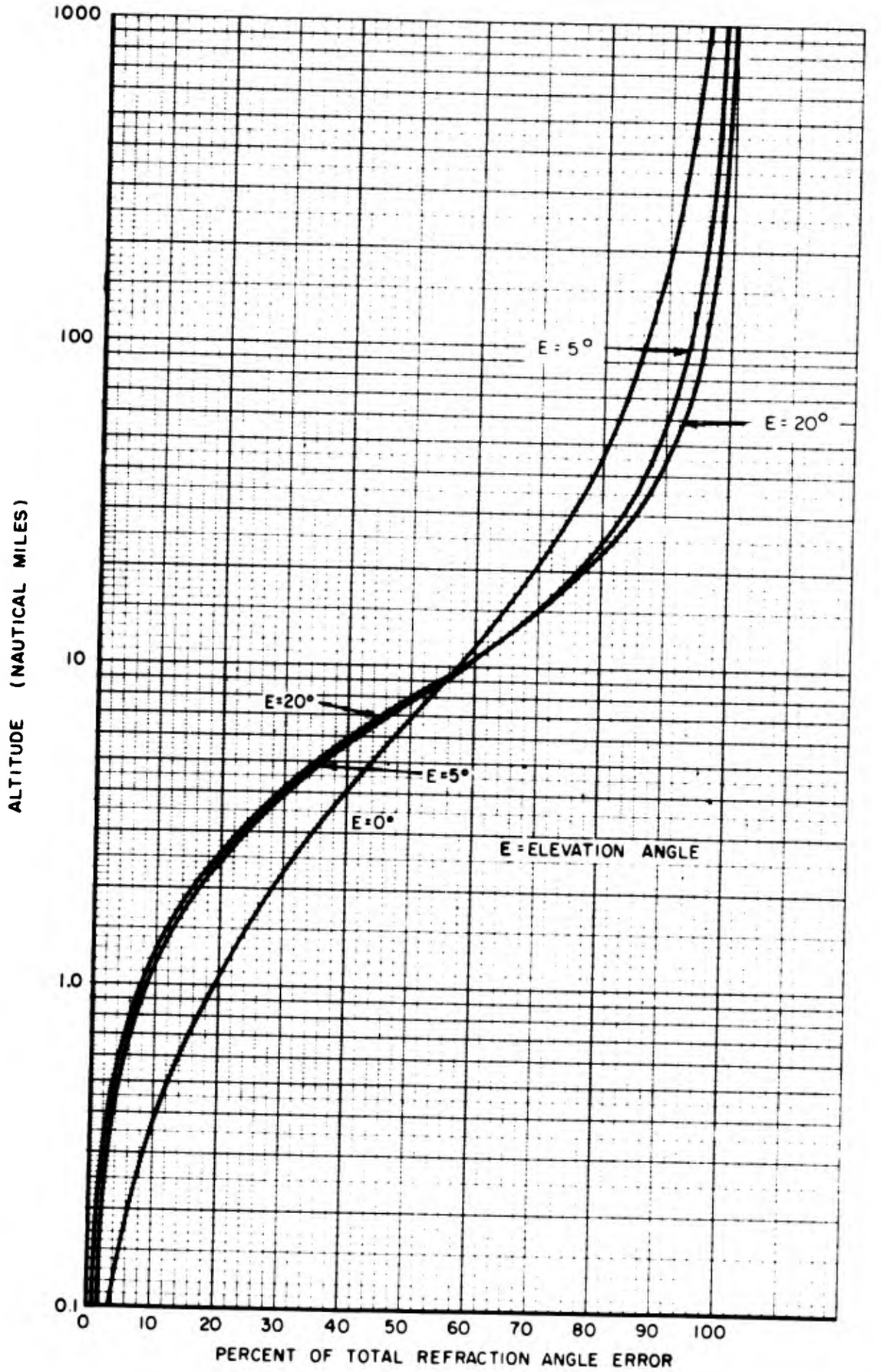

Figure 5.4-6. Percentage of Total Refraction for a Standard Atmosphere with Zero Per Cent Relative Humidity

It should be mentioned that the refraction error computations were performed utilizing the base of the ionospher, instead of the surface of the earth, as the point of origin of the ray path. This assumption required that, in the mathematical equations of the stratified layer method, the radius of the earth, r_o, be replaced by $(r_o + h_o)$ where h_o is the height of the ionosphere above the earth's surface. In addition, it is necessary to replace the ground elevation angle, α_o, with the ionospheric elevation angle, α_I, where

$$\alpha_I = \cos^{-1}\left[\frac{r_o}{r_o + h_o}\cos\alpha_o\right] \qquad (5.4\text{-}1)$$

The ionospheric elevation angle is plotted in Figure 5.4-7 for an assumed h_o of 80 km. It is seen that, at this height level, the minimum departure angle of a ray with respect to the tangent plane is about nine degrees.

The refraction errors for the daytime and nighttime models are presented in Figures 5.4-8 and 5.4-9 for 200 mc/sec and 400 mc/sec transmission frequency. It is evident that, for identical propagation conditions, the angle error is inversely proportional to the square of frequency.

It is noted that the refraction error is a maximum in the vicinity of the maximum ionization. The effect of the E-layer on refraction, in comparison to the F-layer where the greatest deviation takes place, appears to be very slight. The daytime angular error is approximately 2.7 times greater than the nighttime error. This compares favorably with the value of 3.1 which is the ratio of the daytime-to-nighttime maximum electron density.

3. TOTAL ATMOSPHERIC REFRACTION

The total refraction error computations at 200 mc/sec and 400 mc/sec, presented in Figures 5.4-10 and 5.4-11, are based on the atmosphere being divided into approximately 540 stratified layers. The region between the upper edge of the troposphere (100,000 feet) and the bottom of the ionosphere (80 km for daytime and 100 km for nighttime) consists of free space or unity refractive index. The "ionosphere neglected" curve was calculated on an assumed unity refractive index in the ionosphere.

It is seen that maximum refraction occurs for propagation along the horizon and that the error increases monotonically with height. The latter effect at the very low elevation angles is contrary to the results shown in Figures 5.4-8 and 5.4-9 in which only ionospheric refraction errors are considered. The monotonic function indicates that the angular bending due to the curvature of the earth and the atmosphere is more predominant than the ionospheric contribution. It is evident, however, that, at an elevation angle of five degrees, the error due to the ionosphere is greater than that resulting from the sphericity of the atmosphere.

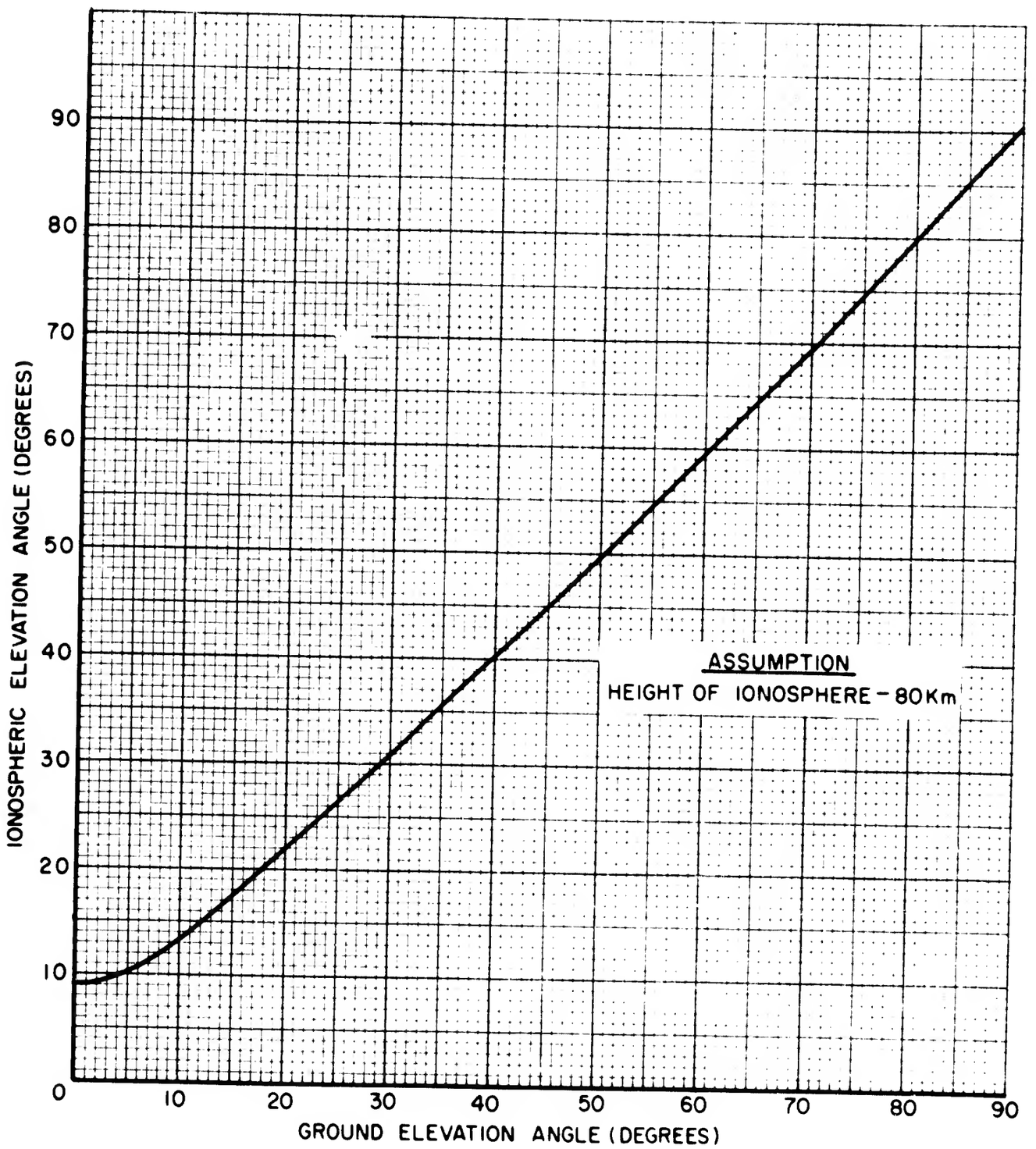

Figure 5.4-7. Relationship Between Ground Elevation Angle and Ionospheric Elevation Angle

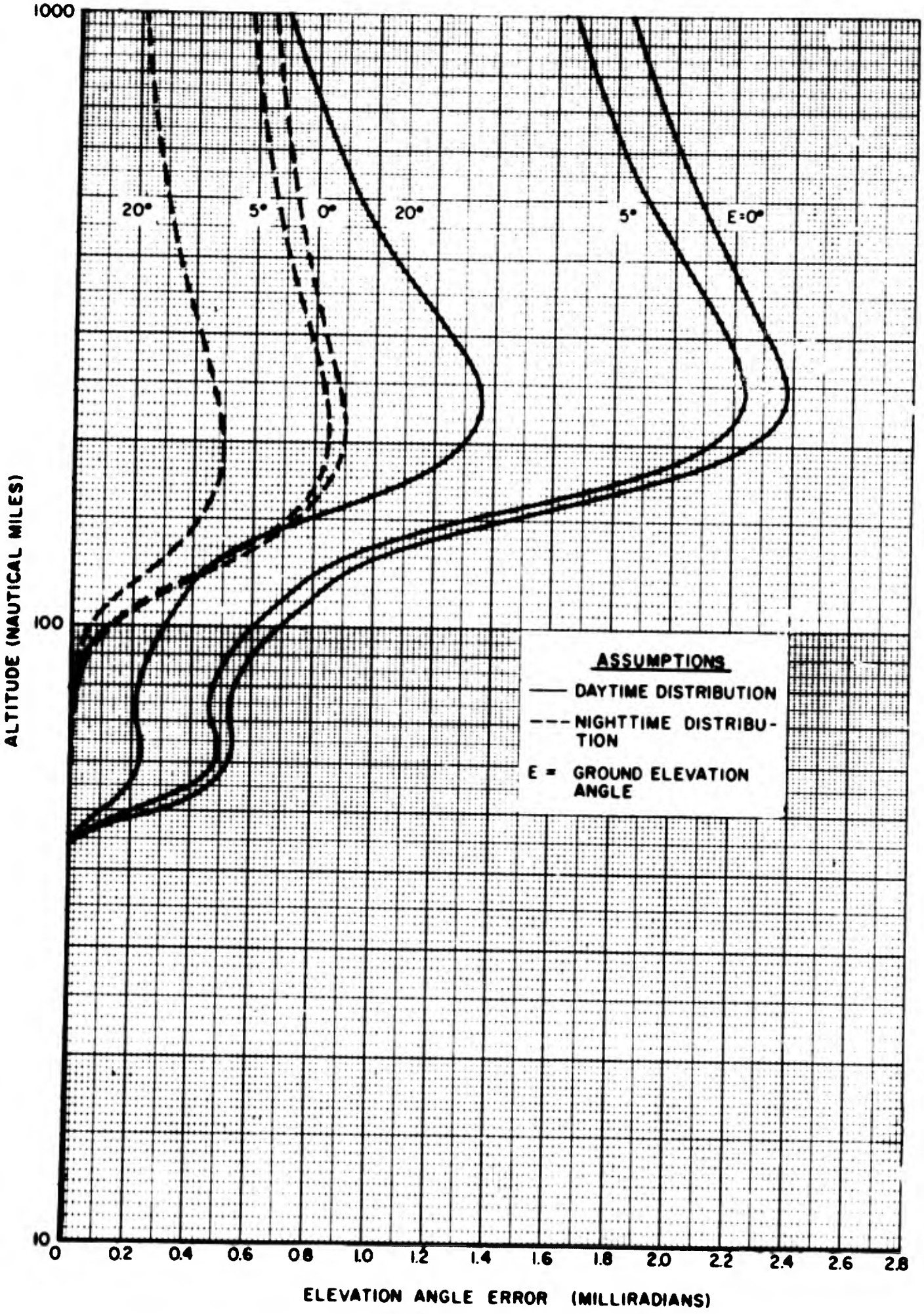

Figure 5.4-8. Ionospheric Refraction Errors at 200 mc.

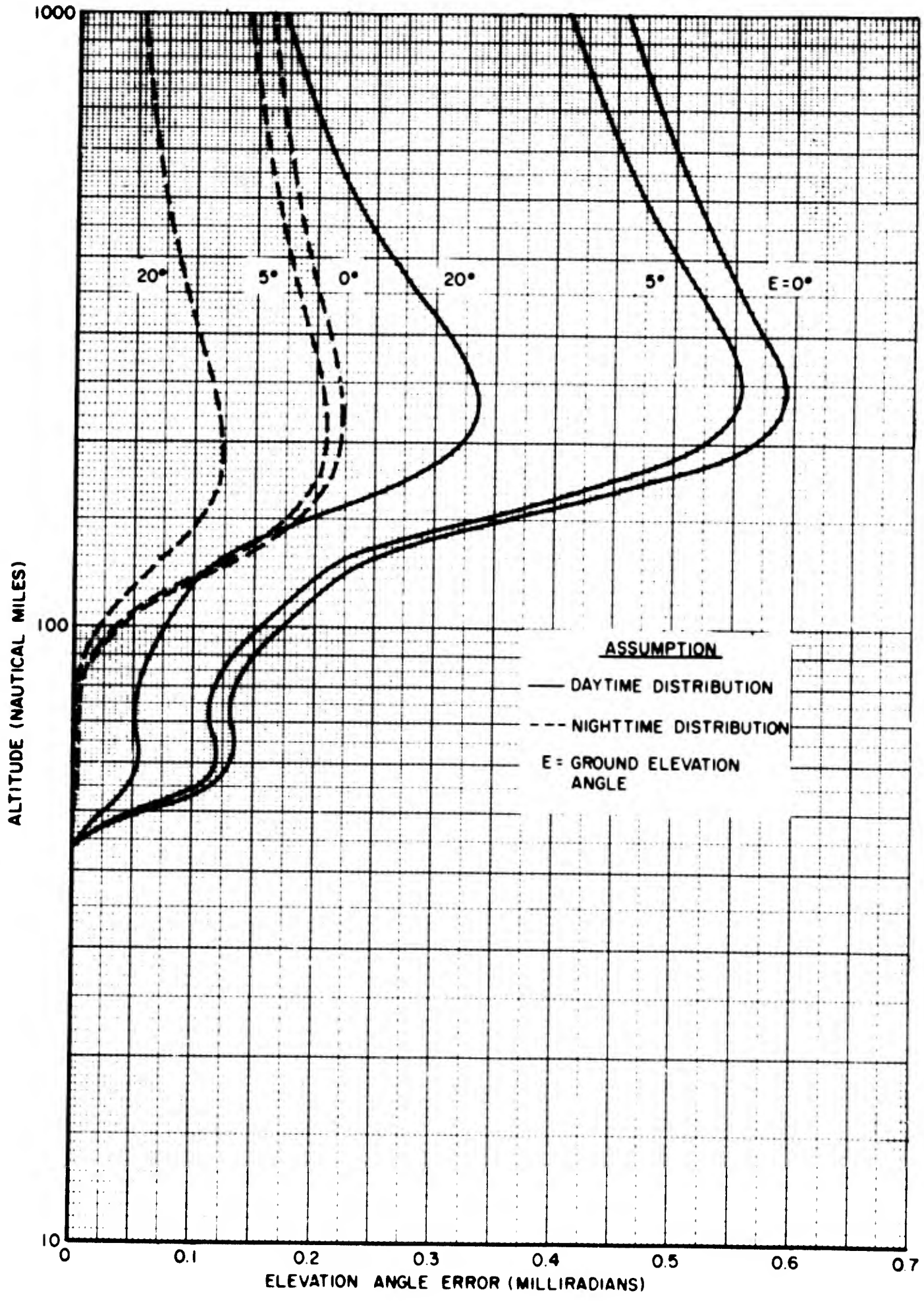

Figure 5.4-9. Ionospheric Refraction Errors at 400 mc.

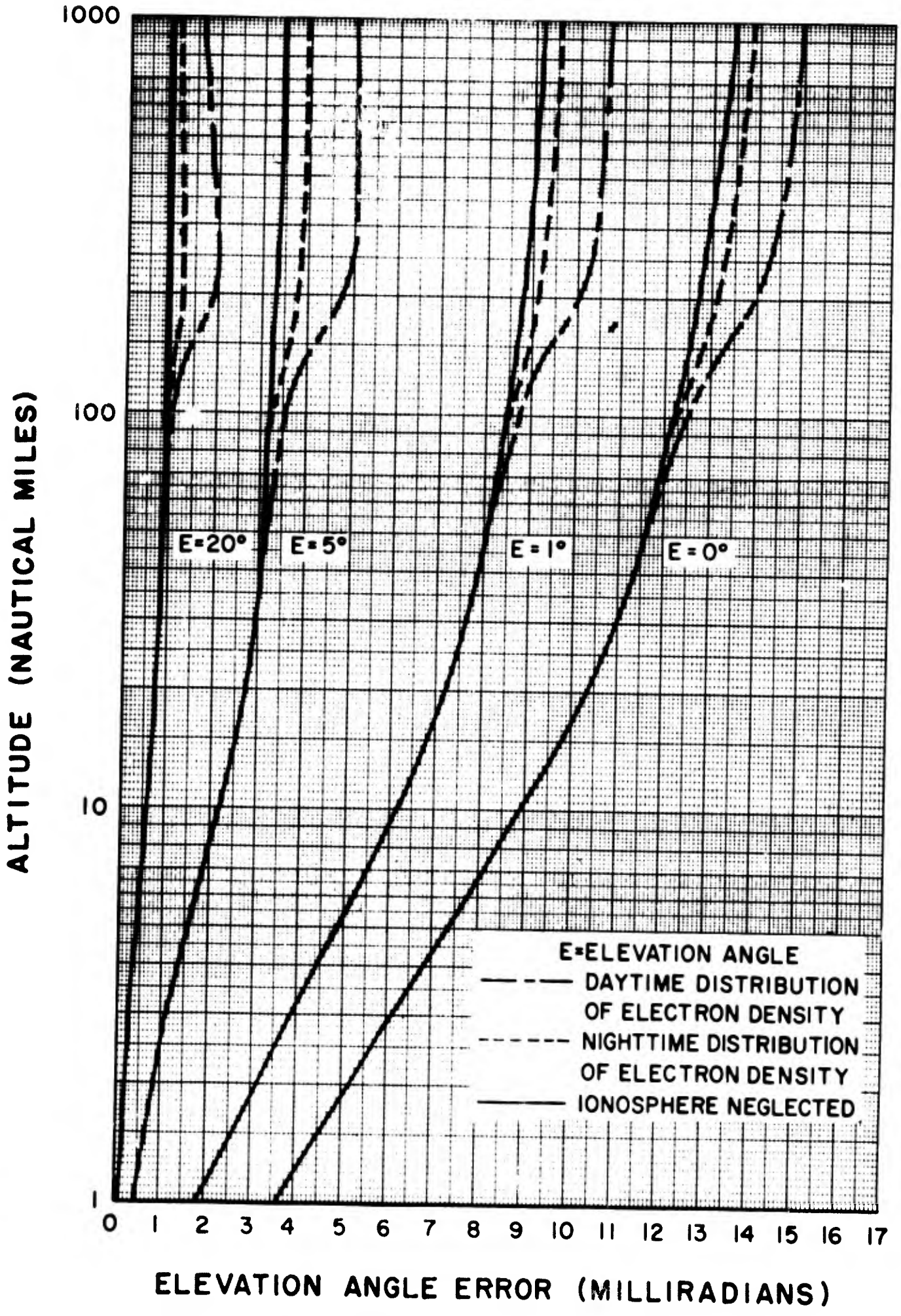

Figure 5.4-10. Total Atmospheric Refraction Errors at 200 mc. for a Standard Atmosphere with One Hundred Per Cent Relative Humidity

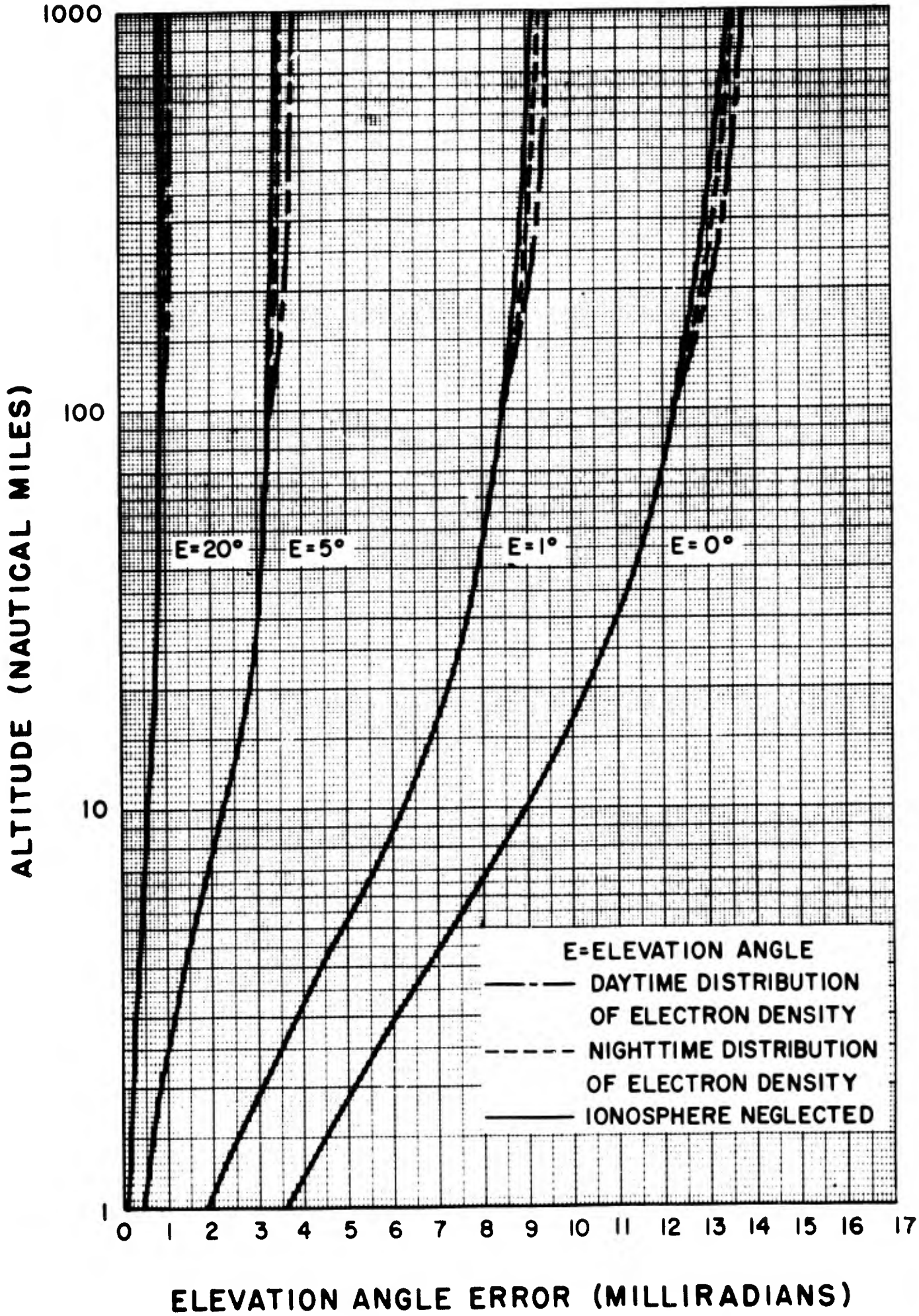

Figure 5.4-11. Total Atmospheric Refraction Errors at 400 mc. for a Standard Atmosphere with One Hundred Per Cent Relative Humidity

The limits of the total atmospheric angular errors for the various tropospheric and ionospheric conditions are plotted in Figures 5 4-12 and 5.4-13. It appears that, at 200 mc/sec and zero degree elevation angle, an error between 0.51 and 0.89 degree may be present while, at 400 mc/sec, the upper limit decreases to approximately 0.82 degree.

C. RANDOM REFRACTIVE ERRORS

Radiosonde observations in the troposphere reveal that wide variations exist from day to day and even from hour to hour in the measured index of refraction. These large-scale irregularities which are usually found at height levels up to approximately 5000 to 10,000 feet are influenced, to a large extent, by the weather and season. Under these conditions, the refractivity may vary as much as 20 N-units within a height interval of only 100 to 200 feet.

In addition to the large scale irregularities, small-scale variations in the refractive index have been observed by means of microwave refractometer techniques. The standard deviation fluctuation in the refractivity which is presumably the result of atmospheric turbulence is usually on the order of 0.25 to 0.3 N-units.

Since the atmospheric bending of electromagnetic waves is wholly dependent upon the refractive index profile along the path traveled by the waves, random variations of this parameter will necessarily produce a continuous fluctuation in the angular position of a radar target.

A study of the effects of large-scale irregularities, as reported by Engelman and Colin (2), indicates that, for an elevation angle of 13 degrees and a height of 50,000 feet, the angular refraction error could change by 0.1 milliradian within a several-hour period. In addition, it was found that, from meteorological measurements taken at the same time, the angular error computed along a path from Syracuse, New York, was 0.84 milliradian,while from Rome, New York, which is only 40 miles distant, it was 0.91 milliradian This discrepancy can be attributed to horizontal inhomogeneities in the refractive index profile. During this period, the average total angular correction was about 0.8 milliradian with a standard deviation of approximately 0.05 milliradian. An interesting conclusion borne out by this investigation is the disclosure that most of the variations in the angular correction could be correlated and attributed to the variation in the surface refractive index.

Based on Engelman and Colin's results, it appears that the deviations in the refraction angle error due to meteorological observations made along different propagation paths may be on the order of ten per cent of the mean value. An estimate of the deviation for low angles of elevation is illustrated in Figure 5 4-14 together with the Engelman-Colin measurement These plots are derived from the average refraction calculation presented in Figures 5.4-2 and 5.4-3.

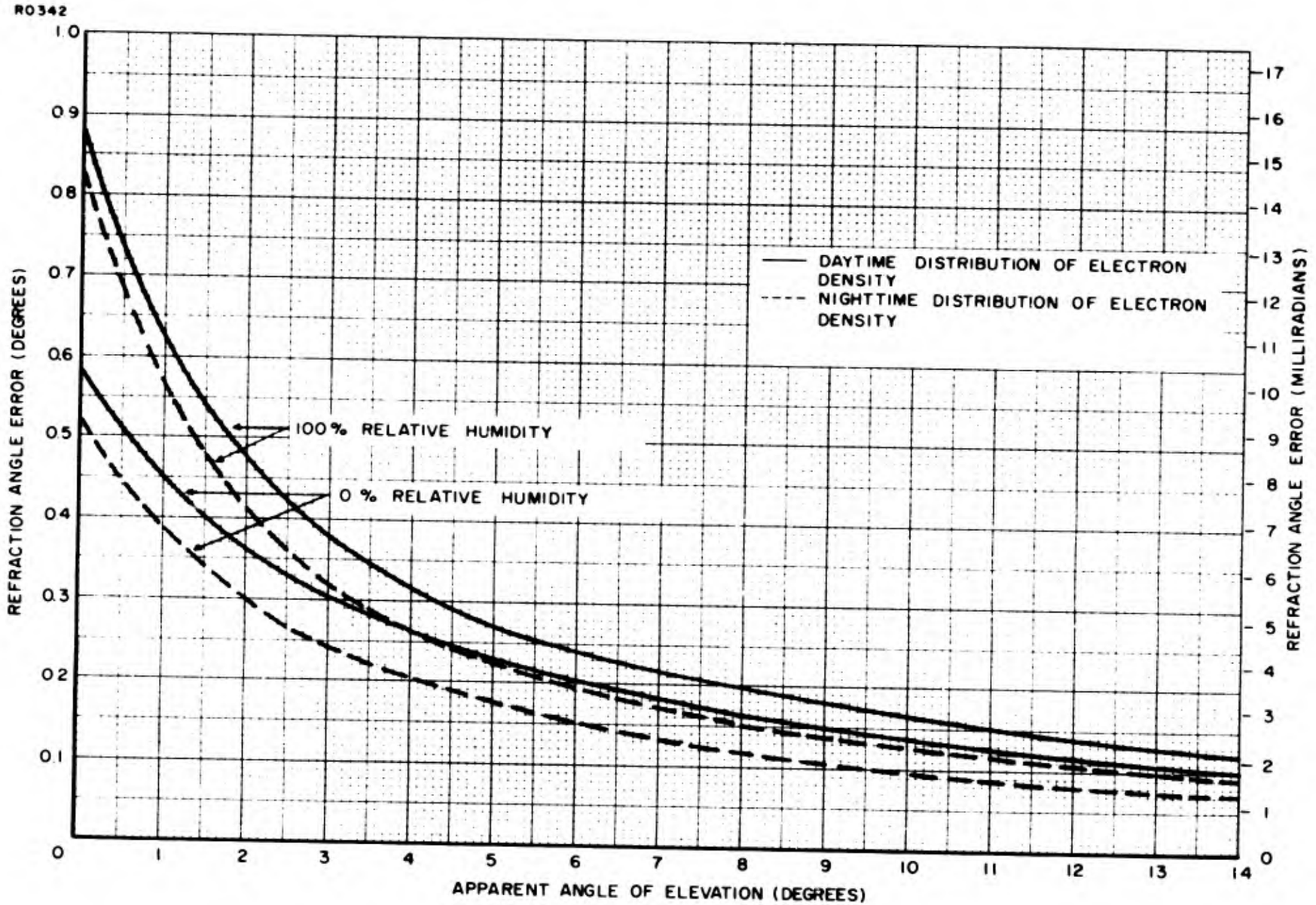

Figure 5.4-12. Limits of Total Atmospheric Refraction Errors at 200 mc.

R0341

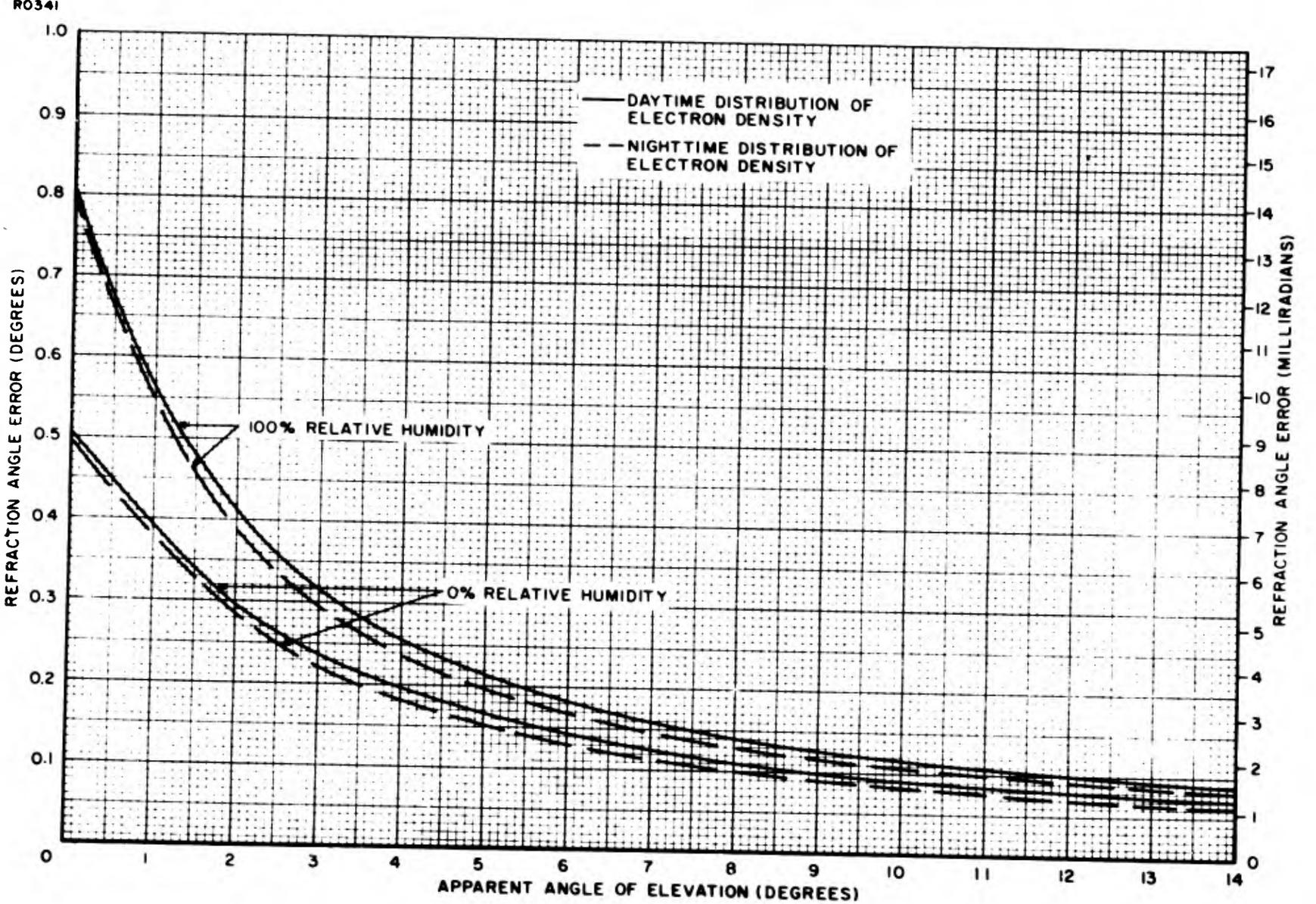

Figure 5.4-13. Limits of Total Atmospheric Refraction Errors at 400 mc.

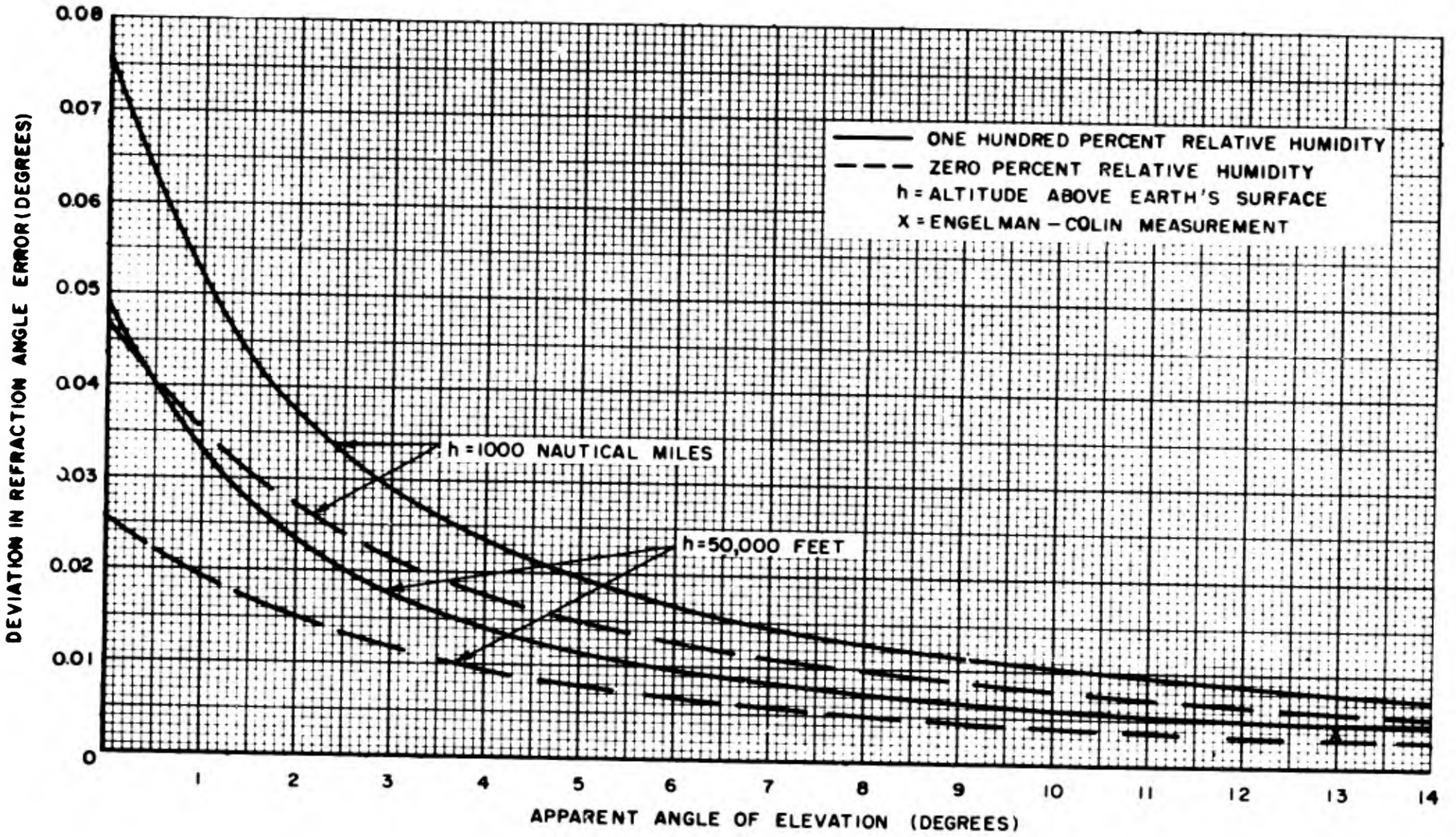

Figure 5.4-14. Estimate of Deviation in Refraction Angle Error due to Meteorological Observations Made along Different Propagation Path

When radiosonde measurements of meteorological conditions are conducted in the vicinity of a radar installation, they generally do not describe the true atmospheric conditions along the paths traversed by the radio waves. Because of this, the theoretically calculated angular refraction which would normally be used to correct radar data could, in essence, be in error. Since experimental and theoretical verification of the magnitudes of this effect is not available at the present time, the data in Figure 5.4-14 could be employed, as a first approximation, in the evaluation of this problem.

With regard to small-scale irregularities and turbulence in the troposphere, Muchmore and Wheelon (3) have developed a theoretical relationship for estimating the fluctuation of the apparent angular position of the target. The total mean-square angular deviation in the angle of arrival is given by

$$\overline{\phi^2} \approx \frac{4 \times (10^{-12}) \sqrt{\pi}\, L\, \overline{\Delta N^2}}{\ell_o} \qquad (5.4\text{-}2)$$

where L is the path length through the turbulence; ℓ_o, the scale length of the turbulent eddy; and $\overline{\Delta N^2}$, the mean-squared fluctuation in the refractivity, N.

Figure 5.4-15 is a plot of the rms angular deviation based on ℓ_o = 200 feet, $\overline{\Delta N^2}$ = 0.5 and an assumed height thickness of 25,000 feet for the turbulent region. It is seen that at three degree elevation angle, the rms fluctuation may be on the order of 0.0045 degree or 0.08 milliradian.

The small scale irregularities also introduce fluctuations in the phase of radio wave signals. According to Muchmore and Wheelon (3), the mean-squared-phase shift in a single ray assuming an isotropic scale of turbulence is approximated by the function

$$\overline{\alpha^2} \approx \frac{8 \times 10^{-12} \pi^2 \ell_o L\, \overline{\Delta N^2}}{\lambda^2} \qquad (5.4\text{-}3)$$

This relationship is applicable for a point antenna. The phase shift for a finite antenna aperture is given by

$$\overline{\theta^2} \approx \overline{\alpha^2} \left(1 - \frac{R^2}{\ell_o^2} + \cdots \right) \qquad (5.4\text{-}4)$$

where R is the radius of the antenna. For standard parabolic antennas, $\ell_o > R$.

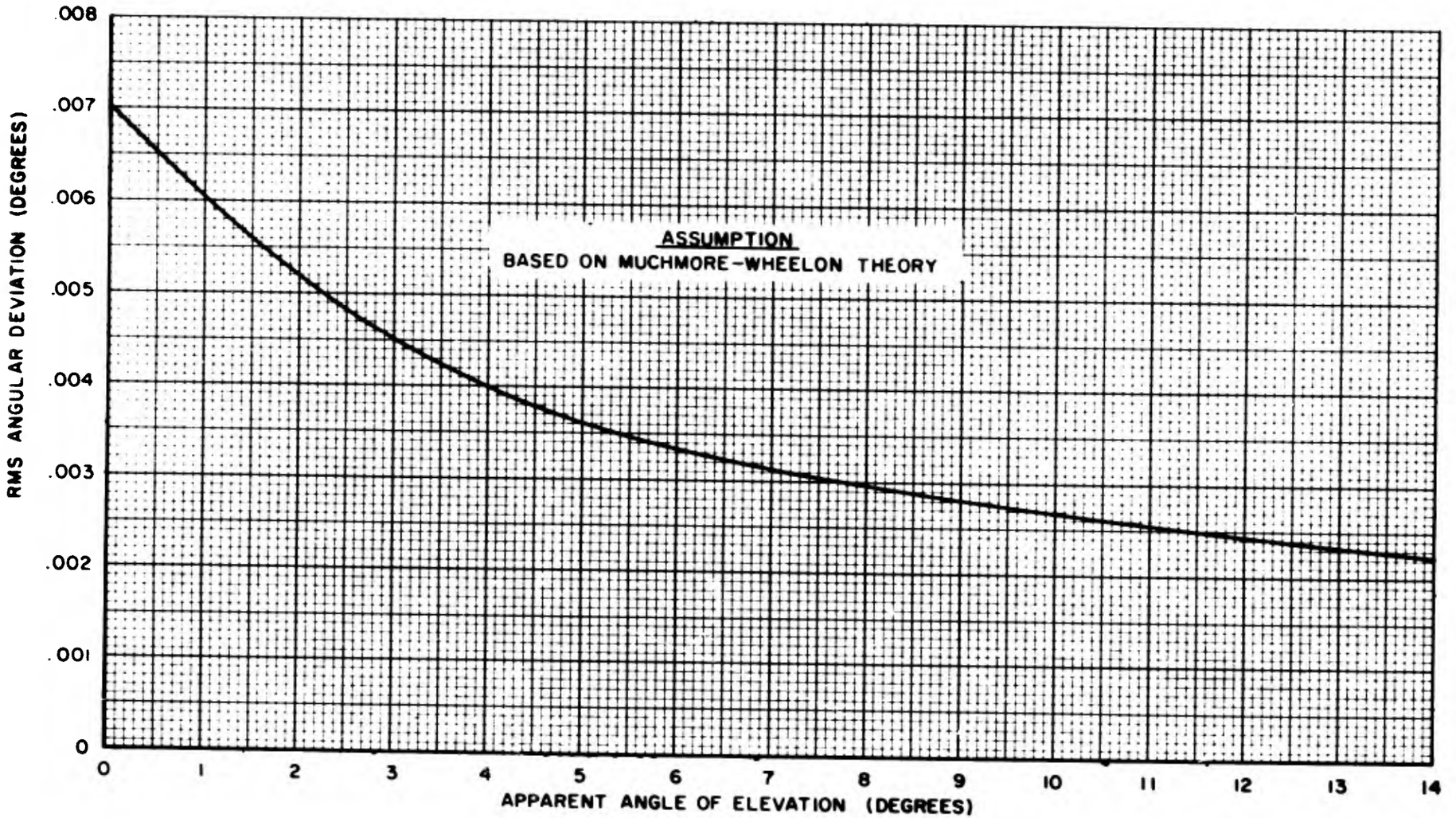

Figure 5.4-15. Estimate of RMS Deviation in Angle of Arrival

The rms phase jitter for a single ray at an elevation angle of two degrees and a frequency of 1200 mc/sec is, therefore, about 4.6 degrees. When two receiver locations are considered which are separated by distance, S, the instantaneous phases at these positions will be correlated if $S < \ell_o \approx 200$ feet. If the separation, S, is greater than the atmospheric scale length, ℓ_o, then the phases at the two receivers are uncorrelated and the phase difference will have an rms variation of $[2\overline{\alpha^2}]^{1/2}$.

D. EXPERIMENTAL MEASUREMENTS OF TOTAL ATMOSPHERIC REFRACTION

Experimental measurements of the total deviation of solar radiation in the entire atmosphere have been performed by McCready, Pawsey and Payne-Scott (4) and by Marner and Ringoen (5) whose results are given in Figure 5.4-16.

Marner's and Ringoen's measurements at 34,500 mc/sec were made with a radio sextant. The rms variation in the radio refraction is indicated by the vertical bars while the dashed line through the data represents the average refraction. A preliminary investigation of the variation of refraction with weather conditions gave evidence that the refraction increased slightly with an increase in water-vapor content. Since ionospheric ray bending effects are minute at radio frequencies of 34,500 mc/sec, it can be concluded that the refractive deviations were caused entirely by the tropospheric medium.

The curve through the McCready, et al, data was deduced on the basis of an assumed linear variation of refractive index with height. The pertinent constants in the linear relationships were evaluated from the average values of refractive index at the ground appropriate to the observed humidity and temperature. Since there was a high degree of correlation between the theoretical curve and the experimental data, the authors concluded that all the refractive effects took place in the troposphere, with the ionosphere contributing nothing. This conclusion is somewhat erroneous since theoretical calculations seem to indicate that, at 200 mc/sec, ionospheric refraction is appreciable. It would appear that the difference between the 200 mc/sec and 34,500 mc/sec data can be attributed to the ionosphere.

It is of interest to note that the optical refractive curve presented in McCready's original paper coincides rather closely with Marner's average refraction curve.

A comparison of the data presented in Figures 5.4-4 and 5.4-16 clearly reveals that Marner's curve falls within the bounds set up by the limits of refraction error theoretically postulated.

The corrections for parallax and refractive effects for observed optical elevation angles of the sun, as given by Bowditch (6), is plotted in Figure 5.4-17. It is seen that the angle correction decreases with increasing ground temperature. Parallax is the apparent displacement of a celestial body, which is a finite distance away from the earth, caused by the fact that observations are made on the earth's surface and not at the earth's center. The parallax corrections for the sun at zero degree and 20 degree elevation are nine seconds of arc and eight seconds of arc, respectively.

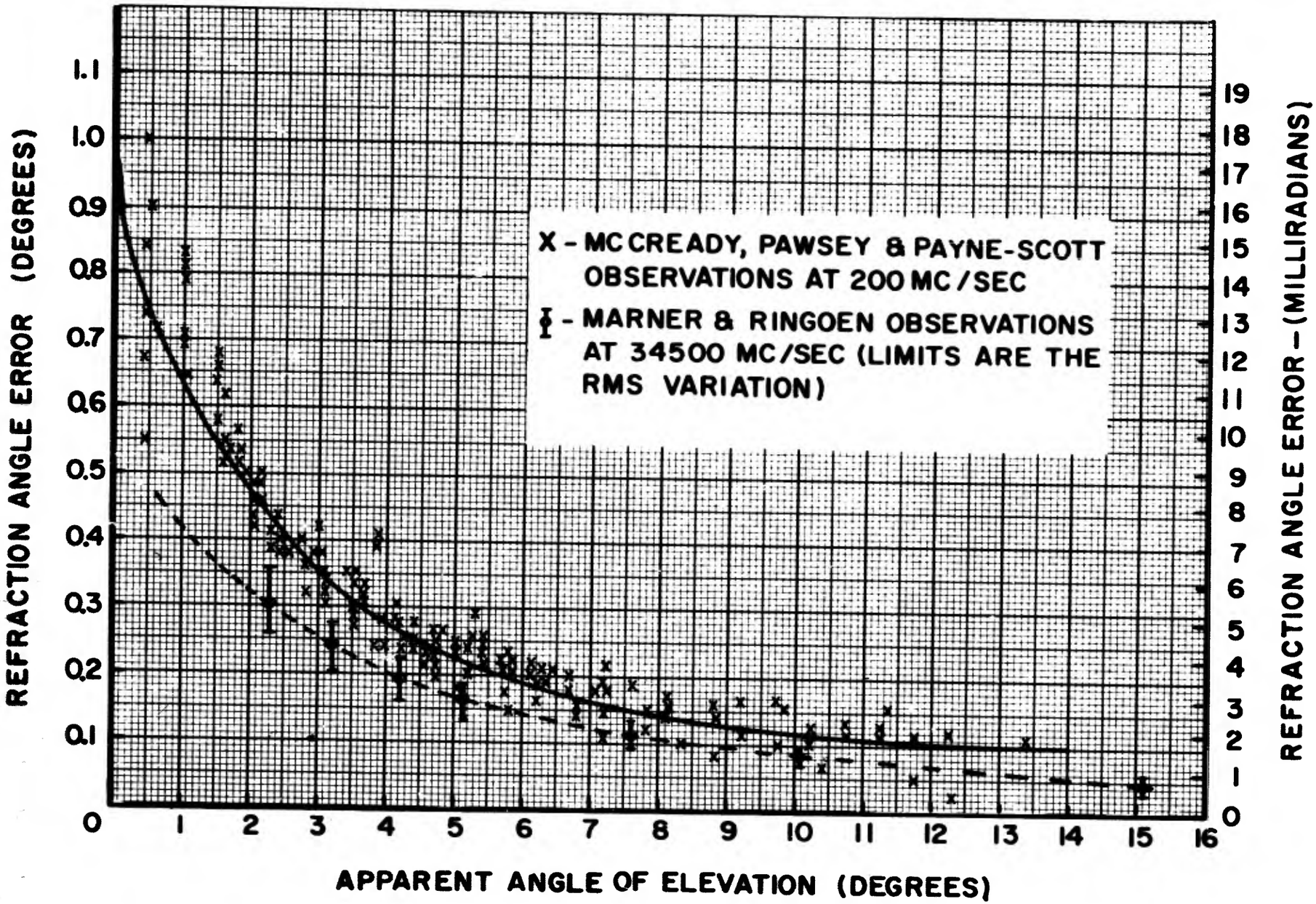

Figure 5.4-16. Average Atmospheric Refraction for Propagation of Solar Radiation Through the Atmosphere

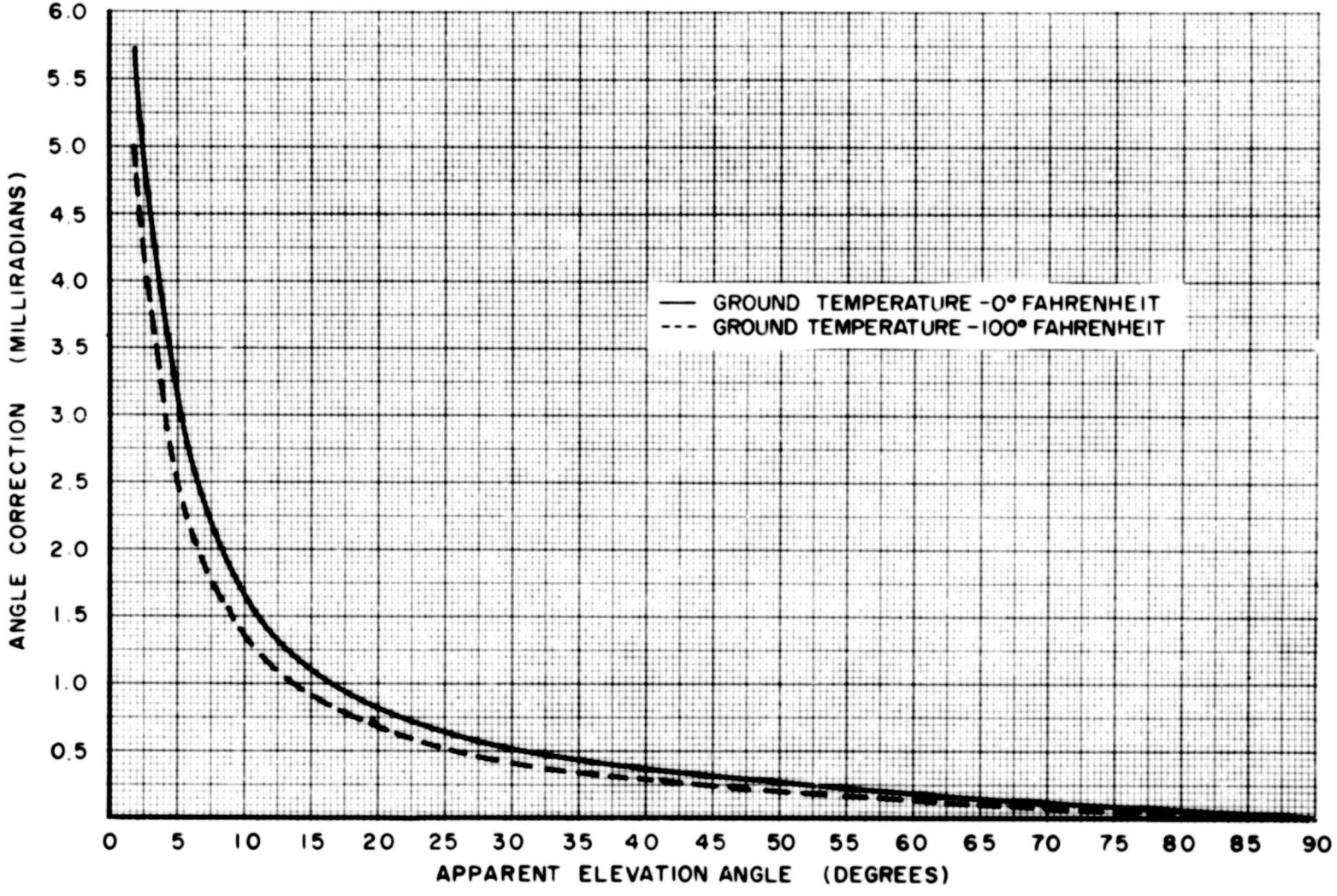

Figure 5.4-17. Correction for Parallax and Refraction Effects for Observed Optical Elevation Angles of the Sun

E. REFERENCES

1. Harris, A. R., "Azimuthal Refraction - A Study of Atmospheric Properties Affecting Radar Accuracy," General Electric Company Unclassified Report, February, 1957.

2. Engelman, A. and Colin, L., "An Analysis of the Time and Space Scale Problems in Radio Meteorology," Paper presented at the URSI-IRE Meeting, Washington, D.C., May 1957.

3. Muchmore, R. B., and Wheelon, A. D., "Line-of-Sight Propagation Phenomena - I Ray Treatment," Proceedings of IRE, Vol. 43, pp. 1437-1449, Oct. 1955.

4. McCready, L. L., Pawsey, J. L. and Payne-Scott, Ruby; "Solar Radiation at Radio Frequencies and its Relation to Sunspots," Proceedings of Royal Society A., Vol. 190, p. 357, 1947.

5. Marner, G. R. and Ringoen, R. M.; "Atmospheric Refraction of 8.7 mm Radiation," Collins Radio Co., Report No. CTR-162, April 1956.

6. Bowditch, N.; "American Practical Navigation," U. S. Navy Dept., Hydrographic Office, No. 9, 1943.

5.5 - TIME DELAYS IN THE ATMOSPHERE

A. INTRODUCTION

Time delays or range errors are always inherent in radar target measurements. This effect is present primarily because the velocity of electromagnetic propagation in the atmosphere is slightly less than the free space velocity. An additional source of error is the increase in path-length brought about by the refractive bending of the propagated ray. In the computations (by the stratified layer method) of the data presented in this section, both factors are taken into account.

B. TROPOSPHERIC TIME DELAY

The tropospheric range errors plotted in Figures 5.5-1 and 5.5-2 are valid for the two standard atmospheric models described in Section 5.2. The same number of stratified layers utilized in the tropospheric refraction calculations were also employed in this analysis.

It is seen that the magnitude of the range error is a direct function of the elevation angle or path length and also a function of the amount of humidity in the air, the value at zero per cent relative humidity being about 80 per cent of the value at 100 per cent relative humidity.

For a one-way transmission path, a maximum range error of approximately 381 feet is possible for propagation along the horizon. Irrespective of the atmospheric model, approximately 57 per cent of the retardation occurs below the 10,000-foot altitude for horizon transmissions while, at five degree elevation angle and at the same altitude, only 34 per cent takes place.

C. IONOSPHERIC TIME DELAY

Figures 5.5-3 and 5.5-4 are graphs of range error for the daytime and the nighttime models of electron density presented in Section 5.2. As in the case of the ionospheric refraction computations, the base of the ionosphere, i.e., the 80 km altitude for the daytime distribution and 100 km for the nighttime, was taken as the point of origin of the ray trajectory.

It is evident that: (1) the range error is a maximum during the daytime, increasing with low elevation angles; (2) the error is inversely proportional to the square of frequency; (3) the major portion of the time delay occurs below an altitude of 300 nautical miles.

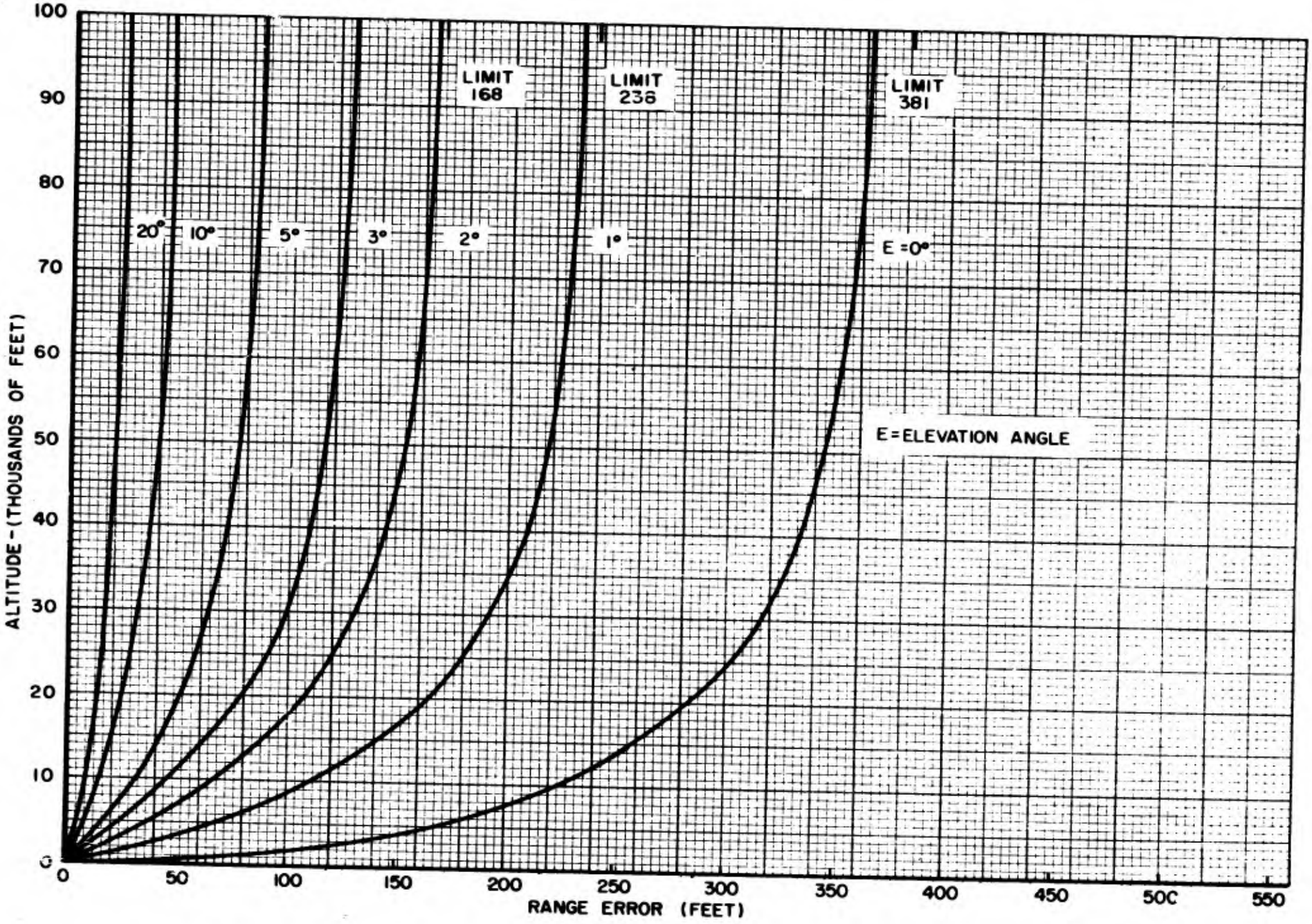

Figure 5.5-1. Atmospheric Range Errors for a Standard Atmosphere with One Hundred Per Cent Relative Humidity, One-Way Transmission Path

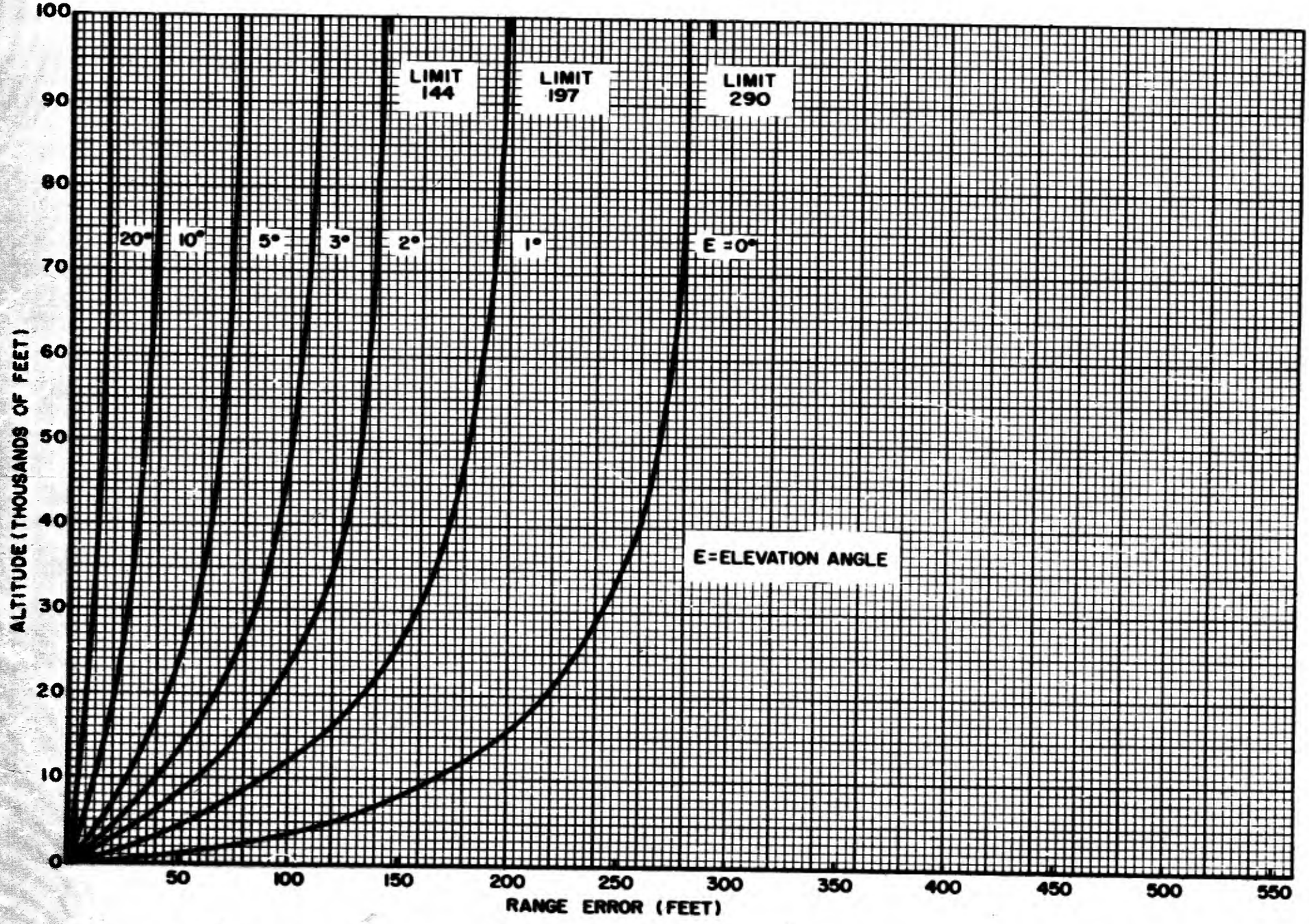

Figure 5.5-2. Atmospheric Range Errors for a Standard Atmosphere with Zero Per Cent Relative Humidity, One-Way Transmission Path

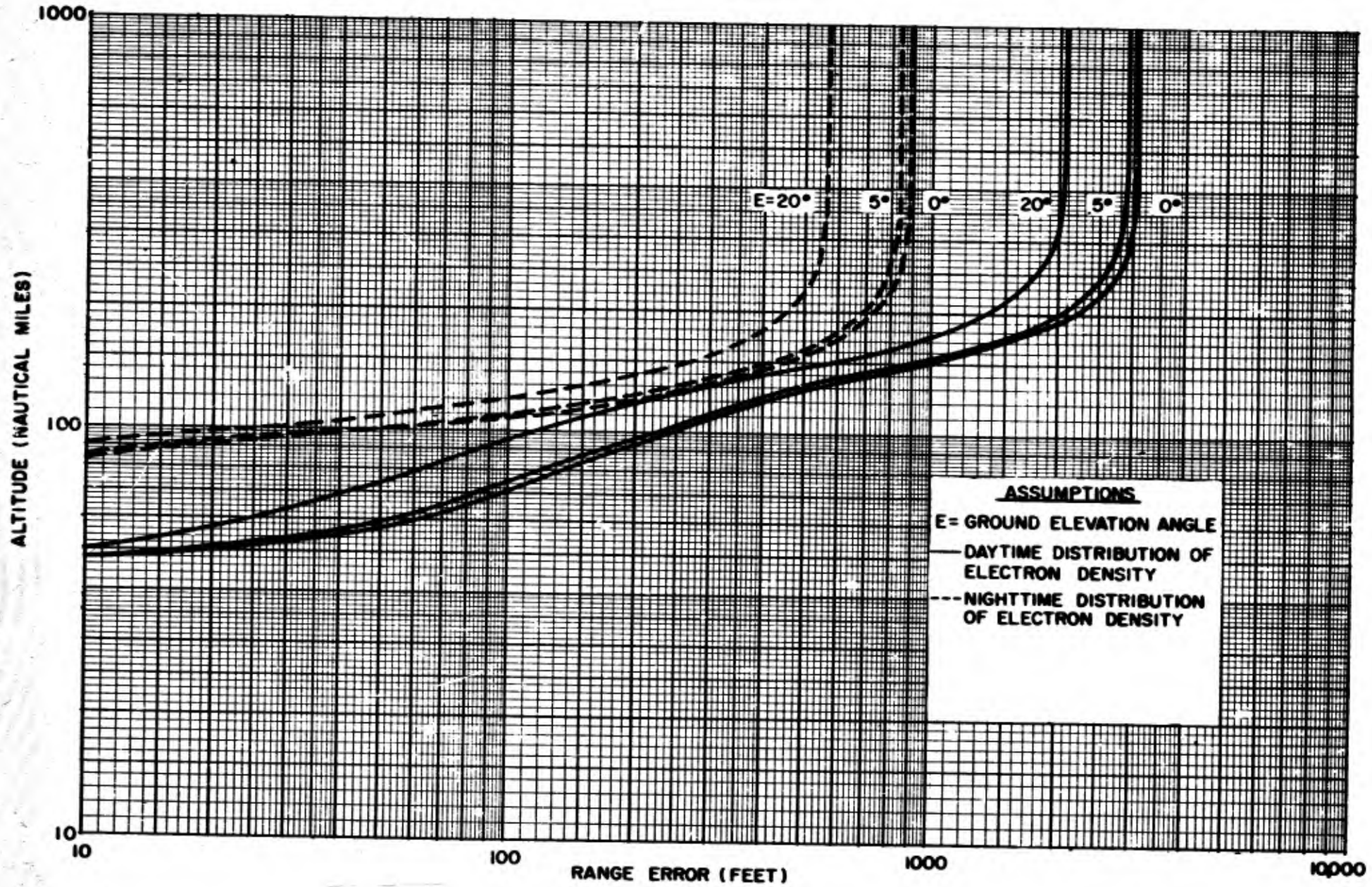

Figure 5.5-3. Ionospheric Range Errors at 200 mc., One-Way Transmission Path

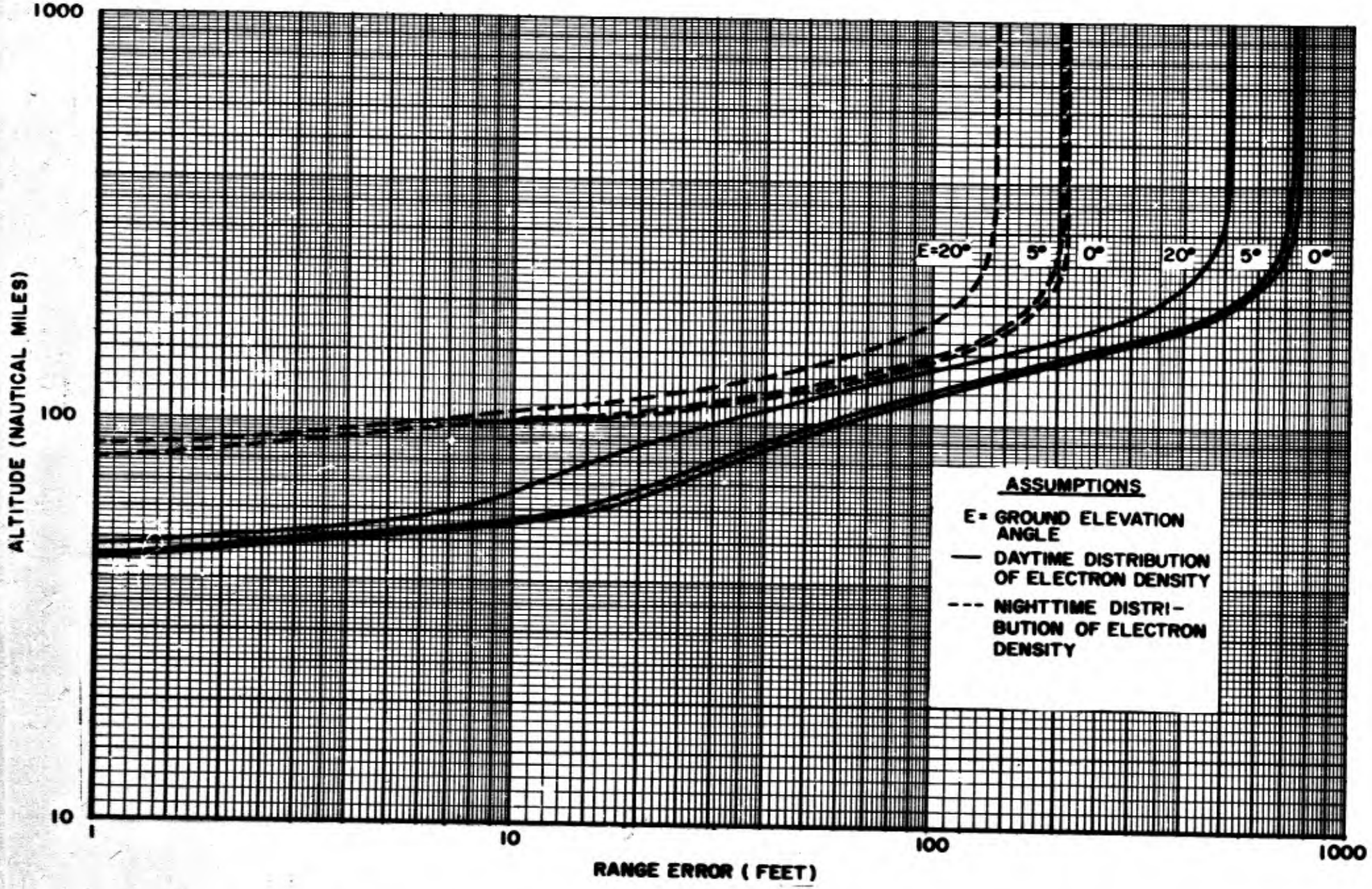

Figure 5.5-4, Ionospheric Range Errors at 400 mc., One-Way Transmission Path

At 200 mc/sec, for a one-way transmission path, the maximum error is on the order of 3000 feet. It is noted that this value is approximately eight times larger than the maximum error introduced by the troposphere.

It follows, from the inverse square of frequency dependency, that, at a frequency of about 575 mc/sec, the tropospheric and ionospheric contributions to the propagational time delays are of the same order of magnitude. Above 575 mc/sec, the tropospheric error is the more predominant one.

5.6 - DOPPLER EFFECTS DUE TO THE ATMOSPHERE

A. INTRODUCTION

Due to the propagational anomaly of refraction of radio waves traversing the atmosphere, an error is introduced in the determination of the line-of-sight or radial velocity of a moving target. This error results from the fact that the direction of the refracted ray at the target differs slightly from the fictitious line-of-sight or apparent path direction. The Doppler error, introduced by the incorrect assumption of the magnitude of the refractive index at the target location in the deviating medium, is believed to be indeterminate and is, therefore, not considered in this analysis.

It should be mentioned that, unlike the refraction and range errors, the Doppler errors are not cumulative. In other words, the total Doppler error, for a target traversing the ionosphere, is only the localized error at the specific point in the medium. The troposphere merely acts as a refractive medium.

B. TROPOSPHERIC EFFECT

A target, T, is traveling with a velocity, V, in an arbitrary direction in the refractive medium. The components of target velocity for the various orientations shown in Figure 5.6-1 are

$$V_r = V \cos (\psi + \Delta\alpha_T) \tag{5.6-1}$$

$$V_d = V \cos \psi \tag{5.6-2}$$

$$V_a = V_d \cos (\Delta\alpha) \tag{5.6-3}$$

where V_r, V_d and V_a are the components of V in the ray path direction, in the direct path direction and in the apparent path direction, respectively. The angle, $\Delta\alpha$, is the refractive error angle while $\Delta\alpha_T$ is the angle between the ray path and the direct path at the target location.

The error introduced in the measurement of the target Doppler velocity, ΔV, is given by

$$\Delta V = V_a - V_r \tag{5.6-4}$$

Expanding the cosine term of Equation (5.6-1) and then substituting the resulting expression, together with Equations (5.6-2) and (5.6-3) in Equation (5.6-4), it follows that the velocity error can be written in the form

$$\Delta V = V\cos\psi \left[\cos (\Delta\alpha) - \cos (\Delta\alpha_T)\right] + V\sin\psi \sin (\Delta\alpha_T) \tag{5.6-5}$$

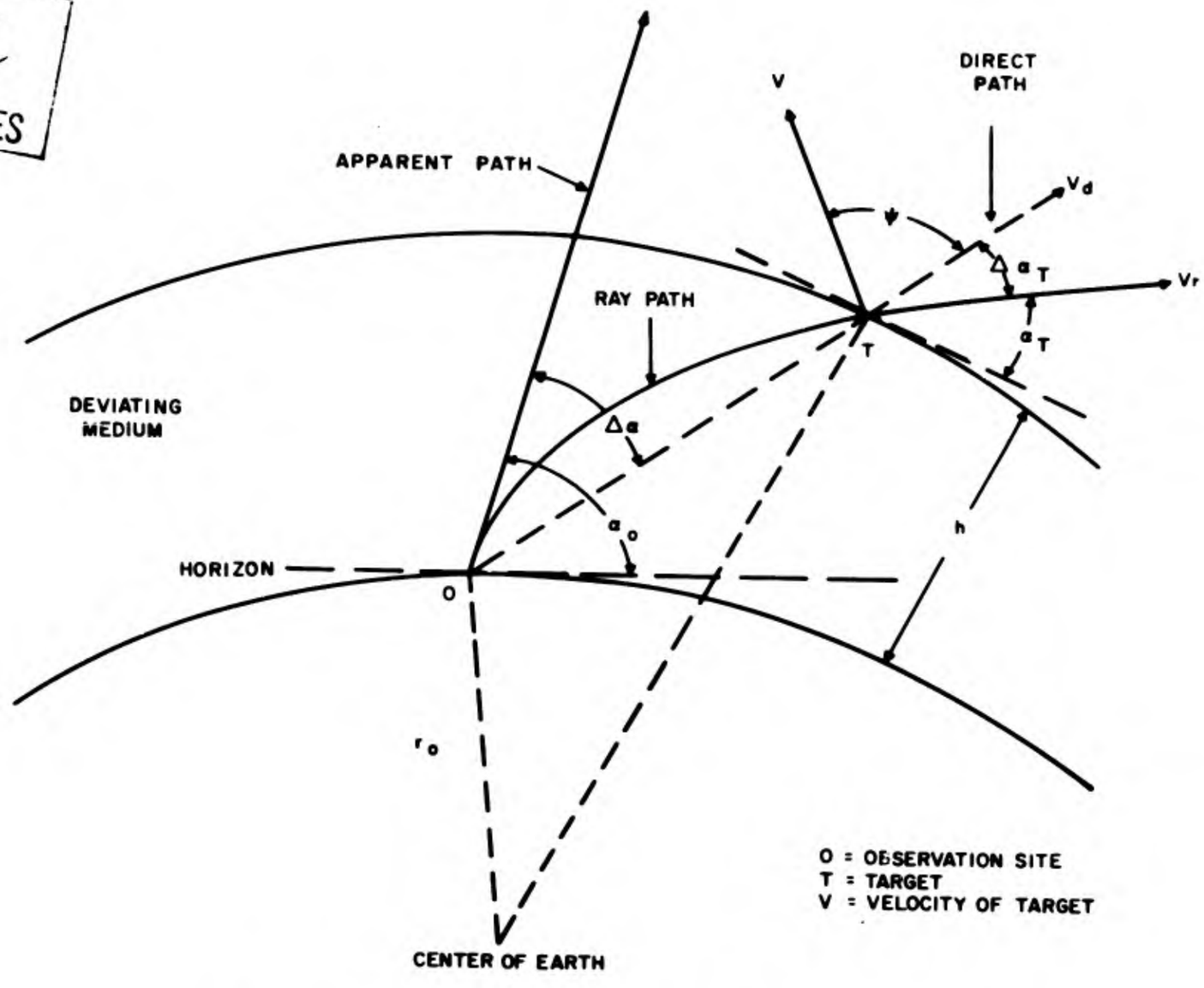

Figure 5.6-1. Deviation of Ray Path at Target Position

Since $\Delta\alpha$ and $\Delta\alpha_T$ are very small angles, the trigonometric functions can be expanded in a series. Neglecting higher order terms, it follows that

$$\Delta V \cong V\cos\psi \left[\frac{(\Delta\alpha_T)^2}{2} - \frac{(\Delta\alpha)^2}{2}\right] + V\sin\psi\,(\Delta\alpha_T) \qquad (5.6\text{-}6)$$

Since the magnitudes of $(\Delta\alpha_T)^2$ and $(\Delta\alpha)^2$ are of the order of microradians, the target radial velocity component, $V\cos\psi$, can be neglected. Thus, to a first approximation

$$\Delta V \cong V\sin\psi\,(\Delta\alpha_T) \qquad (5.6\text{-}7)$$

It is seen that the Doppler velocity error in the radial direction attributed to refraction is composed only of the tangential velocity component of target velocity, $V\sin\psi$. The error is a maximum when the velocity vector is perpendicular to the direction of the direct path and is a minimum when the target is moving along the direct line-of-sight path.

It is of interest to note that the identical expression for the Doppler velocity error, given by Equation (5.6-7) would have been obtained if ΔV had been defined by

$$\Delta V = V_d - V_a \qquad (5.6\text{-}8)$$

In other words, the magnitude of the refraction error angle is not significant and can be neglected in this analysis.

According to the general concept of the Doppler effect, the reflection of a radio wave from a moving object results in a signal returne o a fixed transmitting-receiving system whose frequency differs from the transmitted frequency. Analytically, this phenomenon is written as

$$f' = \frac{c - V\cos\psi}{c + V\cos\psi}\, f \qquad (5.6\text{-}9)$$

where f is the transmitted frequency; f', the apparent reflected frequency; V, the velocity of the moving object; c, the velocity of light in free space; and ψ, the orientation angle (see Figure 5.6-1).

It is seen that when the target is moving away from the observing site, $\psi = 0^o$, the reflected frequency is less than the transmitted frequency. For an object moving towards the observer, $\psi = 180^o$, the reflected frequency is greater than the transmitted frequency.

Equation (5.6-9) can be expressed as

$$f_d = -\frac{2V\cos\psi}{c + V\cos\psi}\, f \qquad (5.6\text{-}10)$$

where f_d is the difference between the apparent reflected frequency and the transmitted frequency.

Since $c >> V$, the frequency difference reduces to

$$f_d = - \frac{2 V \cos \psi}{c} f \qquad (5.6\text{-}11)$$

The error, encountered in the measurement of the Doppler frequency, is merely

$$d(f_d) = - \frac{2f}{c} \cos \psi \, dV \qquad (5.6\text{-}12)$$

This expression, of course, assumes that f and ψ are errorless quantities. The term, $\cos \psi \, dV$, is the component of target velocity error in the radial direction.

Substituting Equation (5.6-7) in this relationship, it follows that the Doppler frequency error due to refraction is

$$d(f_d) = - \frac{2f}{c} V \sin \psi \, (\Delta \alpha_T) \qquad (5.6\text{-}13)$$

With regard to the angle, $\Delta\alpha_T$, this parameter can be evaluated from Snell's law for spherically stratified surfaces and from the law of sines. It can be readily shown that

$$\Delta\alpha_T = \cos^{-1} \left[\frac{r_o}{r_o + h} \cos (\alpha_o - \Delta\alpha) \right] - \cos^{-1} \left[\frac{n_G r_o}{n_T (r_o + h)} \cos \alpha_o \right] \qquad (5.6\text{-}14)$$

where n_G and n_T are the refractive indices at the ground and target, respectively; r_o, the radius of the earth, h, the target height above the earth's surface; and α_o, the apparent elevation angle of the target.

The function, $\Delta\alpha_T$, is plotted in Figure 5.6-2 at height levels of 100,000 feet and 100 nautical miles, where n_T is practically zero It is seen that, for a given height, $\Delta\alpha_T$ decreases monotonically with elevation angle. The region of maximum $\Delta\alpha_T$, depicted in Figure 5.6-3 for zero degree elevation angle, centers in the vicinity of 25,000 feet for the 100 per cent relative humidity model (see Section 5.2), and 40,000 feet for the zero per cent relative humidity model

Figure 5.6-4 illustrates the Doppler frequency error for the two tropospheric models based on an assumed target speed of 20,000 ft/sec, target altitude of 100,000 ft and $\psi = 90^o$.

It is seen that the greatest Doppler frequency error occurs for the standard atmosphere with one hundred per cent relative humidity. The error is directly proportional to frequency and at 100 mc/sec, and zero degree elevation angle, the maximum error is approximately 16 cycles/sec

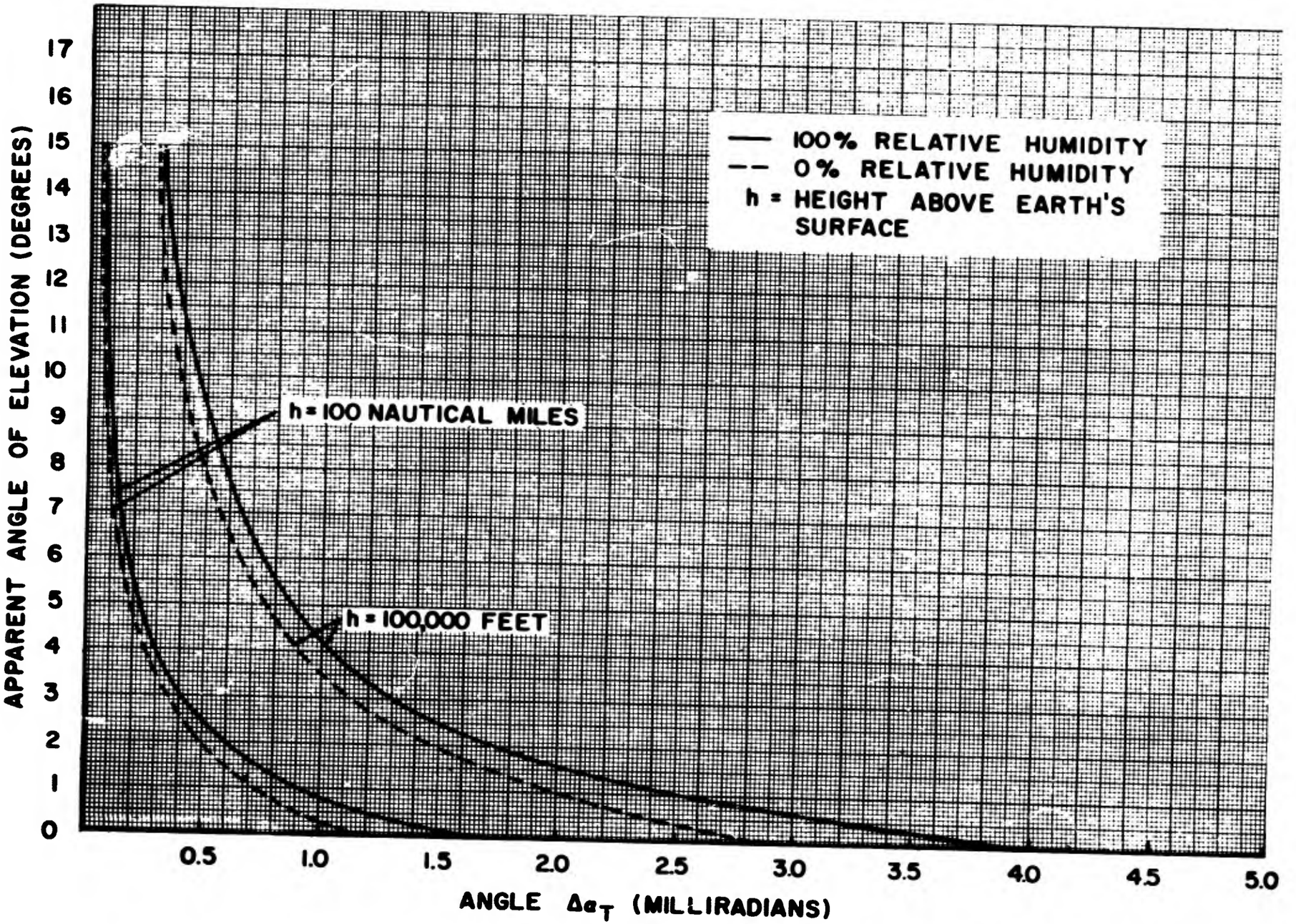

Figure 5.6-2. Angle $\Delta\alpha_T$ for the Troposphere

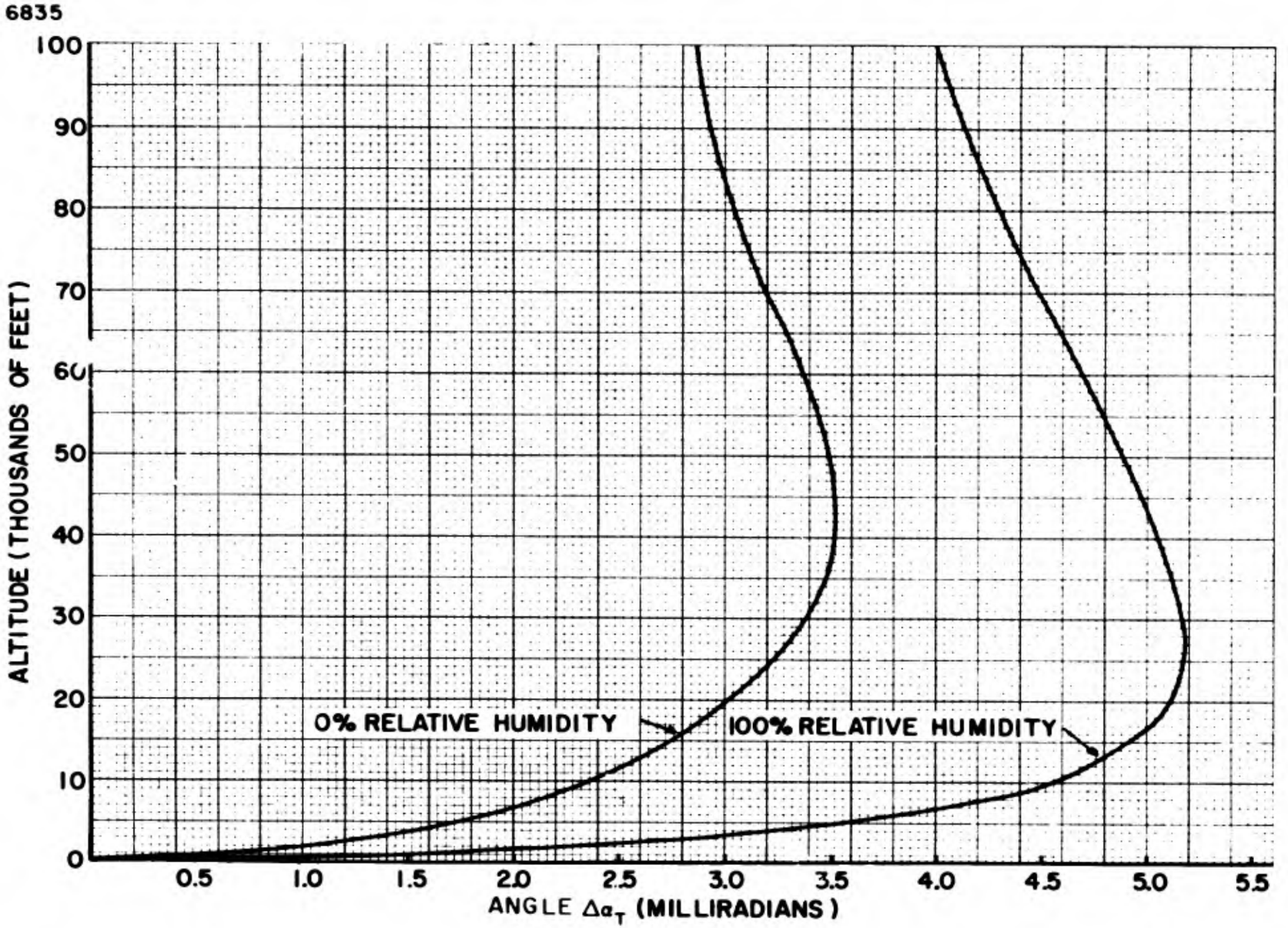

Figure 5.6-3. Region of Maximum $\Delta\ \alpha_T$ in the Troposphere for Zero Degree Elevation Angle

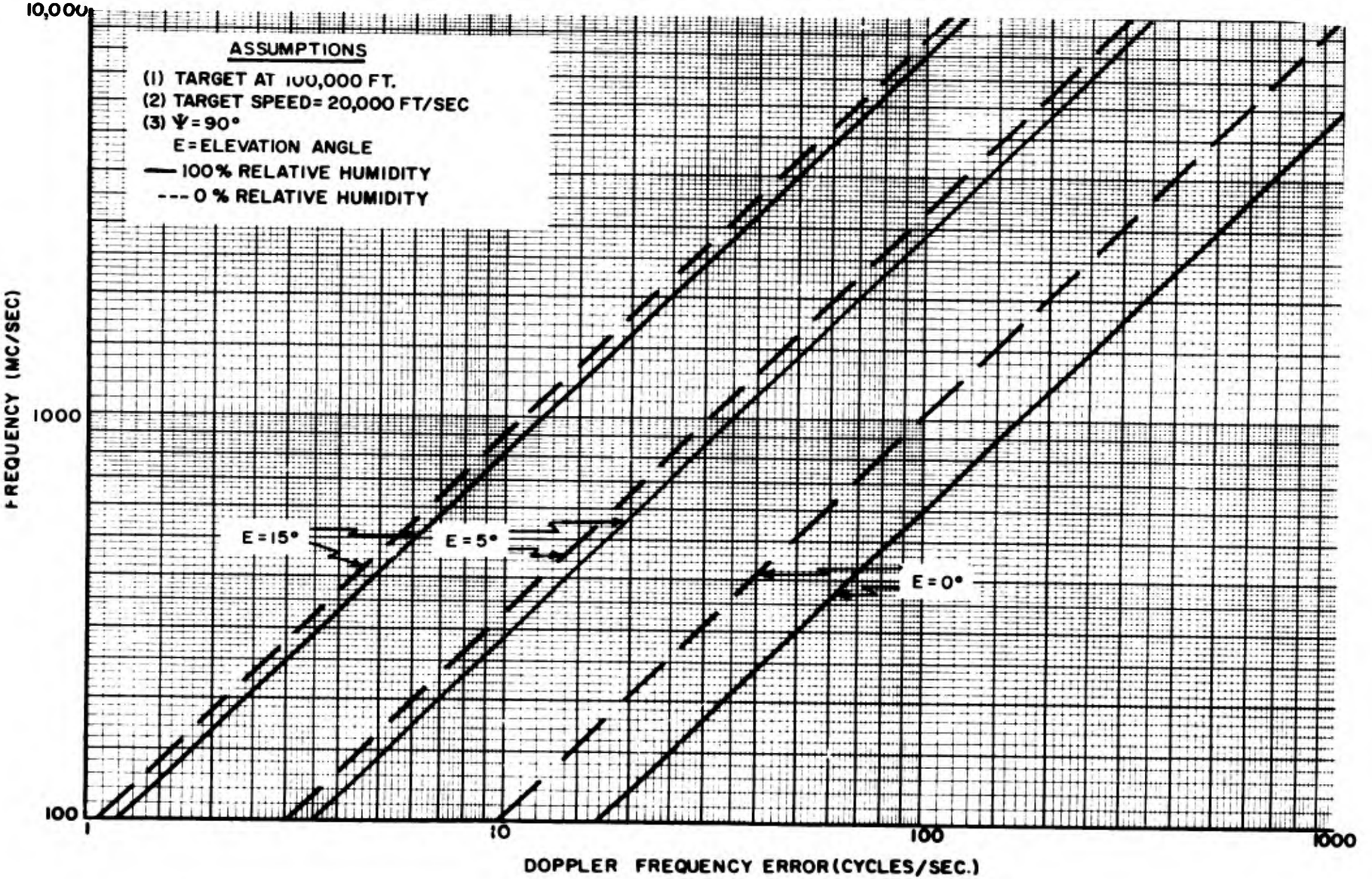

Figure 5.6–4. Doppler Frequency Error in the Troposphere

C. IONOSPHERIC EFFECT

The mathematical derivation of the Doppler frequency error presented above is valid for the ionosphere problem. However, in applying Equation (5.6-14) to conditions in the ionosphere, the following modifications are required: (1) the radius of the earth, r_o, is replaced by $r_o + h_o$ where h_o is the height of the lower edge of the ionosphere above the earth's surface; (2) the target height, h, is measured vertically from the lower edge of the ionosphere; (3) the ground refractive index, n_G, now becomes n_I, the index of refraction at the entrance into the ionosphere which, for all practical purposes, is unity; (4) the ground elevation angle is replaced by the ionospheric elevation angle which is defined as the angle between the incident ionosphere ray and the tangent plane.

It can be shown that when the effect of atmospheric refraction is neglected, the relationship between the ground elevation angle, α_o, and the ionospheric elevation angle, α_I, is merely

$$\alpha_I = \cos^{-1}\left[\frac{r_o}{r_o + h_o}\cos\alpha_o\right] \qquad (5.6\text{-}15)$$

From simple geometric considerations, it can be readily demonstrated that the angle, $\Delta\alpha_T$, for the ionosphere is a maximum at the level of maximum electron density and, as illustrated in Figure 5.6-5 is inversely proportional to the square of frequency.

Figure 5.6-6 depicts the variation of $\Delta\alpha_T$ at a frequency of 200 mc/sec as a function of elevation angle for an assumed target height of 300 km for the daytime electron density model and 250 km for the nighttime model.

From the results presented in Figure 5.6-7, it is seen that the Doppler frequency error is at maximum during the daytime and at low elevation angles. For an assumed target speed of 20,000 ft/sec and $\psi = 90^o$, the error, at 100 mc/sec and at a ground elevation angle of zero degrees which is analogous to an ionospheric elevation angle of about 9^o, is on the order of 51 cycles/sec. For the nighttime, under similar conditions, the error is only 17 cycles/sec. It should be mentioned that, for the ionosphere, the Doppler frequency error is inversely proportional to frequency.

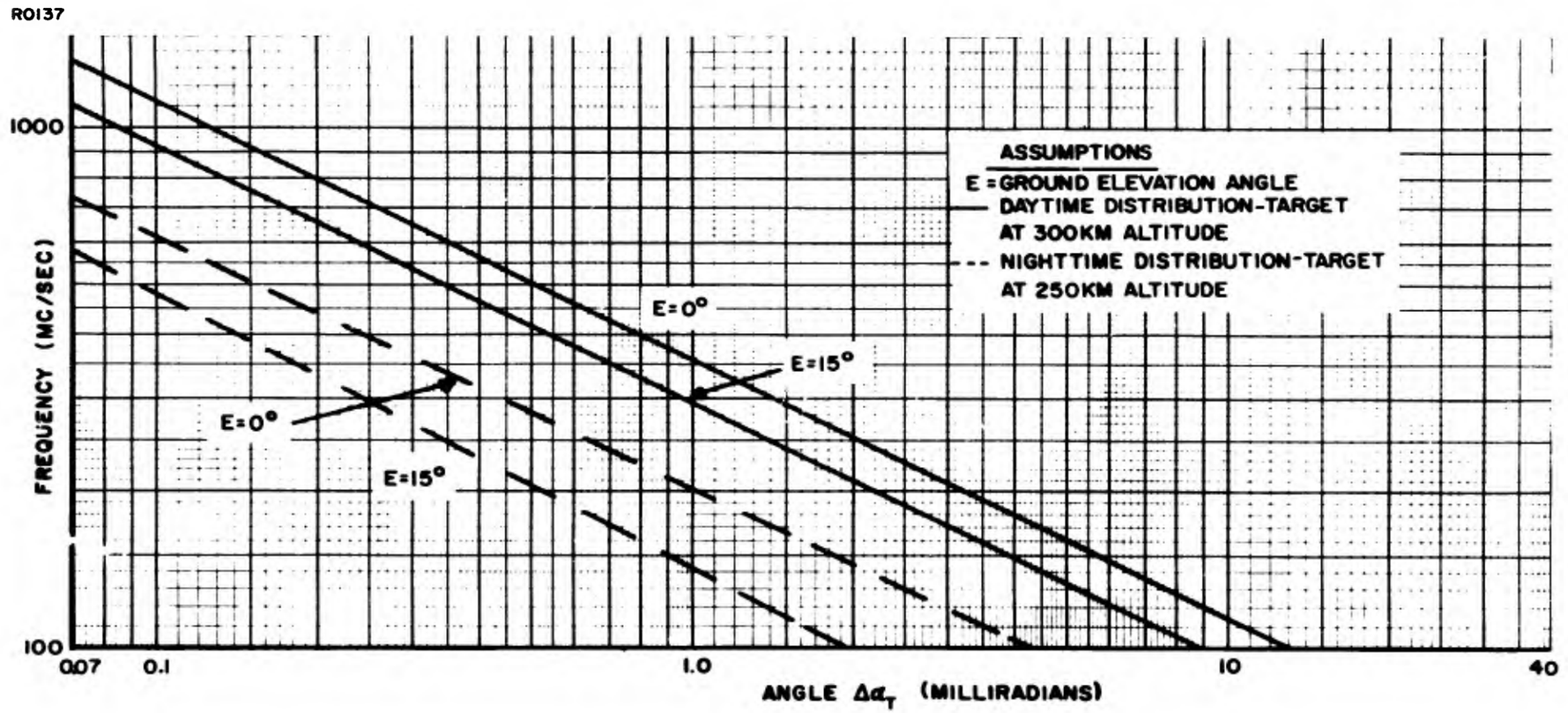

Figure 5.6-5. Angle $\Delta\alpha_T$ for the Ionosphere as a Function of Frequency

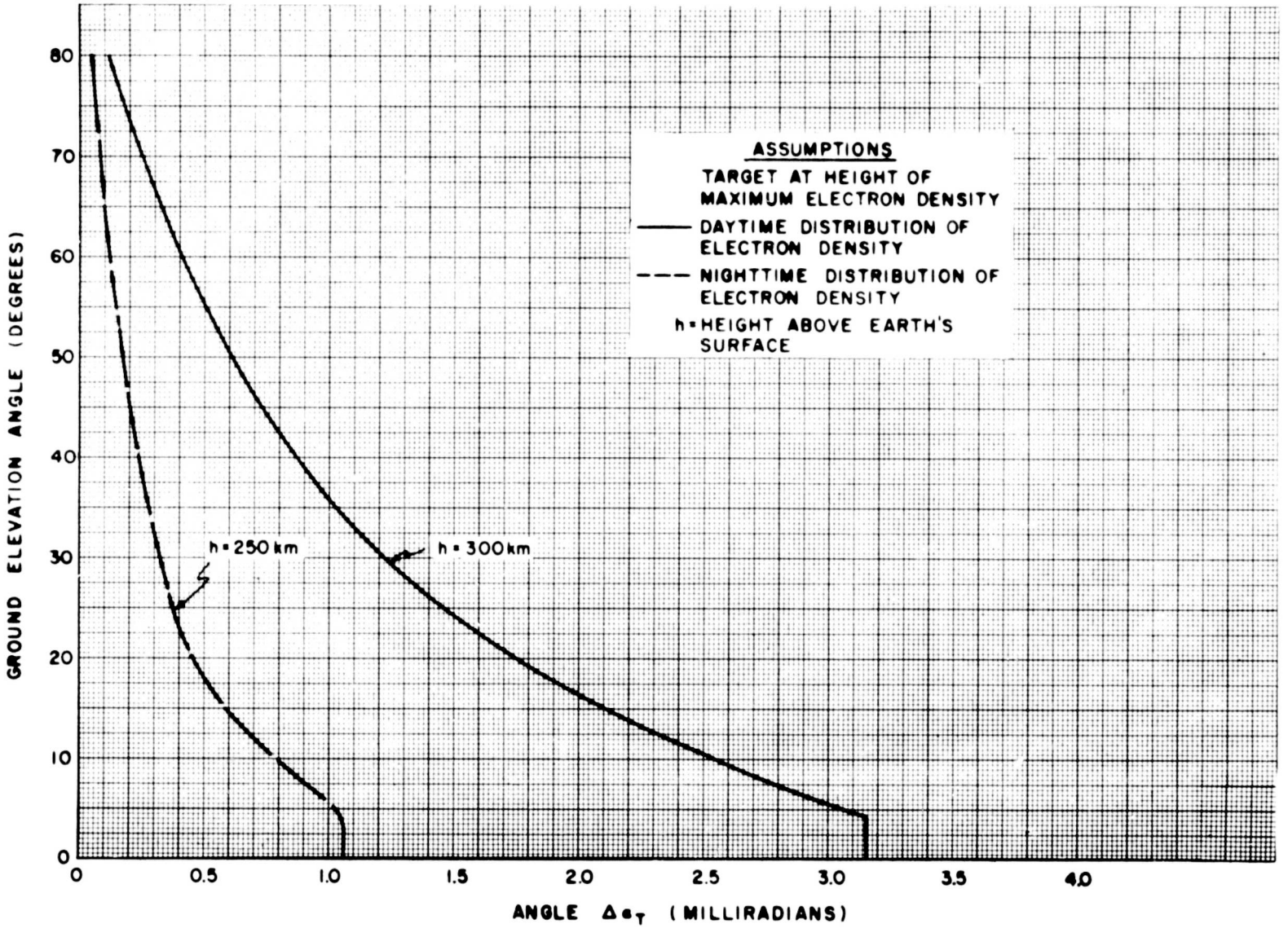

Figure 5.6-6. Angle $\Delta\alpha_T$ for the Ionosphere at 200 mc.

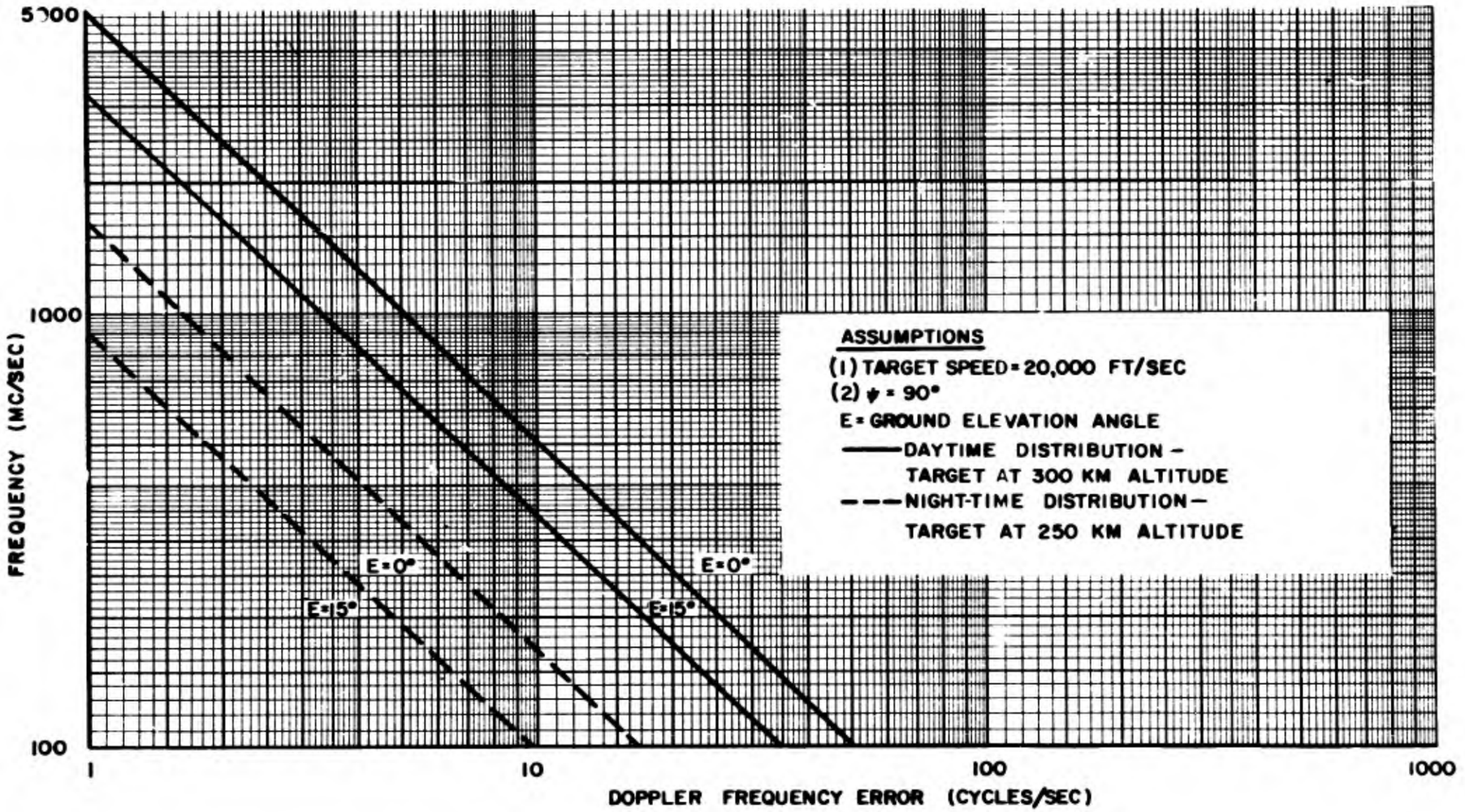

Figure 5.6-7. Doppler Frequency Error in the Ionosphere

6.1 - PROPAGATION OF RADIO WAVES THROUGH AN IONIZED MEDIUM WITH APPLICATION TO THE IONOSPHERE

A. IN THE ABSENCE OF THE EARTH'S MAGNETIC FIELD AND ELECTRON COLLISIONS

When an electromagnetic wave passes through an ionized medium, a periodic force is imposed on both the electrons and ions. If it is assumed that a plane-polarized wave is incident on the medium having a field strength

$$E = E_o \sin \omega t \tag{6.1-1}$$

then the differential equation for the motion of the electrons can be given by

$$m \frac{d^2x}{dt^2} = e E_o \sin \omega t \tag{6.1-2}$$

where e is the electron charge (4.8×10^{-10} esu); m, the electron mass (9.1×10^{-28} gm); and ω, the angular frequency of the incident wave. Since the mass of an ion is 1839 times greater than the mass of an electron, the motion of the ions can be neglected.

Integrating Equation (6.1-2), it follows that the velocity of the electron is

$$\frac{dx}{dt} = - \frac{eE_o}{m\omega} \cos \omega t \tag{6.1-3}$$

The motion of the electrons produces a convection current density, i_c, defined by

$$i_c = N_e e \frac{dx}{dt} \tag{6.1-4}$$

where N_e is the number of electrons/cm^3. Upon substitution, this expression becomes

$$i_c = - \frac{N_e e^2 E_o}{m\omega} \cos \omega t \tag{6.1-5}$$

The electric field gives rise to a displacement current density, i_D, given by

$$i_D = \frac{K}{4\pi} \frac{\delta E}{\delta t} \tag{6.1-6}$$

where K is the dielectric constant of the medium with no electrons present. The displacement current simplifies to

$$i_D = \frac{K\omega E_o}{4\pi} \cos \omega t \tag{6.1-7}$$

The total current density, i, is merely the sum of Equations (6.1-5) and (6.1-7)

$$i = \left[K - \frac{4\pi N_e e^2}{m\omega^2} \right] \frac{E_o \omega}{4\pi} \cos \omega t \qquad (6.1\text{-}8)$$

It is evident that the presence of electrons reduces the dielectric constant from K to

$$\left[K - \frac{4\pi N_e e^2}{m\omega^2} \right]$$

For a medium in which the conductivity is zero, the index of refraction is simply the square root of the dielectric constant. Since in free space, the dielectric constant is unity, the presence of electrons in the ionosphere causes a decrease in the index of refraction to

$$n = \left[1 - \frac{4\pi N_e e^2}{m\omega^2} \right]^{\frac{1}{2}} \qquad (6.1\text{-}9)$$

The phase velocity of the wave, V_p, which is the velocity with which a point of constant phase moves, is given by

$$V_p = \frac{c}{n} \qquad (6.1\text{-}10)$$

or

$$V_p = \frac{c}{\left[1 - \frac{4\pi N_e e^2}{m\omega^2} \right]^{\frac{1}{2}}} \qquad (6.1\text{-}11)$$

It is interesting to note that the vibration of electrons in an ionized medium has the effect of increasing the phase velocity of the wave. If no electrons are present, $N_e = O$, the phase velocity is simply c, the velocity of propagation in free space. As the electron density increases, the phase velocity increases. The phase velocity approaches infinity as the denominator decreases to zero. When this condition arises, further wave propagation is impossible.

In the case of the ionosphere, the maximum electron density of an ionized layer can be determined by transmitting radio waves vertically incident to the ionosphere. Reflections will occur up to the frequency for which the denominator in Equation (6.1-11) equals zero. If the frequency is still increased, the radio waves will penetrate the layer, resulting in no further reflections. The limiting frequency, ω_c, at which the reflections begin to disappear is called the critical frequency of the layer and is given by

$$\omega_c^2 = \frac{4\pi N_e e^2}{m} = 3.18 \times 10^9 N_e \left(\frac{\text{Radians}}{\text{Sec}} \right)^2 \qquad (6.1\text{-}12)$$

It is evident, therefore, that an alternative definition for the index of refraction is

$$n = \sqrt{1 - \frac{\omega_c^2}{\omega^2}} \tag{6.1-13}$$

The group velocity of the wave, which is the velocity of an imaginary observer who remains at the same point on the envelope of the advancing wave, is given by

$$V_g = \frac{d\omega}{d\gamma} \tag{6.1-14}$$

where γ is the phase constant defined by

$$\gamma = \frac{\omega}{V_p} \tag{6.1-15}$$

It can be readily shown that

$$V_g = \frac{V_p}{1 - \frac{\omega}{V_p}\frac{dV_p}{d\omega}} \tag{6.1-16}$$

Substituting Equation (6.1-10) in this expression, it follows that

$$V_g = \frac{1}{\frac{n}{c} + \frac{\omega}{c}\frac{dn}{d\omega}} \tag{6.1-17}$$

Differentiating Equation (6.1-13) with respect to ω and substituting in Equation (6.1-17), it is found that

$$V_g = nc \tag{6.1-18}$$

It is interesting to note that the group velocity of the wave in the ionosphere is obviously less than the free space velocity of propagation and that

$$V_g V_p = c^2 \tag{6.1-19}$$

which is the condition existing for electromagnetic propagation in a wave guide.

B. IN THE ABSENCE OF THE EARTH'S MAGNETIC FIELD; ELECTRON COLLISIONS PRESENT

The preceding analysis neglects the collisions of the vibrating electrons with the ions and neutral particles In the absence of collisions, the electrons, which vibrate under the influence of the imposed field, reradiate the energy in phase with the incoming signal. The result is that there is no loss in the energy of the wave.

When the effect of collisions is taken into account, a damping term is introduced into the equation of motion which results in the absorption of energy from the electromagnetic wave traversing the ionized medium. The electrons, colliding with the other particles, give up some of their energy to these particles. The ultimate effect of this phenomenon is the absorption of signal energy.

Since the mathematical derivations beyond this point are tedious, only results will be stated. Reference is made to Mitra (1) for more detailed information.

The introduction of electron collisions in the ionosphere renders it an absorbing medium having a conductivity, σ, given by

$$\sigma = \frac{N_e e^2 \nu}{m(\omega^2 + \nu^2)} \tag{6.1-20}$$

where ν is the electron angular collision frequency. The dielectric constant is now a complex quantity defined by

$$K' = K - \frac{4\pi j\sigma}{\omega} \tag{6.1-21}$$

The complex index of refraction, M, is given by

$$M^2 = K' = \left(n - \frac{jck}{\omega}\right)^2 \tag{6.1-22}$$

where k is the absorption per unit length of path. The term, ck/ω, is the absorption per length of path $\lambda/2\pi$ where λ is the free space wavelength.

The complex index of refraction can also be written as

$$M^2 = 1 + \frac{1}{\alpha + j\beta} \tag{6.1-23}$$

where

$$\alpha = \frac{-m\omega^2}{4\pi N_e e^2} \tag{6.1-24}$$

and

$$\beta = \frac{m\omega\nu}{4\pi N_e e^2} \tag{6.1-25}$$

From Equations (6 1-22) and (6 1-23) and neglecting higher orders of $[ck/\omega]^2$, it can be shown that

$$n = \left[1 - \frac{4\pi N_e e^2}{m(\omega^2 + \nu^2)} \right]^{\frac{1}{2}} \qquad (6\ 1\text{-}26)$$

and that

$$k = \frac{2\pi N_e e^2 \nu}{cn(\omega^2 + \nu^2)} \qquad (6.1\text{-}27)$$

According to Nicolet (2) at altitudes of 80 km, 100 km, 120 km and 140 km, the angular collision frequencies are about 4×10^6 radians/sec, 1.5×10^5 radians/sec, 10^4 radians/sec and 2×10^3 radians/sec, respectively. Thus, at a frequency of 100 mc/sec, it is valid to assume that $\omega^2 >> \nu^2$. This approximation is greatly improved at the higher frequencies It follows that the absorption coefficient simplifies to

$$k = \frac{N_e e^2 \nu}{2\pi cnmf^2} \qquad (6.1\text{-}28)$$

where f is in cycles/sec.

It is noted that the absorption coefficient is directly proportional to the electron density and collision frequency and inversely proportional to the refractive index and the square of the frequency. The absorption tends to a maximum as the refractive index tends to a minimum

C. IN THE PRESENCE OF THE EARTH'S MAGNETIC FIELD AND ELECTRON COLLISIONS

The theory of propagation of electromagnetic waves through an ionized medium in the presence of an external magnetic field is often referred to as the magneto-ionic theory.

The equation of motion of an electron in the region of ionization is, for the general case,

$$m\ddot{\underline{r}} = -e\underline{E} - g\dot{\underline{r}} - \frac{e}{c}(\underline{r} \times \underline{H}) \qquad (6.1\text{-}29)$$

where $\underline{E}$ is the electric field vector; $\underline{H}$, the magnetic field vector; $\underline{r}$, the displacement vector of the electron; and g, the frictional coefficient ($=m\nu$). The dots over the vector, $\underline{r}$, denote differentiation with respect to time

Assuming plane wave propagation along the x-axis with no component of the earth's magnetic field along the y-axis, shown in Figure 6.1-1, then the equations of motion in scalar form can be readily written Eventual solution of these equations, where it is assumed that the incident electron field varies sinusoidally with time, leads to the general form of the complex index of refraction, M.

$$M^2 = (n - j\frac{ck}{\omega})^2 \tag{6.1-30}$$

$$M^2 = 1 + \frac{2}{2(\alpha + j\beta) - \frac{\gamma_T^2}{1 + \alpha + j\beta} \pm \left[\frac{\gamma_T^4}{(1 + \alpha + j\beta)^2} + 4\gamma_L^2\right]^{\frac{1}{2}}} \tag{6.1-31}$$

while the polarization vector of the wave, P, is

$$P = \frac{H_Z}{H_Y} = -\frac{j}{\gamma_L}\left[\frac{1}{M^2 - 1} - (\alpha + j\beta)\right] \tag{6.1-32}$$

where

$$\alpha = -\frac{\omega^2}{\omega_c^2} \qquad \gamma_T = \frac{\omega\omega_H}{\omega_c^2}\sin\theta$$

$$\beta = \frac{\omega\nu}{\omega_c^2} \qquad \omega_H = \frac{He}{mc} \tag{6.1-33}$$

$$\gamma_L = \frac{\omega\omega_H}{\omega_c^2}\cos\theta$$

The quantity, He/mc, is the gyromagnetic frequency of the electron about the earth's magnetic field while θ is the propagation angle, i.e., the angle between the magnetic field vector and the direction of propagation, illustrated in Figure 6.1-1. The terms, H_Z and H_Y, are the components of the magnetic field intensity of the wave along the Z- and Y-directions, respectively.

It is noted that there are two possible values for the complex index of refraction which indicate two different modes of propagation. The waves travel independently in the ionized medium and each has a polarization vector associated with it. In the general case, at the low frequencies, the waves are elliptically polarized with opposite senses of rotation. At frequencies on the order of 100 mc/sec, the waves are circularly polarized.

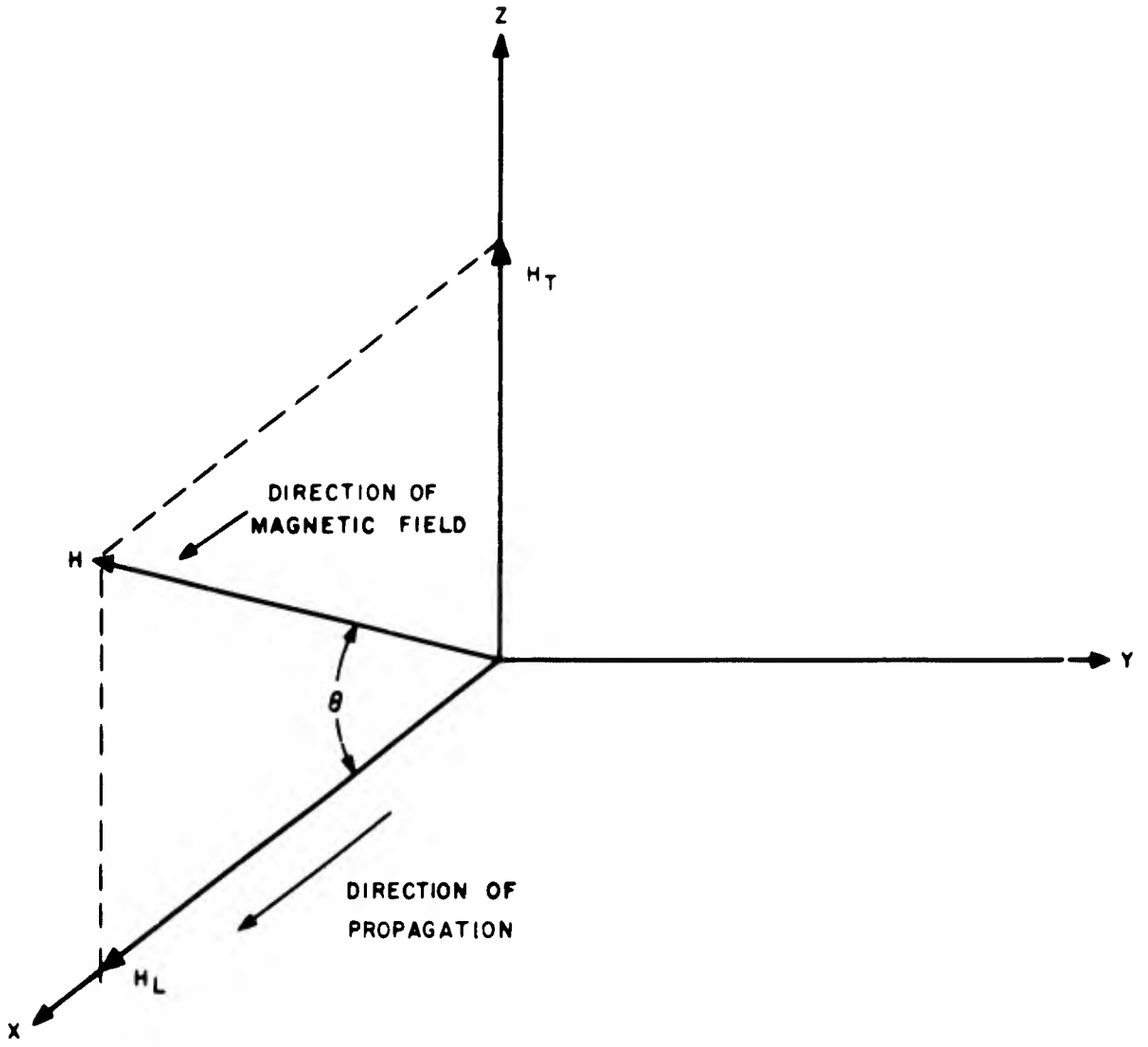

Figure 6.1-1. Coordinate System for Magneto-Ionic Theory

Since Equations (6.1-31) and (6.1-32) are quite complicated in their present form, simplification can be accomplished by considering the effect of electron collisions at frequencies in the VHF and UHF range.

It is seen that

$$\alpha + j\beta = \alpha \left(1 - j \frac{\nu}{\omega}\right) \tag{6.1-34}$$

As shown in the preceding section, $\omega >> \nu$. Thus, to a first approximation, β can be neglected, which implies that the absorption coefficient, k, is zero.

For the daytime model of electron density, presented in Section 5.2, the maximum electron density in the F_2-layer is 12.5×10^5 electrons/cm^3. Hence, it follows from Equation (6.1-12) that, at 100 mc/sec,

$$\left|\alpha\right| = \left|\frac{\omega^2}{\omega_c^2}\right| = 99.3 \tag{6.1-35}$$

For higher frequencies or smaller concentrations of electron density, the magnitude of α increases. Since $\alpha >> 1$, it is evident that

$$1 + \alpha + j\beta \approx \alpha \tag{6.1-36}$$

Referring to Equation (6.1-31), it is noted that when the approximation given by Equation (6.1-36) is taken into account, the complex index of refraction reduces to a real quantity given by

$$n_{o,e}^2 = 1 + \frac{2}{2\alpha - \frac{\gamma_T^2}{\alpha} \pm \left[\frac{\gamma_T^4}{\alpha^2} + 4\gamma_L^2\right]^{\frac{1}{2}}} \tag{6.1-37}$$

This expression, on substituting in the definitions of α, γ_T and γ_L, becomes

$$n_{o,e}^2 = 1 - \frac{1}{\frac{\omega^2}{\omega_c^2} - \frac{\omega_H^2}{2\omega_c^2}\sin^2\theta \pm \frac{\omega\omega_H}{\omega_c^2}\left[\left(\frac{\omega_H \sin^2\theta}{2\omega}\right)^2 + \cos^2\theta\right]^{\frac{1}{2}}} \tag{6.1-38}$$

The subscripts o and e indicate that there are now two values for the refractive index, the former (positive sign) being associated with the ordinary mode of propagation while the latter (negative sign) with the extraordinary mode of propagation.

The polarization vector, Equation (6 1-32) also simplifies to

$$P_{o,e} = -\frac{j}{\gamma_L}\left[\frac{1}{n_{o,e}^2} - \alpha\right] \tag{6.1-39}$$

Case 1 - Quasi-Longitudinal Propagation

The quasi-longitudinal mode of propagation can be represented by the condition that

$$4\frac{\omega^2}{\omega_H^2} >> \sin^2\Theta \tan^2\Theta \tag{6.1-40}$$

To satisfy this inequality, the propagation angle, Θ, is restricted within a range which is dependent upon the transmission frequency. In order for the term, $4\omega^2/\omega_H^2$, to maintain at least a minimum factor of 50 greater than ($\sin^2\Theta\tan^2\Theta$), the propagation angle is restrained between $0^o \leq \Theta \leq 86.6^o$ at a frequency of 100 mc/sec. At 400 mc/sec, however, this limitation increases to approximately $0^o \leq \Theta \leq 89.6^o$.

According to the inequality given by Equation (6 1-40), the index of refraction, Equation (6.1-38), reduces to

$$n_{o,e}^2 = 1 - \frac{\omega_c^2}{\omega^2\left[1 \pm \frac{\omega_H}{\omega}\cos\Theta\right]} \tag{6.1-41}$$

The magnitude of the magnetic field intensity, H, at any point on the earth is given by, according to Chapman and Bartels (3),

$$H = H_o\,(1 + 3\sin^2\psi)^{\frac{1}{2}} \tag{6 1-42}$$

where ψ is the geomagnetic latitude and H_o is the equatorial magnetic intensity ($\approx$0.31 gauss). It is seen that the maximum magnetic field intensity at the geomagnetic pole is approximately 0.62 gauss. For this value of H, the gyromagnetic frequency, ω_H is 10.55×10^6 radians/sec Comparing this value with propagating frequencies above 100 mc/sec, it is evident that $(\omega_H/\omega)^2 << 1$ Since $(\omega/\omega_c)^2 >> 1$, Equation (6.1-41) can be expanded by the binomial series Neglecting higher order terms, there results

$$n_{o.e} \approx 1 - \frac{\omega_c^2}{2\omega^2\left[1 \pm \frac{\omega_H}{\omega}\cos\Theta\right]} \tag{6.1-43}$$

Separating the two indices of refraction and again utilizing the binomial expansion, it is seen that

$$n_o \approx 1 - \frac{\omega_c^2}{2\omega^2}\left[1 - \frac{\omega_H}{\omega}\cos\Theta\right] \tag{6.1-44}$$

$$n_e \approx 1 - \frac{\omega_c^2}{2\omega^2}\left[1 + \frac{\omega_H}{\omega}\cos\Theta\right] \tag{6.1-45}$$

It follows that the difference in the index of refraction for the two modes of propagation is

$$\Delta n = \frac{\omega_c^2 \omega_H}{\omega^3}\cos\Theta \tag{6.1-46}$$

where $\Delta n = n_o - n_e$. This expression can also be written as

$$\Delta n = \frac{N_e e^3 H}{2\pi^2 m^2 cf^3}\cos\Theta \tag{6.1-47}$$

The polarization vector, Equation (6.1-39), on substituting in the definitions of γ_L and α and Equation (6.1-41), becomes

$$P_o = +j \qquad P_e = -j \tag{6.1-48}$$

These relationships definitely show that both the ordinary and extraordinary components are circularly polarized. Based on the coordinate system used to define P, Equation (6.1-32), the former has a left-handed sense of rotation, i.e., when viewed in the direction of propagation, the locus of the end of the electric field intensity vector in a plane perpendicular to the propagation direction rotates in a counter-clockwise fashion, while the latter has a right-handed sense of rotation.

When the direction of propagation is in the reverse direction to that of the magnetic field, the ordinary ray has a right-handed sense of rotation while the extraordinary ray rotates in a left-handed sense.

Case 2 - Quasi-Transverse Propagation

The condition for quasi-transverse propagation is denoted by the inequality

$$\sin^2\Theta \tan^2\Theta >> \frac{4\omega^2}{\omega_H^2} \tag{6.1-49}$$

which is merely the reverse of Equation (6.1-40). For this condition to be valid, the angle, Θ, must be on the order of 89.8° at 100 mc/sec. As the frequency is increased, Θ rapidly approaches 90 degrees.

The real part of the complex index of refraction, Equation (6.1-38), simplifies to

$$n_{o,e}^2 = 1 - \frac{2\omega_c^2}{2\omega^2 - \omega_H^2 \sin^2\Theta \pm \omega_H^2 \sin^2\Theta} \qquad (6.1\text{-}50)$$

Expanding this function by the binomial series and neglecting higher order terms, it can be shown that the individual indices become

$$n_o \approx 1 - \frac{\omega_c^2}{2\omega^2} \qquad (6.1\text{-}51)$$

$$n_e \approx 1 - \frac{\omega_c^2}{2\omega^2}\left[1 + \frac{\omega_H^2}{\omega^2}\sin^2\Theta\right] \qquad (6.1\text{-}52)$$

It is noted that the ordinary refractive index, n_o, is independent of the earth's magnetic field and is identical with the index of refraction derived for electromagnetic propagation in the absence of the earth's magnetic field and electron collisions. The term, $[1 + (\omega_H/\omega)^2 \sin^2\Theta]$, represents the correction due to the presence of the earth's magnetic field.

The difference in the refractive indices is, therefore, given by

$$\Delta n = \frac{\omega_c^2 \omega_H^2}{2\omega^4} \sin^2\Theta \qquad (6.1\text{-}53)$$

or

$$\Delta n = \frac{N_e e^4 H^2}{8\pi^3 m^3 c^2 f^4} \sin^2\Theta \qquad (6.1\text{-}54)$$

With regard to the polarization of the two modes of propagation, substituting Equation (6.1-50) in Equation (6.1-39) reveals that, for quasi-transverse propagation,

$$P_o = 0 \qquad P_e = -j\infty \qquad (6.1\text{-}55)$$

In other words, the ordinary wave is linearly polarized in the direction parallel to the earth's magnetic field. The extraordinary wave is also linearly polarized but in the direction perpendicular to the earth's magnetic field.

D. REFERENCES

1. Mitra, S. K.; "The Upper Atmosphere," The Asiatic Society of Calcutta, 1952.

2. Nicolet, M.; "The Collision Frequency of Electrons in the Ionosphere" Journal of Atmospheric and Terrestrial Physics, Vol. 3, p. 200, 1953.

3. Chapman, S. and Bartels, J.; "Geomagnetism" Vol. I, Oxford University Press, 1940.

6.2 - IONOSPHERIC POLARIZATION EFFECTS

A. INTRODUCTION

When a linearly polarized electromagnetic wave enters an ionized medium in the presence of an external magnetic field, such as encountered in the ionosphere, the wave separates into two independent components both, in the general case, elliptically polarized with opposite senses of rotation. For frequencies in the UHF range, the two components, which are referred to as the ordinary and the extraordinary waves, are circularly polarized.

As the ionosphere is traversed, the two waves progress with different velocities of propagation which result in the phase relationship between them to be continuously changing. On leaving the ionosphere, the circularly polarized components recombine to form a linearly polarized wave which is rotated with respect to the original linear wave. This phenomenon is commonly referred to as the Faraday effect.

The magnitude of the angular rotation is a function of the integrated electron density along the transmission path, the angle between the direction of propagation and the direction of the magnetic line of force, and the transmission frequency.

B. THEORETICAL CONSIDERATIONS

Since a circularly polarized wave is basically composed of two harmonic orthogonal signals which are 90° out of phase with one another, only one of the linearly polarized waves from each of the two circularly polarized components, i.e., the ordinary and the extraordinary waves need be considered in analyzing the polarization rotational effects of the ionosphere.

The electric field intensities of two linearly polarized progressive waves can be written as

$$E_o = a\, e^{j(\omega t - \gamma_1 s)} \tag{6.2-1}$$

$$E_e = a\, e^{j(\omega t - \gamma_2 s)} \tag{6.2-2}$$

where the subscripts, o and e, refer to the ordinary and the extraordinary modes of propagation, respectively The phase constants, γ_1, and γ_2, are defined by

$$\gamma_{1,2} = \frac{\omega}{V_{p1,2}} \tag{6.2-3}$$

where V_p is the phase velocity of the wave and ω is the angular transmission frequency.

Since, by definition, the refractive index of the media is

$$n_{1,2} = \frac{c}{V_{p1,2}} \tag{6.2-4}$$

it follows therefore that

$$\gamma_{1,2} = \frac{\omega n_{1,2}}{c} \tag{6.2-5}$$

where c is the velocity of electromagnetic waves in free space.

The difference in phase between the two waves traversing a distance, ds, is given by

$$d\phi = (\gamma_1 - \gamma_2)\, ds \tag{6.2-6}$$

Substituting Equation (6.2-5) in this expression, it is seen that

$$d\phi = \frac{\omega}{c} \Delta n\, ds \tag{6.2-7}$$

where $\Delta n = n_1 - n_2$.

This relationship defines the phase shift for a one-way propagation path. When two-way transmission paths are considered, an additional factor of two is introduced. It should be noted that $d\phi$, as given by Equation (6.2-7), is the differential phase shift between the two magneto-ionic components. The resultant polarization rotation is merely one-half this value. Thus, taking these two items into consideration, the total polarization shift for a two-way propagation path becomes

$$\phi(s) = \frac{\omega}{c} \int_{s_1}^{s_2} \Delta n\, ds$$

where s_1, and s_2 are the limits of the path.

In terms of a vertical height variable, this expression becomes

$$\phi(h) = \frac{\omega}{c} \int_{h_1}^{h_2} \Delta n\, f(h)\, dh \tag{6.2-8}$$

where

$$f(h) = \frac{r_o + h}{\left[(r_o + h)^2 - (r_o \cos E)^2\right]^{\frac{1}{2}}} \tag{6.2-9}$$

and r_o is the radius of the earth and E is the elevation angle of the antenna beam. The parameter, f(h), is plotted in Figure 6.2-1 as a function of height. It is seen that, as the height or elevation angle is increased, f(h) tends to approach unity.

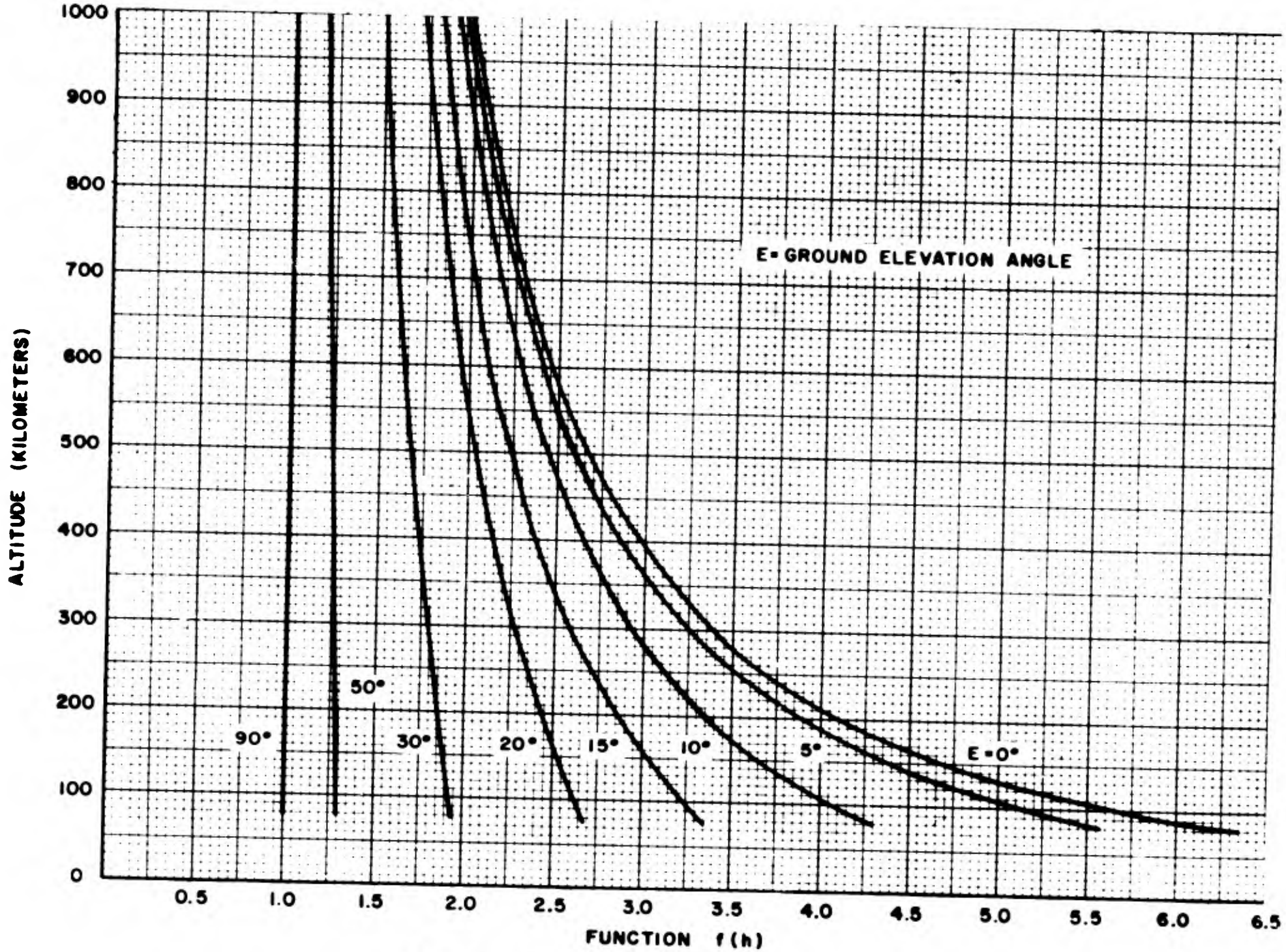

Figure 6.2-1. Ionospheric Function, f(h)

According to the theory of propagation of electromagnetic waves, presented in Section 6-1, the difference in the refractive indices between the ordinary and the extraordinary waves, for quasi-longitudinal propagation, is given by

$$\Delta n = \frac{N_e e^3 H}{2\pi^2 m^2 c f^3} \cos \Theta \qquad (6.2\text{-}10)$$

where N_e is the electron density [electrons/cm^3]; H, the earth's magnetic field (gauss); e, the electron charge [4.8×10^{-10} esu]; m, the electron mass [9.1×10^{-28}gm]; f, the transmission frequency (cycles/sec)

The total two-way polarization rotation (in radians) on substituting Equation (6.2-10) in Equation (6.2-8) becomes

$$\phi (h) = \frac{e^3}{\pi m^2 c^2 f^2} \int_{h_1}^{h_2} f (h) H \cos \Theta N_e \, dh \qquad (6.2\text{-}11)$$

In terms of the values of the known constants, this expression reduces to

$$\phi (h) = \frac{4.7233 \times 10^4}{f^2} \int_{h_1}^{h_2} f (h) H \cos \Theta N_e \, dh \qquad (6.2\text{-}12)$$

where the altitude limits, h_1 and h_2, are in centimeter units. It is noted that the total rotation is directly proportional to the magnetic field and inversely proportional to the square of frequency

In the case of quasi-transverse propagation, it is shown in Section 6-1 that the difference in the refractive indices is

$$\Delta n = -\frac{N_e e^4 H^2}{8\pi^3 m^3 c^2 f^4} \sin^2 \Theta \qquad (6.2\text{-}13)$$

where $89.8^\circ \leq \Theta \leq 90^\circ$ for frequencies in the 100 mc/sec range.

The two-way polarization rotation, therefore, evaluates to

$$\phi (h) = \frac{e^4}{4\pi^2 m^3 c^3 f^3} \int_{h_1}^{h_2} f (h) H^2 \sin^2 \Theta N_e \, dh \qquad (6.2\text{-}14)$$

or simply

$$\phi\,(h) = \frac{6\ 6087 \times 10^{10}}{f^3} \int_{h_1}^{h_2} f\,(h)\, H^2 \sin^2\Theta\, N_e\, dh \qquad (6.2\text{-}15)$$

It is evident that, for this mode of propagation, the polarization is directly proportional to the magnetic field squared and inversely proportional to the cube of frequency.

The calculations of the one-way polarization rotation, plotted in Figure 6.2-2 as a function of elevation angle, are based on the following assumptions; target located at a height of 1000 km; transmission frequency of 100 mc/sec; magnetic field of 0.62 gauss; and longitudinal propagation It is evident that, assuming identical propagation conditions, the polarization shift, from transmission along the horizon is approximately 3.5 times greater than that at an angle of 90 degrees In addition, for a given elevation angle, the daytime shift is on the order of 3 8 times greater than the nighttime effect.

The polarization rotation for the two modes of propagation is shown in Figures 6.2-3 and 6.3-4. It is seen that, for the longitudinal case, the rotation is about 100 times greater than the transverse condition

According to Figures 6.2-5 and 6.2-6, for transmissions at zero degree elevation angle and daytime conditions, 95 per cent of the total polarization shift is attained at a height of 550 km while, for the nighttime distribution, it is reduced to the 470 km level.

According to the theory of propagation of electromagnetic waves, presented in Section 6-1, the difference in the refractive indices between the ordinary and the extraordinary waves, for quasi-longitudinal propagation, is given by

$$\Delta n = \frac{N_e e^3 H}{2\pi^2 m^2 c f^3} \cos \Theta \qquad (6.2\text{-}10)$$

where N_e is the electron density [electrons/cm^3]; H, the earth's magnetic field (gauss); e, the electron charge [4.8×10^{-10} esu]; m, the electron mass [9.1×10^{-28}gm]; f, the transmission frequency (cycles/sec)

The total two-way polarization rotation (in radians) on substituting Equation (6.2-10) in Equation (6.2-8) becomes

$$\phi (h) = \frac{e^3}{\pi m^2 c^2 f^2} \int_{h_1}^{h_2} f(h)\, H \cos \Theta N_e \, dh \qquad (6.2\text{-}11)$$

In terms of the values of the known constants, this expression reduces to

$$\phi (h) = \frac{4.7233 \times 10^4}{f^2} \int_{h_1}^{h_2} f(h)\, H \cos \Theta N_e \, dh \qquad (6.2\text{-}12)$$

where the altitude limits, h_1 and h_2, are in centimeter units. It is noted that the total rotation is directly proportional to the magnetic field and inversely proportional to the square of frequency

In the case of quasi-transverse propagation, it is shown in Section 6-1 that the difference in the refractive indices is

$$\Delta n = -\frac{N_e e^4 H^2}{8\pi^3 m^3 c^2 f^4} \sin^2 \Theta \qquad (6.2\text{-}13)$$

where $89.8^\circ \leq \Theta \leq 90^\circ$ for frequencies in the 100 mc/sec range.

The two-way polarization rotation, therefore, evaluates to

$$\phi (h) = \frac{e^4}{4\pi^2 m^3 c^3 f^3} \int_{h_1}^{h_2} f(h)\, H^2 \sin^2 \Theta N_e \, dh \qquad (6.2\text{-}14)$$

or simply

$$\phi\,(h) = \frac{6.6087 \times 10^{10}}{f^3} \int_{h_1}^{h_2} f\,(h)\, H^2 \sin^2\Theta\, N_e\, dh \qquad (6.2\text{-}15)$$

It is evident that, for this mode of propagation, the polarization is directly proportional to the magnetic field squared and inversely proportional to the cube of frequency.

The calculations of the one-way polarization rotation, plotted in Figure 6.2-2 as a function of elevation angle, are based on the following assumptions; target located at a height of 1000 km; transmission frequency of 100 mc/sec; magnetic field of 0.62 gauss; and longitudinal propagation. It is evident that, assuming identical propagation conditions, the polarization shift, from transmission along the horizon is approximately 3.5 times greater than that at an angle of 90 degrees In addition, for a given elevation angle, the daytime shift is on the order of 3 8 times greater than the nighttime effect.

The polarization rotation for the two modes of propagation is shown in Figures 6.2-3 and 6.3-4. It is seen that, for the longitudinal case, the rotation is about 100 times greater than the transverse condition

According to Figures 6.2-5 and 6.2-6, for transmissions at zero degree elevation angle and daytime conditions, 95 per cent of the total polarization shift is attained at a height of 550 km while, for the nighttime distribution, it is reduced to the 470 km level.

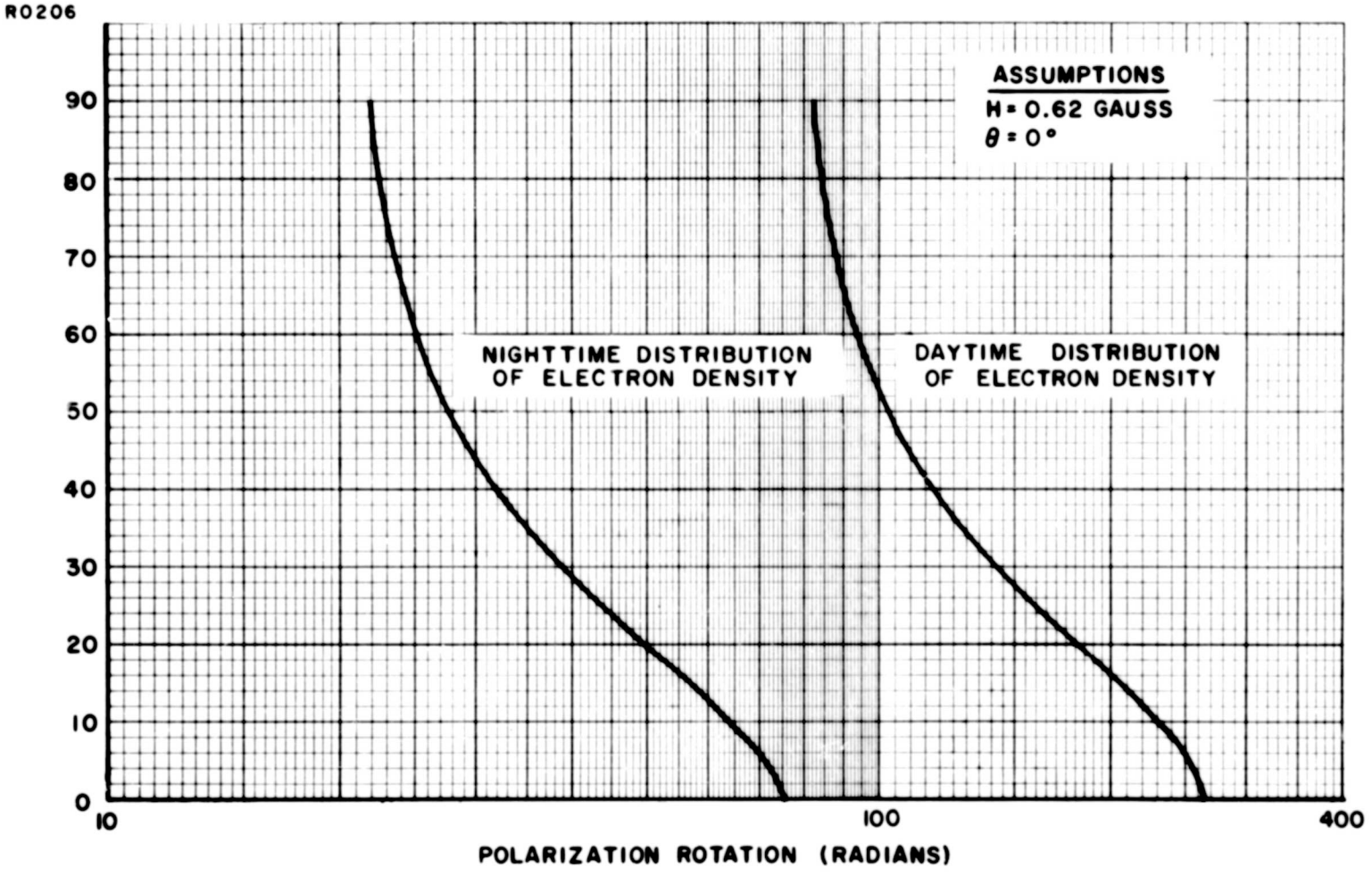

Figure 6.2-2. Polarization Rotation at 100 mc. for Target at 1000 km. Height, Two-Way Transmission Path and Longitudinal Propagation

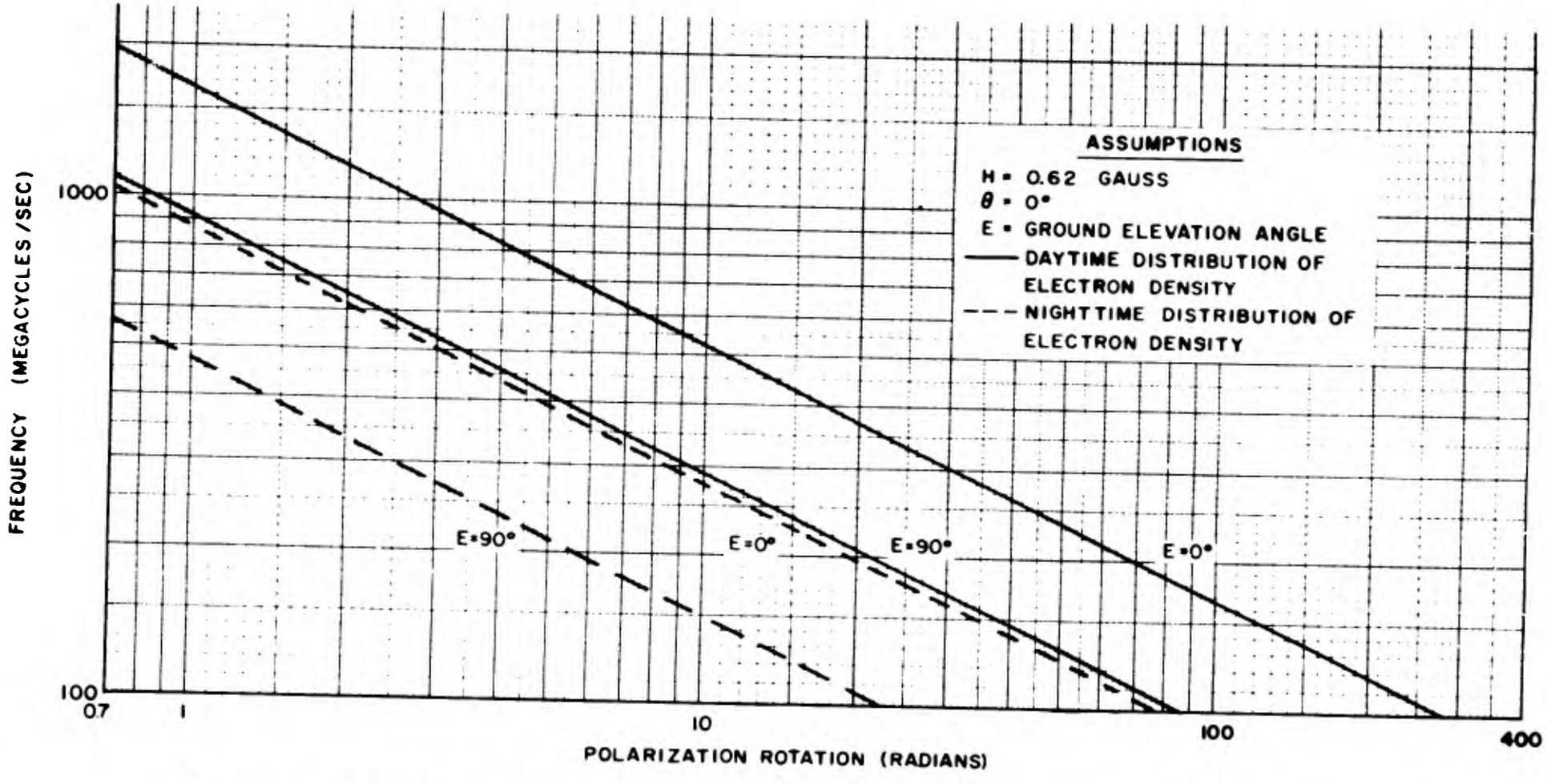

Figure 6. 2-3. Polarization Rotation as a Function of Frequency for a Target at 1000 km Height, Two-Way Transmission Path and Longitudinal Propagation

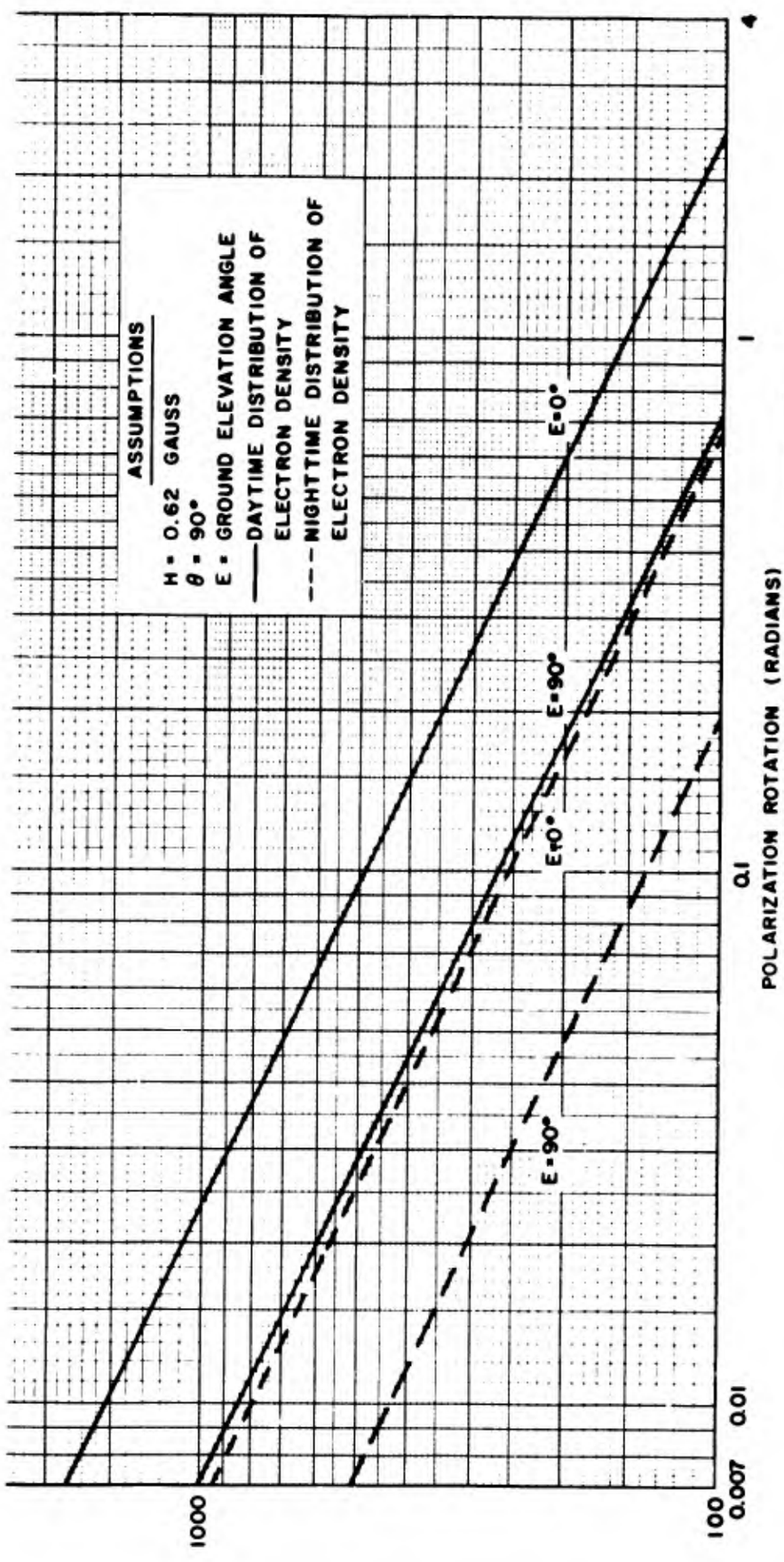

Figure 6. 2-4. Polarization Rotation as a Function of Frequency for a Target at 1000 km Height, Two-Way Transmission Path and Transverse Propagation

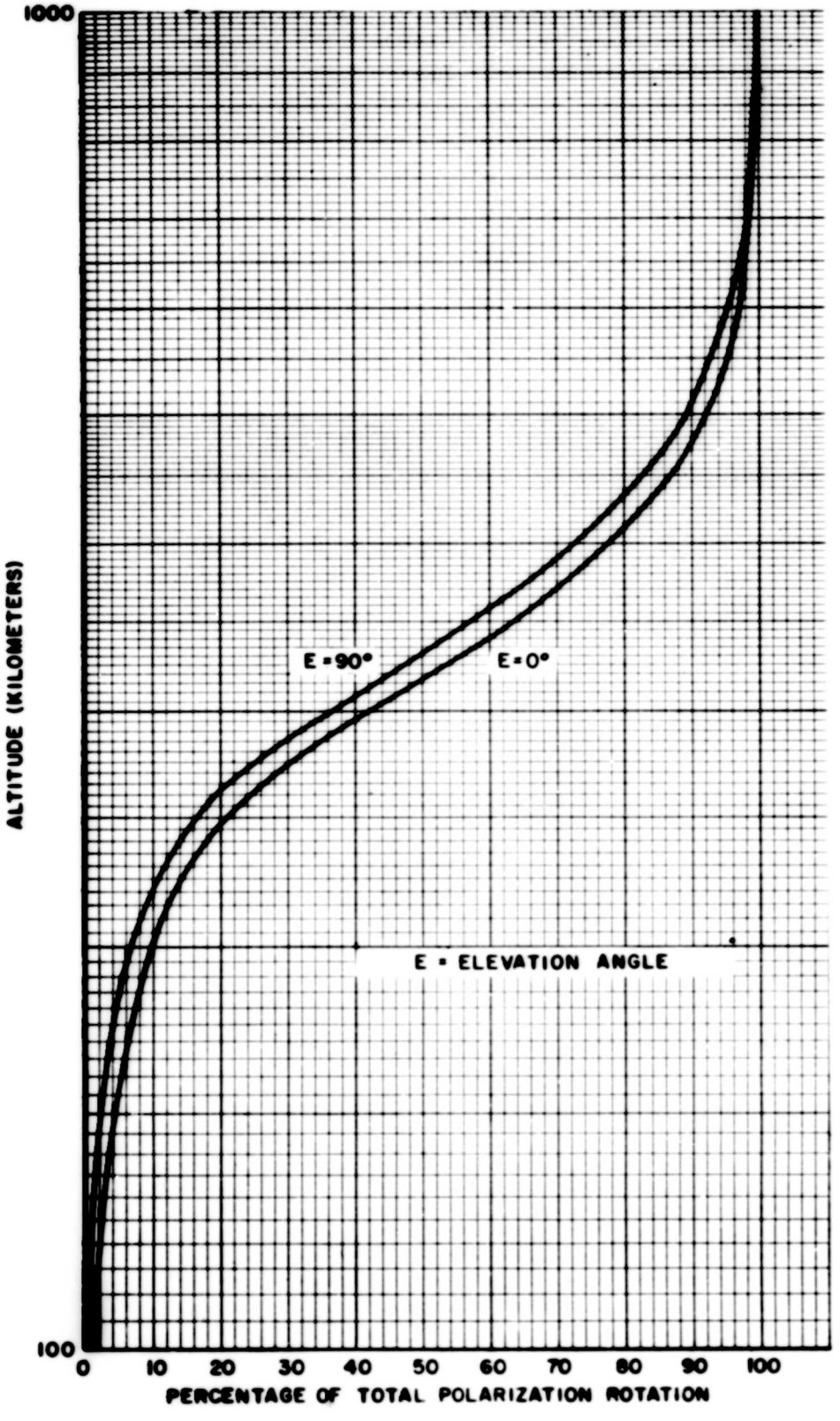

re 6.2-5. Percentage of Total Polarization Rotation as a Function of Altitude for Daytime Distribution of Electron Density

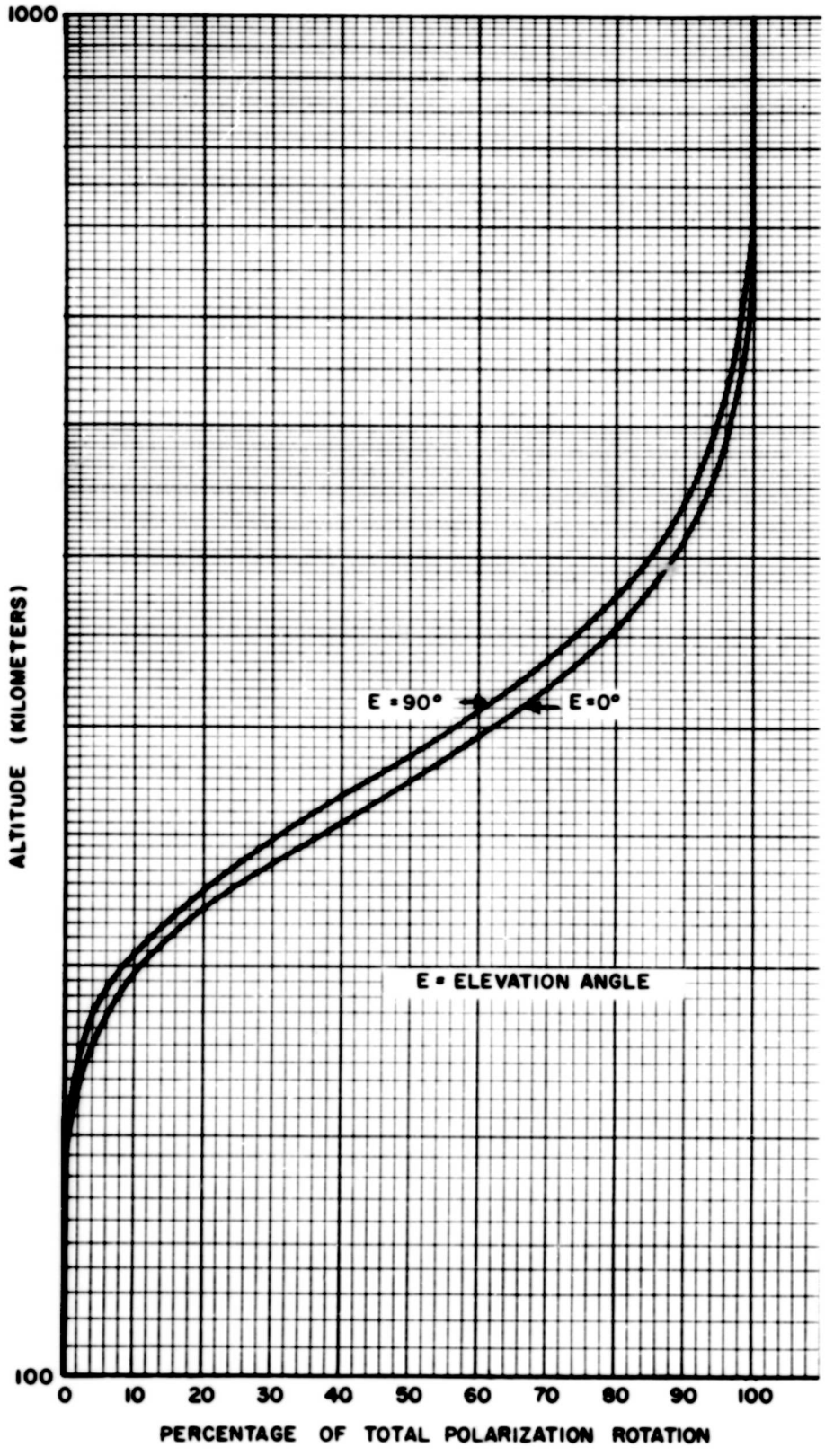

Figure 6.2-6. Percentage of Total Polarization Rotation as a Function of Altitude for Nighttime Distribution of Electron Density

6 3 - ATMOSPHERIC ATTENUATION OF RADIO WAVES

A. TROPOSPHERIC ATTENUATION

The absorption of radio waves in the lower atmosphere is the result of the presence of both free molecules and suspended particles such as dust grains and water drops condensed in fog and rain. In a non-condensed atmosphere, oxygen and water vapor are the substances which cause absorption

Theoretical calculations of the anticipated absorption of electromagnetic waves by oxygen and water vapor have been made by Van Vleck (1). His values of the decay constant of oxygen at frequencies of 300 mc/sec, 1000 mc/sec, 3000 mc/sec and 10,000 mc/sec are 0.0014 db/km, 0 0050 db/km, 0.0066 db/km, and 0.0072 db/km, respectively.

The theoretical values of the ratio of water vapor absorption to the density of water vapor at 3000 mc/sec and 10,000 mc/sec are 0.000025 and 0.00039 db/km per gm/m^3, respectively. At temperate latitudes in the summer with a temperature of 20°C, the water vapor density is about 7.5 gm/$meter^3$. At saturation at 20°C, this value may be as high as 17 gm/$meter^3$. It is quite apparent, therefore, that for frequencies below 3000 Mc/sec, the attenuation by water vapor will be negligible.

It should be mentioned that at certain regions of the electromagnetic frequency spectrum, the absorption by oxygen and water vapor are a maximum because of resonance effects. For oxygen, the region occurs at wavelengths in the vicinity of 0.25 cm and 0.5 cm. At the latter wavelength, the decay constant is approximately 14 db/km. For water vapor, at the resonance wavelength of 1.35 cm, the absorption is 0.020 db/km per gm/m^3.

The decay constant, γ, is related to the amplitude, a, by the function

$$a = 10^{-0.05\gamma L} \qquad (6.3\text{-}1)$$

where L is the effective path length. The decrease in signal strength, for a radio wave traversing an absorbing region, is in addition to the free space or inverse square law attenuation.

The total two-way attenuation due to oxygen, as predicted by Van Vleck, is shown in Figure 6.3-1 These curves were derived on the assumption that the oxygen content is effective to an altitude of 25,000 feet It is seen that, for an elevation angle of 3°, 1.6 db absorption can be anticipated at 3000 mc/sec The absorption of water vapor at this frequency is quite insignificant.

The experimental observations of Aarons, Barron and Castelli (2) at 9350 mc/sec indicate an atmospheric attenuation on the order of 0 00585 db/km. Their results which are also plotted in Figure 6 3-1 are slightly less than the theoretical values.

The extremes of atmospheric absorption, as estimated by Gardner (3), are shown in Figure 6 3-2. For a ray tangent to the earth's surface, there is a difference in the

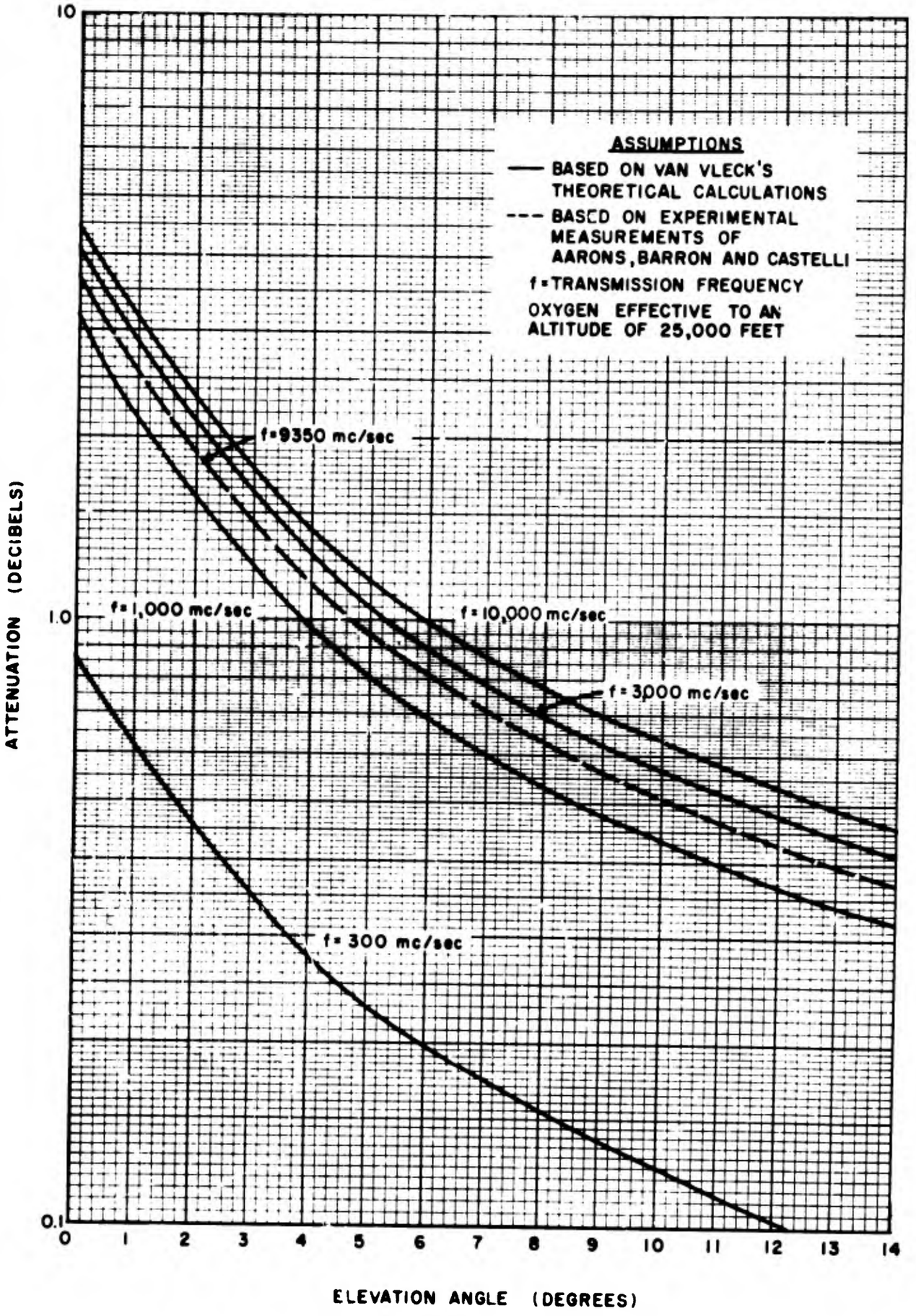

Figure 6.3-1. Attenuation in the Troposphere due to Oxygen, Two-Way Transmission Path

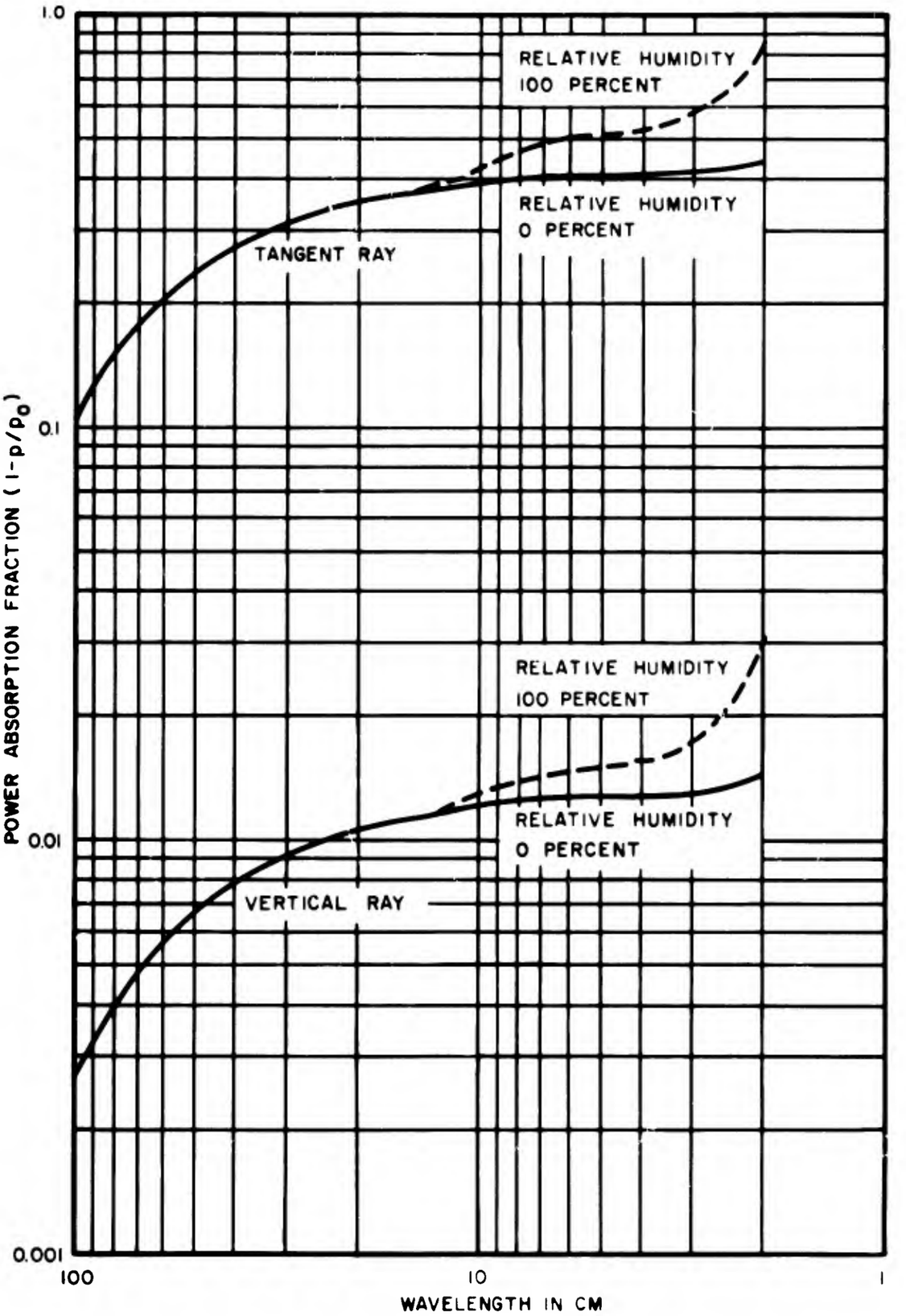

ure 6.3-2. One-Way Atmospheric Absorption Extremes as a Function of Wavelength (after Gardner)

absorption of 0.25 db between an atmosphere with one hundred per cent relative humidity and one with zero per cent relative humidity. According to Gardner's calculations, at 10 cm, the maximum atmospheric attenuation for a two-way propagating path is approximately 4.7 db. This value compares favorably with the data presented in Figure 6.3-1.

With regard to the effect of rain clouds and storms on radio wave transmissions, Hitschfeld and Marshall (4) express the one-way radar attenuation by rain, A, in decibels by the relationship

$$A = K R r \tag{6.3-2}$$

where R is the rate of rainfall in mm/hour and r is the path lengh of the intervening rain in miles. The value of the parameter, K, in db $[\text{mm hour}^{-1}\ \text{mile}]^{-1}$, corresponding to an R of about 30 mm/hour, is 0.00098, 0.013, 0.08 for a frequency of 3000 mc/sec, 5250 mc/sec and 9350 mc/sec.

Figure 6.3-3 is a plot of the two-way attenuation based on Hitschfeld's and Marshall's data for an assumed heavy rainfall of 30 mm/hour. At a frequency of 3000 mc/sec and a storm path of 20 miles, the two-way signal attenuation evaluates to approximately 1.2 db.

B IONOSPHERIC ATTENUATION

An electromagnetic wave passing through an ionized medium imposes a periodic force on the electrons, causing them to vibrate. The absorption of signal energy occurs when the electrons, colliding with other particles, are forced to give up some of their energy to these particles.

To determine the total absorption of electromagnetic waves traversing the ionosphere, it is necessary to consider the familiar problem of a plane wave in a homogeneous, partially-conducting dissipative medium. The field intensity can be expressed in the form

$$E = E_o e^{j\omega(t - qs)} \tag{6.3-3}$$

or

$$E = E_o e^{-ks}\, e^{j\omega(t - \frac{s}{V_p})} \tag{6.3-4}$$

where

$$q = \frac{1}{c}\left(n - j\frac{ck}{\omega}\right) \tag{6.3-5}$$

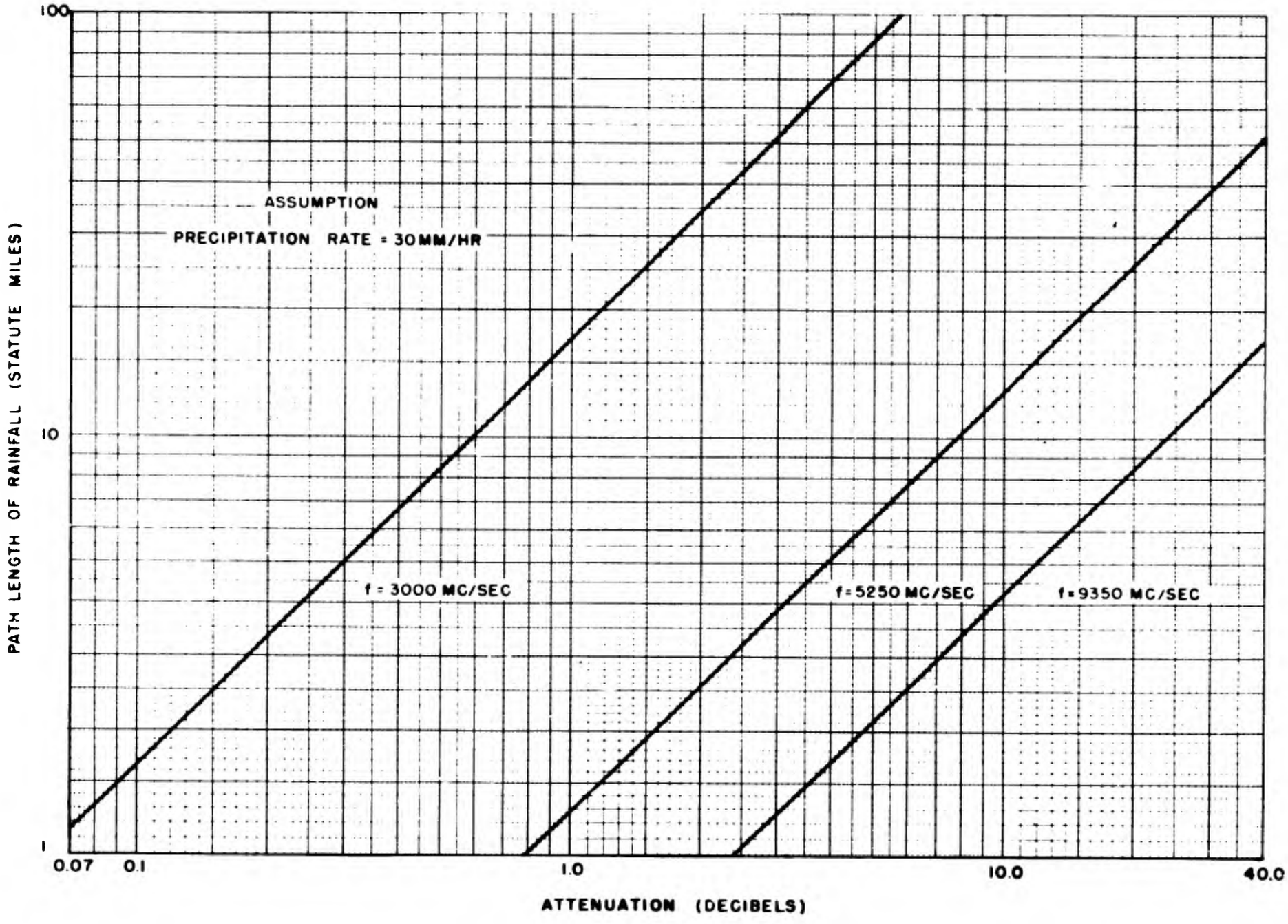

Figure 6.3-3. Attenuation due to Rainfall, Two-Way Transmission Path

and n is the index of refraction of the medium; V_p, the phase velocity of the wave; k, the absorption coefficient of the medium; and c, the velocity of light in free space. The factor e^{-ks}, indicates that the amplitude of the wave is attenuated logarithmically with increasing distance, s. The total attenuation, A, in decibels is given by the integral

$$A = 20 \log e^{-\int_{s_1}^{s_2} k\, ds} \tag{6.3-6}$$

or

$$A = -8.68 \int_{s_1}^{s_2} k\, ds \tag{6.3-7}$$

where s_1 and s_2 are the limits of the path.

In the ionosphere, there are two types of absorption; (1) non-deviative absorption and (2) deviative absorption. The term, non-deviating region absorption, is ordinarily given to absorption in a medium where the frequency is sufficiently high that the ray is not bent back for reflection. In such a case, the index of refraction does not differ greatly from unity. When the refractive index is much less than one, resulting in considerable deviation of the wave from its original direction of propagation, the absorption is called deviating. In the deviating region, the index of refraction varies from point to point along the traversed path. For transmissions in the ionosphere at frequencies above 100 Mc/sec, it is evident from Sections 5.2 and 5.4 that non-deviative absorption is predominant.

It has been shown in Section 6.1 that, when the earth's magnetic field is neglected and the transmitted frequency is greater than the electron collision frequency, the latter being valid for frequencies in the VHF range, the absorption coefficient of the medium, k, is given by

$$k = \frac{N_e e^2 \nu}{2\pi cnmf^2} \tag{6.3-8}$$

where N_e is the electron density; e, the electron charge; m, the electron mass; ν, angular collision frequency, and f, the transmission frequency.

Substituting Equation (6 3-8) in Equation (6.3-7) and assuming non-deviative type of absorption, $n \cong 1$, the total attenuation becomes

$$A\,(db) = -(8.68)\, \frac{e^2}{2\pi\, cmf^2} \int_{h_1}^{h_2} f(h)\, N_e\, \nu\, dh \tag{6.3-9}$$

where the path differential, ds, is expressed in terms of the height differential by

$$ds = f(h)\, dh \tag{6.3-10}$$

As discussed in Section 6.2, the function, f(h) is given by

$$f(h) = \frac{r_o + h}{\left[(r_o + h)^2 - (r_o \cos E)^2\right]^{\frac{1}{2}}} \tag{6.3-11}$$

where r_o is the radius of the earth, h, the height above the earth's surface, and E, the elevation angle.

The ionospheric attenuation at 100 mc/sec for a one-way transmission path is plotted as a function of elevation angle in Figure 6.3-4. These calculations are based on the model of collision frequency and the two models of electron density described in Section 5.2.

As shown in Figure 6.3-5, for the daytime model at zero degree and 90 degree elevation angle, 90 per cent of the total attenuation is attained at a height of 110 km and 116 km, respectively.

Figure 6.3-6 is a plot of ionosphere attenuation as a function of frequency. It is seen that the attenuation is inversely proportional to the square of frequency, with the daytime absorption being considerably greater than the nighttime effect.

Ionospheric attenuation under abnormal conditions, such as aurora, is of extreme interest. The observations of 81.5 Mc/sec extra-terrestrial signals from discrete sources by Little and Maxwell (5) showed a decrease in signal amplitude of about 10 per cent during an aurora.

Little (6) has reported that 65 mc/sec extra-terrestrial radio waves have also undergone absorption during aurorae. He found that the frequency of occurence of absorption in excess of 10 per cent to be most prevalent at midday and least frequent during the evening. The absorption was strongly correlated with polar blackout, a condition in which low frequency pulsed radio waves vertically incident in the ionosphere are no longer reflected and are completely absorbed. In addition, his results also indicated good correlation between auroral absorption and geomagnetic K indices which are a measure of the activity of the earth's magnetic field.

C. REFERENCES

1. Kerr, D E.; "Propagation of Short Radio Waves", Radiation Laboratory Series, Vol 13, McGraw-Hill Book Co., 1951.

2. Aarons, J., Barron, W R. and Castelli, J P., "Radio Astronomy Measurements at VHF and Microwaves", Proceedings of the IRE, Vol 46, pp 325-335, Jan 1958.

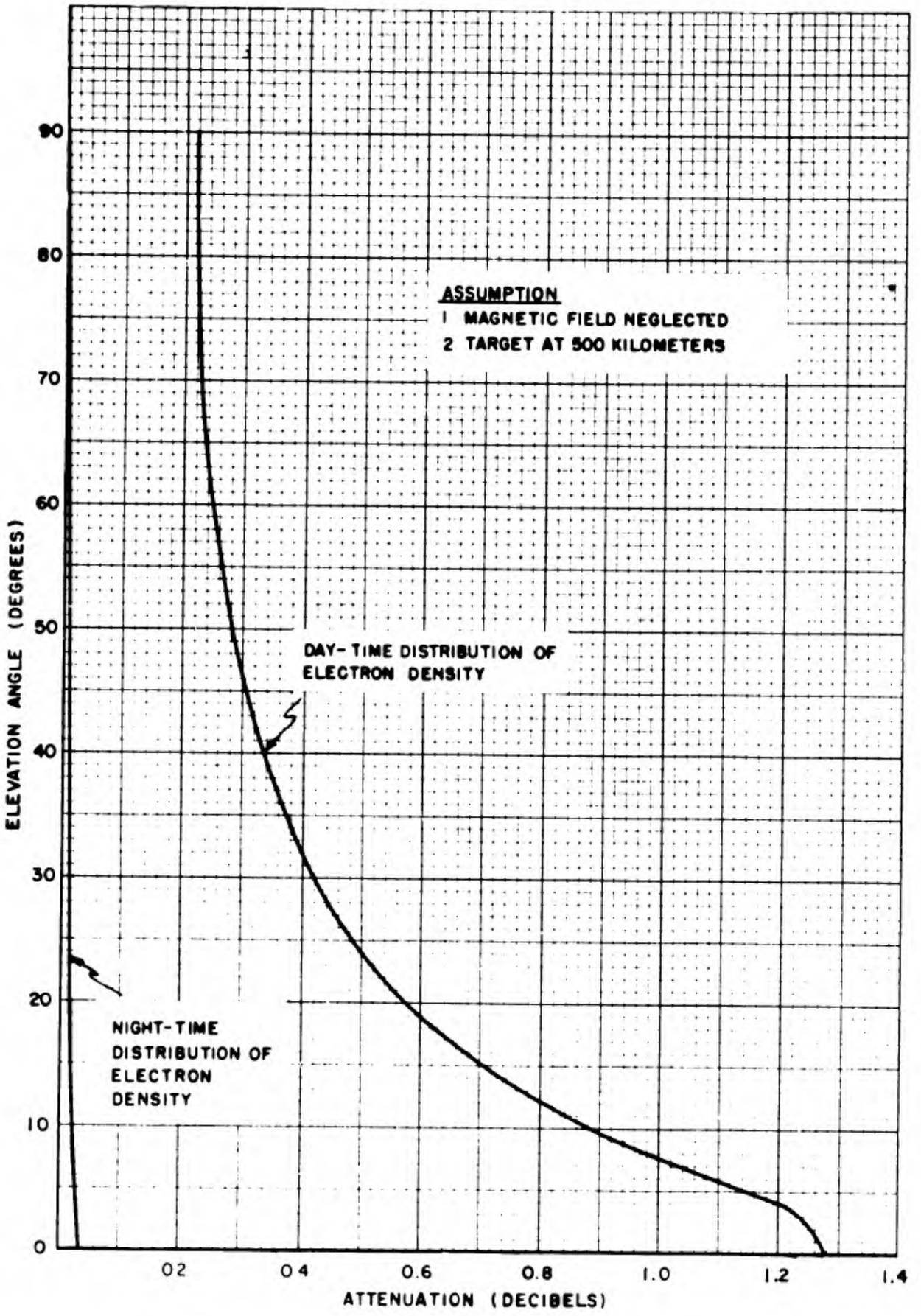

Figure 6.3-4. Ionospheric Attenuation at 100 mc., One-Way Transmission Path

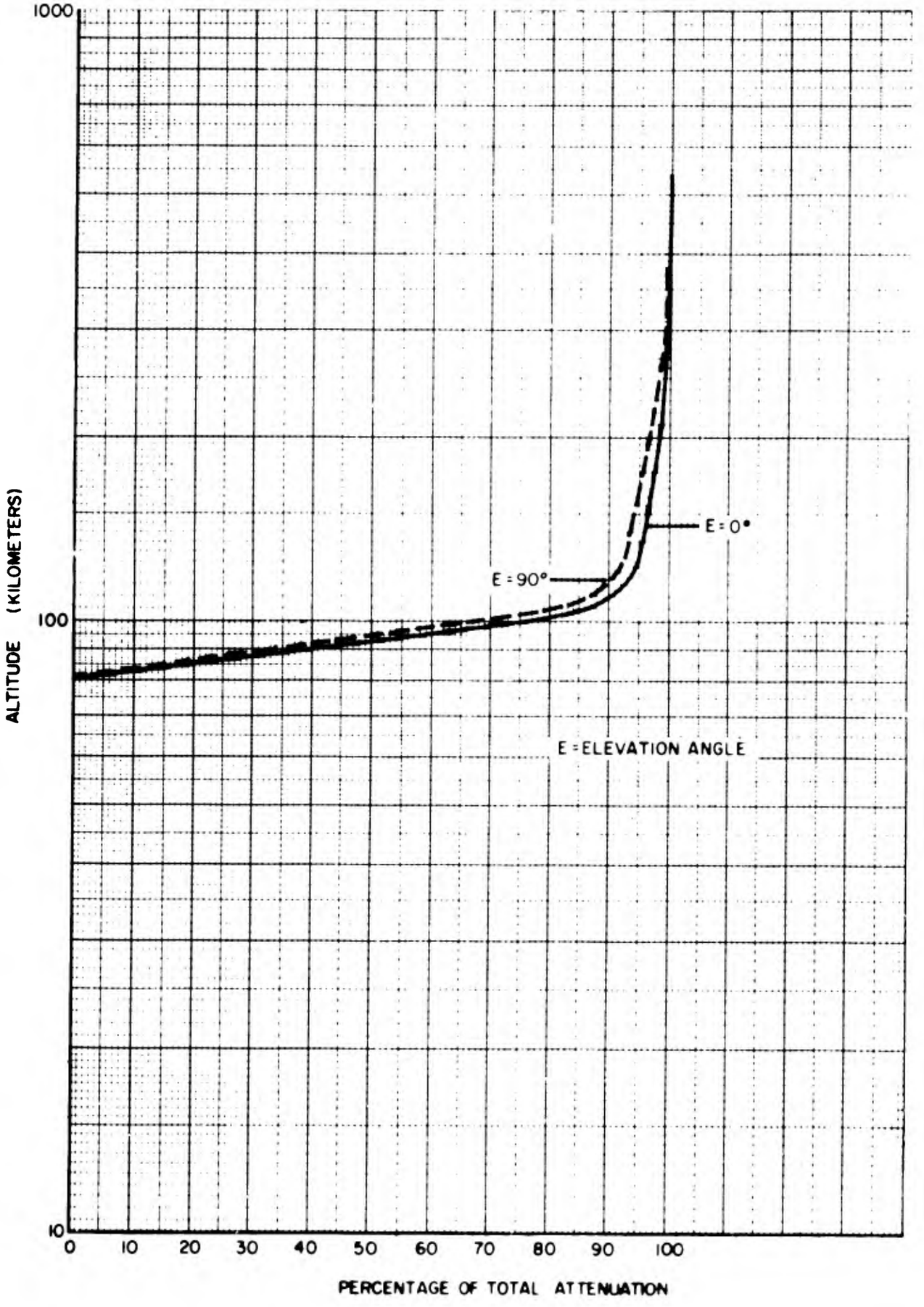

Figure 6.3-5. Percentage of Ionospheric Attenuation as a Function of Altitude for Daytime Distribution of Electron Density

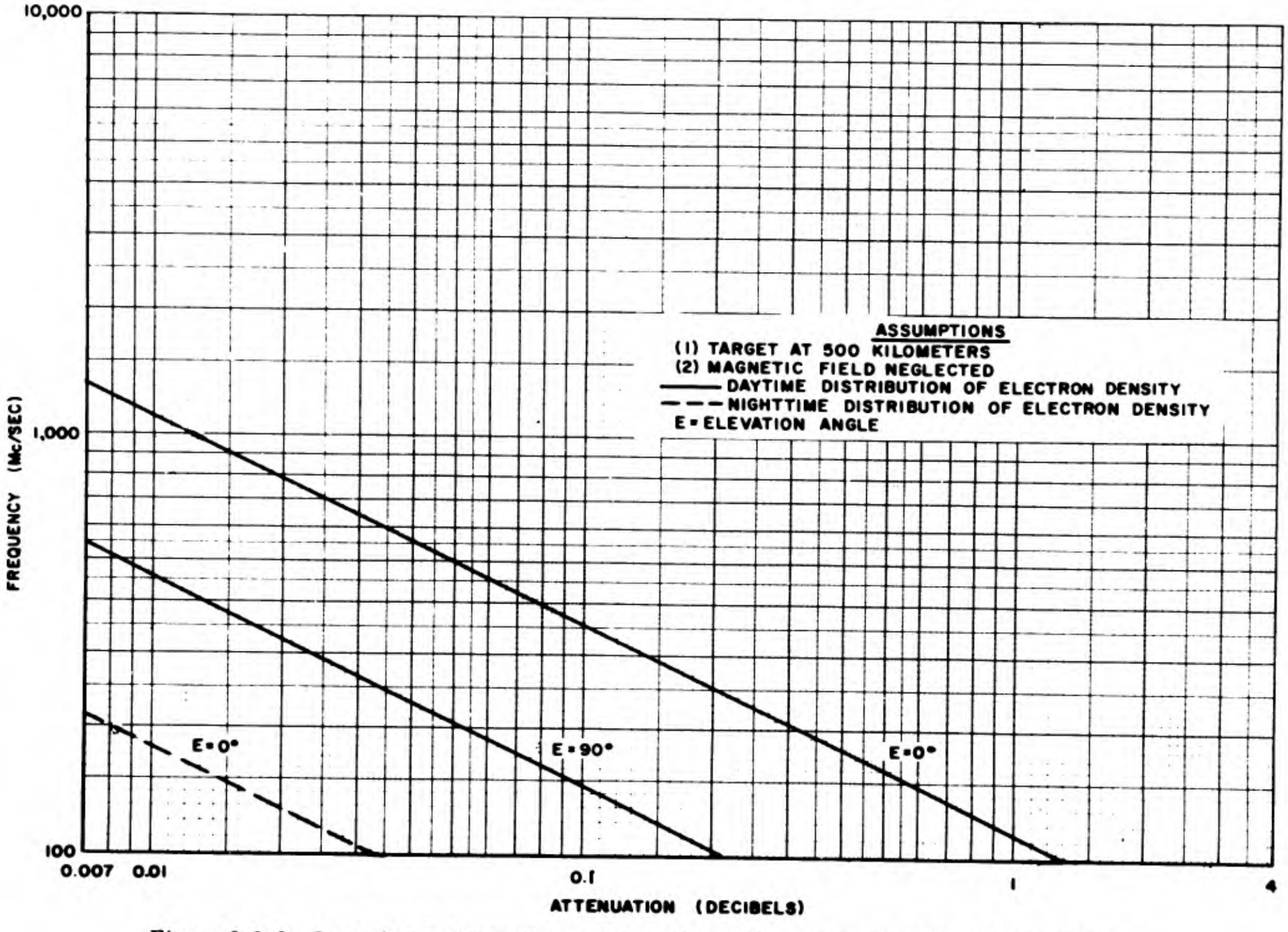

Figure 6.3-6. Ionospheric Attenuation as a Function of Frequency, One-Way Transmission Path

3. Gardner, R.; "Antenna Noise Temperature Study", Airborne Instruments Laboratory, Final Engineering Report, Contract DA-49-170sc-1547.

4 Hitschfeld, W. and Marshall, J.S.; "Effect of Attenuation on the choice of Wavelength for Weather Detection by Radar", Proceedings of the IRE, Vol 42, pp 1165-1168, July 1954.

5. Little, C. G. and Maxwell, A., "Scintillation of Radio Stars During Aurorae and Magnetic Storms", Journal of Atmospheric and Terrestrial Physics, Vol. 2, p 356, 1952.

6. Little, C. G.; "High Latitude Ionospheric Observations Using Extra-Terrestrial Radio Waves", Proceedings of the IRE, Vol. 42, p 1700,Nov. 1954.

6 4 - THE AURORA

A. GENERAL CONSIDERATIONS

1. INTRODUCTION

The auroral phenomena, according to present-day concepts, are believed to be produced by high-speed charged particles or corpuscular matter which are ejected from the sun during a solar flare and then guided to the polar regions by the action of the earth's magnetic field

The intense ultra-violet radiation which is also emitted during a solar eruption appears almost simultaneously with the observed solar flare in the form of ionization changes in the earth's atmosphere Auroral activity is very closely related to earth current fluctuations, intense geomagnetic variations and disturbed ionospheric conditions in the polar region.

The aurora is observable as a luminous display in the northern and southern polar regions. In the northern latitude it occurs most frequently in the region of 67^{o} geomagnetic latitude On either side of this zone, the frequency of auroral activity decreases. The lower altitude limit of the aurora is at approximately 100 kilometers and the upper limit, which is the level of sunlit aurora maximum, at about 1100 kilometers. Some of the many different classifications of the visual aurora are homogeneous arcs, homogeneous bands, pulsating arcs, pulsating surfaces, arcs with ray structure, bands with ray structure, glows, draperies, rays and aurora.

2. AURORAL REFLECTIONS

Radio reflections from the aurora were first observed by Harang and Stoffregen in 1938 (1) at a frequency of 40 mc/sec and at ranges of 400-700 km. Lovell, Clegg and Ellyett (2) using meteor detection equipment operating at a frequency of 46 mc/sec obtained echoes apparently from a luminescent cloud at the end of an auroral stream at ranges of the order of 460-480 km.

Auroral echoes at 30 mc/sec have been reported by McKinley and Millman (3). Most of the echoes occurred between 300-700 km although some appeared as close as 150 km. Assuming that the drift in the range of auroral echoes represents radial velocities, they obtained values of velocity ranging from 500-800 meters/sec. These velocities are approximately the same as those found by Störmer for the slow drift of auroral formations over the surface of the earth

Aspinall and Hawkins (4) experimental results at 72 mc/sec indicate that diffuse auroral echoes were visible at ranges of 600-800 km and that discrete echoes appeared at ranges of 400-900 km with durations of the order of 100 seconds. The

diffuse echoes were apparently correlated with visual glows and arcs and the discrete echoes with auroral rays. Drift velocities of both discrete and diffuse echoes were observed to lie within 1.0 - 1.5 km/sec.

Auroral echoes were simultaneously recorded at 56 mc/sec and 106 mc/sec by Currie, Forsyth and Vawter (5) It appeared that echoes occurred when the auroral forms exhibited some ray structure and then only from parts of the aurora which are at elevation angles less than 15^{o} above the horizon The height distribution of the centers from which the echoes appeared to originate were in the E-layer of the ionosphere between 105-118 km, corrected for atmospheric refraction These results agree closely with the height distributions of photographic observations of aurora. McNamara and Currie's analysis of this auroral data (6) has shown that the echoes observed at these two frequencies were due to direct reflections from auroral structures. The echo range distribution on 56 mc/sec was between 500-1100 km with the maximum number of echoes occurring between 700-800 km.

3 CHARACTERISTICS OF AURORAL ECHOES

Auroral echoes have been found to have rapid and erratic amplitude fluctuations Amplitude measurements by Bowles (7, 8) at 50 mc/sec and 145 mc/sec have shown that the power-spectrum of the fading has frequency components of roughly equal strength from zero frequency to a cut-off frequency between 100 cycles/sec and 400 cycles/sec According to Booker (9), the fading of auroral echoes may be due to a wind-like motion of the scattering columns of ionization but with speeds up to ten times greater than the wind movements associated with a quiet ionosphere The most probable value of wind magnitudes in the normal E-layer, as reported by Millman (10), seems to range between 40-90 meters/sec.

Variations in the polarization of radio echoes from the aurora have been noted in the investigations of McNamara and Currie (11) The observations were made at frequencies of 56 mc/sec and 106 5 mc/sec The transmitted signals were horizontally polarized and were received on both vertically and horizontally polarized antennae Based on 66% of 489 measurements at 56 mc/sec, the most probable ratio, horizontal to vertical component of field strength, was 1 1 and the mean power ratio was 3 db. For the remaining 34% of the measurements, the received signal was horizontally plane polarized. The mean power ratio was 5 db for all the measurements. The polarization ratios often differed widely for echoes occurring simultaneously at different ranges It was often noted that the polarization changed from plane to the de-polarized state, or vice versa, within a few minutes Seventy-eight observations on 106 5 mc/sec showed no change in the state of polarization. On 56 mc/sec, a definite polarization ratio dependence on range was found the maximum mean polarization ratio being located between 550-650 km It has been suggested that multiple scattering within the reflecting region could cause the de-polarization of the signals

Harang and Landmark (12, 13) have reported that, at a frequency of 35 mc/sec, auroral echoes were sometimes completely depolarized and other times nearly plane polarized. At 74 mc/sec, there was no change in the plane of polarization from that of the transmitted signal.

4. RADIO NOISE FROM AURORA

The existence of noise that appeared to emanate from the aurora was found by Forsyth, Petrie and Currie (14) They detected pulses of 1-5 μsec in duration at a frequency of 3000 mc/sec The pulses were most numerous when the antenna was directed at bright active types of aurora. An attempt to repeat this experiment by Chapman and Currie (15) was unsuccessful They attributed the failure to detect the auroral radio noise to the decrease in the intensity of auroral displays and sunspot activity.

5. RECENT EXPERIMENTAL MEASUREMENTS

The azimuth distributions of auroral echoes have indicated the existence of some form of aspect sensitivity It has been clearly established that the echoes are most frequenty obtained when the radar antenna beam is oriented toward the magnetic north pole. Dyce's observations (16) at 51 7 mc/sec show a scatter in angle about magnetic north of the order of ±60 degrees.

According to the experimental investigations of the Lincoln Laboratory (17), the University of Alaska (18) and the Defense Research Telecommunications Establishment (19), it appears that, in order to detect radar-auroral reflections, the direction of electromagnetic propagation must be nearly perpendicular to the auroral ionization which is presumably aligned along the lines of force of the earth's magnetic field. In addition to the requirement of perpendicularity, it is necessary that this geometric condition take place at ionospheric heights (80 km and above) and in geographic regions of high auroral activity

With regard to the aspect sensitivity of auroral echoes, the recent Stanford Research Institute results (20) reveal that at a frequency of 216 mc/sec, 398 mc/sec and 780 mc/sec, the maximum off perpendicular angle which gave rise to auroral reflections were 12°, 10° and 6°, respectively These data imply the possible existence of a frequency dependence for the angle between the direction of propagation and the earth's magnetic field

An estimate of the frequency dependence of the reflected echo power obtained from non-simultaneous data at three frequencies, as reported by the Stanford Research Institute (20), indicates that when the target, i.e., the auroral ionization, does not fill the antenna beam (discrete-type-echo), the dependency is given by

$$\frac{P_{f_1}}{P_{f_2}} \propto \left(\frac{f_2}{f_1}\right)^{5 \pm 2}$$

where P_{f1} and P_{f2} are the reflected powers associated with the frequencies, f_1 and f_2, respectively

When the target fills the antenna beam (diffuse-type-echo), the power frequency relationship is

$$\frac{P_{f_1}}{P_{f_2}} \propto \left(\frac{f_2}{f_1}\right)^{3-2}$$

From radar-auroral observations at 488 mc/sec and 944 mc/sec, Blevis reports an approximate fourth power-frequency dependence for the discrete-type echo (21)

As for auroral-Doppler effects, maximum Doppler shifts of ±6 kc/sec have been noted at 398 mc/sec (20). In addition to being shifted, the spectrum of the auroral signal is also spread by as much as 3 kc/sec Doppler components of as much as 3 db above noise have been observed at frequencies as far removed as ±4 kc/sec from the carrier frequency of 488 mc/sec (21)

B. THEORIES OF AURORAL REFLECTIONS

1 INTRODUCTION

There are two basic differences in the theories which attempt to explain the mechanism of auroral reflections One hypothesis is that, in order to detect auroral echoes, the radar beam must be perpendicular to the auroral ionization which is aligned along the lines of the earth's magnetic field The other hypothesis, which rejects the perpendicular requirement, states that auroral echoes are the result of scattering from highly ionized regions present during auroral disturbances at E-layer heights.

As discussed below, the partial reflection theory and the Booker-Gordon scattering theory are proponents of the former hypothesis while the critical reflection theory advances the latter

2 PARTIAL REFLECTION THEORY

This theory, as advocated by Herlofson (22), assumes that the electromagnetic radiation is at normal incidence to the large plane surface which forms the boundary between the ionized and the nonionized regions If the ionized region were large and the boundary sharp, the free electron density within the aurora need not be greater than the density of the daytime E-layer to produce auroral reflections.

The power received by a receiving antenna in free space which is separated by a distance, R, from a transmitter is given by

$$P_r = \left(\frac{P_t G_t}{4\pi R^2}\right) A_r \qquad (6\ 4\text{-}1)$$

where P_t is the transmitted peak power, and G_t is the gain of the transmitting antenna relative to an isotropic antenna The parameter, A_r, is the effective area of the receiving antenna defined by

$$A_r = \frac{G_r \lambda^2}{4\pi} \qquad (6.4\text{-}2)$$

where G_r is the gain of the receiving antenna relative to an isotropic antenna. The term in the parenthesis is the power density of the transmitted wave at the receiving antenna.

If the signal is returned to a radar transmitting-receiving system from a perfectly reflecting plane surface located at a distance, R, the distance traversed by the wave is 2R. The received signal power becomes

$$P_r = P_t G^2 \left(\frac{\lambda}{8\pi R}\right)^2 \qquad (6\ 4\text{-}3)$$

where $G = G_t = G_r$

This equation can be rewritten as

$$A_o^2 P_r' = P_t G^2 \left(\frac{\lambda}{8\pi R}\right)^2 \qquad (6.4\text{-}4)$$

where A_o is the numerical amplitude of the signal and P_r' is the received power corresponding to a signal having unity amplitude

If the reflecting plane surface is not a perfect reflector, the power received is somewhat less The decrease in power is directly proportional to the power reflection coefficient of the surface In other words, Equation (6 4-4) is modified to

$$A_o^2 P_r' = P_t G^2 \left(\frac{\lambda}{8\pi R}\right)^2 \rho_p \qquad (6.4\text{-}5)$$

where ρ_p is the power reflection coefficient

For an electromagnetic wave at normal incidence to the boundary separating two media having different indices of refraction, n_1 and n_2, the reflection coefficient for power (23) is

$$\rho_p = \frac{(n_1 - n_2)^2}{(n_1 + n_2)^2} \qquad (6\ 4\text{-}6)$$

In the case of the ionosphere it has been shown that the index of refraction, n, neglecting electron collision frequency and the earth's magnetic field is given by (see Section 6 1)

$$n = \left[1 - \frac{4\pi N_e e^2}{m\omega^2} \right]^{\frac{1}{2}} \qquad (6\ 4\text{-}7)$$

where N_e is the electron density, and e and m are the electron charge and electron mass, respectively

Assuming that the transmitting frequency is greater than the critical frequency of the ionospheric medium which implies that

$$\omega^2 >> \frac{4\pi N_e e^2}{m}$$

then to a first approximation

$$n \approx 1 - \frac{2\pi N_e e^2}{m\omega^2} \qquad (6\ 4\text{-}8)$$

Substituting Equation (6 4-8) in Equation (6 4-6) and assuming that one medium is free space with unity refractive index, then the power reflection coefficient reduces to

$$\rho_p \approx \left(\frac{N_e e^2}{4\pi mf^2} \right)^2 \qquad (6\ 4\text{-}9)$$

The amplitude reflection coefficient, ρ_A, which is the square root of the power reflection coefficient, is plotted in Figure 6.4-1 as a function of electron density and frequency. It is evident that for frequencies above 100 mc/sec and for a normal F_2-layer maximum electron density, $\rho_A \cdots 1$

Substituting Equation (6 4-9) in Equation (6 4-5), it follows that

$$A_o = \frac{N_e e^2 cG}{32\pi^2 mRf^3} \left(\frac{P_t}{P'_r} \right)^{\frac{1}{2}} \qquad (6.4\text{-}10)$$

It is noted that the amplitude of the received signal is inversely proportional to the third power of frequency This implies that the amplitude of an auroral echo at frequency, f, is about 18 db below the echo amplitude reflected at a frequency, 1/2 f This analysis, of course assumes identical antenna gains and transmitter powers for both frequencies

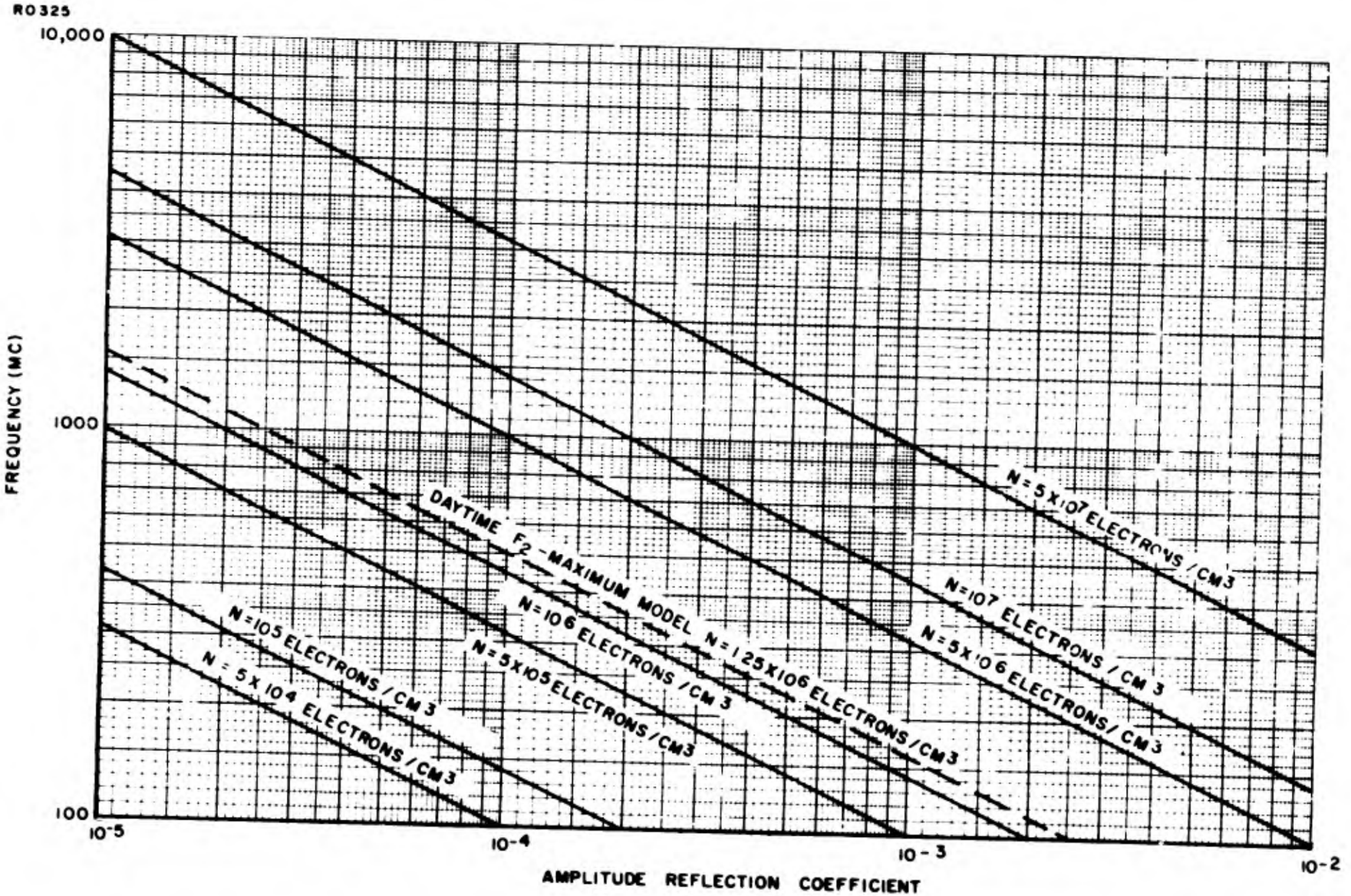

Figure 6.4-1. Amplitude Reflection Coefficient as a Function of Electron Density

To be more realistic in comparing the amplitude ratio of auroral echoes received at two different frequencies, transmitting and receiving systems with identical performances and characteristics should be employed In essence, this requires that the product of $(P_t G_t A_r)$ be a constant for both frequencies It necessarily follows that the echo amplitude, A_o, is now inversely proportional to the square of frequency and that the amplitude of an auroral echo at frequency, f, is now only 12 db below the echo amplitude reflected at frequency, 1/2 f.

If there is diffuseness in the boundary of the ionized region and absorption is present, the amplitude of the returned signal given by Equation (6 4-10) will be modified. Herlofson (22) and Forsyth (24) have shown that the echo amplitude, A, can be represented by

$$A = A_o e^{-\frac{4\pi^2 a^2}{\lambda^2} - \alpha\lambda^2} \qquad (6\ 4\text{-}11)$$

where "a" is the thickness of the boundary and α is a constant for the wave path. The term, $\alpha\lambda^2$, takes into account the effect of attenuation From dual frequency measurements at 56 mc/sec and 106 5 mc/sec Forsyth (24) reports electron densities of the order of $N \doteq 8 \times 10^6$ electrons/cm^3 as computed by this theory

A plane reflecting surface would result in auroral echoes appearing at a single precise range. Since auroral echoes have been observed simultaneously at different ranges and azimuth angles, Aspinall and Hawkins (4) have modified this theory by replacing the plane reflecting surface with a cylindrical surface Equation (6 4-10) is modified by the term $[b/(b + R)]^2$ where b is the radius of the cylindrical surface. To correspond with the visual appearance of an auroral ray, the cylindrical radius can be assumed to be about one kilometer Aspinall and Hawkins have computed the ionization density of the reflecting region of the aurora to be of the order of 6×10^5 electrons/cm^3.

3. SCATTERING THEORY

The Booker-Gordon tropospheric scattering theory (25, 26) has been applied to account for auroral reflections by scattering from inhomogeneities in the auroral ionization. According to the Booker-Gordon theory, the power scattered in any direction by a turbulent medium is given by

$$\sigma_T(\theta, X) = \frac{\overline{\left(\frac{\Delta\epsilon}{\epsilon}\right)^2} \left(\frac{2\pi\ell}{\lambda}\right)^3 \sin^2 X}{\lambda \left[1 + \left(\frac{4\pi\ell}{\lambda}\right)^2 \sin^2\frac{\theta}{2}\right]^2} \qquad (6.4\text{-}12)$$

where $\sigma_T(\theta, X)$ is the tropospheric scattered power per unit solid angle per unit incident power density per unit element of volume; θ, the scattering angle measured from the direction of incidence (normal to the wave front); X, the scattering angle measured from the direction of the incident electric field; and ℓ, the scale of turbulence of the medium. The term, $\overline{(\Delta\epsilon/\epsilon)^2}$, is the mean-square fractional deviation of the dielectric constant from the average. For scattering in any direction at right angles to the incident electric field, such as forward or back scattering, $\sin^2 X$ is unity. In the case of back scattering, which is of immediate interest, θ is equal to π radians.

It follows, therefore, that the scattered power is

$$\sigma_T(\pi, \frac{\pi}{2}) = \frac{\overline{\left(\frac{\Delta\epsilon}{\epsilon}\right)^2} \left(\frac{2\pi\ell}{\lambda}\right)^3}{\lambda\left[1 + \left(\frac{4\pi\ell}{\lambda}\right)^2\right]^2} \tag{6.4-12}$$

To express this relationship for scattering occurring in the ionosphere, the dielectric constant of the ionosphere, ϵ must be in terms of electron density. Since the dielectric constant is equal to the square of the refractive index, n, then, neglecting the earth's magnetic field and electron collision frequency, it follows that

$$\epsilon = 1 - \frac{4\pi N_e e^2}{m\omega^2} = 1 - \frac{\omega_c^2}{\omega^2} \tag{6.4-13}$$

where ω_c is the critical frequency.

The change in the dielectric constant is merely

$$\Delta\epsilon = -\frac{\Delta N_e}{N_e}\frac{\omega_c^2}{\omega^2} \tag{6.4-14}$$

and therefore

$$\frac{\Delta\epsilon}{\epsilon} = \frac{-\frac{\Delta N_e}{N_e}\frac{\omega_c^2}{\omega^2}}{1 - \frac{\omega_c^2}{\omega^2}} \tag{6.4-15}$$

Assuming that the electron densities in the aurora are less than the critical density necessary for reflection, or in other words, $\omega^2 >> \omega_c^2$, it follows that

$$\frac{\Delta \epsilon}{\epsilon} = - \frac{\Delta N_e}{N_e} \frac{\lambda^2}{\lambda_c^2} \tag{6 4-16}$$

where λ_c is the critical wavelength. It is evident from this relationship, that the mean-square fractional deviation of the dielectric constant from the average is

$$\overline{\left(\frac{\Delta \epsilon}{\epsilon}\right)^2} = \overline{\left(\frac{\Delta N_e}{N_e}\right)^2} \frac{\lambda^4}{\lambda_c^4} \tag{6.4-17}$$

It follows, therefore, that, for the ionosphere, the back scattered power becomes

$$\sigma_I \left(\pi, \frac{\pi}{2}\right) = \frac{\overline{\left(\frac{\Delta N_e}{N_e}\right)^2} \left(\frac{2\pi \ell}{\lambda_c}\right)^3}{\lambda_c \left[1 + \left(\frac{4\pi \ell}{\lambda}\right)^2\right]^2} \tag{6.4-18}$$

According to the radar equation, as discussed by Ridenour (27) the power returned from a target having a radar cross section, σ, is given by

$$P_r = \left(\frac{P_t G_t}{4\pi R^2}\right) \left(\frac{\sigma}{4\pi R^2}\right) \left(\frac{G_r \lambda^2}{4\pi}\right) \tag{6.4-19}$$

where the first two terms in the parentheses express the power density in the reflected wave at the receiving antenna. The last term is the effective cross section of the receiving antenna.

In terms of echo amplitude, as discussed in the preceding section, this relationship may be written as

$$A_o = \frac{G\lambda \sigma^{\frac{1}{2}}}{(4\pi)^{3/2} R^2} \left(\frac{P_t}{P'_r}\right)^{\frac{1}{2}} \tag{6.4-20}$$

The radar cross-section in terms of the Booker-Gordon scattering cross-section is

$$\sigma = 4\pi \, V \, \sigma_I \left(\pi, \frac{\pi}{2}\right) \qquad (6\ 4\text{-}21)$$

where V is the volume of the reflecting region. Substituting Equations (6 4-18) and (6 4-21) in Equation (6 4-20), it follows that

$$A_o = \frac{G\lambda}{4\pi R^2} \left(\frac{P_t}{P'_r}\right)^{\frac{1}{2}} \left\{ \frac{V \overline{\left(\frac{\Delta N_e}{N_e}\right)^2} \left(\frac{2\pi \ell}{\lambda_c}\right)^3}{\lambda_c \left[1 + \left(\frac{4\pi \ell}{\lambda}\right)^2\right]^2} \right\}^{\frac{1}{2}} \qquad (6\ 4\text{-}22)$$

Assuming that $\ell \gg \lambda$, Equation (6 4-22) reduces to

$$A_o = \frac{G c^3}{(4\pi)^3 \ell^2 R^2} \left(\frac{P_t}{P'_r}\right)^{\frac{1}{2}} \left(\frac{V}{\lambda_c}\right)^{\frac{1}{2}} \frac{\left\{ \overline{\left(\frac{\Delta N_e}{N_e}\right)^2} \left(\frac{2\pi \ell}{\lambda_c}\right)^3 \right\}^{\frac{1}{2}}}{f^3} \qquad (6.4\text{-}23)$$

It is seen that the echo amplitude is inversely proportional to the cube of frequency. A similar result was obtained for the partial reflection theory.

4. CRITICAL REFLECTION THEORY

This theory assumes that auroral reflections are from small volumes of highly intense ionization concentrations This mechanism is similar to that which causes vertical incident ionospheric reflections According to the ray theory of wave propagation, vertical incident ionospheric reflections occur at the height where the index of refraction equals zero. It has been previously shown (see Section 6.1) that, for reflection, the critical frequency is

$$\omega_c^2 = \frac{4\pi N_e e^2}{m} \qquad (6.4\text{-}24)$$

where the value of electron density is taken at the point of reflection. As shown in Figure 6 4-2. the electron densities required to reflect frequencies above 100 mc/sec are in excess of the values existing in the non-auroral ionosphere

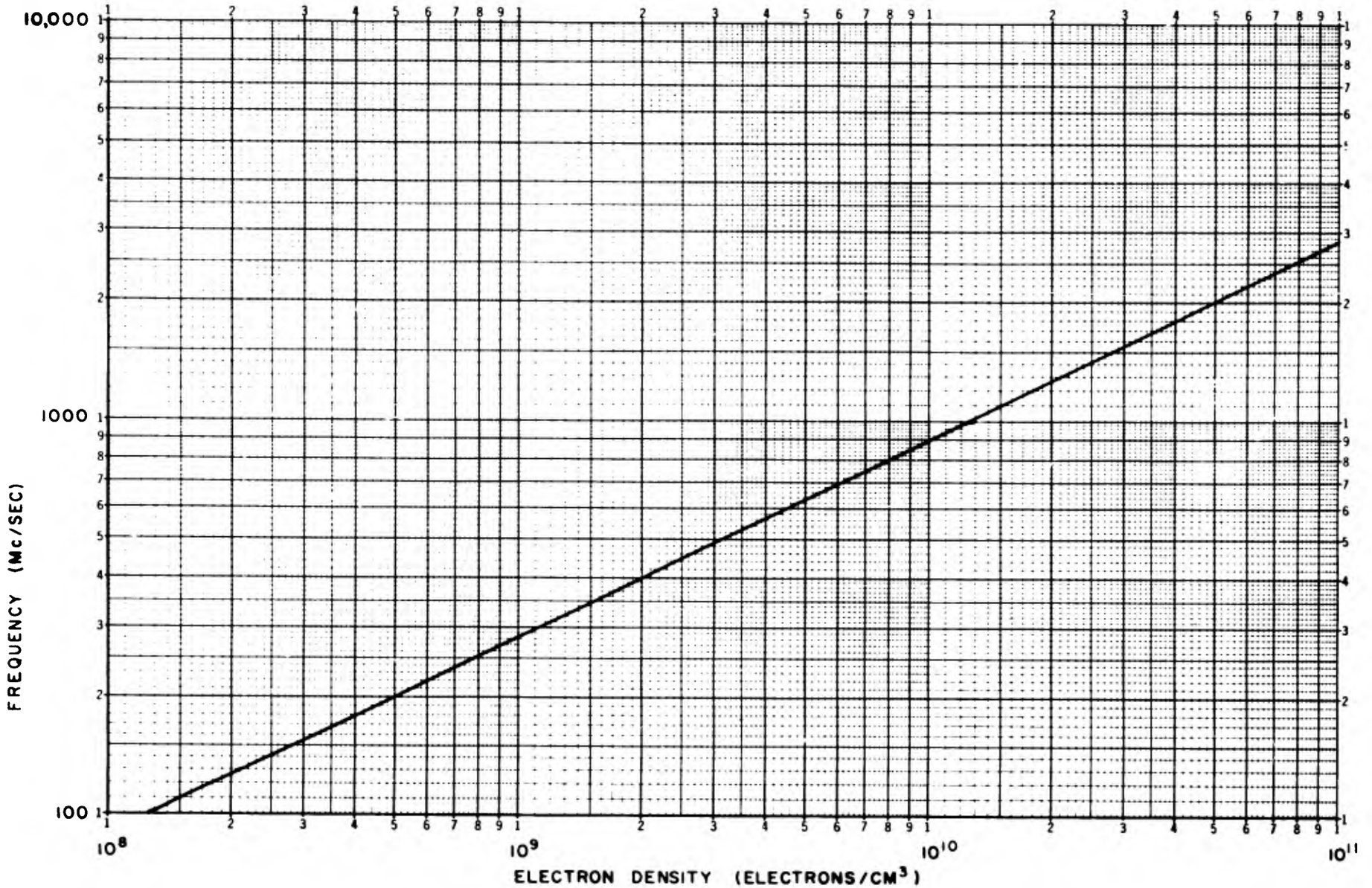

Figure 6.4-2. Values of Electron Density for High Critical Frequency Reflections

According to this theory. the power received from auroral reflections is based entirely on the supposition that the reflecting surface has a unity reflection coefficient. From Equation (6 4-5), it is seen that echo amplitude, which is given by

$$A_o = \frac{Gc}{8\pi Rf} \left(\frac{P_t}{P'_r} \right)^{\frac{1}{2}} \qquad (6.4\text{-}25)$$

is inversely proportional to frequency.

Assuming two transmitting systems in which (P_t) and (G) are held constant, then, at frequency, f, the received amplitude is 6 db below the amplitude obtained at 1/2 f. When both systems have identical operating characteristics, namely ($P_t G_t A_r$) constant, then the amplitudes returned at f and 1/2 f should be equal. The only stipulation is that the electron densities in the aurora are sufficiently high to cause reflections.

Forsyth (24) is of the opinion that critical-frequency reflections are responsible for the auroral echoes observed simultaneously at frequencies of 56 mc/sec and 106.5 mc/sec. The electron sensities required to reflect 56 mc/sec and 106.5 mc/sec radio waves are about 4×10^7 electrons/cm^3 and 1.4×10^8 electrons/cm^3 respectively.

C. THE GEOMETRY OF RADAR-AURORAL REFLECTIONS

1. INTRODUCTION

Recent experimental results (17, 18, 19) indicate that radar-auroral reflections originate from regions in space which satisfy, to a first approximation, the condition of perpendicularity of the propagation direction with the magnetic lines of force.

Assuming that the perpendicularity requirement is valid, it is then highly desirable to estimate beforehand the geometric configuration of auroral propagation for any location on the earth's surface.

Two methods are discussed for calculating the angle between the direction of the earth's magnetic line of force and the direction of electromagnetic propagation (28, 29). This angle will henceforth be referred to as the propagation angle.

One method, purely theoretical, is based on the supposition that the earth's magnetic field can be approximated by the field of a magnetic dipole located at the earth's center. The other method is a graphical one wherein magnetic data obtained from isomagnetic maps are incorporated in the solution

The basic assumptions which both techniques embody are that the earth is spherical and that the bending of the waves due to the refractive properties of the atmosphere is negligible

2. THEORETICAL METHOD

This method is based on the assumption that the earth's magnetic field may be approximated by a magnetic dipole having a geomagnetic pole at 78.6° north latitude and 70.1° west longitude.

The geomagnetic configuration, illustrated in Figure 6 4-3, is fundamentally to determine the propagation angle θ for any geographic location, antenna azimuth bearing A, antenna elevation angle E. and reflection height above the earth's surface h. The various symbols refer to the following:

P_s	the reflection point in space
P_G	the reflection point projected vertically downward on the earth's surface
R	slant range from the radar location to P_s
I	magnetic inclination angle
a	point of intersection of the direction of electromagnetic propagation with the plane tangent to the earth's surface at P_G
b	point of intersection of the direction of the magnetic line of force with the plane tangent to the earth's surface at P_G
$\overline{P_G b}$	line in tangent plane whose orientation coincides with a geomagnetic longitude plane
α	azimuth bearing of the radar location with respect to P_G measured positive in a clockwise direction from geomagnetic north
e	angle formed by the intersection of the propagation vector and the vertical connecting P_s and P_G
r_o	radius of the earth

From the law of cosines it is seen that

$$\overline{ab}^2 = \overline{aP_s}^2 + \overline{bP_s}^2 - 2\overline{aP_s}\ \overline{bP_s} \cos(180 - \theta) \qquad (6.4\text{-}26)$$

$$\overline{ab}^2 = \overline{P_G a}^2 + \overline{P_G b}^2 - 2\overline{P_G a}\ \overline{P_G b} \cos \alpha \qquad (6.4\text{-}27)$$

When the two expressions are equated, it follows that

$$h^2 + 2\overline{aP_s}\ \overline{bP_s} \cos\theta = -h^2 - 2\overline{P_G a}\ \overline{P_G h} \cos\alpha \qquad (6.4\text{-}28)$$

where

$$h^2 = \overline{aP_s}^2 - \overline{P_G a}^2 = \overline{bP_s}^2 - \overline{P_G b}^2 \qquad (6.4\text{-}29)$$

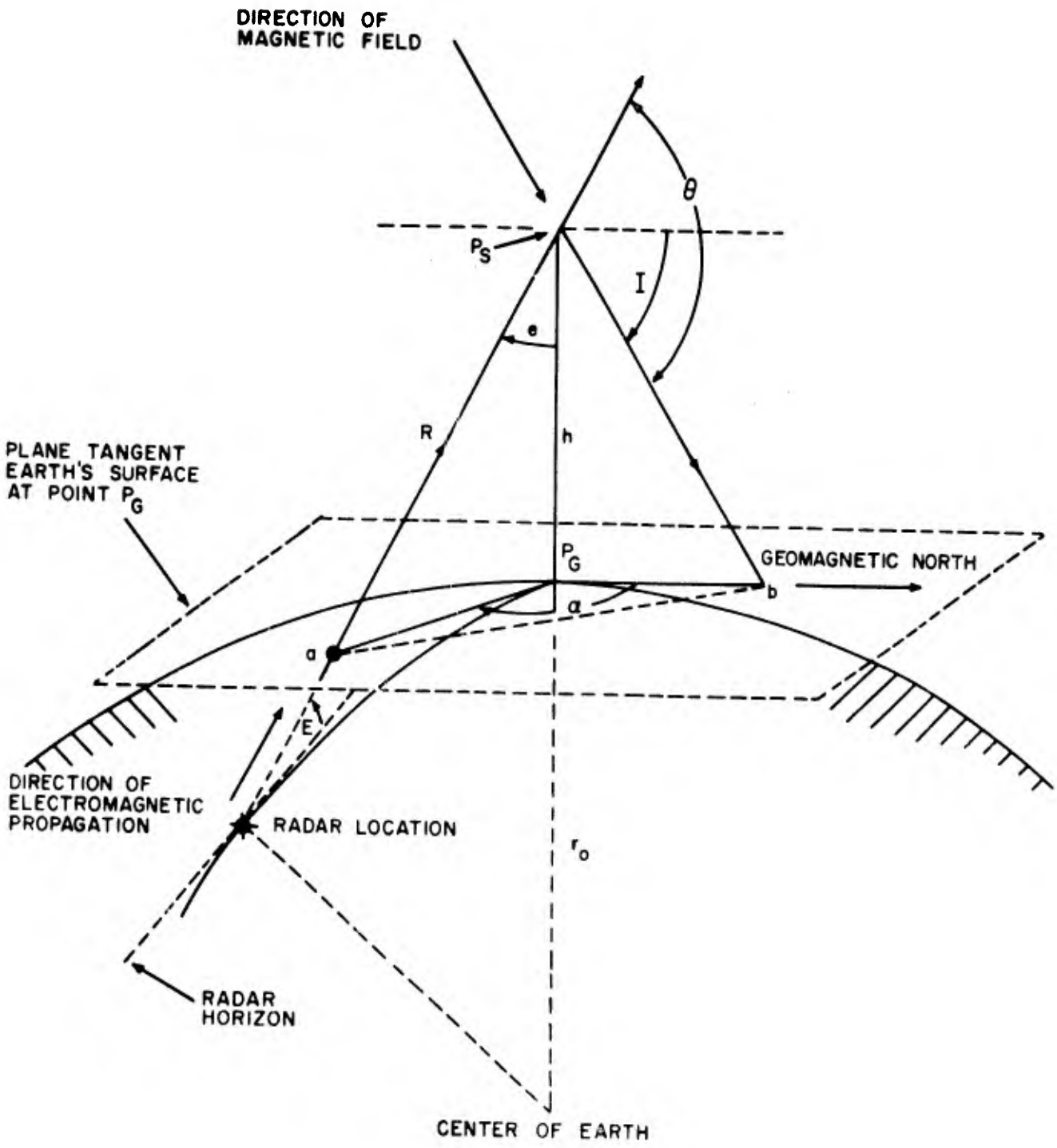

Figure 6.4-3. Radar-Auroral Geometric Configuration

Since

$$\sin e = \frac{\overline{P_G a}}{\overline{aP_s}} \qquad \cos e = \frac{h}{\overline{aP_s}}$$

$$\sin I = \frac{h}{\overline{bP_s}} \qquad \sin I = \frac{\overline{P_G b}}{\overline{bP_s}} \tag{6.4-30}$$

Equation (6.4-29) simplifies to

$$\cos \theta = -\cos e \sin I - \sin e \cos I \cos \alpha \tag{6.4-31}$$

The next step in the solution of the propagation angle is to specify the angles, e, I, and α, in terms of known parameters. For this problem, it is assumed that the known parameters are λ_R and ϕ_R, the geographic longitude and latitude of the radar observation site; λ_M and ϕ_M, the geographic longitude and latitude of the geomagnetic north pole; and the radar coordinates, A, E, and h.

Referring to Figure 6.4-3, the angle e can be evaluated from the law of sines by

$$e = \sin^{-1} \left[\frac{r_o}{r_o + h} \cos E \right] \tag{6.4-32}$$

The inclination, or magnetic dip I, specifies the direction of the total magnetic intensity vector with respect to the horizon and, by definition, is measured positive in the downward direction.

According to Chapman (30), the inclination is only a function of the geomagnetic latitude at the particular point in question, which in this case is P_s or its vertical projection on the earth's surface. In other words, the angle I can be written as

$$I = \tan^{-1} \left[2 \tan \psi_P \right] \tag{6.4-33}$$

where ψ_P is the geomagnetic latitude of P_s. It should be mentioned that since latitude (and also longitude) is invariant with altitude, ψ_P is to be used in lieu of ψ_{Ps} or ψ_{PG}. The subscript Ps, when employed in the text, refers solely to the point P_s.

It can be readily shown that ψ_P is expressible by the function

$$\psi_P = \sin^{-1}\left[\frac{z_{Ps}}{(x_{Ps}^2 + y_{Ps}^2 + z_{Ps}^2)^{\frac{1}{2}}}\right] \tag{6.4-34}$$

where the terms x_{Ps}, y_{Ps}, and z_{Ps}, are components of the vector defined by the matrix equation

$$\begin{Bmatrix} x_{Ps} \\ y_{Ps} \\ z_{Ps} \end{Bmatrix} = [a_{ij}] \begin{Bmatrix} R \sin E \\ R \cos E \sin A \\ R \cos E \cos A \end{Bmatrix} + \{a_i'\} \tag{6.4-35}$$

It should be noted that x, y, and z are the components of a rectangular coordinate system having its origin at the earth's center. The z-axis passes through the geomagnetic pole, and the x-axis passes through the zero-degree geomagnetic longitude meridian which is coincident with that great-circle arc containing the south geographic pole. This is schematically illustrated in Figure 6.4-4.

From simple trigonometric considerations, it can be shown that the radar $-P_s$ slant range of Figure 6.4-3 is given by

$$R = -r_o \sin E + \left[(r_o + h)^2 - (r_o \cos E)^2\right]^{\frac{1}{2}} \tag{6.4-36}$$

The symbol a_{ij} is the element of a 3×3 rotation matrix $[a_{ij}]$. The first subscript i represents the row and the second subscript j the column occupied by the elements which are given by

$$\begin{aligned}
a_{11} &= \cos(\lambda_M - \lambda_R) \sin \phi_M \cos \phi_R - \cos \phi_M \sin \phi_R \\
a_{12} &= \sin(\lambda_M - \lambda_R) \sin \phi_M \\
a_{13} &= -\cos(\lambda_M - \lambda_R) \sin \phi_M \sin \phi_R - \cos \phi_M \cos \phi_R \\
a_{21} &= -\sin(\lambda_M - \lambda_R) \cos \phi_R \\
a_{22} &= \cos(\lambda_M - \lambda_R) \\
a_{23} &= \sin(\lambda_M - \lambda_R) \sin \phi_R
\end{aligned} \tag{6.4-37}$$

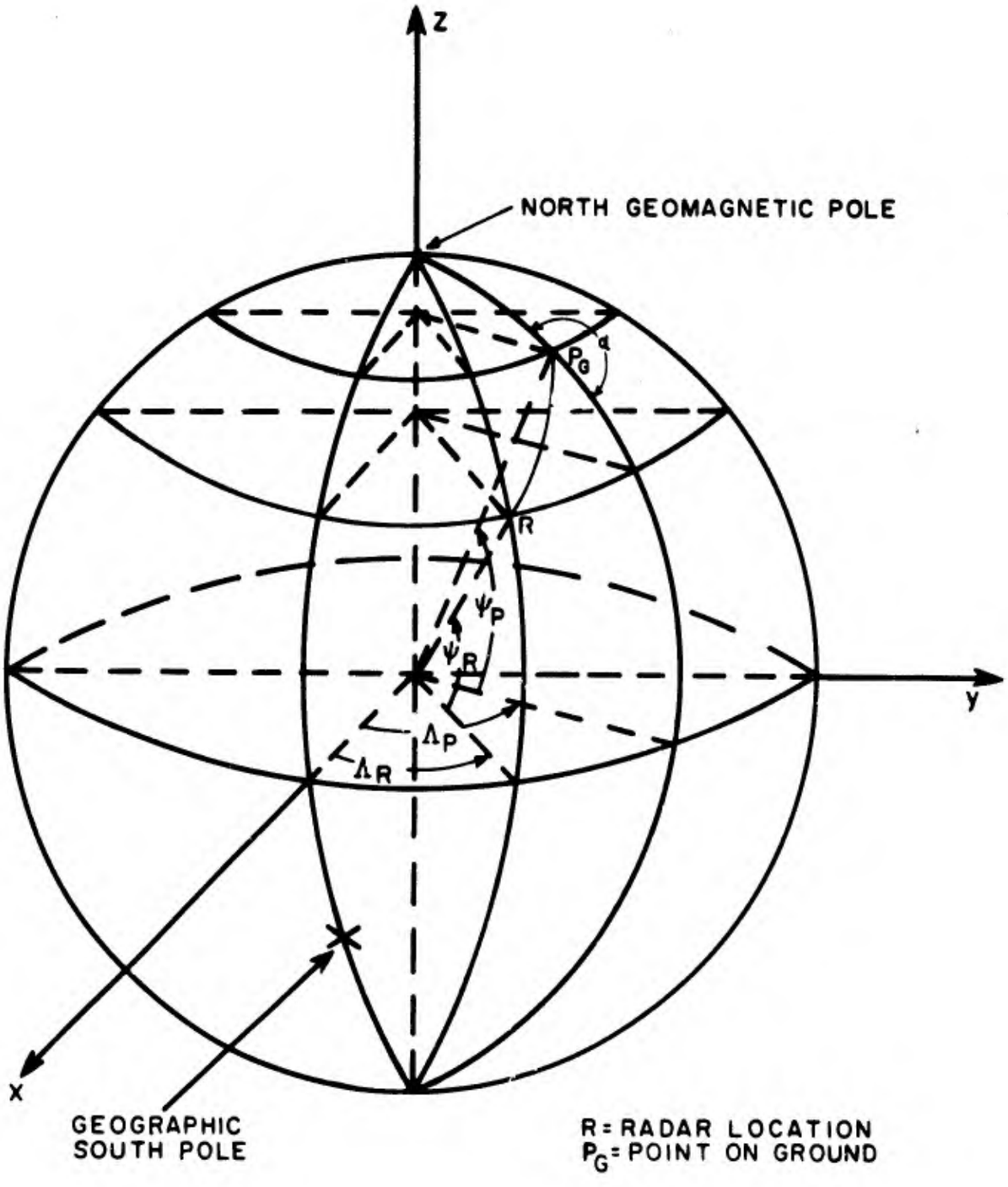

Figure 6.4-4. Geomagnetic Coordinate System

$$a_{31} = \cos(\lambda_M - \lambda_R)\cos\phi_M \cos\phi_R + \sin\phi_M \sin\phi_R$$

$$a_{32} = \sin(\lambda_M - \lambda_R)\cos\phi_M \qquad (6.4\text{-}37)$$

$$a_{33} = -\cos(\lambda_M - \lambda_R)\cos\phi_M \sin\phi_R + \sin\phi_M \cos\phi_R$$

The elements of the one-column translation matrix $\{a_i'\}$ are simply

$$a_1' = r_o a_{11}$$

$$a_2' = r_o a_{21} \qquad (6.4\text{-}38)$$

$$a_3' = r_o a_{31}$$

When x_{Ps}, y_{Ps}, and z_{Ps} of Equation (6.4-35) are evaluated by matrix multiplication and then Equations (6.4-36), (6.4-37) and (6.4-38) are substituted in the resulting expressions, it can be shown that the denominator of Equation (6.4-34)reduces to

$$\left[x_{Ps}^2 + y_{Ps}^2 + z_{Ps}^2\right]^{\frac{1}{2}} = r_o + h \qquad (6.4\text{-}39)$$

and that the coordinate Z_{Ps} is given by

$$z_{Ps} = a_{31}\left[r_o + R\sin E\right] + a_{32}R\cos E\sin A + a_{33}R\cos E\cos A \qquad (6.4\text{-}40)$$

Thus, it is seen that the magnetic inclination angle, which is one of the variables of Equation (6.4-31) can be determined directly from Equations (6.4-34), (6.4-37), (6.4-39) and (6.4-40).

In solving for the propagation angle, all that remains is to express the geomagnetic bearing angle α, depicted in Figure 6.4-4 as a function of the given parameters. It can be shown from spherical trigonometry that α is expressible by

$$\alpha = \tan^{-1}\left[\frac{\sin(\Lambda_P - \Lambda_R)\cos\psi_R}{\cos(\Lambda_P - \Lambda_R)\sin\psi_P\cos\psi_R - \cos\psi_P\sin\psi_R}\right] \qquad (6.4\text{-}41)$$

where Λ_R and ψ_R are the geomagnetic longitude and latitude, respectively, of the radar observation site.

The geomagnetic longitude of P_s or P_G, Λ_P, is defined by

$$\Lambda_P = \tan^{-1}\left[\frac{y_{Ps}}{x_{Ps}}\right] \tag{6.4-42}$$

where, according to Equation (6.4-35)

$$x_{Ps} = a_{11}\left[r_o + R \sin E\right] + a_{12} R \cos E \sin A + a_{13} R \cos E \cos A \tag{6.4-43}$$

$$y_{Ps} = a_{21}\left[r_o + R \sin E\right] + a_{22} R \cos E \sin A + a_{23} R \cos E \cos A \tag{6.4-44}$$

As for Λ_R and ψ_R, they are similarly expressed by Equations (6.4-34) and (6.4-42), with subscript Ps, however, replaced by the subscript R. Since coordinate transformations at the radar location require that R = 0, it becomes quite evident that the components of a point on the earth's surface, x_0, y_0, and z_0, are merely given by the matrix elements, a_1', a_2', and a_3' respectively.

It follows that

$$\psi_R = \sin^{-1}\left[\cos\left(\lambda_M - \lambda_R\right) \cos \phi_M \cos \phi_R + \sin \phi_M \sin \phi_R\right] \tag{6.4-45}$$

$$\Lambda_R = \tan^{-1}\left[\frac{-\sin\left(\lambda_M - \lambda_R\right) \cos \phi_R}{\cos\left(\lambda_M - \lambda_R\right) \sin \phi_M \cos \phi_R - \cos \phi_M \sin \phi_R}\right] \tag{6.4-46}$$

Equations (6.4-45) and (6.4-46) are simple transformations for expressing geomagnetic coordinates in terms of geographic coordinates.

3 GRAPHICAL METHOD

The graphical method involves the utilization of ground-observed magnetic data in the solution of the propagation angle defined by Equation (6.4-31). According to this equation, θ is a function of three parameters, e, which is the angle given by Equation (6.4-32), the inclination angle, I, and the angle, α.

From simple geometric considerations, it can be shown that the magnetic declination D is related to α by

$$\alpha = \gamma - D \tag{6.4-47}$$

where γ is the geographic azimuth of the radar measured at the same ground location used to describe α. It should be recalled that in the previous section, α was referred to as the geomagnetic bearing angle, since measurements were taken with respect to geomagnetic north.

Since magnetic data at ionospheric altitudes are not readily available, it can be assumed, as a first approximation, that the surface values of magnetic inclination and declination are invariant at all heights. Thus, the magnetic elements, D and I, can be scaled from the isogonic and isoclinic charts issued by the U.S. Navy Hydrographic Office or by the Canadian Department of Mines and Technical Surveys.

The epoch 1955.0 isomagnetic publications of the latter organization were employed in this investigation. The angular dimensions of γ were also determined from these maps with little difficulty.

4. COMPARISON OF METHODS

The spatial distribution of the propagation-magnetic field orientation has been determined for Fairbanks, Alaska (65°N, 147.5°W), under the following conditions: (1) azimuth coverage of 360°, (2) elevation coverage in discrete steps up to 30°, and (3) reflection heights of 100 km and 150 km. Calculations based on both the theoretical and the graphical method were performed. Because of the somewhat complex mathematical relationships encountered in the theoretical approach, the former was programmed on an IBM 709 computer.

The magnetic-field aspects as seen from Fairbanks are presented in Figures 6.4-5 and 6.4-6. It is noted that the theoretical results are slightly lower than those obtained graphically. Minimum propagation angle exists in the direction of geomagnetic north (A = + 30°) for the theoretical case and in the direction of magnetic north denoted by the magnetic declination of 29°E (A = + 29°) for the graphical case.

The effect of elevation orientation on the propagation angle is shown in Figure 6.4-7 where observations are taken along the direction of geographic north (A = 0°). It is seen that the angle between the direction of propagation and the earth's magnetic field is minimum at approximately 4° elevation at the 100 km level. As the height increases, there is a noticeable change in the position of the elevation angle at which the minimum propagation angle occurs. It is apparent that, for a fixed elevation angle, the magnitude of the propagation angle increases with height.

5. CONCLUSIONS

Both the theoretical and graphical techniques will yield only approximate results although the latter appears to be the more accurate. The method that should be employed in a given problem is dependent on such factors as the degree of accuracy required, the availability of a digital computer, and the scarcity of magnetic data at the particular geographic location in question.

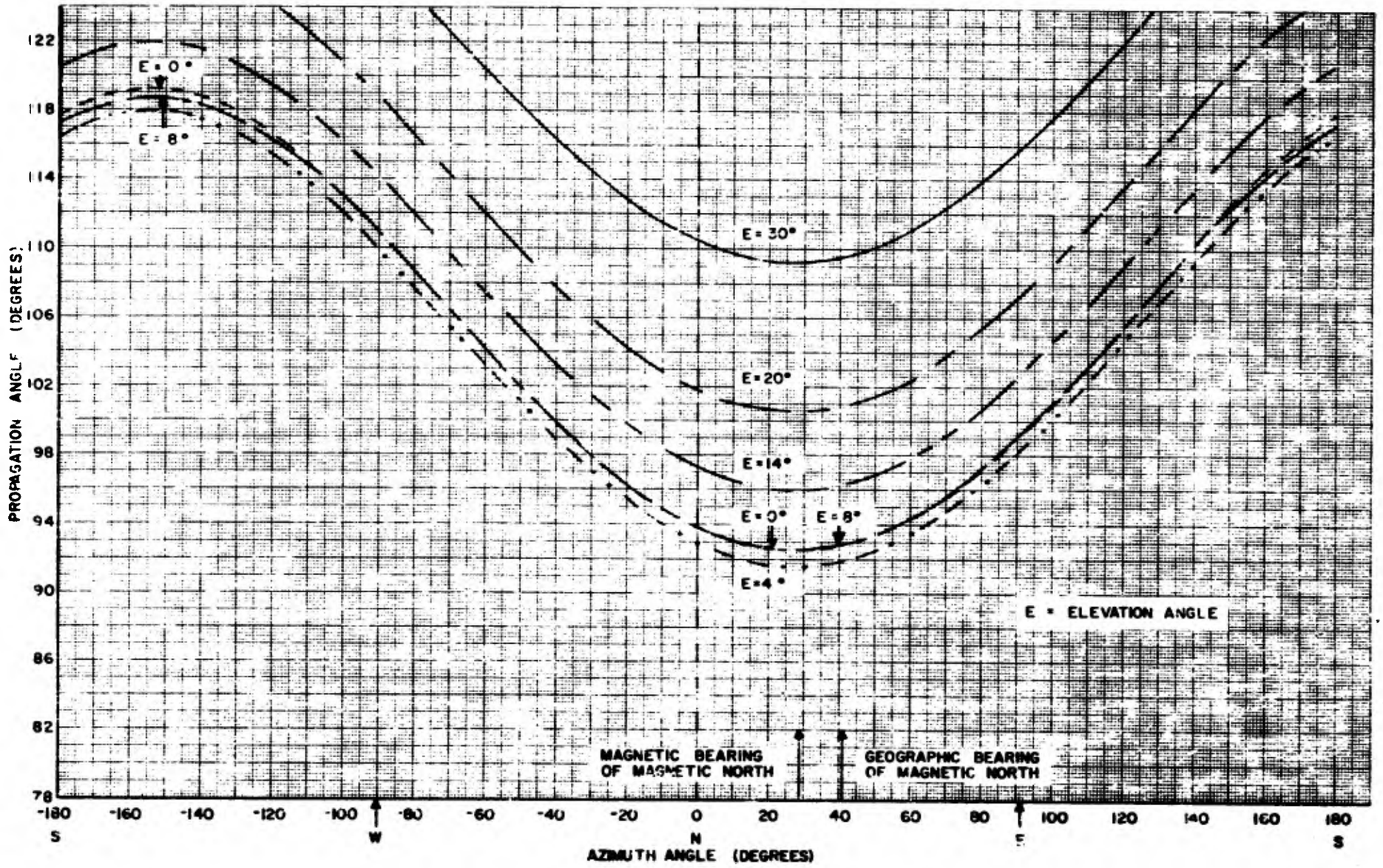

Figure 6.4-5. Propagation Angle at 100 km. Height as Viewed from Fairbanks, Theoretical Method

Since magnetic data at ionospheric altitudes are not readily available, it can be assumed, as a first approximation, that the surface values of magnetic inclination and declination are invariant at all heights. Thus, the magnetic elements, D and I, can be scaled from the isogonic and isoclinic charts issued by the U. S. Navy Hydrographic Office or by the Canadian Department of Mines and Technical Surveys.

The epoch 1955.0 isomagnetic publications of the latter organization were employed in this investigation. The angular dimensions of γ were also determined from these maps with little difficulty.

4. COMPARISON OF METHODS

The spatial distribution of the propagation-magnetic field orientation has been determined for Fairbanks, Alaska (65°N, 147.5°W), under the following conditions: (1) azimuth coverage of 360°, (2) elevation coverage in discrete steps up to 30°, and (3) reflection heights of 100 km and 150 km. Calculations based on both the theoretical and the graphical method were performed. Because of the somewhat complex mathematical relationships encountered in the theoretical approach, the former was programmed on an IBM 709 computer.

The magnetic-field aspects as seen from Fairbanks are presented in Figures 6.4-5 and 6.4-6. It is noted that the theoretical results are slightly lower than those obtained graphically. Minimum propagation angle exists in the direction of geomagnetic north (A = + 30°) for the theoretical case and in the direction of magnetic north denoted by the magnetic declination of 29°E (A = + 29°) for the graphical case.

The effect of elevation orientation on the propagation angle is shown in Figure 6.4-7 where observations are taken along the direction of geographic north (A = 0°). It is seen that the angle between the direction of propagation and the earth's magnetic field is minimum at approximately 4° elevation at the 100 km level. As the height increases, there is a noticeable change in the position of the elevation angle at which the minimum propagation angle occurs. It is apparent that, for a fixed elevation angle, the magnitude of the propagation angle increases with height.

5. CONCLUSIONS

Both the theoretical and graphical techniques will yield only approximate results although the latter appears to be the more accurate. The method that should be employed in a given problem is dependent on such factors as the degree of accuracy required, the availability of a digital computer, and the scarcity of magnetic data at the particular geographic location in question.

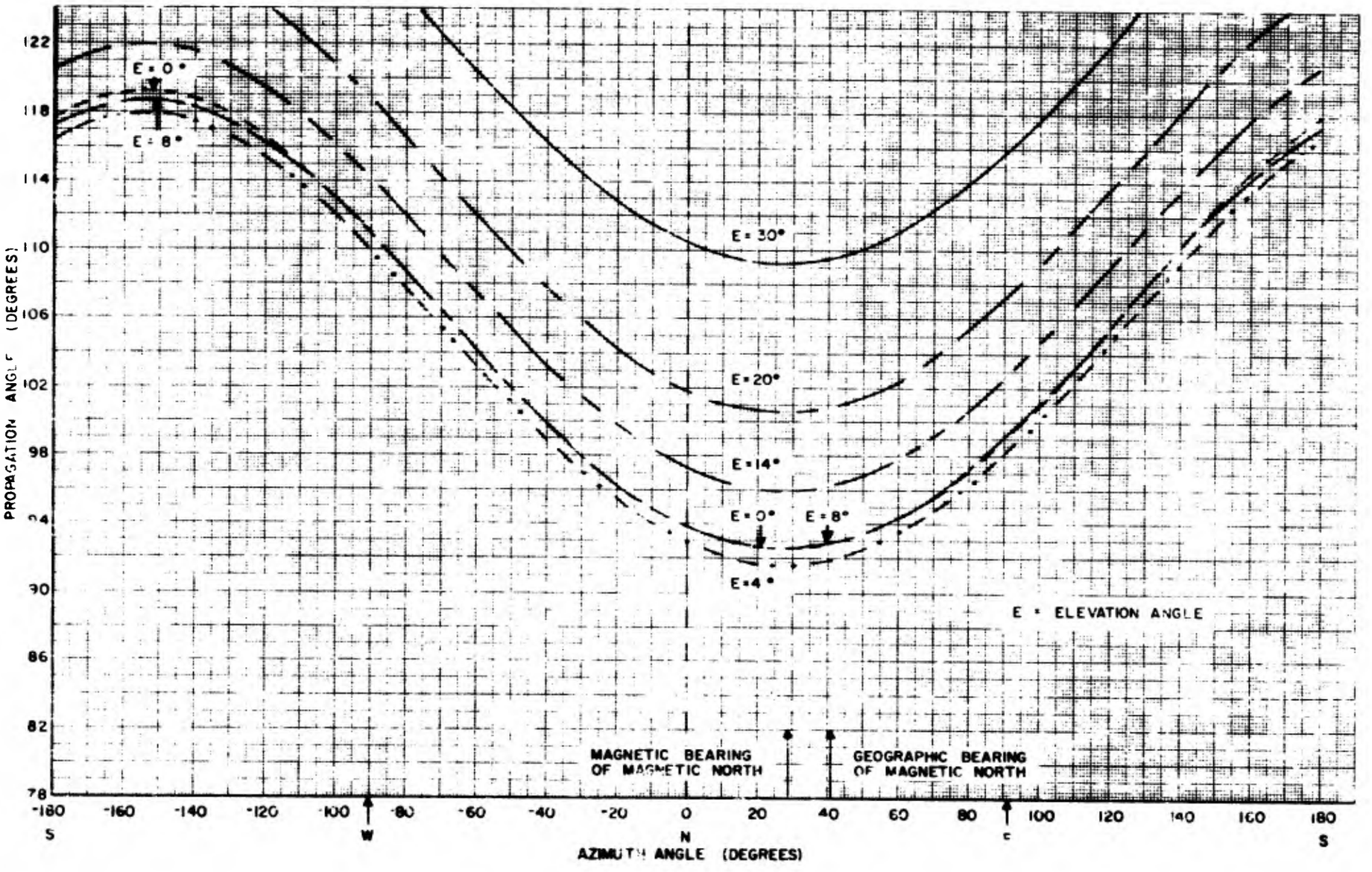

Figure 6.4-5. Propagation Angle at 100 km. Height as Viewed from Fairbanks, Theoretical Method

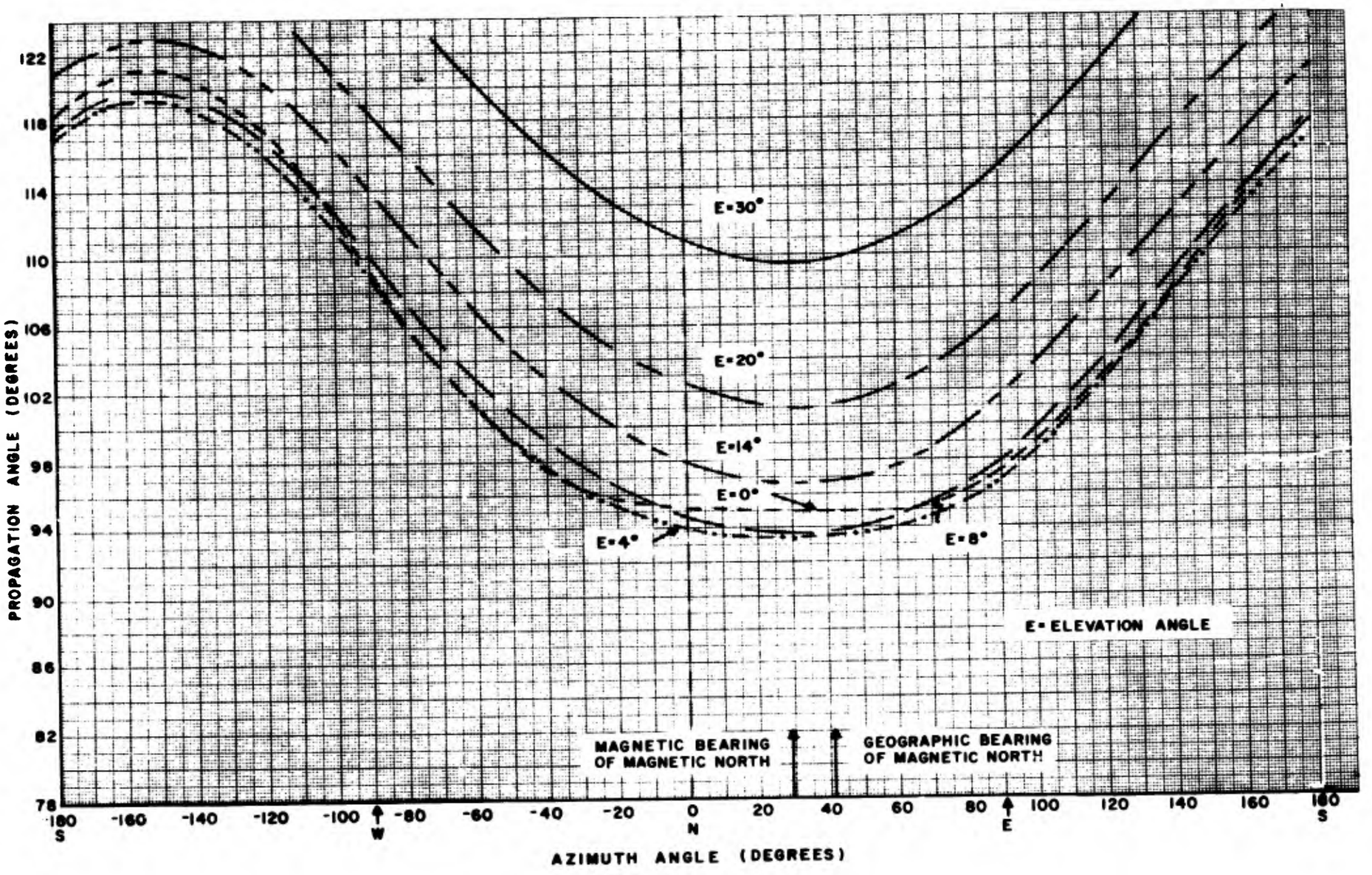

Figure 6.4-6. Propagation Angle at 100 km. Height as Viewed from Fairbanks, Graphical Method

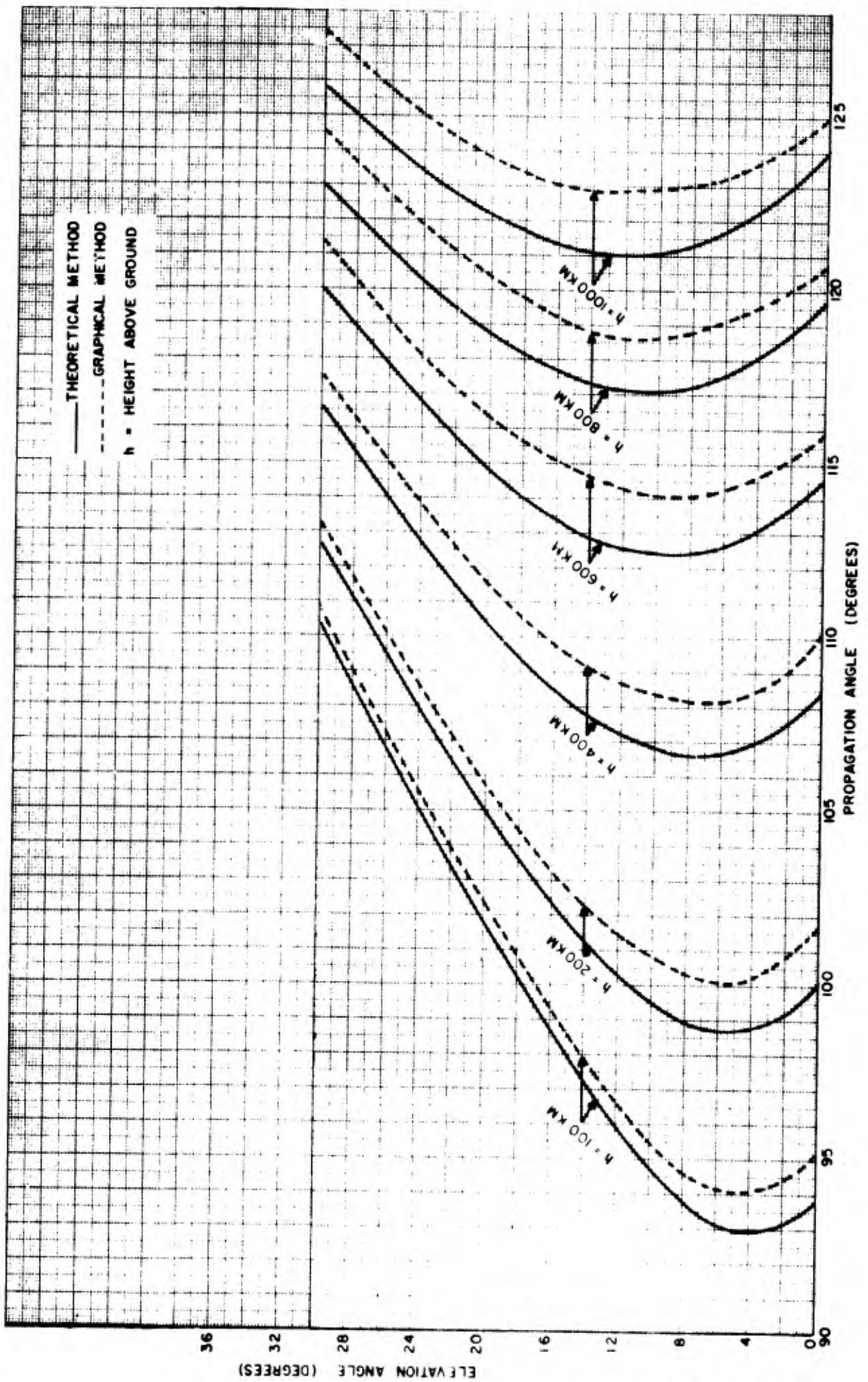

Figure 6.4-7. Propagation Angle as Viewed from Fairbanks along the Direction of Geographic North ($A = 0^{o}$)

The accuracy of the graphical method can be improved considerably by the use of refined magnetic data This necessitates the employment of extrapolated values of magnetic declination and inclination at heights above the earth's surface in lieu of the observational ground-level data

For magnetic field geometries at great heights, the theoretical method should suffice. This is principally substantiated by the fact that, at large distances from the earth's surface, the earth's magnetic field should tend to approach that of a centered magnetic dipole.

D. REFERENCES

1. Harang, L and Stroffregen, W ; "Scattered Reflections of Radio Waves from a Height of more than 1000 Km," Nature, Vol. 142, p. 832, Nov 1938.

2. Lovell, A. C. B., Clegg, J. A. and Ellyett, C. D.; "Radio Echoes from the Aurora Borealis," Nature, Vol. 160, p 372, 1947

3. McKinley, D. W. R. and Millman, P. M.; "Proceedings of the Conference on Auroral Physics," Geophysical Research Paper No. 30, Air Force Cambridge Research Center, p. 131, July 1954

4. Aspinall, A. A. and Hawkins, G. S.; "Radio Echo Reflections from the Aurora Borealis," Journal of British Astronomical Association, Vol. 60, p. 130, 1950.

5. Currie, B. W., Forsyth, P. A. and Vawter, F. E.; "Radio Reflections from Aurora," Journal of Geophysical Research, Vol. 58, p. 179, June 1953.

6. McNamara, A. G. and Currie, B. W.; "Radio Echoes During Aurorae," Journal of Geophysical Research, Vol. 59, p 279, June 1954.

7. Bowles, K ; "The Fading Rate of Ionospheric Reflections from the Aurora Borealis at 50 Mc/sec," Journal of Geophysical Research, Vol. 57, p. 191, June 1952.

8. Bowles, K ; "Analysis of the Fading of Very High Frequency Radio Waves Propagated by the Aurorally Disturbed Ionosphere," Technical Report No. 15, School of Electrical Engineering Cornell University, June 1954.

9. Booker, H. G., Gartlein, C. W. and Nichols, B.; "Interpretations of Radio Reflections from the Aurora," Journal of Geophysical Research, Vol. 60, p. 1, March 1955.

10 Millman, G. H., "A Study of Ionospheric Winds and Turbulence Utilizing Long Radio Waves," Annales de Geophysique, Vol 8, p 365, 1952

11. McNamara, A. G. and Currie, B. W., "Polarization of Radio Echoes from Aurorae," Nature, Vol 174, p 1153, Dec 18, 1954

12. Harang, L. and Landmark, B.; "Radio Echoes Observed during Aurorae and Terrestrial Magnetic Storms Using 35 and 74 mc/sec Waves Simultaneously," Nature, Vol. 171, p. 1017, June 6, 1953.

13. Harang, L. and Landmark, B ; "Radio Echoes Observed during Aurorae and Geomagnetic Storms Using 35 and 74 mc/sec Waves Simultaneously," Journal of Atmospheric and Terrestrial Physics, Vol 4, p. 322, 1954.

14. Forsyth, P. A., Petrie, W., and Currie, B. W ; "Auroral Radiation in the 3000 mc Region," Nature, Vol. 164, p 453, 1949.

15. Chapman, R. P. and Currie, B. W.; "Radio Noise from Aurora," Journal of Geophysical Research, Vol. 58, p. 363, Sept 1953.

16. Dyce, R. B.; "Communication Aspects of VHF Auroral Reflections," Technical Report No. 23, School of Electrical Engineering, Cornell University, June 1955.

17. Fricker, S. J., Ingalls, R. P., Stone, M. L. and Wang, S. C.; "UHF Radar Observations of Aurora," Journal of Geophysical Research, Vol. 62, p. 527-546, Dec. 1957.

18. Peterson, A. M., Leadabrand, R L., and Dyce, R. B., "398 Mc Auroral Echoes Observed at College, Alaska." Paper presented at the URSI-IRE Meeting, Washington, D.C., May 1957

19. Chapman, J. H., Blevis, B. C., Green, F D., Serson, H. V. and Cameron, E. A. "Preliminary Data on Radar Reflections from Aurora at 488 Mc/sec," Defense Research Telecommunications Establishment, Report No 44-2-1, May 1957.

20. Presnell, R. I., Leadabrand, R. L., Dyce, R. B., Schlobohm, J. C. and Berg, M. R.; "Upper Atmosphere Clutter Research - Part I: VHF and UHF Auroral Investigations at College, Alaska," Stanford Research Institute, Contract No. AF 30(602)-1762, April 1959

21. Blevis, B. C.; "UHF Radar Propagation Research at Ottawa," Paper presented at the URSI-IRE Meeting, Washington, D. C., May 1957.

22. Herlofson, N ; "Interpretation of Radio Echoes from Polar Auroras," Nature, Vol 160, p 867, Dec 20, 1947

23. Slater, J. C. and Frank, N H.; "Electromagnetism," McGraw-Hill Book Co., 1947.

24. Forsyth, P. A.; "Radio Measurements and Auroral Electron Densities," Journal of Geophysical Research, Vol. 58, p 53, March 1953

25. Booker, H. G. and Gordon, W. E.; "A Theory of Radio Scattering in the Troposphere," Proceedings of Institute of Radio Engineers, Vol. 38, p. 401, April 1950.

26. Gordon, W. E.; "The Scattering of Radio Waves by Tropospheric Scattering," Research Report EE 163, School of Electrical Engineering, Cornell University, Sept. 1953.

27. Ridenour, L. N.; "Radar Systems Engineering," Radiation Laboratory Series, Vol. 1, McGraw-Hill Book Co., Inc., 1947.

28. Millman, G. H.; "The Geometry of Radar-Auroral Reflections," General Electric Technical Information Series Report No. R58EMH3, March 1958.

29. Millman, G. H.; "The Geometry of the Earth's Magnetic Field at Ionospheric Heights," Journal of Geophysical Research, Vol. 64, pp. 717-726, July 1959.

30. Chapman, S.; "The Earth's Magnetism," Methuen and Company, 1951.

6 5 - METEORS

A. GENERAL CONSIDERATION

1. INTRODUCTION

Meteoric particles impinging on the earth's atmosphere are heated by collisions with ions and other particles. This phenomena, which takes place in the ionosphere at altitudes between approximately 80-120 km, produces incandescence and an ionization trail extending along the path of the meteor.

Depending upon the transmitter frequency, power level and system sensitivity, radar equipments may be confronted with the radiation backscattered from the columns of ionization. Radar echo returns from meteor trails can give rise to false targets which, in turn, would result in a serious clutter problem For extremely high powered radars, meteor echoes can be received on side lobes as well as in the main antenna beam.

The effect of meteoric ionization on any active radar system is dependent upon the geometry of the antenna beam pattern in the E-region of the ionosphere with respect to the meteoric trail under observation For radar-target ranges greater than approximately 700 nautical miles, the meteor echoes can be effectively eliminated by range gating.

2 CHARACTERISTICS OF METEORIC IONIZATION

Meteoroids which produce visual ionization trails weigh approximately 10^{-3} gram and have a radii on the order of 10^{-2} cm The trails which are detectable by radio waves, however, are most likely formed by smaller meteoroids The entry velocity (with limits between 11-72 km/sec, and the mass of the particles and the orientation of the trail with respect to the tangent plane at the earth's surface determine, to a large extent, the height at which the ionization density is a maximum A combination of diffusion and ionospheric turbulence are the basic phenomenon which distort the trail formation.

Meteors are classified into two types, shower and sporadic. The shower meteors travel in a group around the sun in fixed elliptical orbits The meteors in a given shower have the same velocity and appear to originate from a fixed point on the celestial sphere, i e., the radiant The major meteor showers together with their celestial coordinates and dates of activity are listed in Table 6 5-1. The sporadic meteors, on the other hand, are random in nature; that is, the radiants and velocities are variable from meteor to meteor Approximately 75 per cent of the meteoric particles that enter the earth's atmosphere are of this type

TABLE 6.5-1

MAJOR METEOR SHOWERS

SHOWER	DECLINATION (DEGREES)	RIGHT ASCENSION (DEGREES)	DATE OF OCCURRENCE	MAXIMUM ACTIVITY
Quandrantid	48	232	Jan. 1-5	Jan. 3
Lyrid	31	271	April 20-23	April 21
Eta-Aquarid	-1	337	May 3-7	May 5
Arietid and Zeta Perseid	25	45	June 9-13	June 11
Beta Taurid	20	86	July 1-3	July 2
Delta Aquarid	-17	337	July 21-August 5	July 28
Perseid	57	47	August 6-17	August 12
Giacobinid	54	262	Oct. 8-12	Oct. 10
Orionid	15	95	Oct. 19-23	Oct. 21
Taurid	14	54	Nov. 1-13	Nov. 7
Geminid	32	112	Dec. 6-17	Dec. 13
Ursid	76	217	Dec. 20-24	Dec. 22

NOTE - The declination and right ascension are average values.

There are two types of meteor echoes which have been observed by radar techniques; (1) the "tail" (or main) echo which is due to the reflection from the thin trail of ionization formed by the passage of the meteor in the atmosphere; (2) the "head" echo which is attributed to the reflection from the meteoroid and its moving cloud of ions.

Radar echoes backscattered from meteoric ionization have been found to be aspect sensitive in that maximum signals are returned when the incident radio waves are perpendicular to the trail (1, 2, 3)

According to the theoretical studies of meteor rate and radiants by Eshelman, Gallagher, and Mlodnosky (4), a maximum number of meteors enters an observer's hemisphere during the early hours of the morning (0600 hours local time) and during the autumnal equinox while the minimum is at 1800 hours local time and at the vernal equinox. In addition, the amount of diurnal variation decreases with latitude while the amount of seasonal variation increases with latitude.

3. EXPERIMENTAL MEASUREMENTS

The characteristics of radar-meteor returns observed by the AN/FPS-17 radar (5) operating in the 200 mc per frequency range reveal that, of a total of 66,984 meteors recorded, 98 per cent of the echoes were less than one second in duration, while 70 per cent were less than 0.2 second in duration. An average rate of 28 meteors per hour were recorded for non-shower meteors, as compared to a maximum rate of 485 per hour recorded during a shower period

Preliminary experimental results of the Stanford Research Institute (6) indicate that, during non-shower periods, the rate of occurrence of meteor echoes for favorable hours of the day is approximately 200 per hour at 100 mc/sec and 0.5 per hour at 400 mc/sec.

Experimental measurements by McKinley (7) show that, at the lower frequencies, the meteor clutter problem is more severe. Operating at a frequency of 32 mc/sec and a peak power level of 200 kw, 400 to 500 meteor echoes per hour were recorded for an average non-shower period.

According to theory (8), at the short wavelengths, the number of meteor returns is directly proportional to the square root of the transmitted power and inversely proportional to the cube of frequency. Thus at frequencies above 400 mc/sec, the number of meteor echoes should decrease, assuming that the system parameters remain constant.

B. THEORIES OF METEORIC REFLECTIONS

1. INTRODUCTION

The theories of radio-wave reflections from meteoric ionization discussed in this section are those proposed by Eshelman (8).

In utilizing scattering theory for low density ionization trails, i.e., under-dense trails in which the line density is less than 10^{14} electrons/meter, it is assumed that each free electron is acted upon by the incident electromagnetic wave and that the scattered field is the vector sum of the fields scattered from each individual electron. At the long wavelengths ($\lambda > 3$ meters), the trail is considered to be a long cylinder of constant radius while, at the short wavelengths, ($\lambda < 3$ meters), the trail is assumed to be a paraboloid of revolution generated by a moving point-source of ionization.

In the case of high density ionization trails (line density $> 10^{14}$ electrons/meter), and at the long wavelengths, the total reflection process is assumed to take place at the surface of the ionization trail where the condition of critical reflection is satisfied, i.e., the frequency of the incident radiation is equal to the plasma frequency of the trail. Solutions have not yet been obtained for the short wavelengths and high-density trails.

2. LOW-DENSITY TRAILS

The maximum echo intensity received by specular reflection from an underdense meteor trail, irrespective of wavelength, can be expressed by the function

$$P_R(\max) = P_T I_o q^2 \left(\frac{V\lambda^2}{16\pi^2 D}\right)^2 \quad T^2 e^{-(8\pi^2 r_i^2/\lambda^2)} \tag{6.5-1}$$

where

$$I_o = \frac{G_T G_R \lambda^2}{(4\pi)^3 R_o^4} \quad 4\pi \left(\frac{\mu_o e^2}{4\pi m}\right)^2 \tag{6.5-2}$$

$$T = 1 - e^{-2C} \tag{6.5-3}$$

$$C^2 = \frac{32\pi^4 D^2 R_o}{V^2 \lambda^3} \tag{6.5-4}$$

and where I_o is the received intensity per unit transmitted power for one electron; q, the electron line-density (electrons/meter); V, the velocity of meteor (meters/sec), D, the diffusion coefficient (meter^2/sec); r_i, the initial radius of the cloud of ionization formed near the meteoric particle (meters); R_o, the range to the specular reflection point (meters); G_T and G_R, gain of transmitting and receiving antennas, respectively, relative to an isotropic antenna; P_T, the transmitted peak power; λ, the transmitted wavelength. The term, $(\mu_o e^2/4\pi m)$, is the classical electron radius (2.8178×10^{-15} meter) where μ_o is the permeability of free space [12.57×10^{-7} weber/amp-meter]; e, the electron charge (1.6×10^{-19} coulomb); and m, the electron mass [9.1×10^{-31} kg].

The transition wavelength, λ_T, between the short and long wavelength models is given by

$$\lambda_T = \frac{2^{\frac{7}{3}} \pi^{\frac{4}{3}} D^{\frac{2}{3}} R_o^{\frac{1}{3}}}{V^{\frac{2}{3}}} \tag{6.5-5}$$

For average values of D, R_o and V, λ_T reduces to approximately 3 meters.

At the long wavelengths, when $\lambda >> \lambda_T$, $T^2 = 4C^2$. Thus, Equation (6.5-1) reduces to

$$P_R(\max) = P_T I_o q^2 \frac{\lambda R_o}{2} e^{-(8\pi^2 r_i^2/\lambda^2)} \qquad (6.5\text{-}6)$$

When $\lambda << \lambda_T$ which is applicable for the short wavelengths, T = 1. It follows then that

$$P_R(\max) = P_T I_o q^2 \left(\frac{V\lambda^2}{16\pi^2 D}\right)^2 e^{-(8\pi^2 r_i^2/\lambda^2)} \qquad (6.5\text{-}7)$$

The variation of echo intensity with time is not the same for the short and the long wavelength case. According to Eshelman (8), the intrinsic duration, τ, of a meteoric echo, which is defined as the duration of a rectangular pulse having an intensity equal to the maximum intensity of the actual echo and having an energy equal to the actual echo energy, is given by

$$\tau = \frac{4\pi^2 D R_o}{T^2 V^2 \lambda} \qquad (6.5\text{-}8)$$

For $\lambda >> \lambda_T$, $T^2 = 4C^2$ and, therefore, this expression reduces to

$$\tau = \frac{\lambda^2}{32\pi^2 D} \qquad (6.5\text{-}9)$$

which is the time it takes for the intensity to decay exponentially to e^{-1} (approximately 36.8 per cent) of its maximum value.

For the case $\lambda << \lambda_T$, it follows that, since $T^2 = 1$,

$$\tau = \frac{4\pi^2 D R_o}{V^2 \lambda} \qquad (6.5\text{-}10)$$

This relationship corresponds to the time it takes the short wavelength echo to exceed $[1 + (\pi^2/4)]^{-1}$, i.e., 28.8 per cent, of its maximum value.

3. HIGH-DENSITY TRAILS

The maximum energy reflected from an over-dense meteoric trail, for the long wavelength case, is given by

$$P_R(\max) = P_T I_o q^{\frac{1}{2}} \frac{\lambda R_o}{4\pi \left(\frac{\mu_o e^2}{4\pi m}\right)^{3/2} e^{0.5}} \tag{6.5-11}$$

while the intrinsic echo duration which, for this particular condition, is the total duration of the echo, is expressed by

$$\tau = \frac{\lambda^2 q}{4\pi^2 D} \left(\frac{\mu_o e^2}{4\pi m}\right) \tag{6.5-12}$$

An over-dense trail implies that the reflection process is specular and that the density of the ionization in the trail must satisfy the condition

$$fc^2 = 8 \times 10^7 N_e/\text{sec}^2 \tag{6.5-13}$$

where fc is the plasma or critical frequency in cycles/sec while N_e is the electron density in electrons/cm^3.

4. LOW-DENSITY TRAILS AND NON-SPECULAR REFLECTION

In detecting the ionization formed near the meteoroid (or the "head" echo), the geometry of the direction of propagation with the direction of meteor travel is such that non-specular reflection is most likely not attained. The intensity of the non-specular echo for the under-dense trail, at all wavelengths, is given by

$$P_R = P_T I q^2 \left(\frac{\lambda}{4\pi \cos\Theta}\right)^2 e^{-(8\pi^2 r_i^2/\lambda^2)} \tag{6.5-14}$$

where I is similar to I_o, defined by Equation (6.5-2) with the exception that R_o is replaced by R, the radar-range to the head of the trail. The angle, Θ, which is the angle between the propagation direction and meteor trail axis, measured at meteor head, must be less than $\Theta = \tan^{-1}(R/L)$ for Equation (6.5-14) to be valid where L is the length of the meteor trail. Since the meteor travels with a velocity, V, the time duration of the echo merely becomes $\tau = L/V$ seconds.

C. ASPECT ANGLE OF SHOWER METEORS

The validity of the hypothesis that the direction of propagation must be perpendicular at some point on the meteor trail for maximum signal return can be experimentally verified utilizing meteor showers Since meteor showers appear to originate from a fixed point on the celestial sphere, their radiant directions can be predicted with a reasonable degree of accuracy It is then possible, by the procedure outlined in this section, to calculate the orientation of the radiant direction with respect to any antenna axis configuration.

The geometry of the shower meteor aspect angle problem is illustrated in Figure 6.5-1 The aspect angle, ξ, which is defined as the angle between the direction of propagation and the direction of the meteor radiant can be expressed by

$$\bar{S} \cdot \bar{R} = \cos\xi \tag{6 5-15}$$

where $\bar{S}$ is the unit vector denoting the propagation direction and $\bar{R}$, the shower meteor radiant unit vector

Since

$$\bar{S} = \bar{i} \cos E' \sin A' + \bar{j} \cos E \cos A' + \bar{k} \sin E' \tag{6 5-16}$$

$$\bar{R} = \bar{i} \cos E \sin A + \bar{j} \cos E \cos A + \bar{k} \sin E \tag{6 5-17}$$

it follows that

$$\cos \xi = \cos E' \sin A' \cos E \sin A + \cos E' \cos A' \cos E \cos A + \sin E' \sin E \tag{6 5-18}$$

where A' and E' are the azimuth and elevation angles of the direction of propagation; and, A and E, the azimuth and elevation angles in the direction of the radiant The terms, $\bar{i}$, $\bar{j}$, and $\bar{k}$, are the unit vectors that form the coordinate system at the observation point

The equations can be simplified to the form

$$A' = A + \cos^{-1}\left[\frac{\cos \xi}{\cos E \cos E'} - \tan E \tan E'\right] \tag{6 5-19}$$

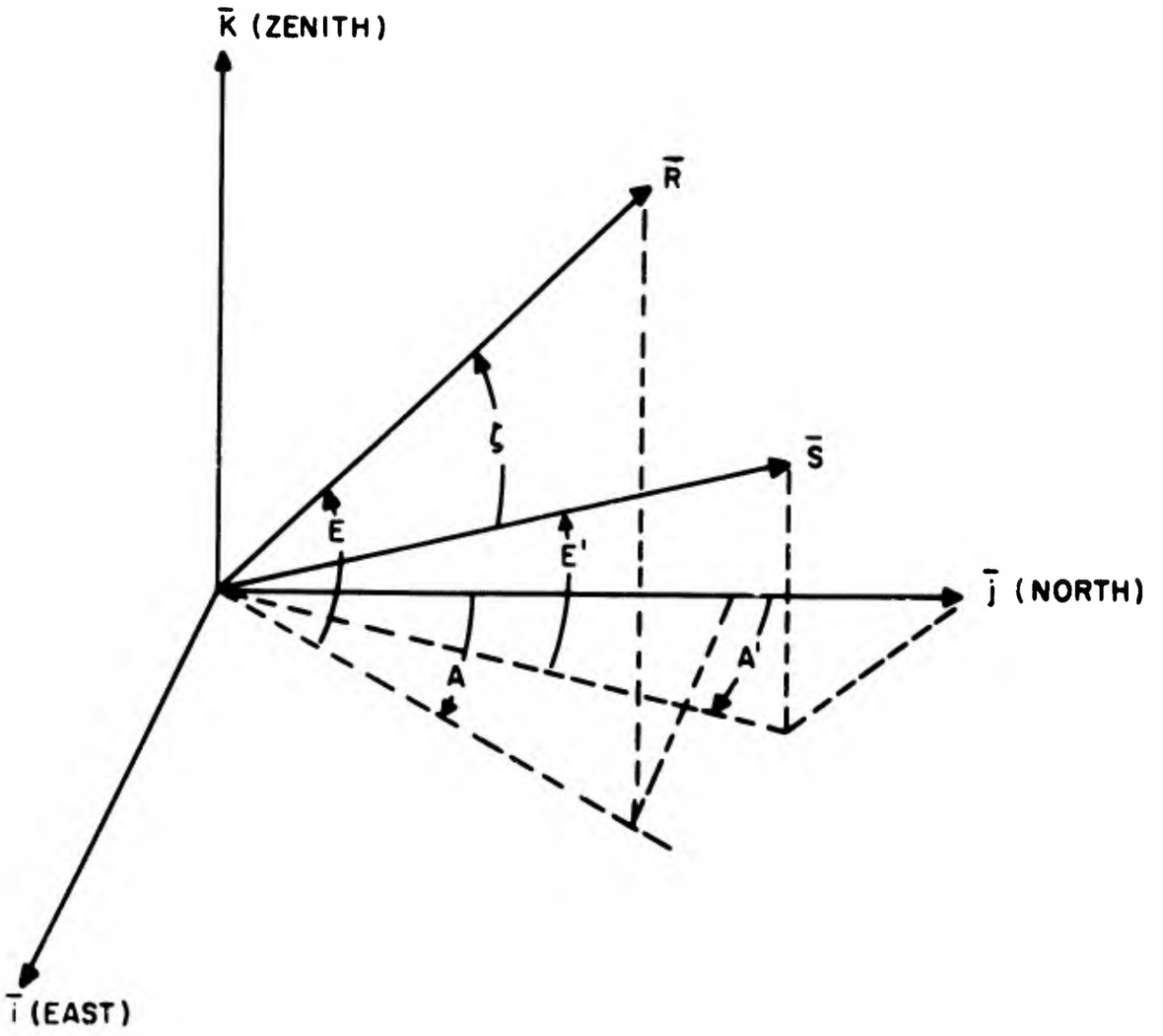

Figure 6.5-1. Meteor Shower Radiant Aspect Angle

For a given meteor shower, the orbital path as observed from a location on the earth's surface can be readily determined It can be shown (see Section 6 8 that

$$\sin D = \sin E \sin L - \cos E \cos L \cos A \qquad (6.5\text{-}20)$$

where D is the declination angle of the meteor shower and L is the observer's latitude.

In order to solve Equation (6 5-19) it is necessary to assume a value for ξ and E'. Since E and A are known for each shower, the azimuth, A', can be obtained. It is noted that, for a given aspect angle and elevation angle, there are two possible solutions for A'. The time of radiant crossing at specific angular orientations can be found by the procedure outlined in Section 6.8

D. REFERENCES

1. Hey, J. S. and Stewart, G. S , "Derivation of Meteor Stream Radiants by Radio Reflection Methods " Nature Vol. 158. p 481 1946

2. Hey, J. S. and Stewart, G. S. "Radar Observations of Meteors," Proceedings of Physical Society, Vol 59, p 858, 1947

3. Lovell, A. C. B., Banwell, C J and Clegg J A . "Radio Echo Observations of the Giacobinid Meteors. 1946," Monthly Notice of Royal Astronomical Society, Vol 107, p 164, 1947

4. Eshelman, V. R., Gallagher P. B., and Mlodnosky R F , "Meteor Rate and Radiant Studies," Stanford University, Final Report. Contract No AF19(604)-1031, Feb 1957.

5. "Meteor Trail Echo Experiments Using the AN/FPS-17 Radar." General Electric Company Engineering Report for RADC Contract No. AF30(602 -1416, July 1957.

6. Leadabrand, R. L., Dolphin L and Peterson A M. "Upper Atmosphere Clutter Research - Part III Preliminary Results of Radar Investigations of Meteor Echoes at 100 and 400 mc," Stanford Research Institute, Final Report for RADC Contract No. AF30(602 -1462, October 1957

7. McKinley, D W. R. "Dependence of Integrated Duration of Meteor Echoes on Wavelength and Sensitivity," Canadian Journal of Physics Vol 32 pp 450-467, 1954.

8. Eshelman, V. R., "Short-Wavelength Radio Reflections from Meteoric Ionization. Part I Theory for Low-Density Trails " Stanford University Scientific Report No 5. Contract No AF19(604)-1031 August 1956

6.6 - THE MOON

A. CHARACTERISTICS OF LUNAR ECHOES

1. INTRODUCTION

The first radio reflections from the moon, using conventional radar techniques, were recorded at a frequency of 111.5 mc/sec at moonrise and moonset by the U.S Army Signal Corps (1). A more complete description of the Signal Corps results are described by DeWitt and Stodola (2). In order to obtain the required sensitivity, they used a receiver bandwidth of about 50 cycles/sec, transmitter pulse length of 0.25 seconds and a transmitter peak power of 3 kw. The experimental results showed that the returned echo amplitude was often times less than the theoretically computed one and, on occasions, could not be detected. In addition, the signal amplitude underwent unexpected fluctuations having periods of several minutes which they attributed to anomalous ionospheric refraction.

Kerr and Shain (3) of Australia performed the moon reflection experiments at 20 mc/sec also, during moonrise and moonset. Their records indicated a rather slow amplitude fluctuation rate which they also attributed to ionospheric refraction phenomenon. The rapid amplitude fluctuations having periods of a few seconds were explained by assuming that the moon's surface consisted of many random scatterers in relative motion, brought about by the moon's libration.

The characteristics of lunar echoes such as libration fading of the order of 2-3 cycles/sec and pulse lengthening to approximately one lunar radius have also been noted by many investigators operating in the UHF range (4, 5, 6). The latter phenomenon indicates the possibility that the moon is a quasi-rough reflector at the frequency of observations.

The employment of radar techniques to reflect signals off the moon's surface for studying the characteristics of the ionosphere by means of the Faraday effect was first reported by Browne (7) and Evans (8, 9). Their equipment consisted of a 10 kw peak power transmitter, operating with a 30 millisecond pulse length and a pulse repetition frequency of 0.6 pulses/sec, and an antenna whose size was approximately 250 square meters. The degree of rapid echo amplitude fading was found to be due to the moon's libration and was a function of the position of the moon in its orbit. By comparing, the slow signal amplitude fading on two close spaced frequencies, 120.0 mc/sec ±0.6%, which was due to the rotation of the plane of polarization by the ionosphere, Evans (8, 9) was able to deduce the ionospheric electron content during periods when the moon crossed the meridian at Manchester, England.

Bauer and Daniels (10) performed similar measurements at a frequency of 151.11 mc/sec employing a bistatic radar system operating between Belmar, New Jersey and Urbana, Illinois. The absolute values of the total electron content were evaluated from these measurements.

The lunar observations of Hill and Dyce (11) at Menlo Park, California on 106.1 mc/sec, however, did not permit an accurate determination of the electron content because of the ambiguity in resolving the number of polarization rotations of the wave.

Radar-lunar experiments operating in the 400 mc/sec frequency range have been conducted at Trinidad, B.W.I. (6) and at the Millstone Hill facility (4). At the former location, the time variation of the electron content above the height of the F-layer maximum has been determined while, at the latter, a study of the reflectivity characteristics of the moon's surface has been undertaken.

2. DOPPLER SHIFT IN TRANSMISSION FREQUENCY

According to the laws of planetary motion, the orbit of a body moving under the influence of gravitational attraction is in the form of a conic section. In the case of the moon, the orbital path is elliptical, with a mean eccentricity of 0.055. Thus, there is a component of the moon's orbital velocity directed toward the center of the earth. Due to the earth's rotation, there is an additional velocity component along the earth-moon line-of-sight, its magnitude being a function of the latitude of the observation site and the moon's hour angle. The resultant of these two velocity components introduces a Doppler shift in the frequency of the signal reflected from the moon. The Doppler shift at 120 mc/sec as reported by Browne (7), is approximately ±50 cycles/sec for observations taken when the hour angle of the moon is less than 30 minutes of time. Doppler shifts as large ±1000 cycles/sec at 400 mc/sec have been recorded by the Lincoln Laboratory (12).

B. RAPID FADING OF SIGNAL AMPLITUDE

The rapid fluctuations of radar pulses reflected from the moon's surface are usually attributed to the libration which is defined as the oscillatory motion of the moon about an axis which itself changes with time. There are three principle causes of libration: (1) libration in latitude -- this results from the fact that the axis of rotation of the moon is tilted about 6.5° to the plane of revolution. Thus, from a fixed position on the earth, varing amounts of the moon's northern hemisphere and southern hemisphere are visible, (2) libration in longitude -- this is due to the fact that the period of rotation of the moon is constant, but the speed along the orbit varies in accordance with Kepler's second law for planets, (3) diurnal libration -- this is the result of the rotation of the earth. As the earth rotates, the position of the moon relative to an observer on the earth is continually changing.

The effect of the moon's libration on the reflected signal can be explained by assuming that the moon's surface consists of a random number of scatterers. The amplitude of the reflected pulse, as observed on the earth's surface, is the resultant of the signals reflected from each of the scattering elements. Since the moon undergoes an apparent rocking motion, or libration, the signals scattered from various parts of its surface are continuously undergoing changes in phase and amplitude which, in turn, produces fluctuations in the resultant signal.

According to Browne (7), at a frequency of 120 mc/sec, the maximum doppler broadening of the signal power spectrum due to libration is of the order of ±2 cycles/sec, which is detectable in the form of pulse-to-pulse fading.

C. SYSTEM REQUIREMENTS FOR RADAR-LUNAR TRANSMISSIONS

In order for a radar system to be capable of detecting and processing lunar echoes, stringent requirements are imposed on the parameters of the transmitter and receiver equipment. An estimate of the system parameters can be readily made by evaluating the radar equation.

The power returned from a target embodied in free space, P_r, according to the radar equation, is given by (13)

$$P_r = \left(\frac{P_t G_t}{4\pi R^2}\right)\left(\frac{\sigma}{4\pi R^2}\right)\left(\frac{G_r \lambda^2}{4\pi}\right) \qquad (6.6\text{-}1)$$

where P_t is the transmitted peak power; σ, the target cross-sectional area; R, the radar-target range, G_t and G_r, the gain of the transmitting and the receiving antenna, respectively, relative to an isotropic antenna; λ, the transmission wavelength. The first two parentheses express the power density in the reflected wave at the receiving antenna while the last parenthesis is the effective cross-sectional area of the receiving antenna.

Assuming a monostatic system which, basically, utilizes a single antenna for both transmitting and receiving, then $G_t = G_r = G$.

The gain of an antenna is expressible in terms of either the effective antenna area, A_e, or the physical antenna area, A, by the relationship

$$G = \frac{4\pi}{\lambda^2} A_e = \frac{4\pi}{\lambda^2} pA \qquad (6.6\text{-}2)$$

where p is the antenna efficiency factor. For a parabolic reflector, the equivalent, projected, antenna area is merely

$$A = \frac{\pi D^2}{4} \qquad (6.6\text{-}3)$$

where D is its diameter.

According to Nyquist's formulation of the thermal noise concept, the total internal receiver noise power, N, is given by

$$N = KTBF \qquad (6.6\text{-}4)$$

where K is Boltzmann's constant (1.38×10^{-23} watt-sec/degree Kelvin), T, the absolute temperature ($\approx 290^{\circ}$ Kelvin), B, the receiver bandwidth (cycles/sec); F, the receiver noise figure.

Thus, substituting Equation (6.6-2) and (6.6-3) in Equation (6.6-1), the radar echo signal-to-receiver noise ratio can be written as

$$\frac{P_r}{N} = \frac{\pi P_t D^4 p^2 \sigma}{4^3 \lambda^2 R^4 KTBF} \tag{6.6-5}$$

The relationship is valid when no signal integration is utilized and is applicable to any target configuration and radar-target orientation. With regard to the lunar problem, however, the parameters in Equation (6.6-5) can be further evaluated.

Since the moon's orbital path around the earth is elliptical, the earth-lunar distance is continously varying as a function of time. The distance from an observer on the earth's surface to the nearest point on the moon's surface can be readily determined from simple geometric considerations.

As illustrated in Figure 6.6-1, it is evident from the law of sines that

$$\frac{\sin \alpha_p}{r_o} = \frac{\sin \left[90 - (E + \alpha_p) \right]}{R + r} \tag{6.6-6}$$

where r_o is the radius of the earth (3963 statute miles); r, is the radius of the moon (1080 statute miles); α_p, the parallax angle of the moon; E, the elevation angle of the antenna beam; R, the earth-lunar distance.

Rewriting this expression in terms of R, it follows that

$$R = r_o \frac{\cos E}{\tan \alpha_p} - r_o \sin E - r \tag{6.6-7}$$

Further simplification can be made by noting that

$$\frac{\cos E}{r_o + R_1 + r} = \frac{\sin \alpha_p}{r_o} \tag{6.6-8}$$

and

$$\sin \alpha_h = \frac{r_o}{r_o + R_2 + r} \tag{6.6-9}$$

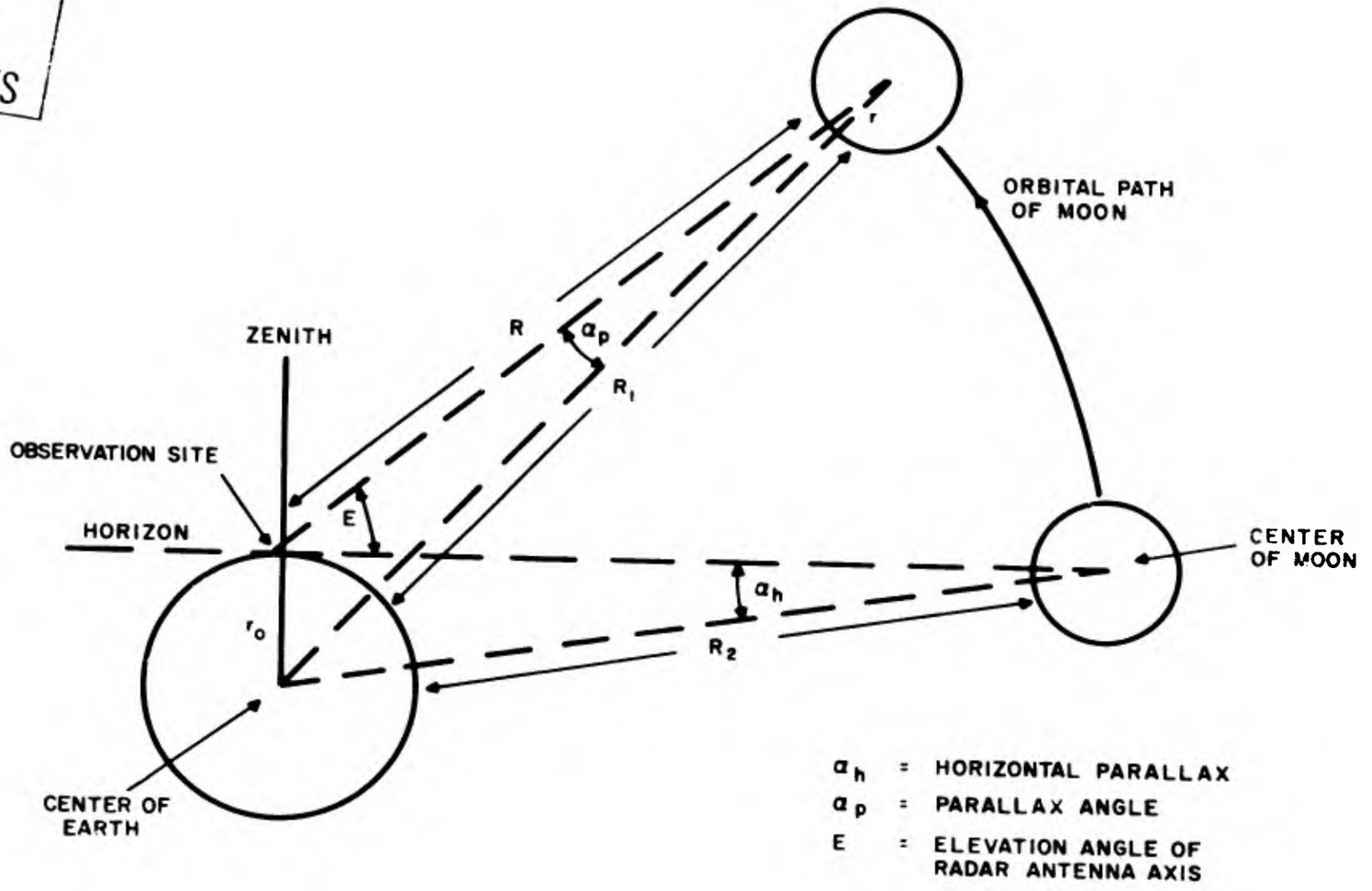

Figure 6.6-1. Earth-Moon Geometry

where the angle, α_p, is the horizontal parallax

To a first approximation it is valid to assume that $R_1 \approx R_2$ and, since α_p and α_h are extremely small angles, $\tan \alpha_p \approx \sin \alpha_p \approx \alpha_p$ and $\sin \alpha_h \approx \alpha_h$ Based on these assumptions and on Equations (6.6-8) and (6.6-9), it is seen that the radar lunar range becomes

$$R = \frac{13,624,972}{\alpha_h} - (3963) \sin E - 1080 \qquad (6.6\text{-}10)$$

where R is in statute miles and α_h is in minutes of arc The magnitude of α_h, as tabulated in the American Nautical Almanac varies between approximately 53 9 and 61.3 minutes of arc during a lunar month. Thus, for observations along the horizon, the minimum and maximum distance to the surface of the moon is approximately 221,200 and 251,700 statute miles, respectively. The mean earth-moon distance is often quoted as 239,000 statute miles

For an idealized spherical target whose surface is smooth and perfectly reflecting, the target cross-section is given by the projected area

$$\sigma = \pi r^2 \qquad (6.6\text{-}11)$$

where r is the radius of the spherical target

Since the moon is not a perfectly smooth and totally reflecting body, the radar cross-section of the moon must be modified to include the following factors

$$\sigma = \pi r^2 \rho q \qquad (6.6\text{-}12)$$

where ρ is the power reflection coefficient of the moon's surface and q is the directivity factor of the moon's surface

The reflection coefficient for power is defined by

$$\rho = \left(\frac{n_1 - n_2}{n_1 + n_2} \right)^2 \qquad (6.6\text{-}13)$$

This definition is applicable for an electromagnetic wave at normal incidence to the boundary separating two media having different indices of refraction, n_1 and n_2. Since the dielectric constant, ϵ is equal to the square root of the refractive index and assuming that one medium is free space, i e , unity refractive index, Equation (6 6-13) reduces to

$$\rho = \left(\frac{1 - \sqrt{\epsilon}}{1 + \sqrt{\epsilon}} \right)^2 \qquad (6.6\text{-}14)$$

The moon's surface is assumed to consist of rock with a dielectric constant between 4-5. Thus, the power reflection coefficient of the moon can be considered to be on the order of 0.11-0.15.

The directivity factor is introduced in the case of the moon since its surface is comparatively rough. Although the radiation is scattered in all directions, there is an increase in the amount of energy scattered back. The magnitude of q has been suggested to range from 4.0 to 5.7, the latter value being obtained from optical measurements.

It should be mentioned that the cross-sectional area of the moon which is effective in estimating the signal-to-noise ratio of a lunar echo is dependent upon the length of the transmitted pulse.

Since the radius of the moon is approximately 1740 km (1080 statute miles), it takes approximately 11.6 milliseconds for an electromagnetic wave to travel from the moon's surface to its limb and to be reflected back again to the surface. Thus, for radar transmissions having a pulse width, τ, greater than 11.6 milliseconds, the total projected area of the moon is basically the effective target cross-sectional area.

When $\tau < 11.6$ milliseconds, the lunar radar cross-section is reduced. It is evident that, for this case, the depth of penetration, d, i.e., the pulse length in units of distance, as shown in Figure 6.6-2, is related to the pulse width by

$$d = \frac{\tau c}{2} \tag{6.6-15}$$

where c is the free space velocity.

It can be readily shown that "a", the radius of lunar projected area which now must be considered, is given by

$$a = \left[r\tau c - \left(\frac{\tau c}{2} \right)^2 \right]^{\frac{1}{2}} \tag{6.6-16}$$

or simply

$$a = \frac{c}{2} \left[2t\tau - \tau^2 \right]^{\frac{1}{2}} \tag{6.6-17}$$

where t =11.6 milliseconds. Thus, it is evident that for the general case, the radar cross-section defined by Equation (6.6-12), should be modified to

$$\sigma = \pi a^2 \rho q \tag{6.6-18}$$

The decrease in the effective lunar cross-section is presented in Figure 6.6-3 as a function of the pulse length of the incident radiation.

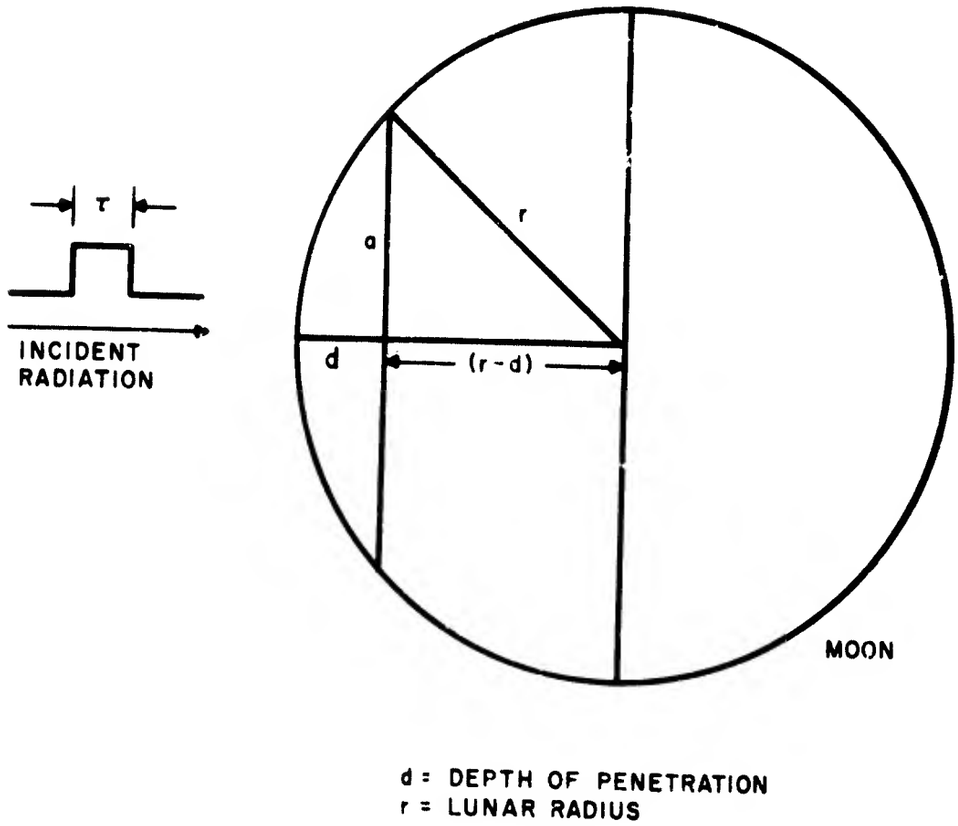

Figure 6.6-2. Lunar Cross Section Geometry

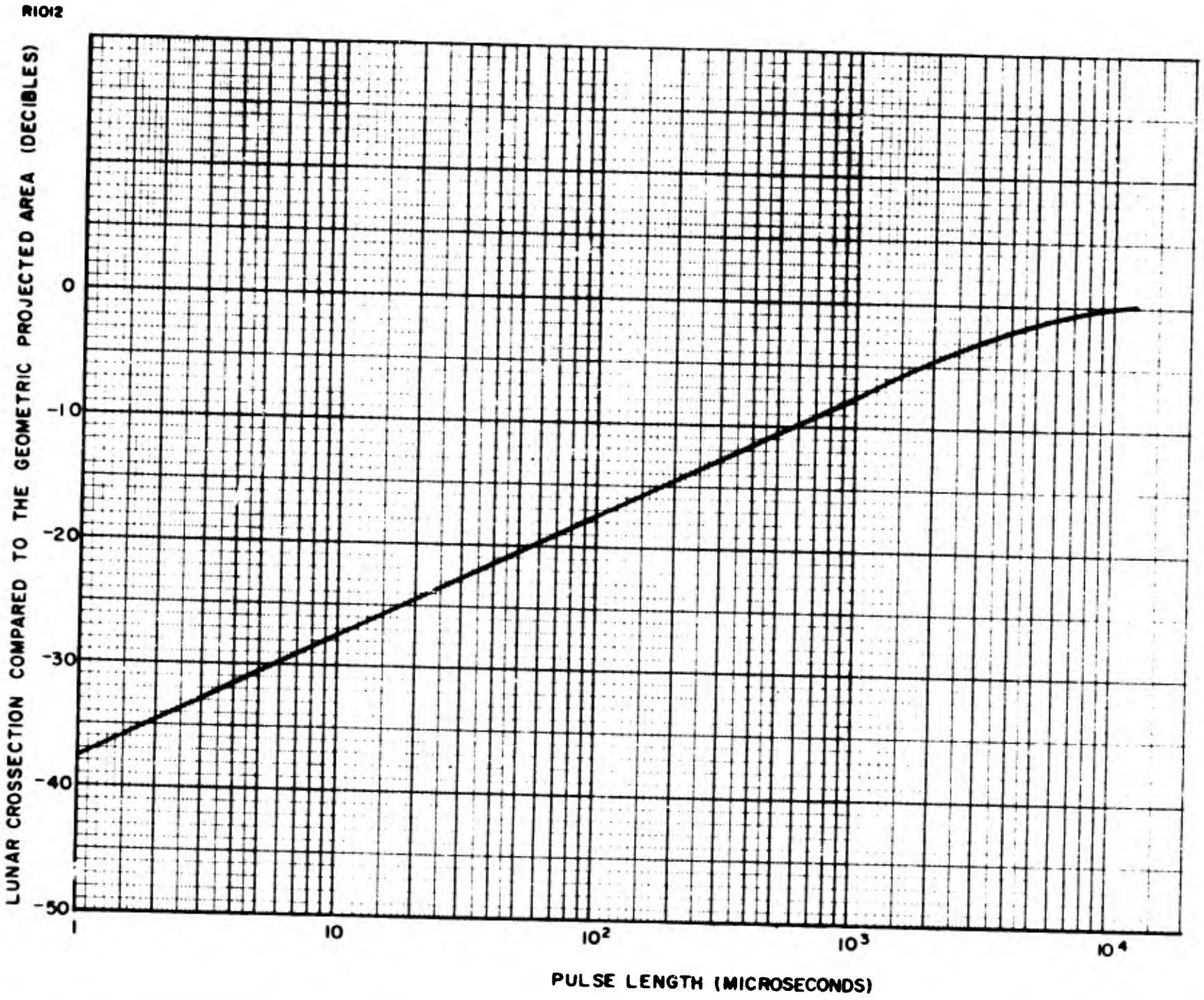

Figure 6.6-3. Decrease in the Effective Lunar Cross Section as a Function of Pulse Length of the Transmitted Signal

Substituting Equation (6.6-18) in Equation (6.6-5), it follows that

$$\frac{P_r}{N} = \frac{\pi^2 P_t D^4 p^2 \rho q a^2}{4^3 \lambda^2 R^4 KTBF} \qquad (6.6\text{-}19)$$

This expression can be written in the form for $\tau > 11.6$ milliseconds,

$$\frac{P_r}{N} = 8.926 \times 10^{-6} \left(\frac{P_t D^4}{BF \lambda^2} \right) \qquad (6.6\text{-}20)$$

where $p = 0.6$, $\rho = 0.12$, $q = 4.5$, $R = 239{,}000$ statute miles and where D is in feet and λ is in meters.

In Figures 6.6-4 and 6.6-5, the radar-lunar signal-to-receiver noise ratio, defined by Equation (6.6-19), is plotted as a function of system parameters for a transmission frequency of 400 mc/sec and 900 mc/sec, respectively. This type of graphical presentation can be used to estimate either the reflected signal-to-receiver noise characteristics for various equipment configurations or the radar parameters necessary to attain a specific signal-to-noise ratio.

For example, assuming $f = 900$ mc/sec, $P_r/N) = 19$ db, $D = 18$ ft, then $(P_t/BF) = 10$ db. For a noise figure of 10 db and a bandwidth of 100 cycles/sec the transmitter power required is approximately 10 kw.

D. REFERENCES

1. Webb, H.D., "Army Radar Contacts the Moon", Sky and Telescope, Vol. 5, pp. 3, 1946.

2. DeWitt, J. H. and Stodola, E. K., "Detection of Radio Signals Reflected from the Moon", Proceedings of I.R.E., Vol. 37, pp. 229-242, March 1949.

3. Kerr, F. J. and Shain, C. A., "Moon Echoes and Transmissions Through the Ionosphere", Proceedings of I.R.E., Vol. 39, pp. 230-242, March 1951.

4. Pettengill, G. H., "Measurements of Lunar Reflectivity Using the Millstone Radar", Proceedings of I.R.E., Vol. 48, pp. 933-934, May 1960.

5. Leadabrand, R. L., Dyce, R. B., Fredriksen, A., Presnell, R. I., and Schlobohm, J. C., "Radio Frequency Scattering from the Surface of the Moon", Proceedings of I.R.E., Vol. 48, pp. 932-933, May 1960.

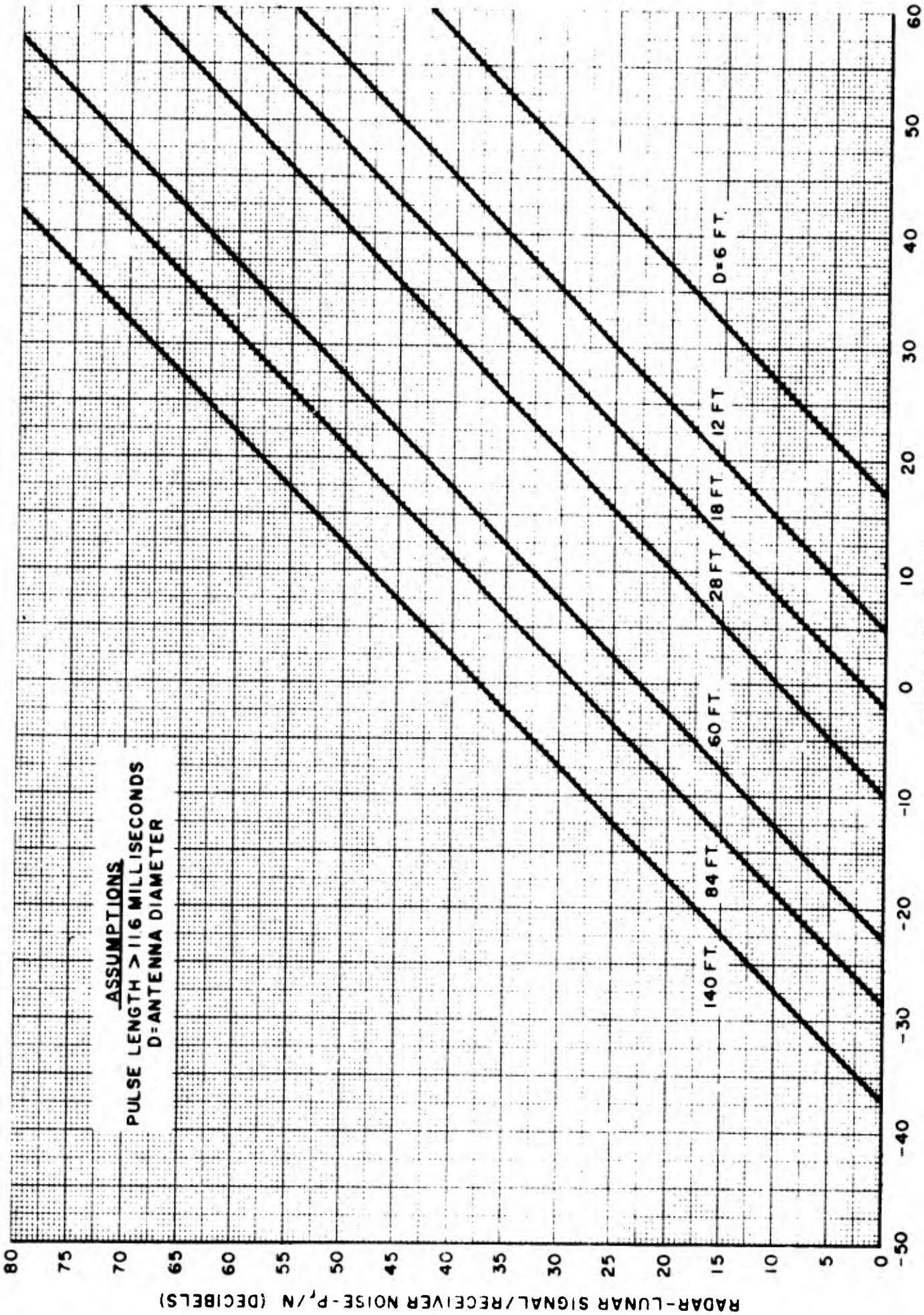

Figure 6.6-4. Radar-Lunar Signal-to-Receiver Noise Ratio as a Function of System Parameters for Transmission Frequency of 400 mc

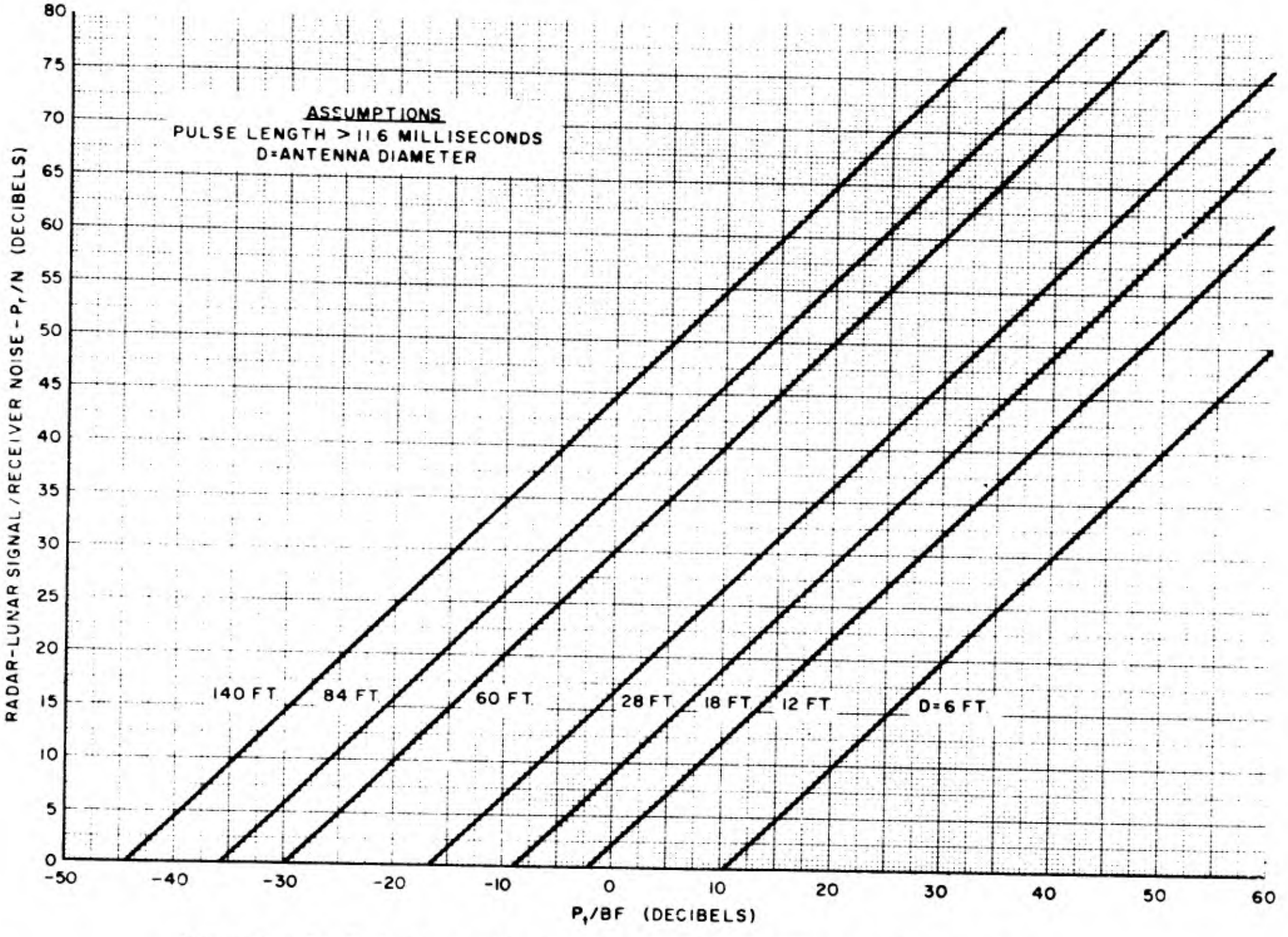

Figure 6.6-5. Radar-Lunar Signal-to-Receiver Noise Ratio as a Function of System Parameters for Transmission Frequency of 900 mc

6. Millman, G.H., Sanders, A.E. and Mather, R.A., "Radar-Lunar Investigations at a Low Geomagnetic Latitude". Paper presented at the URSI-IRE meeting. Washington, D.C., May 1960.

7. Browne, I.C., Evans, J.V., Hargreaves, J.K., and Murray, W.A.S., "Radio Echoes from the Moon", Proceeding of Physical Society, B, Vol. 69, pp 901-920, Sept. 1956.

8. Evans, J.H., "The Measurement of the Electron Content of the Ionosphere by the Lunar Radio Echo Method", Proceedings of Physical Society, B, Vol. 69, pp 953-955, Sept. 1956.

9. Evans, J. H., "The Electron Content of the Ionosphere", Journal of Atmospheric and Terrestrial Physics, Vol. 11, pp 259-271, 1957

10. Bauer, S.J. and Daniels, F. B., "The Measurement of Ionospheric Electron Content by the Lunar Radio Technique", Journal of Geophysical Research, Vol. 64, pp 1371-1376, October, 1959.

11. Hill, R.A. and Dyce, R. B., "Some Observations of Ionospheric Faraday Rotation on 106.1 mc/sec", Journal of Geophysical Research, Vol. 65, pp 173-176, 1960.

12. Fricker, S.J., Ingalls, R.P., Mason, W.C., Stone, M.L. and Swift, D.W., "Characteristics of Moon-Reflected UHF signals", Lincoln Laboratory, Technical Report No. 187, December 1958.

13. Ridenour, L.N., "Radar Systems Engineering", M.I.T. Radiation Laboratory Series, Vol. 1, McGraw-Hill Book Co., Inc., 1947.

6 7 - EXTRA TERRESTRIAL RADIO NOISE SOURCES

A. INTRODUCTION

The sun, the galactic center and discrete radio stars are astronomical sources which emit electromagnetic waves in the radio frequency spectrum When this cosmic radiation is intercepted by an antenna and enters into a receiver, it affects the system sensitivity in the same manner as thermal receiver noise. The effective receiver noise temperature is a function of the actual receiver temperature, the background noise intercepted by the antenna and the lossiness of the networks connecting the receiver to the antenna Since the extra terrestrial radio noise contributes to this temperature and hence may tend to reduce system sensitivity, it must be taken into account in the analysis of radar systems

B. DISCRETE NOISE SOURCES

1. EQUIVALENT ANTENNA TEMPERATURE

The distribution of energy for frequencies in the radio spectrum of a black body radiator, according to the Rayleigh-Jeans radiation law, is

$$b = \frac{2 k T_b}{\lambda^2} \qquad (6.7\text{-}1)$$

where b is the energy emitted per steradian per second by a unit area of surface, expressed in watts meter^{-2} (cycles/sec)$^{-1}$ steradian^{-1}, k Boltzmann's constant (1.38×10^{-23} watts-sec/degree Kelvin); T_b, the absolute temperature of the black body; and λ, the radiated wavelength.

The flux density, S, which is a measure of the radiation from a discrete source whose angular dimension is small with respect to the antenna beamwidth is given by

$$S = b \Omega \qquad (6.7\text{-}2)$$

where Ω is the solid angle, in steradians, subtended by the source at the point of observation and S is in watts meter^{-2} (cycles/sec)$^{-1}$

The power available at a receiving system is therefore

$$P = (1/2) S A_e B \qquad (6\ 7\text{-}3)$$

where A_e is the effective area of the receiving antenna and B is the receiver bandwidth The factor of one-half enters into this relationship simply because an antenna is generally capable of accepting only one of two orthogonal polarizations

According to Nyquist's formulation of the thermal noise concept (1), the thermal noise intercepted by an antenna is

$$P = k T_a B \tag{6.7-4}$$

where T_a is the apparent antenna temperature

From Equations (6.7-3) and (6.7-4), it follows that the apparent antenna temperature can be expressed in terms of the flux density by the function

$$T_a = \frac{S A_e}{2k} \tag{6.7-5}$$

Substituting Equations (6.7-1) and (6.7-2) in this relationship, it is seen that the apparent antenna temperature can also be defined in terms of the black body temperature of a distance source by

$$T_a = \frac{T_b \Omega A_e}{\lambda^2} \tag{6.7-6}$$

The apparent temperature of an antenna is usually composed of contributions from many external noise sources such as the sky background radiation, the radiation from a warm earth scattered by particles into the main lobe of an antenna, the leakage from a warm earth into the minor lobe pattern of an antenna and the reradiation from an absorbing medium. Mathematically, the apparent temperature is given by

$$T_a = T_{a1} + T_{a2} + T_{a3} + \cdots T_{an} \tag{6.7-7}$$

where T_{ai} is the apparent noise temperature resulting from one of the above sources

If the celestial noise radiator has an angular area larger than the angular dimensions of the antenna beamwidth, then, neglecting other sources, the temperature of this source determines the antenna temperature

If the angular size of the source is small compared to the antenna angular beam size, then to a first approximation, the apparent antenna temperature due to this source is given by

$$T_a = \frac{A_b}{A_a} T_b \tag{6.7-8}$$

where A_a and A_b are the angular areas of the antenna beam and celestial body, respectively.

With reference to Equation (6.7-6) a more accurate determination of the apparent antenna temperature would be obtained by integrating over solid angle such that

$$T_a = \frac{1}{4\pi} \int G T_b \, d\Omega \qquad (6.7\text{-}8)$$

where G is the antenna gain defined by

$$G = \frac{4\pi A_e}{\lambda^2} \qquad (6.7\text{-}9)$$

2. THE SUN

The sun radiates high intensity electromagnetic wave noise greatly in excess of the black body intensity of 6000°K deduced from optical and thermal data.

If the radio noise from the sun is observed continuously, it is found that, during sunspot activity, irregular increases of radio noise can occur lasting for periods of several days at a time. The radio noise is enhanced on the order of 10-20 db greater than the base level of the quiet sun. As reported by Shapley and Davis (2), a noise burst, recorded at 480 mc/sec, which accompanied a major solar flare, was 1000 times the normal output of the entire sun.

In addition to the increase in the general level of radio noise, when sunspots are visible and active, sudden bursts of a few seconds duration and rapid fluctuations of the flux density are a common characteristic of a solar disturbance. According to Payne-Scott, Yabsley and Bolton (3), when the noise is examined on several frequencies, in the majority of cases, a noise burst appears on one frequency but not on the others. When the noise burst does appear on several frequencies, most often it first shows up on the highest frequency and then, after a few seconds interval, on the lower frequencies.

The characteristics of the five different classes of solar radio waves, compiled by Pawsey and Bracewell (4), are given in Table 6.7-1.

The theoretical total flux density in the radio frequency spectrum of solar energy received at the earth's surface in terms of apparent black-body temperature is, according to Equations (6.7-1) and (6.7-2),

$$S = \frac{2k T_b \pi}{\lambda^2} \left(\frac{r}{R}\right)^2 \qquad (6.7\text{-}10)$$

where

$$\Omega = \pi \left(\frac{r}{R}\right)^2 = 6.79 \times 10^{-5} \text{ steradian} \qquad (6.7\text{-}11)$$

and where r is the radius of the photosphere (6.96×10^5 km)

TABLE 6.7-1

SOLAR RADIO WAVE CHARACTERISTICS

CLASS	BASIC COMPONENT (THERMAL)	SLOWLY VARYING COMPONENT	NOISE STORM	UNPOLARIZED BURST	
				OUTBURST	ISOLATED BURST
Wavelength Range	Unlimited	3-60 cm	1-15m	1cm to 15 m	50cm to 50m
Duration	---	Weeks or Months	Hours or Days	Minutes	Seconds
Polarization	Random	Trace of Circular	Strongly Circular	Random	Random
Place of Origin	Whole Sun	Number of Small Areas	Small Area Above Sunspot	Small Area Rapid Movement	Small Area
Associated Optical Feature	---	Sunspots and Other	Large Sunspot	Flare	Unknown
Remarks	Constant Over Years	27-Day Component	With or Without Numerous Bursts	No Certain Distinction	

and R is the earth-sun distance (1.497×10^8 km). The numerical evaluation of Equation (6.7-10) is

$$S = 1.88 \times 10^{-27} \frac{T_b}{\lambda^2} \text{ watts meter}^{-2} \text{ (cycles/sec)}^{-1} \qquad (6.7\text{-}12)$$

Figure 6.7-1 is a simplified chart which converts the total solar flux density into apparent black-body temperature. As an example, a flux density of 5×10^{-21} watts meter^{-2} (cycles/sec)$^{-1}$, measured by Reber (5) at a frequency of 480 mc/sec, is equivalent to a black-body temperature of 1.05×10^6°K for a disk subtending the same diameter as the sun.

Experimental measured values of the apparent temperature of the quiet sun over a wide range of frequencies are shown in Figure 6.7-2 which is taken from Pawsey and Smerd (6). The solid line through the observational data which is the assumed average linear function between apparent temperature and wavelength, can be expressed by

$$\text{Log } T_b = \text{Log } b_1 + b_2 \text{ Log } \lambda \qquad (6.7\text{-}13)$$

It is noted that this expression is the general form of the equation of a line where b_2 is its slope and b_1 is the log T_b axis intercept. The numerical value of the slope, $b_2 = 1.245$, is obtained by direct measurement with an arbitrary scale in which the logarithmic coordinate axes are disregarded.

From Figure 6.7-2, it is seen that at $\lambda = 0.2$ meters. $T_b = 10^5$°K and hence $b_1 = 7.417 \times 10^5$ It should be noted that, when the wavelength is expressed in centimeters, $b_1 = 2.4 \times 10^3$.

The relationship between the apparent disk temperature and wavelength is therefore

$$T_b = 7.417 \times 10^5 \lambda^{1.245} \qquad (6.7\text{-}14)$$

where λ is in meters.

Combining Equations (6.7-12) and (6.7-14), it is seen that the flux density is directly proportional to frequency and is given by

$$S = \frac{1.394 \times 10^{-21}}{\lambda^{0.755}} \qquad (6.7\text{-}15)$$

Figure 6.7-3 is a plot of this relationship At a frequency of 200 mc/sec, the flux density of the quiet sun is approximately 1.03×10^{-21} watts meter^{-2} (cycles/sec)$^{-1}$ This value compares favorably with Dodson's experimental measurements (7) of 8×10^{-22} watts meter^{-2} (cycles/sec)$^{-1}$ As shown in Figure 6.7-3, at 400 mc/sec, the flux density increases to 1.7×10^{-21} watts meter^{-2} (cycles/sec)$^{-1}$

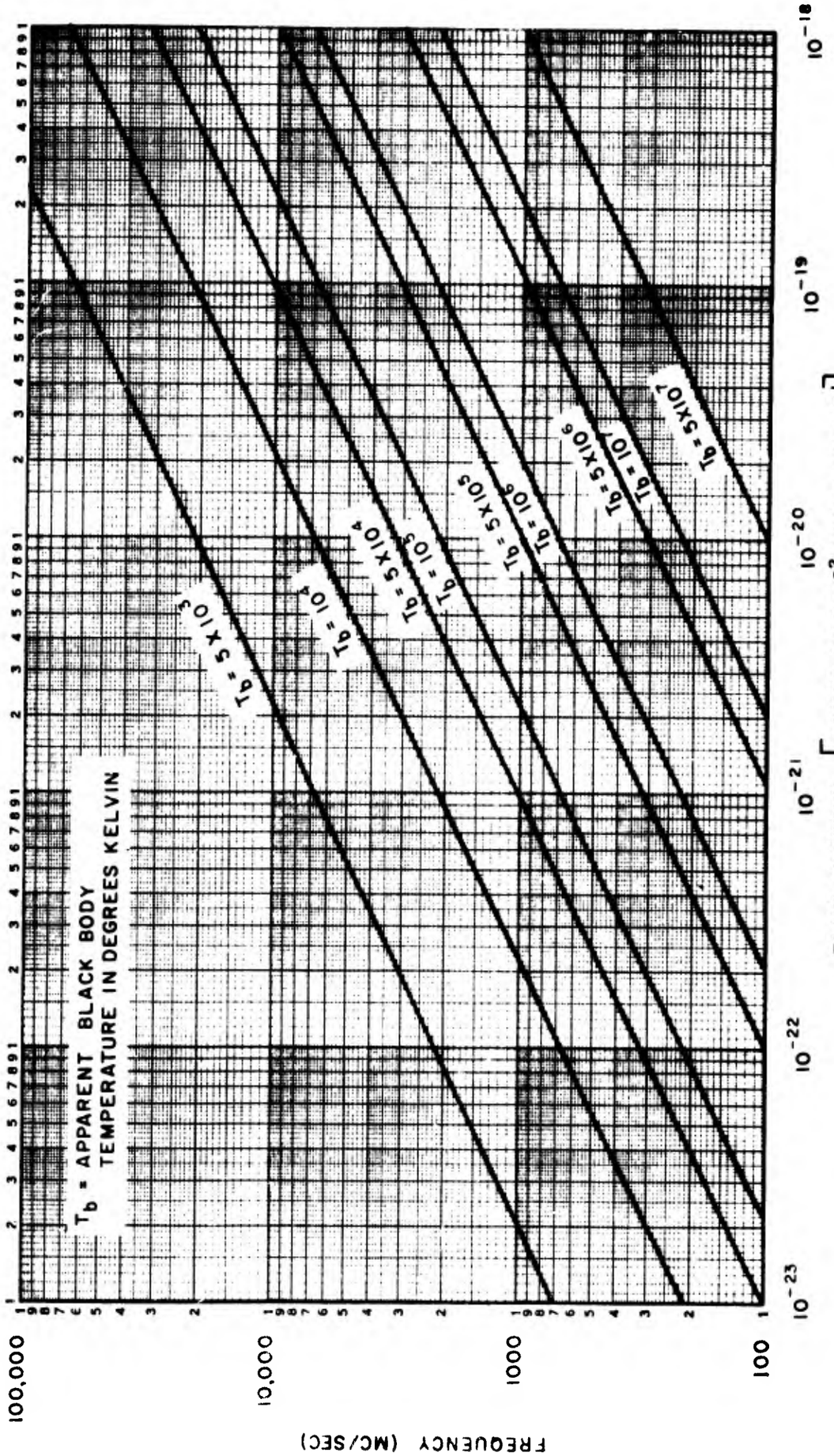

Figure 6.7-1. Conversion of Total Solar Flux Density into Apparent Black Body Temperature

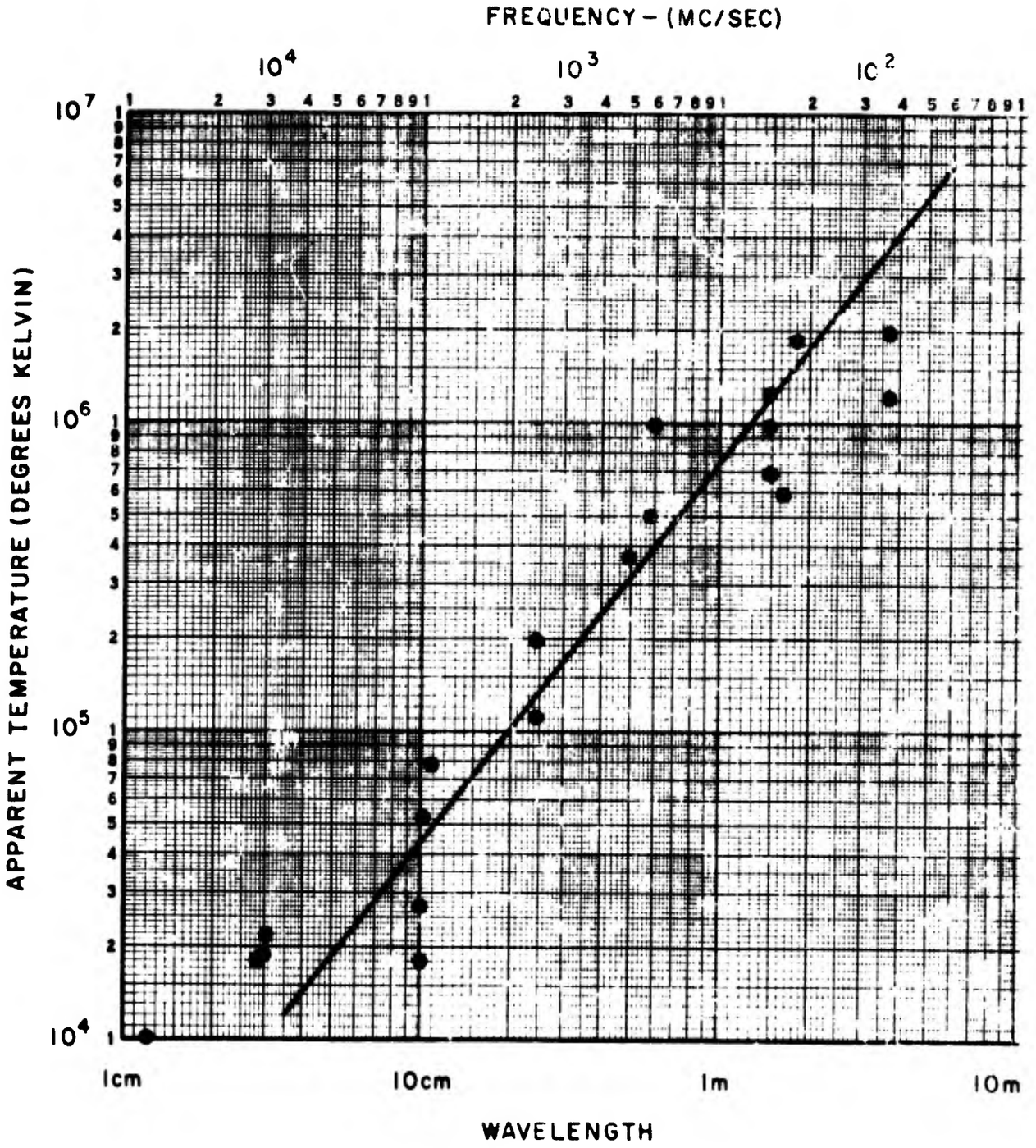

Figure 6.7-2. Experimental Values of the Apparent Temperature of the Quiet Sun

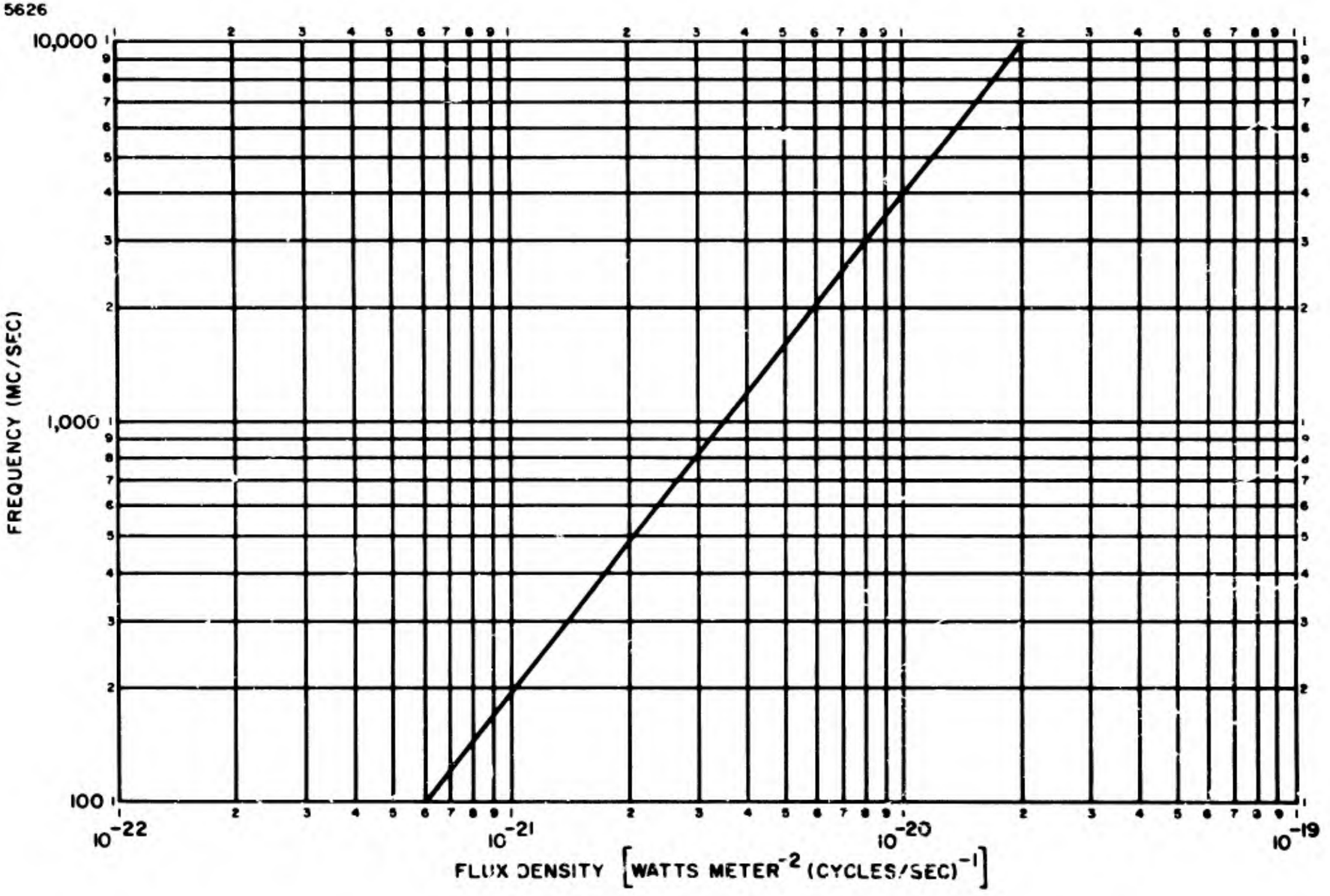

Figure 6.7-3. The Flux Density of a Quiet Sun as a Function of Frequency

3. NON-SOLAR SOURCES

The observations of the fluctuations in 64 mc/sec radiation emanating from a region in the constellation of Cygnus, by Hey, Parsons and Phillips (8), announced the possible existence of discrete noise sources of extra terrestrial origin. The amplitude and the fading rate of the fluctuations were similar in appearance to the radiation from the sun during sunspot activity. Ryle and Smith (9) found that a source in Cassiopeia was more intense than Cygnus and were able to show that the radiation from the two sources were randomly polarized.

In recent years, considerable amount of effort has been devoted to the study of the fluctuations in signal strength of radio stars This scintillation is the result of moving irregularities in the ionosphere, located above the level of F-layer maximum ionization. Little and Maxwell (10) have found that during aurorae, the scintillations are about four times more rapid than during normal conditions which, at 81 mc/sec, is about 1-3 fluctuations per minute. The scintillation rate and the velocity of ionospheric irregularities are approximately proportional to the K index of geomagnetic activity. A similar conclusion was reported by Millman (11) from his investigation of ionospheric winds and turbulence by the three-spaced receiver technique.

A rather complete catalogue of positions and intensities of discrete radio stars has been compiled by Pawsey (12). The major sources which can be detected from locations in both the northern and southern hemisphere are listed in Table 6.7-2.

It should be mentioned that the flux densities are twice that observed in one plane of polarization The asterisks designate the experimental results reported by Wells (13). The flux densities of Cassiopeia at frequencies of 12.5 mc/sec and 15.5 mc/sec are double the values previously quoted.

Figure 6.7-4 is a plot of the flux density of the discrete radio stars. At 200 mc/sec the total radiation from Cassiopeia and Cygnus, which are the more intense sources, is approximately 1.05×10^{-22} watts meter^{-2} (cycles/sec)$^{-1}$ and 6.6×10^{-23} watts meter^{-2} (cycles/sec)$^{-1}$, respectively. It can be shown that the slope of the frequency-flux curve through Cassiopeia and Cygnus can be expressed approximately by the function, $S \propto f^{-0.81}$

C. DISTRIBUTED NOISE SOURCES

1. EQUIVALENT ANTENNA TEMPERATURE

When the source of radiation consists of many individual radiators spatially distributed, the flux density is now defined by the integral

$$S = \int\int b(\theta, \phi)\, d\Omega \qquad (6.7\text{-}16)$$

where the integration is taken over the whole solid angle occupied by the sources.

TABLE 6.7-2

POSITIONS AND INTENSITIES OF DISCRETE RADIO STARS

CONSTELLATION	RIGHT ASCENSION	DECLINATION	FREQUENCY (MC/SEC)	FLUX DENSITY [Watts Meter^{-2} (cycles/sec)$^{-1}$] $\times 10^{-24}$	ANGULAR DIMENSIONS
ANDROMEDA	$00^h\ 40^m\ 15^s \pm 30^s$	$40^\circ\ 50' \pm 20'$	81.5	0.4	
			158.0	1.6	
CASSIOPEIA	$23^h 21^m 12^s \pm 1^s$	$58^\circ\ 32.1' \pm 0.7'$	12.5*	440	
			15.5*	480	
			81.5	220	3' × 4'
			158.0	93	
			3200	15.0	
CENTAURUS	$13^h 22^m 30^s \pm 4^s$	$-42^\circ\ 46' \pm 2'$	60	32.0	
			100	18.5	20'
			101	16.0	
			3200	2.0	
CYGNUS	$19^h 57^m 45.3^s \pm 1^s$	$40^\circ\ 35' \pm 1'$	60	220	
			81.5	135	2'10" × 35"
			100	125	
			101	130	
			158	57	
			3200	7.0	
PERSEUS	$03^h 15^m 15^s \pm 1.5^m$	$41^\circ\ 22' \pm 30'$	81.5	0.95	
			81.5	1.2	
			100	0.9	
			101	2.4	
			158	0.6	
TAURUS	$05^h 31^m 29^s \pm 2.5^s$	$22^\circ\ 00' \pm 3'$	26.75*	53	
			60	18.5	
			81.5	12.5	
			100	18.5	
			101	19.0	3.5' × 5.5'
			160	18.5	
			3200	8.0	
VIRGO	$12^h 28^m 15.5^s \pm 2.5^s$	$12^\circ\ 44' \pm 6'$	18.3	110	
			18.5*	150	
			26.75*	53	
			60	25.0	
			81.5	10.5	2.5' × 5'
			100	12.5	
			101	12	
			3200	1.4	

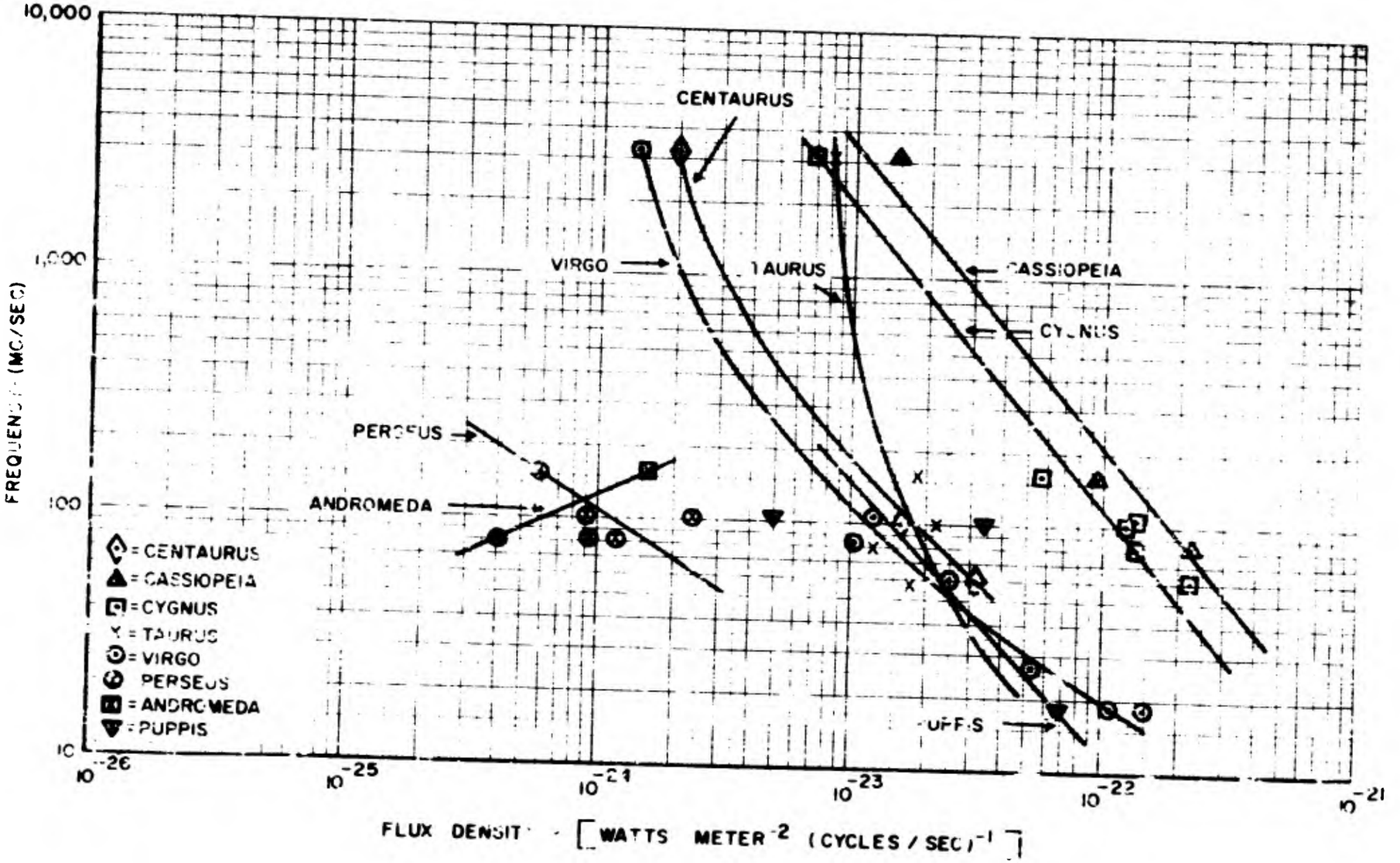

Figure 6.7-4. Flux Density of Discrete Radio Sources as a Function of Frequency

Since the effective antenna area is a function of aspect angles (θ, ϕ), the received power becomes, according to Equation (6.7-3),

$$P = 1/2\ B \iint A_e\ (\theta, \phi)\ b\ (\theta, \phi)\ d\ \Omega \qquad (6.7\text{-}17)$$

The equivalent antenna temperature is, therefore, given by

$$T_a = \frac{1}{\lambda^2} \iint T_b\ (\theta, \phi)\ A_e\ (\theta, \phi)\ d\ \Omega \qquad (6.7\text{-}18)$$

2. GALACTIC SOURCES

The results of observations of the intensity and distribution of radio-frequency radiation from the galaxy at frequencies from 9.5 to over 1000 mc/sec, collected by Piddington (14), are presented in Figure 6.7-5. The slope of the spectrum curve is expressed by $T_b \propto f^{-\gamma}$ where γ is the constant for the portion of the curve in question. The constant, γ, has a value of 2 73 for the central portion of curve B and 2.51 for the central portion of curve A.

The coordinates of the different regions are given in Table 6.7-3. Since the positions of the noise sources were given in galactic coordinates, the conversion to equatorial coordinates was performed from the chart furnished by Pawsey and Bracewell (4). Region A is near the center of the galaxy, while region B is in the Milky Way.

TABLE 6.7-3

DISTRIBUTED NOISE SOURCES

REGION	GALACTIC COORDINATES	EQUATORIAL COORDINATES
A	Latitude = -2°	Declination = -26°
	Longitude = 330°	Right Ascension = $17^{h}35^{m}$
B	Latitude = 0°	Declination = 0°
	Longitude = 180°	Right Ascension = $6^{h}40^{m}$
C	Latitude = -30°	Declination = -29°
	Longitude = 200°	Right Ascension = $5^{h}30^{m}$

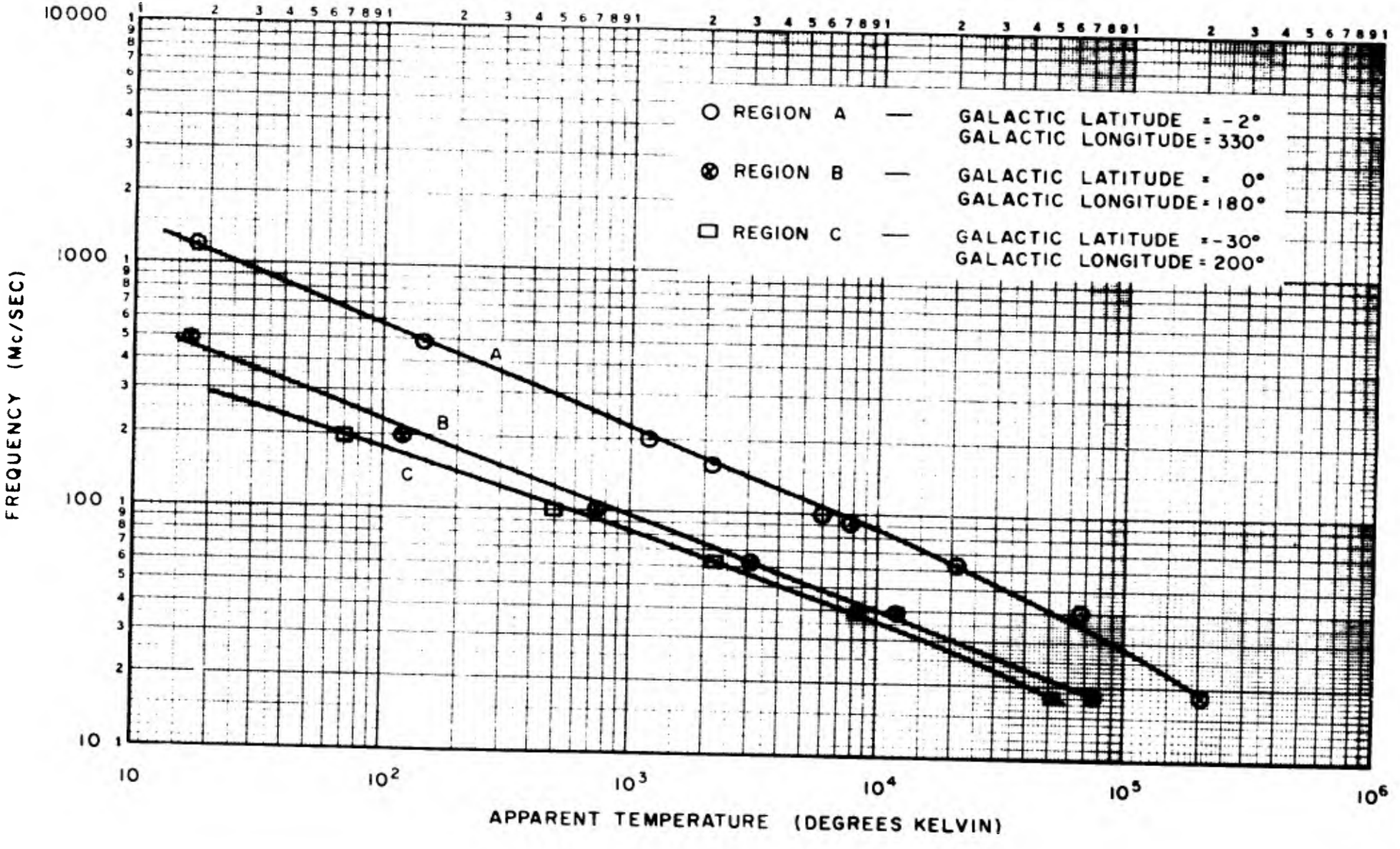

Figure 6.7-5. Apparent Temperature of Galactic Radiation

From galactic radiation measurements at frequencies of 40, 90 and 200 mc/sec, Moxon (15) found that,when the antenna was directed towards the maximum noise radiation at the galactic equator, the relationship between the apparent black body temperature and frequency was $T_b \propto f^{-2.7}$. When the antenna was aimed away from the galactic equator, the temperature-frequency proportionate relationship was $T_b \propto f^{-2.1}$. It was also noticed that the frequency exponent was practically insensitive to galactic longitude variations.

Herbstreit and Johler (16) have reported that, from a comparison of galactic radiation observed on 25 mc/sec and 110 mc/sec, the black-body temperature varied as $T_b \propto f^{-2.4}$

Since the flux density is directly proportional to the square of frequency and the apparent black-body temperature [see Equations (6.7-1) and (6.7-2)], it is, therefore, evident that for galactic noise, the flux density is inversely proportional to frequency. In other words, the flux density decreases with increasing frequency which is contrary to solar noise frequency dependency.

A survey of galactic radio noise on 200 mc/sec has been made by Allen and Gum (17) for the region of the sky south of declination $+45^{\circ}$. The maximum flux density recorded was 2×10^{-20} watts meter^{-2} (cycles/sec)$^{-1}$ steradian^{-1} at galactic latitude -3° and galactic longitude 322°.

According to Piddington (14), galactic radiation at radio frequencies probably originates partly in hot ionized interstellar gas and partly in stellar atmosphere. The ionized gas provides most of the radiation at the higher frequencies and evidences itself by absorption at the lower frequencies.

D. SYSTEM DEGRADATION BY COSMIC RADIATION

An increase in system noise temperature, in essence, alters the maximum range capability of a radar system. According to the radar equation, the maximum range is defined by

$$R_{max} \propto \left(\frac{P_t}{S_{min}}\right)^{\frac{1}{4}} \propto \left(\frac{1}{T_s}\right)^{\frac{1}{4}} \qquad (6.7\text{-}19)$$

where P_t is the transmitted peak power; S_{min}, the minimum detectable signal; and T_s, the system noise temperature

As an example, the apparent antenna temperatures at 1200 mc/sec and the reduction in range brought about by the presence of the quiet sun, the major radio stars and distributed galactic noise regions are presented in Table 6.7-4. Calculations are based on an effective antenna aperture of 430 square meters (50 foot diameter parabolic antenna).

TABLE 6.7-4

REDUCTION IN RADAR RANGE AT 1200 MC/SEC DUE TO THE PRESENCE OF COSMIC NOISE SOURCES

RADIO SOURCE	APPARENT ANTENNA TEMPERATURE (DEGREES KELVIN)	SYSTEM NOISE TEMPERATURE ($T_S = T_A + T_O$)* (DEGREES KELVIN)	PER CENT REDUCTION IN RADAR RANGE
Sun (Quiet)	62500	62790	74.0
Cassiopeia	390	680	19.1
Cygnus	250	540	14.4
Taurus	140	430	9.3
Virgo	31	321	2.5
Center of Galaxy	18	308	1.5
Milky Way	<10	$290 < T_s < 300$	<1.0

*T_o (Receiver Temperature) $\approx 290^{\circ}K$

It is obvious that, for this particular system configuration, the sun is the major source of interference while Cassiopeia, Cygnus, and Taurus are somewhat less effective. The appearance of Virgo, the center of the galaxy and the Milky Way in the antenna beam will not cause any appreciable deterioration of the system. It should be noted that, as the radar transmission frequency is increased, the interference from all the cosmic radio noise sources is reduced

E. REFERENCES

1. Lawson, J. L., and Uhlenbeck, G. E.; "Threshold Signals," Radiation Laboratory Series, Vol. 24, McGraw-Hill Book Co., 1950

2 Shapley, A H. and Davis, R. M., Jr.; "Solar Eruption of May 10, 1949," Science, Vol. 110, p. 159, August 12, 1949.

3. Payne-Scott, R ; Yabsley, D. E. and Bolton, J. G.; "Relative Times of Arrival of Bursts of Solar Noise on Different Radio Frequencies," Nature, Vol. 160, p. 256, 1947

4. Pawsey, J. L. and Bracewell, R. N.; "Radio Astronomy," Oxford University Press, 1955.

5. Reber, G.; "Solar 480 mc/sec Radiation," Nature, Vol. 158, p. 945, 1946.

6 Pawsey, J. L. and Smerd, S. F.; "Solar Radio Emission," Chapter 7, from "The Sun" edited by C. P. Kuiper, University of Chicago Press, 1953.

7 Dodson, H. W.; Hedeman, E. R and Owren, L ; "Solar Flares and Associated 200 mc/sec Radiation," Astrophysical Journal, Vol. 118, p. 169, Sept. 1953.

8 Hey, J. S.; Parsons, S J.; and Phillips, J. W., "Fluctuations in Cosmic Radiation at Radio Frequencies," Nature, Vol. 158, p. 234, 1946.

9. Ryle, M.; and Smith, F. G.; "A New Intense Source of Radio-Frequency Radiation in the Constellation of Cassiopeia," Nature, Vol. 162, p. 462, 1946.

10. Little, C. G. and Maxwell, A.; "Scintillation of Radio Stars During Aurorae and Magnetic Storms," Journal of Atmospheric and Terrestrial Physics, Vol. 2, p. 356, 1952.

11. Millman, G. H., "A Study of Ionospheric Winds and Turbulence Utilizing Long Radio Waves," Annales de Geophysique, Vol. 8, p. 365, 1952.

12. Pawsey, J. L ; "A Catalogue of Reliably Known Discrete Sources of Cosmic Radio Waves," Astrophysical Journal, Vol. 121, p. 1, 1955.

13. Wells, H. W.; "Flux Measurements of Discrete Radio Sources at Frequencies Below 30 Megacycles," presented at the URSI-IRE Meeting, Washington, D.C., May 1956

14. Piddington, J. H.; "The Origin of Galactic Radio Frequency Radiation," Monthly Notices of Royal Astronomical Society, Vol. III, p. 46, 1951.

15. Moxon, L. A.; "Variation of Cosmic Radiation with Frequency," Nature, Vol. 158, p. 758, 1946.

16. Herbstreit, J W and Johler, J. R.; "Frequency Variation of the Intensity of Cosmic Radio Noise," Nature, Vol. 161, p. 515, 1948.

17. Allen, C. W. and Gum, C. S.; "Survey of Galactic Radio-Noise at 200 mc/sec," Australian Journal of Scientific Research, Vol. 3, p. 224, June 1950.

6.8 - ORBITAL PATHS OF CELESTIAL BODIES

A. INTRODUCTION

Oftentimes, in an operational radar system, it is desirable to determine beforehand the location in space of celestial bodies, i.e , the sun, moon, radio stars and meteor radiants, which could introduce noise interference and clutter. In this section, mathematical relationships are presented which will assist in the solution of this problem.

When the angular coordinates of an antenna beam are fixed in position, as the earth rotates, the beam sweeps out, on the celestial sphere, a path of constant declination, but with right ascension which varies with the time of day The presence of a celestial object in the path can be readily resolved when the terrestrial coordinates of the observation site and the celestial coordinates of the astronomical body are known.

B. MATHEMATICAL CONSIDERATIONS

The relationship of the celestial coordinate system with the geographic coordinate system is illustrated in Figures 6 8-1 and 6.8-2. The declination, D, of a point on the celestial sphere is analogous to geographic latitude since it is the angular displacement from the equatorial plane measured positive northward. The right ascension, RA, which corresponds to geographic longitude is the angular position about the celestial pole. It is measured positive east from the meridian containing the Vernal Equinox (or the First Point of Aries) which is the intersection of the plane of the ecliptic, i.e., the plane of the sun's orbit about the earth, with the celestial equator. The Greenwich Hour Angle of Aries, GHA^{γ}, is the angular distance measured positive westward along the celestial equator from the Greenwich meridian to the Vernal Equinox. The local hour angle, ϕ, is the angular displacement between the meridians containing the observation site and the point on the celestial sphere, and is measured positive westward.

It can be readily shown by applying the law of cosines to the spherical triangle of Figure 6.8-3 that the function relating the geographic and celestial coordinates is given by

$$\sin D = \sin E \sin L + \cos E \cos L \cos A \qquad (6.8\text{-}1)$$

where L is the latitude of the observation sight, and A and E are the azimuth and elevation angles of the celestial body as observed at the site, respectively. For the special case when $A = 180^{\circ}$, this equation simplifies to

$$E = \frac{\pi}{2} + D - L \qquad (6\ 8\text{-}2)$$

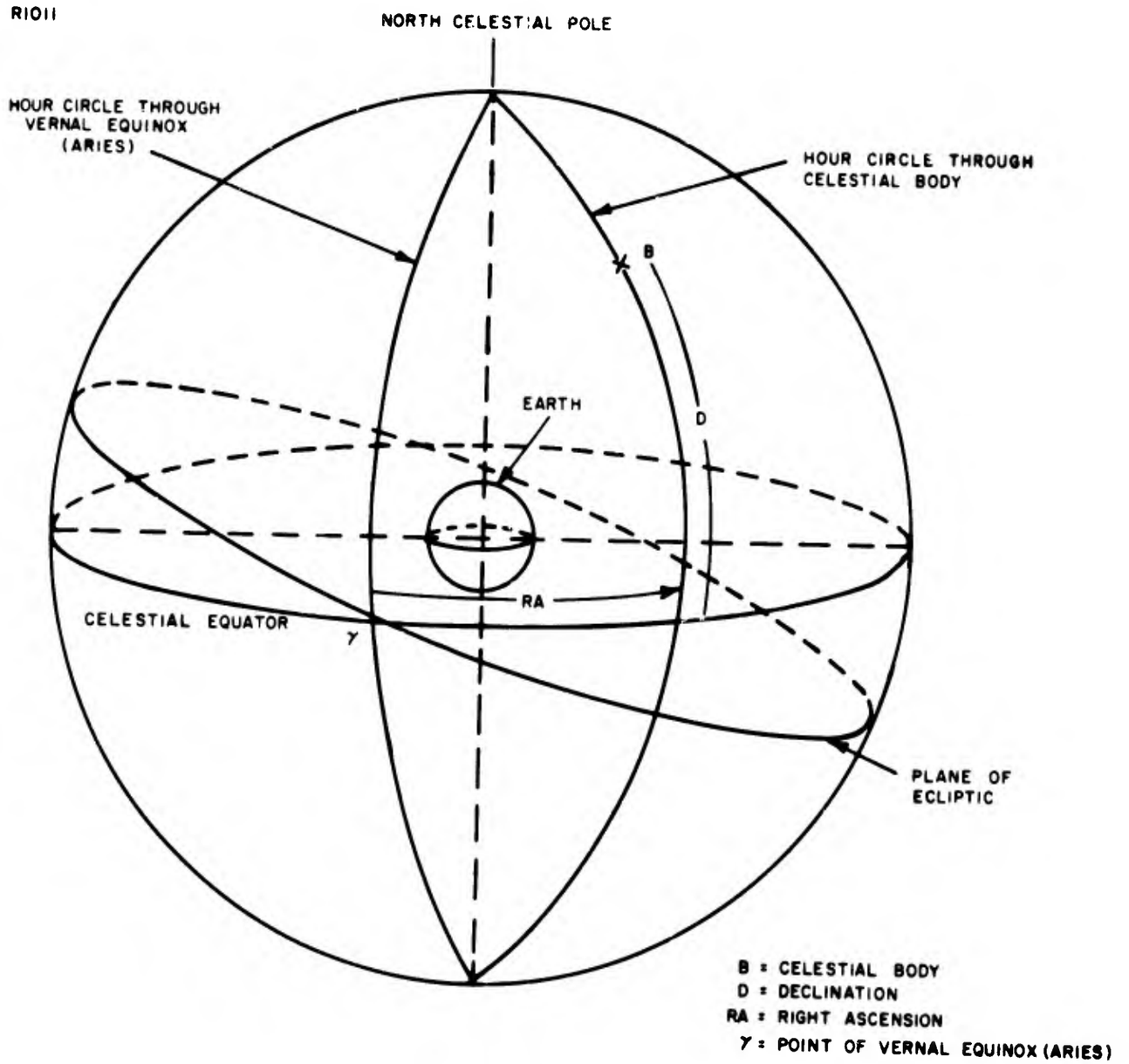

Figure 6.8-1. Celestial Coordinate System

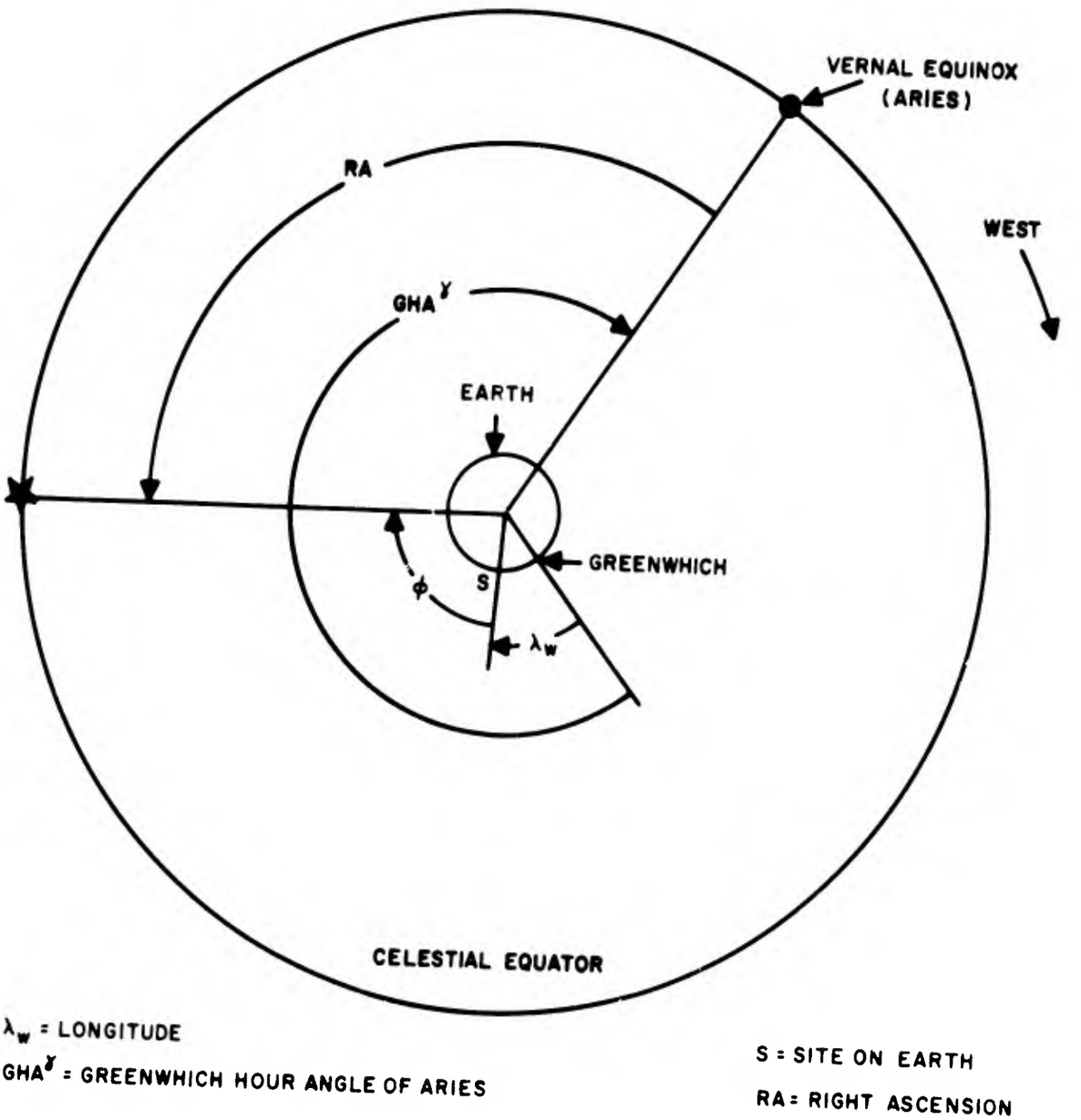

Figure 6.8-2. Celestial Time Coordinates

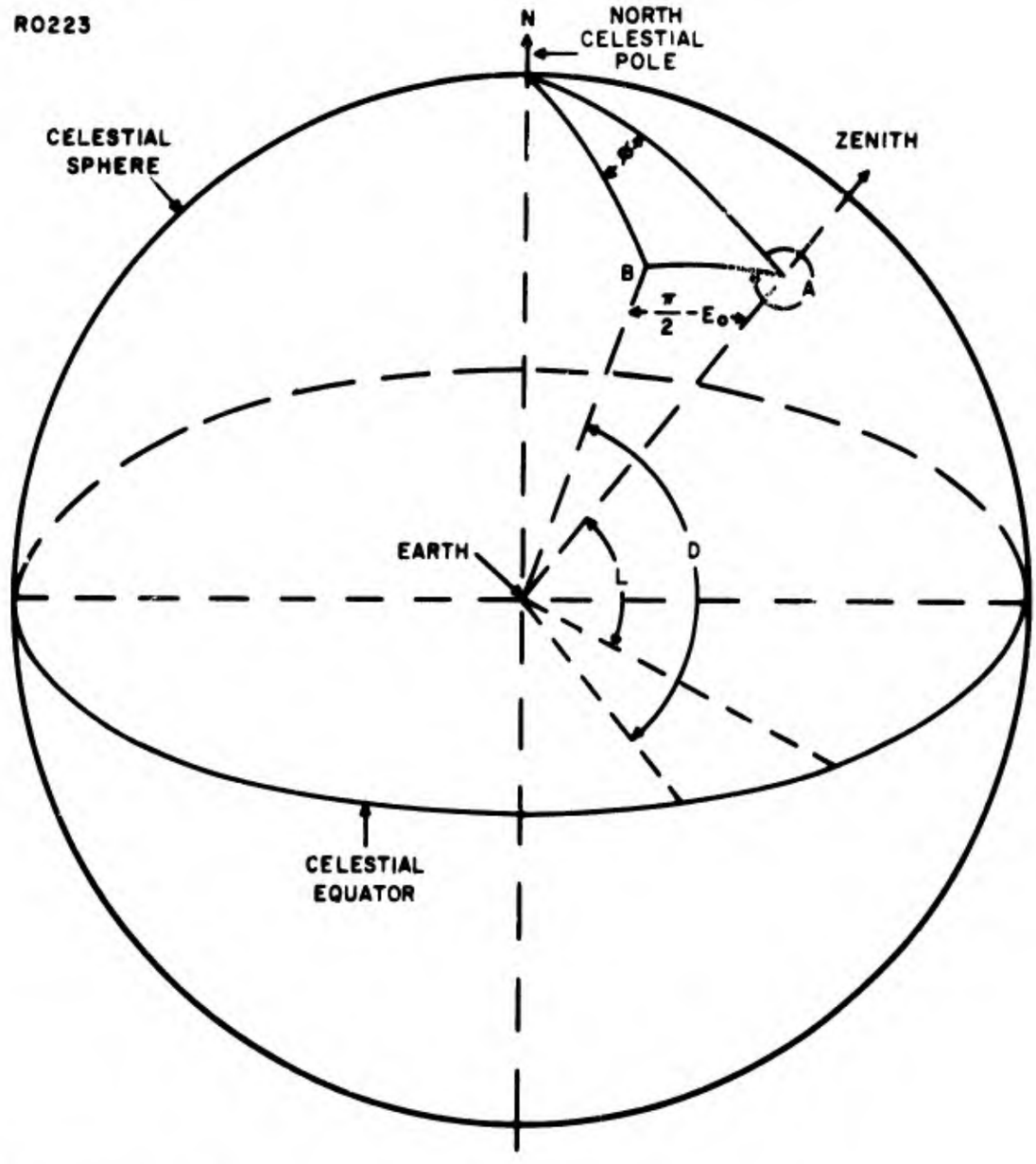

Figure 6.8-3. Astronomical Configuration

For $A = 0^{o}$

$$E = L \pm \left(\frac{\pi}{2} - D \right) \tag{6.8-3}$$

where the two solutions exist only when the condition, $L > [(\pi/2) - D]$, is satisfied.

According to Equation (6.8-1), it is seen that the azimuth and elevation orientations of a celestial body are only dependent upon the observer's latitude and the declination. Since the declination of a radio star is relatively constant, its orbital path as observed from a fixed location on the earth's surface, remains the same from day-to-day. With regard to the sun and the moon, however, both orbital paths are not constant since their declinations are variable functions of time.

The azimuth and elevation positions of the sun and several radio stars, as observed in the northern hemisphere, are plotted in Figures 6.8-4 through 6.8-7. It should be noted that the paths of the radio stars are symmetrical about the observer's meridian.

The duration of time that a celestial body will remain above the horizon at any latitude is of extreme interest. Referring to Figure 6.8-3, it can be shown from spherical trigonometry that, in terms of units of time, the azimuth and elevation coordinates can also be expressed by

$$\sin E = \cos \phi \cos L \cos D + \sin L \sin D \tag{6.8-4}$$

and

$$\tan A = \frac{\sin \phi}{\tan D \cos L - \sin L \cos \phi} \tag{6.8-5}$$

It should be noted that the local hour angle, ϕ, is expressed in sidereal time units and not in solar time. Sidereal time which is based on the rate of motion of the stars differs from solar time in several important aspects: (1) the reference point for solar time is the sun while for sidereal time it is the vernal equinox; (2) the sidereal day begins when the reference point is over the upper branch of the celestial meridian while the solar day starts when the reference point, the sun, crosses the lower branch of the celestial meridian; (3) a mean sidereal day is approximately equal to 23 hours, 56 minutes, 4.09 seconds of mean solar time. Since the sidereal day is shorter than the solar day, a radio star will cross an observer's meridian approximately 3 minutes, 55.91 seconds earlier every day.

The time at which a radio star crosses a given angular position can be determined by utilizing Equations (6.8-4) and (6.8-5) in conjunction with

$$\phi = 360^{o} + GHA^{\gamma} - RA - \lambda_{w} \tag{6.8-6}$$

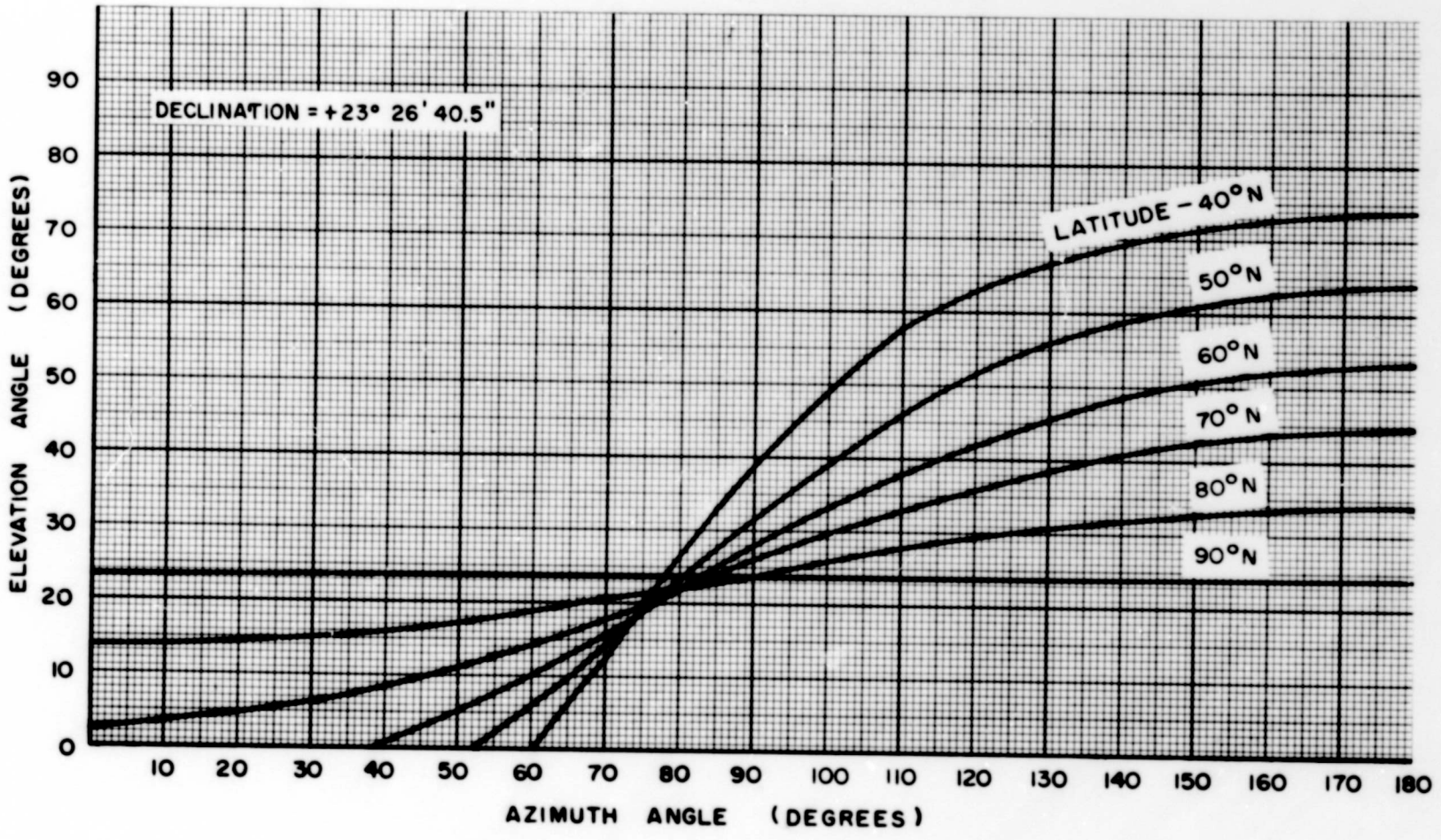

Figure 6.8–4. Antenna Elevation and Azimuth Orientation as a Function of Latitude for the Observation of the Sun at the Summer Solstice

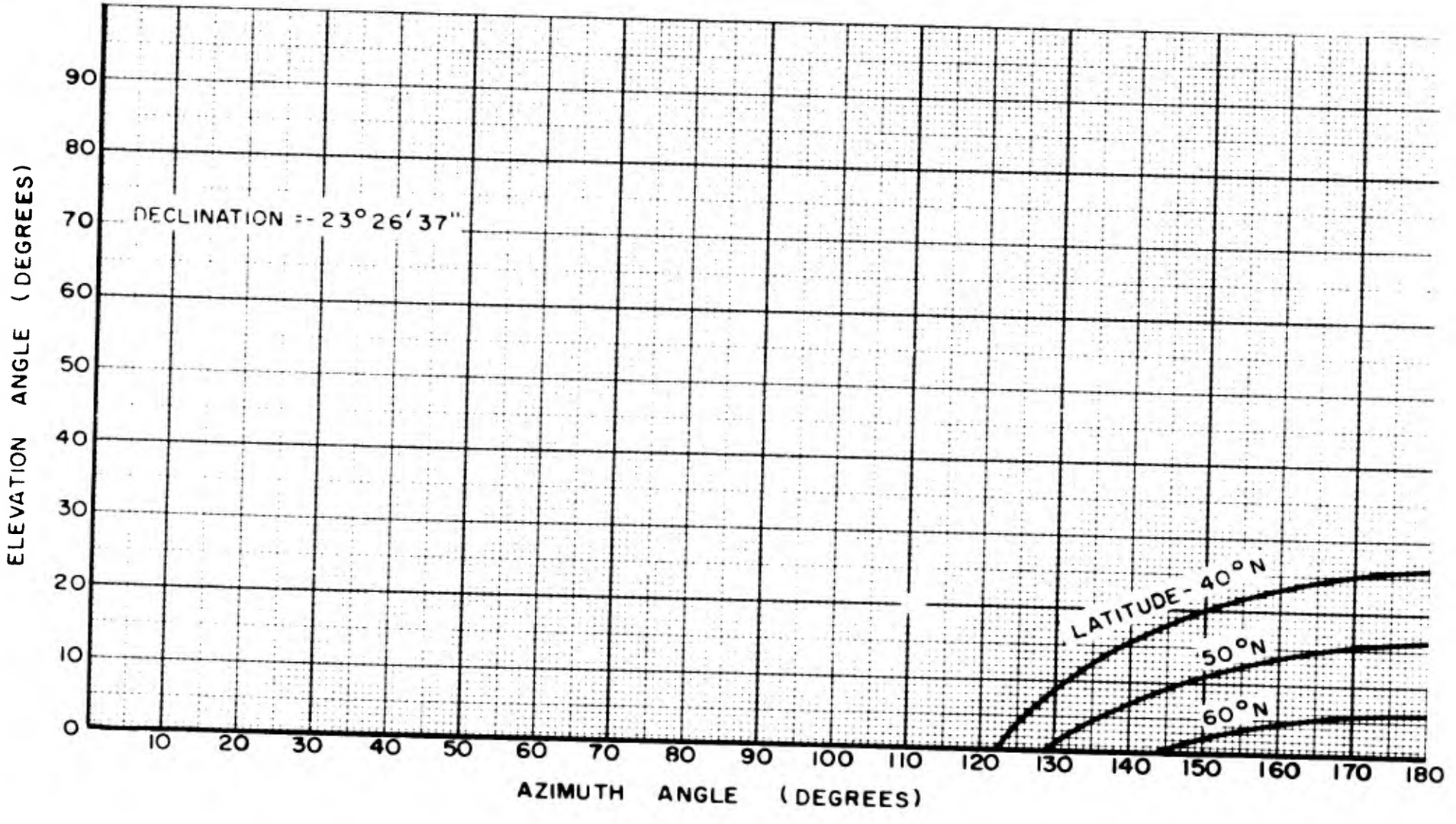

Figure 6.8-5. Antenna Elevation and Azimuth Orientation as a Function of Latitude for the Observation of the Sun at the Winter Solstice

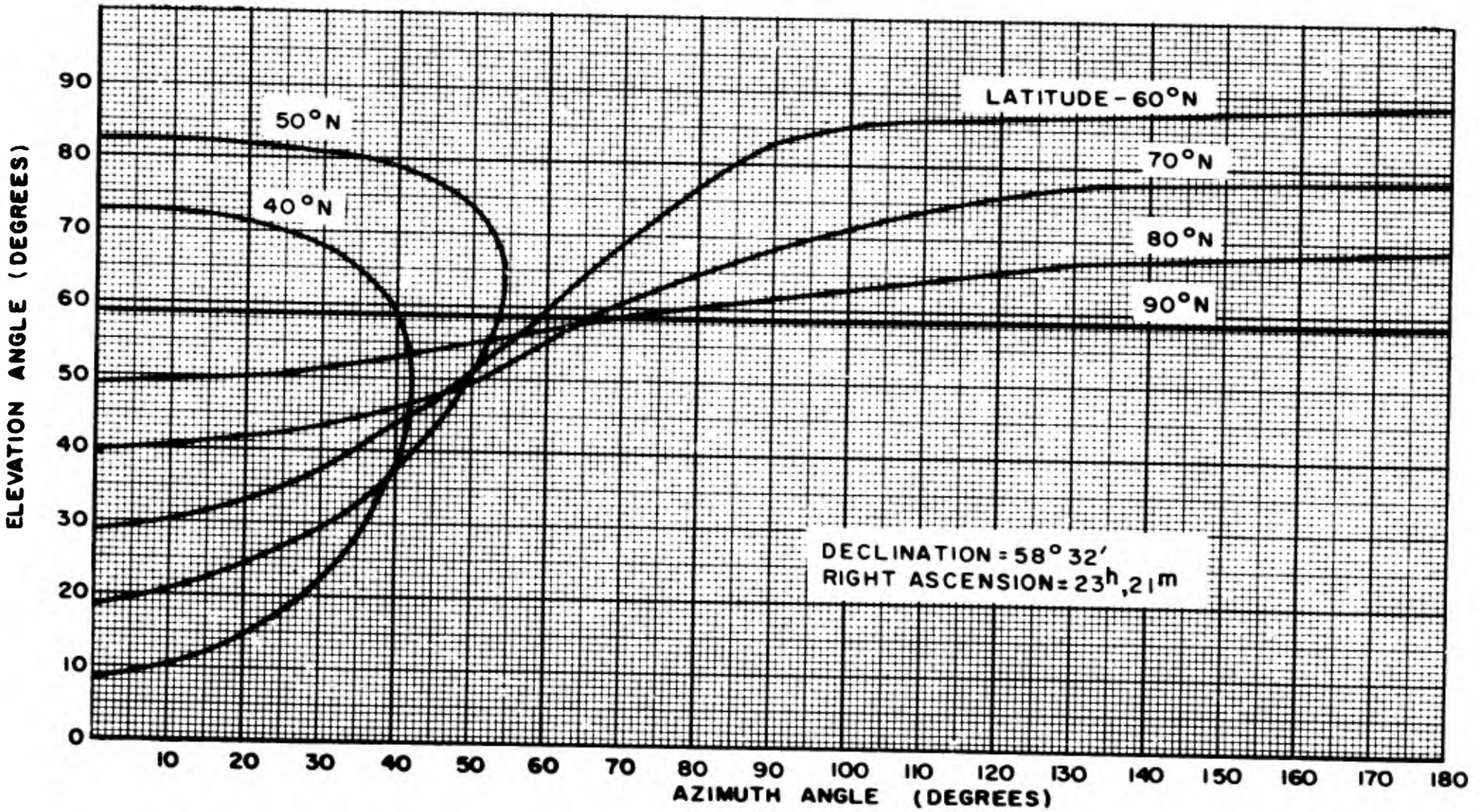

Figure 6.8-6. Antenna Elevation and Azimuth Orientation as a Function of Latitude for the Observation of Cassiopeia

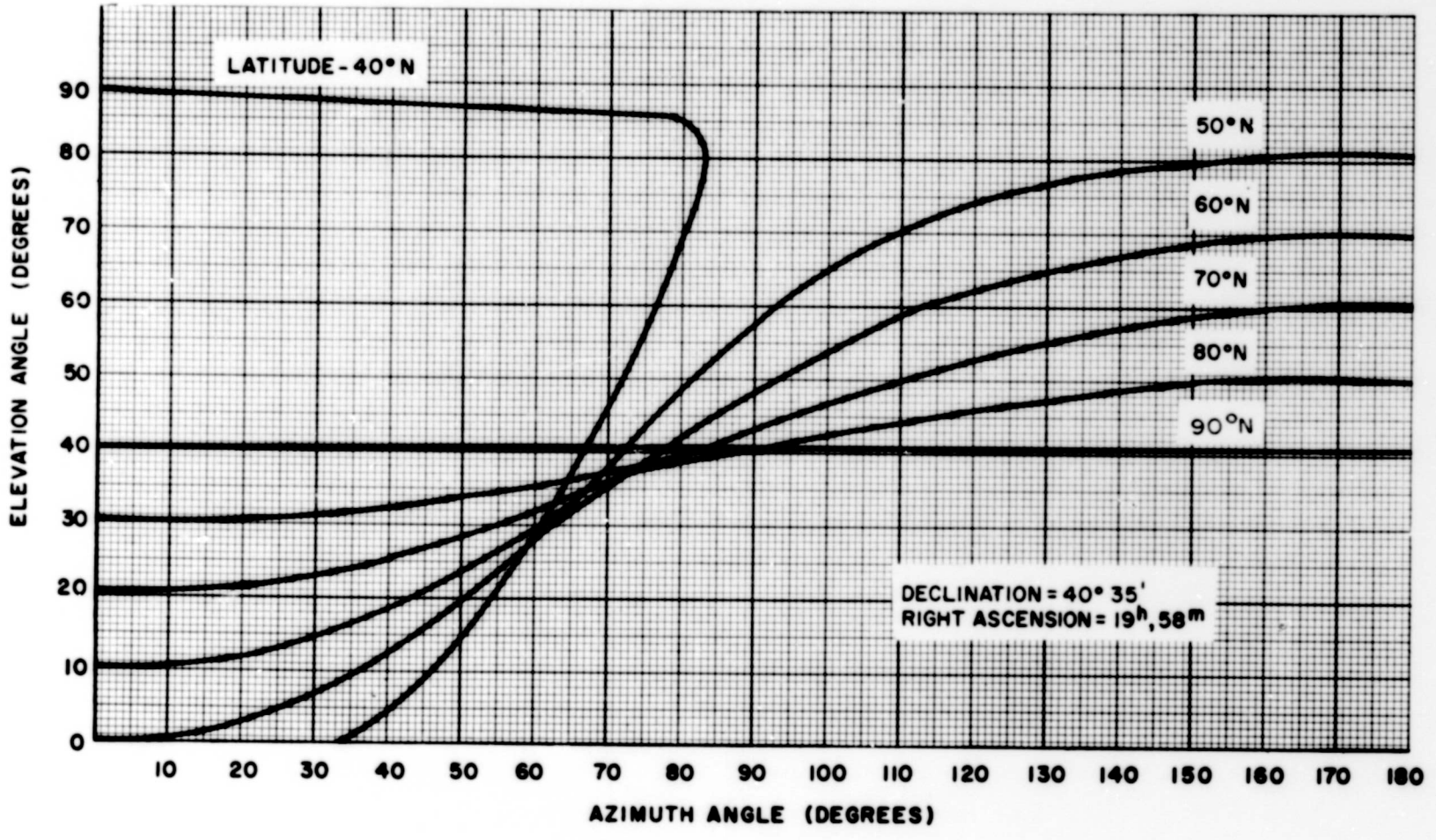

Figure 6.8-7. Antenna Elevation and Azimuth Orientation as a Function of Latitude for the Observation of Cygnus A

where λ_W is the longitude of the observer measured positive westward. This expression is derivable from Figure 6.8-2. The parameter, GHAγ, is listed as a function of time of day in the Nautical Almanac.

With regard to determining the time of passage of the sun and the moon, Equation (6.8-6) is modified to the form

$$\phi = \text{GHA} - \lambda_W \tag{6.8-7}$$

where GHA, the Greenwich hour angle, is, in essence, the local hour angle. This angle, which is also tabulated in the Nautical Almanac, is measured positive westward from Greenwich meridian.

[redacted]

BLANK PAGE